NUI MAYNOOTH

Ollscoil na hÉireann Má Nuad

Simulation, optimization and instrumentation of agricultural biogas plants

Christian Wolf

Student No. 66111684

Doctoral Dissertation

Department of Electronic Engineering

National University of Ireland, Maynooth

February 2013

Head of the Department: Dr. Ronan Farrell

Supervisor: Prof. Dr. Seán McLoone

Abstract

During the last two decades, the production of renewable energy by anaerobic digestion (AD) in biogas plants has become increasingly popular due to its applicability to a great variety of organic material from energy crops and animal waste to the organic fraction of Municipal Solid Waste (MSW), and to the relative simplicity of AD plant designs. Thus, a whole new biogas market emerged in Europe, which is strongly supported by European and national funding and remuneration schemes. Nevertheless, stable and efficient operation and control of biogas plants can be challenging, due to the high complexity of the biochemical AD process, varying substrate quality and a lack of reliable online instrumentation. In addition, governmental support for biogas plants will decrease in the long run and the substrate market will become highly competitive.

The principal aim of the research presented in this thesis is to achieve a substantial improvement in the operation of biogas plants. At first, a methodology for substrate inflow optimization of full-scale biogas plants is developed based on commonly measured process variables and using dynamic simulation models as well as computational intelligence (CI) methods. This methodology which is appliquable to a broad range of different biogas plants is then followed by an evaluation of existing online instrumentation for biogas plants and the development of a novel UV/vis spectroscopic online measurement system for volatile fatty acids. This new measurement system, which uses powerful machine learning techniques, provides a substantial improvement in online process monitoring for biogas plants.

The methodologies developed and results achieved in the areas of simulation and optimization were validated at a full-scale agricultural biogas plant showing that global optimization of the substrate inflow based on dynamic simulation models is able to improve the yearly profit of a biogas plant by up to 70%. Furthermore, the validation of the newly developed online measurement for VFA concentration at an industrial biogas plant showed that a measurement accuracy of 88% is possible using UV/vis spectroscopic probes.

Acknowledgements

This thesis would not have been possible without the help of many friends, companies and research grants but the greatest thanks go to my beloved wife Andrea and to my two little ones Sydney and Jamie, who have always supported and loved me during the last six years and kept my hopes up even during desperate times. I cannot thank you enough!

To my brother Marcus, thank you for reading my thesis, although you did not understand most of it. Your corrections and design ideas made my day.

Furthermore, I would like to thank my supervisors Prof. Dr. Seán McLoone and Prof. Dr. Michael Bongards for their ideas, insight and corrections, which made this PhD what it is today. They are not only mentors but have become dear friends. I could not have asked for better role models, each inspirational, supportive, understanding and patient.

I would also like to thank the many anonymous reviewers from the IWA, IEEE, SAGE and the various conferences, thank you for all your careful and instructive comments that shaped this thesis.

To the staff of the Gummersbach Environmental Computing Center (GECO▶C) from the Cologne University of Applied Sciences, you helped me enjoy my day-job and became close friends. Special thanks go to Peter Kern for always providing me with an open ear and to Daniel Gaida, my biogas pal and mathematics guru for helping me out in so many ways.

In the end, I would like to thank my mum (†16th September 2012) for all her support and wise advice for so many years. I wish you could have seen this!

Science is in a constant state of flux and anybody, who had claimed he would have discovered an eternal truth in science, would only admit that he is not a real scientist.

{Manfred Lütz – Bluff!: The forgery of the world}[1]

[1] Lütz, M., 2012. *Bluff!: Die Fälschung der Welt (Bluff!: The forgery of the world).* München: Droemer.

Table of contents

Table of contents

List of Figures

List of Figures

List of Figures

List of Tables

List of Tables

List of Tables

Nomenclature

Acronym	Definition
ABP	Agricultural Biogas Plant
AD	Anaerobic Digestion
ADM1	Anaerobic Digestion Model No. 1
ANN	Artificial Neural Networks
BOD	Biochemical Oxygen Demand
CH_4	Methane
CI	Computational Intelligence
CO_2	Carbon Dioxide
COD	Chemical Oxygen Demand
CSTR	Continuous Stirred-Tank Reactor
DACE	Design and Analysis of Computer Experiments
FSR	Forward Selection Regression
GA	Genetic Algorithm
GerDA	Generalized Discriminant Analysis
H_2	Hydrogen
H_2S	Hydrogen Sulphide
HRT	Hydraulic Retention Time
IBP	Industrial Biogas Plant
IWA	International Water Association
LCFA	Long Chain Fatty Acids
LDA	Linear Discriminant Analysis
LH	Latin Hypercube
MLP	Multilayer Perceptron
NH_3	Ammonia
NH_4	Ammonium
O_2	Oxygen
ORP	Oxidized Redox Potential
PA	Partial Alkalinity
PLC	Programmable Logic Controller
PLS	Partial Least Squares
PSO	Particle Swarm Optimization
RF	Random Forest
RVM	Relevance Vector Machine
S_2	Sulphur
S-KSM	Sequential Kriging Surrogate Models
SVM	Support Vector Machines
T	Temperature
TA	Total Alkalinity
ThCOD	Theoretical Chemical Oxygen Demand
TIC	Total Inorganic Carbon
TKN	Total Kjeldahl Nitrogen
TOC	Total Organic Carbon
TS	Total Solids
TSS	Total Suspended Solids
UV/vis	Ultraviolet and visible
VFA	Volatile Fatty Acids
VOA	Volatile Organic Acids
VS	Volatile Solids
VSS	Volatile Suspended Solids
WWTP	Waste Water Treatment Plant

1 Introduction

"The apparent goal of the present world system is
to produce more people with […] more for each person […]
if society continues to strive for that goal,
it will eventually reach one of many earthly limitations."

{Donella H. Meadows, *The limits to growth, p. 94*, 1972}

In a world of seven billion people and with an annual population growth of 78 million people (UNPF 2011), resources such as food, water and fossil fuels will become scarce and may even be completely depleted, eventually. Furthermore, the increasing consumption of resources results in an ever increasing production of waste. In 1972 Meadows *et. al* analyzed the consequences of constant growth in a report for the Club of Rome's[2] project on the predicament of mankind (Meadows *et al.* 1972). In a review of the original assumptions and predictions, which was conducted in 2004 (Meadows *et. al* 2004), most of them were found to be surprisingly accurate, which according to Meadows leaves the world with two choices to achieve a sustainable future (Becker 2012): (1) advancement through crisis, or, (2) advancement through proactive change.

Looking at the energy sector in Europe, it is a bit of both. On the one hand, catastrophes such as the tsunami in Japan, which resulted in the meltdown of a nuclear reactor at Fukushima (NISA 2011) showed the world the danger of nuclear power production, which in turn led to policy changes towards renewable energies in many countries in Europe and beyond. On the other hand, many European governments and the European Commission (EC 2009) have developed policies to support and increase sustainable renewable energy production.

In addition to proactive change through political instruments, technical innovations in the area of renewable energy have proven to be a very powerful instrument and the development of highly efficient renewable energy processes and their optimization moves at an unprecedented pace (Da Rosa 2013). Thus, the share of renewable energy in gross final energy consumption in Europe was increased by more than 50% between 2004 and 2010 from 8.1% to 12.5% (Eurostat 2013a) with renewable energy from biomass being the main contributor (Eurostat 2013b).

A relatively small part of the renewable energy from biomass (6.3%) is generated from biogas in so-called biogas or AD[3] plants (Eurostat 2013b). Nevertheless, the biogas market has shown exponential growth, with an increase of 450% and is one of the fastest growing markets in Europe (Eurostat 2013b). The energy-rich biogas, mainly consisting of methane, carbon dioxide, hydrogen and

[2] http://www.clubofrome.org/
[3] AD – Anaerobic Digestion

hydrogen sulphide, is produced from degradable organic material in the absence of oxygen. This conversion is called anaerobic digestion (AD). In general, biogas plants can be divided into two groups: (1) agricultural biogas plants (ABP) and (2) industrial biogas plants (IBP), where ABPs mostly use energy crops and animal waste products for biogas production, and IBPs focus on the digestion of different kinds of waste, for example municipal solid waste (MSW) or organic waste from the food industry as well as waste sludge from WWTP. As the majority of biogas plants in Europe and particularly in Germany are ABPs, the thesis focuses on the optimization and instrumentation of ABPs.

The success of renewable energy from biogas is due to its applicability to a great variety of organic material from energy crops and animal waste to the organic fraction of MSW, and to the relative simplicity of AD plant designs. Furthermore, renewable energy production using AD is not influenced by external weather conditions, which makes it well-suited to stable continuous electrical and thermal energy production. Consequently, renewable energy from biogas is heavily supported by lucrative funding and remuneration schemes at a European and national level (EC 2013, BMU 2011). The effect of this support becomes obvious in Figure 1-1, which shows the development of the number of biogas plants in Germany over the last 20 years. After the first two amendments of the German Renewable Energy Law (REL) in 2004 and 2009 that were in favor of renewable energy from biogas, the number of biogas plants shows a strong increase. With a projected 7,874 biogas plants by 2013 in Germany alone, Germany is the leader in the European biogas market and is a good reference for the current state of the art in biogas technology.

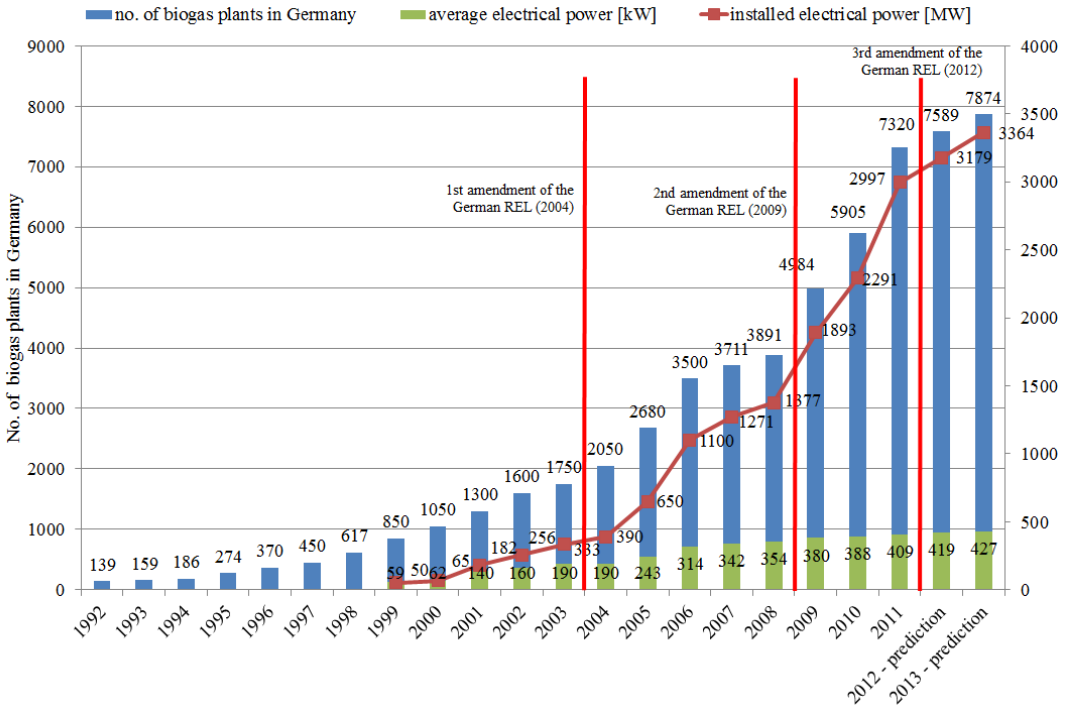

Figure 1-1: Development of the number of biogas plants in Germany over the last 20 years (Fachverband Biogas 2013)

The current state of renewable energy production from biogas in Europe (Figure 1-2) shows that countries in central Europe are the most successful in the biogas market whereas biogas production in countries like Great-Britain, Ireland, Portugal and the majority of the eastern European countries is still in its infancy. This shows the great potential for renewable energy production from biogas in Europe.

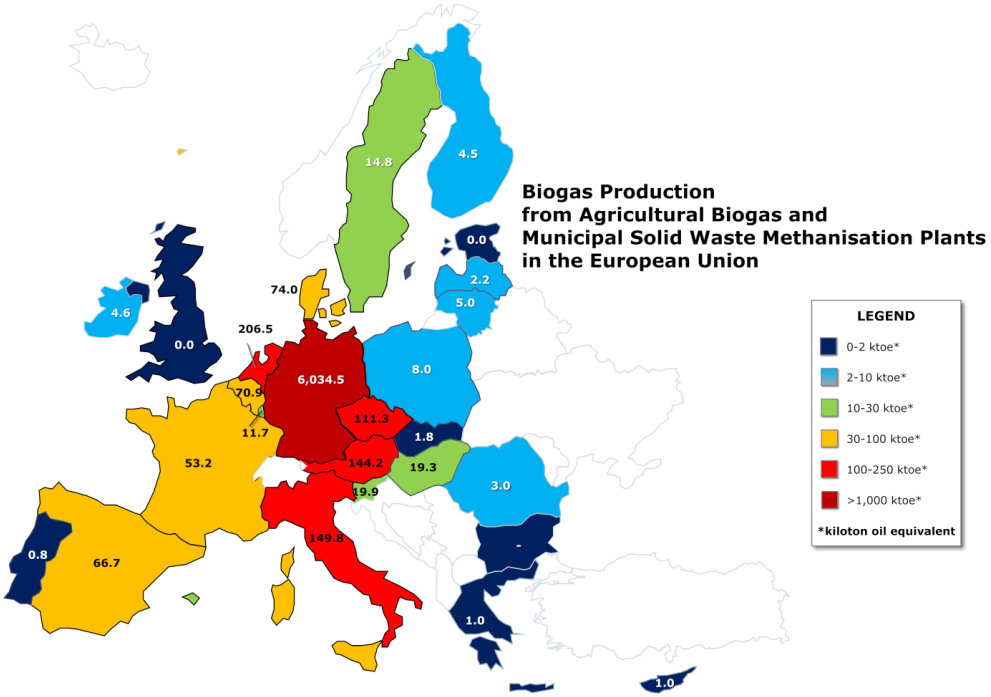

Figure 1-2: Biogas production from Agricultural Biogas and Municipal Solid Waste Methanisation Plants in the European Union (Observ'ER 2012)

Nevertheless, stable and efficient biogas plant operation and control can be difficult, due to the high complexity of the biochemical AD process, which consists of four stages that depend on each other and each requires a different set of optimal process parameters. An analysis of ABP performance in Germany performed by Schmitz in 2008 shows that the average capacity utilization in terms of electrical power production generally is much less than target optimal values of 90-98% (Schmitz 2008).

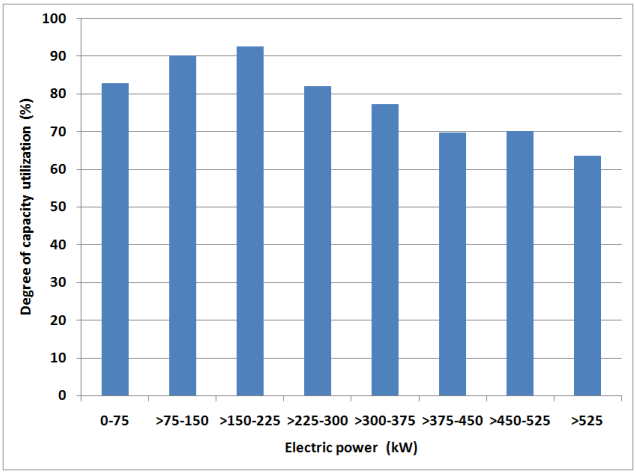

Figure 1-3: Degree of capacity utilization with regard to the average electrical power production of biogas plants in Germany (Schmitz 2008)

While small ABPs seem to reach high degrees of capacity utilization between 80% and 92%, bigger ABPs perform rather poorly with values between 60% and 70%. This clearly indicates that the room for improvement in terms of plant efficiency is huge, if more than 30% of a plant's capacity remains unused.

With regard to steadily decreasing governmental support for ABPs in the long run and a highly competitive substrate market, plant efficiency becomes the major priority in order to assure sustainable plant operation going forward (BMU 2011). Thus, new innovative developments in the area of biogas plant optimization and control are needed to tap the full potential of biogas plants while maintaining process stability. Furthermore, these developments need to work properly within the existing limitations caused by a lack of online instrumentation.

To allow for optimization and control strategies to work in practice, detailed online monitoring of the AD process is a prerequisite. Unfortunately, this is not the case for the majority of ABPs as proven by the German Agency for Renewable Resources (FNR 2009). With less than 70% of German biogas plants measuring biogas yield and biogas quality online, let alone more detailed process operating parameters, it can be concluded that instrumentation of biogas plants is mostly inadequate for process monitoring and control. Therefore, new online measurement systems for biogas plants that are robust, low maintenance and financially feasible, need to be developed.

Being aware of the issues in instrumentation, optimization and control of biogas plants, a great deal of research has been conducted in these areas over the last 20 years (Steyer 2006, Madsen *et al.* 2011). Nevertheless, many of the developed optimization and control strategies and online measurement systems could not be upscaled successfully from lab-, or pilot-scale to full-scale application.

In this thesis tools are developed, adapted and tested that give a new and much more effective approach to the area of optimization and instrumentation of full-scale ABPs:

Based on dynamic simulation models and commonly measured process variables, an optimization toolbox for substrate inflow optimization of ABPs was developed (Gaida and Wolf *et al.* 2011) to maximize process efficiency by increasing biogas yield, quality and degree of substrate degradation while maintaining stable plant operation.

Due to the high complexity of the optimization problem, two new optimization methods based on surrogate models were developed: (1) LH-based S-KSM (Latin Hypercube based Sequential Kriging Surrogate Model optimization) and (2) PSO-based S-KSM (Particle Swarm based Sequential Kriging Surrogate Model optimization). The innovation is the sequential update of a Kriging surrogate model (Matheron 1963) for each iteration of an optimization run, which improves surrogate model accuracy based on intermediate optimization results. The use of Kriging surrogate models in combination with computationally expensive optimization methods significantly reduces the overall number of fitness function evaluations. Thus, optimization performance is substantially increased.

With a combination of these methods and a dynamic simulation model the substrate inflow of a German ABP, named Sunderhook, located in Vreden in northwest Germany was optimized. The results show a fundamental improvement in yearly profit while maintaining process stability.

Furthermore, a UV/vis spectroscopic online measurement system for Volatile Fatty Acids (VFA), a key process parameter of AD, was developed and successfully tested at a full-scale IBP. As measurement accuracy is crucial, a broad set of machine learning methods was used for calibration of the system to compare measurement performance and provide a guideline as to which methods are generally best suited for this kind of application.

1.1 Aims and scope of the thesis

This thesis aims to achieve a substantial improvement in the operation of ABPs by using dynamic simulation models and computational intelligence[4] (CI) methods for substrate inflow optimization, followed by the development of a novel UV/vis spectroscopic online measurement system for VFA using powerful machine learning techniques in order to improve the state of instrumentation of ABPs.

In the first half of the thesis an optimization strategy for the substrate inflow of ABPs, which determines the optimal substrate inflow with regard to biogas production and quality/composition, degree of substrate degradation and process stability based on the current state of the plant, is introduced. The optimization strategy is used in combination with a dynamic simulation model, which

[4] "… Computational Intelligence is defined as a methodology involving computing that exhibit an ability to learn and/or deal with new situations such that the system is perceived to possess one or more attributes of reason, such as generalization, discovery, association and abstraction. The output of a computationally intelligent system often includes predictions and/or decisions. Put another way, computational intelligence comprises practical adaptation concepts, paradigms, algorithms and implementations that enable or facilitate appropriate actions (intelligent behavior) in complex and changing environments." (Eberhart, *et al.* 1996)

is calibrated based on commonly measured process variables to allow for application to a broad variety of ABPs, to optimize the substrate inflow of the full-scale Sunderhook ABP (Vreden, Germany).

Dynamic simulation models are commonly used for development and testing of optimization and control strategies as they offer unique possibilities for testing of strategies under safe conditions. To profit from these features, dynamic simulation models need to be calibrated based on operational data to reflect real operation scenarios. In the case of ABPs, the availability of operational data is a weak point due to a lack of reliable online process measurements and complex analytical methods for substrate characterization. To address this problem, a simulation toolbox for easy model building and calibration based on basic available operational data was developed.

In the second half of the thesis, a practice test of available online measurement systems for biogas plants was conducted at an ABP and IBP to assess the current state of online instrumentation of biogas plants and an UV/vis spectroscopic online measurement system for VFA is developed and validated at a full-scale IBP (Lindlar, Germany) in order to improve online instrumentation of biogas plants. One of the main issues with spectroscopic measurement systems is the complex calibration needed to extract valuable process information from the spectral data sets. To solve this issue, six powerful machine learning techniques are investigated for the calibration of the UV/vis spectroscopic measurement system. The performance results in terms of accuracy and speed can serve as guideline for the use of machine learning methods for calibration of spectroscopic online measurement systems in the future.

Thus, the thesis covers a broad variety of topics from the areas of simulation, optimization and instrumentation of biogas plants with the main goal of substantially improving biogas plant operation in the long run.

1.2 Objectives and contributions

The research presented in this thesis aimed at the development of a methodology for the optimization of ABP operation based on commonly measured process variables using dynamic simulation and CI methods and at the development of robust and reliable online instrumentation for biogas plants using UV/vis spectroscopy and machine learning techniques. The main new contributions of the thesis are as follows:

(1) A detailed survey on recent advances and the current state of the art in the areas of simulation, optimization and instrumentation of biogas plants. The large amount of research conducted in the fields of simulation, optimization and control of AD plants makes it difficult to get an overview of available developments. Thus, a chronological review of developed simulation models, optimization and control strategies as well as online measurement systems for the biogas sector is given. This allows the assessment of the new contributions of the thesis in the

context of previous achievements in the wide field of AD process simulation, optimization and instrumentation.

(2) The development of an open source Matlab®[5] toolbox for the simulation and calibration of biogas plants using basic operational data and based on the Anaerobic Digestion Model No. 1 (ADM1) (Batstone *et al.* 2002). The main advantage of the toolbox is the fast and straight forward design and calibration process, which allows modeling of ABPs without extensive laboratory analysis. Further, the design and calibration of an ADM1-based AD model of the full-scale Sunderhook ABP was performed.

(3) The development of a novel approach for simulation based optimization of complex nonlinear and multi-dimensional fitness functions. The use of global optimization algorithms (such as genetic algorithms or particle swarm optimization) for the optimization of the substrate inflow of biogas plants is computationally expensive as these methods optimize the fitness function by alteration of sets of parameters, whereby a simulation run is calculated for each set of parameters. In this work an alternative method for the optimization of parameters is proposed and tested in a full-scale study: Two novel optimization methods based on Kriging surrogate models of the fitness function, which are sequentially updated during an optimization run, are developed. By using these methods the computation time required can be substantially reduced by up to 98%.

(4) The development of a novel optimization strategy for optimizing the substrate inflow of ABPs. The substrate inflow is the main actuating variable of the AD process and the total amount of substrate fed to a digester as well as the composition of the substrate inflow determine biogas production and process stability. In order to optimize the substrate inflow with respect to total amount of substrate and substrate inflow composition, the ABP optimal substrate inflow optimization problem was defined in detail, taking account of plant efficiency, biogas yield, operating costs and process stability. The evaluation of the performance of the developed optimization strategy for optimizing the Sunderhook ABP substrate feed showed a substantial improvement in plant operation.

(5) The application of the newly developed optimization strategy to the full-scale Sunderhook ABG. The simulation based optimization strategy was successfully applied to the Sunderhook ABG to optimize its substrate inflow. Overall, optimization runs for substrate inflows consisting of up to five different substrates were performed and evaluated. The evaluation shows that yearly profit of the Sunderhook ABP can be substantially improved by up to 70% in the case of the best solution, which equals an increase in yearly net profit of 219,000 €.

(6) The practical testing and evaluation of state of the art online measurement systems for pH, ORP and TS at an ABP and an IBP. Online measurement systems for biogas plants are available in the market but it is difficult for the end user to assess accuracy, maintenance and

[5] http://www.mathworks.com

robustness of the systems during long term operation. Therefore, state of the art online measurement systems for pH, ORP and TS were installed at an ABP and IBP to assess long term stability. Furthermore, measurement values from the online measurement systems were compared to operational data from the plant to evaluate their ability to recognize process disturbances.

(7) The development of a novel UV/vis spectroscopic online measurement system for VFA concentration in digesters. As VFA concentration is one of the most important process parameters, its online measurement provides real-time information about process stability. Therefore, the online measurement of VFA concentration is important but also difficult to realize due to the high TS content of the substrate. The practical testing of the indirect measurement using a UV/vis spectroscopic probe showed that a measurement accuracy of 88% could be achieved.

(8) Evaluation of different machine learning methods for spectral analysis to compare their suitability and performance. The analysis of data from spectroscopic probes is needed for calibration but is a challenge due to the large number of wavelengths and the high nonlinearity of absorption. To allow for a fast and thorough analysis of spectral data sets, analysis of the spectral data was performed using six powerful machine learning methods, which are well-suited to this kind of problem. Results show that by applying dimension reduction and multiple transformations to the data, relevant information can be efficiently extracted, enabling good calibration results to be achieved.

1.3 Outline of the thesis

The remainder of the thesis is organized in six chapters as follows.

Chapter 2 outlines the basic principles for the present work and provides background information on the AD process (section 2.1) as well as on process and operational parameters that are important for monitoring and control applications (section 2.2). Furthermore, a short introduction to ABPs focusing on modes of operation and digester types is given in section 2.3.

Chapter 3 describes the dynamic modeling and simulation of ABPs. Section 3.1 provides a detailed review of dynamic AD models from the last 40 years followed by section 3.2 which provides a complete description of the ADM1 model. Then section 3.3 describes the development and calibration of an ADM1 based AD model for the full-scale Sunderhook ABP using the developed simulation toolbox. Finally section 3.4 provides a short summary of the achieved results on modeling and simulation of ABPs within this chapter.

Chapter 4 focuses on the development of two novel optimization strategies using Kriging surrogate models. Section 4.1 gives a short survey of existing and frequently used metamodeling methods and then focuses on the Kriging approximation, which was chosen as the metamodeling method in this

work. The PSO optimization method and the selection of its parameters are explained in Section 4.2. Section 4.3 then introduces two novel optimization methods using PSO and two different methods to sequentially update the Kriging surrogate model. Method I uses **l**atin **h**ypercube (LH) sampling to update the Kriging model (LH-based S-KSM) and method II uses a separate PSO to update the Kriging model with new positions of the PSO particles (PSO-based S-KSM). The last section investigates the performance of the two novel optimization methods on four test problems and compares the results to conventional PSO optimization.

Chapter 5 presents a novel method for the optimization of ABPs by determining the optimal substrate inflow which maximizes plant efficiency by maximizing biogas yield, minimizing costs and guaranteeing process stability. Section 5.1 gives a short survey of advances in the area of optimization and control of AD plants in general and section 5.2 describes the optimization problem of ABPs with regard to an optimal substrate inflow and introduces the fitness function used in the optimization algorithm. The achieved optimization results based on this fitness function are given in section 5.3 where subsections 5.3.1 to 5.3.4 show the main optimization results of this work based on a combination of S-KSM and PSO. To sum up, a conclusion on the results obtained and their relevance in practice is given in section 5.4.

Chapter 6 describes the practical testing and evaluation of state of the art online measurement systems for biogas plants and the development of a new UV/vis spectroscopic online measurement system using machine learning techniques. In section 6.1 a detailed literature review of the state-of-the-art in online measurement systems is provided together with descriptions of full-scale applications of well-known and innovative monitoring systems. In addition, the current market situation for online measurement systems is analyzed with regard to existing and future technologies. Then section 6.2 introduces and demonstrates the reasons why online measurement systems are urgently needed, giving a practical example from an industrial biogas plant in Germany. Section 6.3 presents and discusses results from a field test of online measurement systems for pH, ORP and TS at an agricultural and an industrial biogas plant highlighting advantages and limitations. The development of a new innovative online measurement system for VFA based on UV/vis spectroscopy is introduced in section 6.4 and its full-scale application at an industrial biogas plant described in detail. The analysis of the spectral data set using powerful machine learning techniques is described in section 6.5. A short summary of the results and the derived conclusion are given in section 6.6.

Chapter 7 summarizes the results and discusses prospects for further research.

1.4 Publications

Anaerobic Digestion – Biogas

Wolf, C., Bongards, M. and McLoone, S., 2007. *Biogas plant substrate feed optimization using computational intelligence methods*. International Conference - Progress in Biogas. Stuttgart-Hohenheim, Germany.

Wolf, C., Bongards, M. and McLoone, S., 2007. *Simulation-based feed-optimization of medium-sized agricultural biogas plants*. 11th IWA World Congress on Anaerobic Digestion. Brisbane, Australia.

Wolf, C., McLoone, S. and Bongards, M., 2008. Biogas plant optimization using genetic algorithms and particle swarm optimization. *IET Irish Signals and Systems Conference (ISSC) 2008; Galway, Ireland*, 244–249.

Wolf, C., McLoone, S. and Bongards, M., 2009. Biogas Plant Control and Optimization Using Computational Intelligence Methods. (Biogasanlagenregelung und -optimierung mit Computational Intelligence Methoden). *at - Automatisierungstechnik*, 57 (12), 638–649.

Wolf, C., 2010. Simulationsbasierte Steuerung von Biogasanlagen mit Particle Swarm Optimierung (Simulation based control of biogas plants using Particle Swarm Optimization). *Conference on Sustainable Technologies and Computational Services for Environmental and Production Processes (STEPS)*, 70–79.

Wolf, C., Gaida, D., Stuhlsatz, A., McLoone, S. and Bongards, M., 2010. Organic acid prediction in biogas plants using UV/vis spectroscopic online-measurements. *Communications in Computer and Information Science* [online], 97 CCIS (PART 1), 200–206.

Gaida, D., Sousa Brito, A.L., Wolf, C., Bäck, T., Bongards, M. and McLoone, S., 2011. Optimal Control Of Biogas Plants Using Nonlinear MPC. *IET Irish Signals and Systems Conference (ISSC 2011)*.

Gaida, D., Wolf, C., and Bongards, M., 2011. *Optimale Betriebsführung von Biogasanlagen mit prozessbegleitender Simulation (Optimal operation of biogas plants with online process simulation)*. ifak workshop: Steuerung, Regelung und Simulation von Biogasanlagen (Operation, control and simulation of biogas plants). Magdeburg, Germany.

Gaida, D., Wolf, C., Bongards, M. and Bäck, T., 2011. MATLAB Toolbox for Biogas Plant Modelling and Optimization. *International Conference Progress in Biogas II - Biogas production from agricultural biomass and organic residues*, 67–70.

Gaida, D., Wolf, C., Meyer, A., Stuhlsatz, J., Lippel, T., Bäck, T., Bongards, M., and McLoone, S., 2011. *State estimation for anaerobic digesters using the ADM1*. International IWA-Symposium on Anaerobic Digestion of Solid Waste and Energy Crops. Vienna, Austria.

Wolf, C., Bongards, M. and Sander, A., 2011. Online-Messtechnik optimiert Biogasanlagen und Faultürme (Online measurement systems optimize biogas plants and WWTP digesters). *wwt - wasserwirtschaft wassertechnik*, 60 (4), 8–16.

Gaida, D., Wolf, C., Kulage, E., Brahmi, D., and Bongards, M., 2012. *Modellbasierte Optimierung und Regelung zur nachhaltigen Energieerzeugung aus Biogas (Model based optimization and control for the sustainable energy production from biogas)*. BIOGAS Jahrestagung und Fachmesse. Bremen, Germany.

Gaida, D., Wolf, C., Bäck, T., and Bongards, M., 2012. *Nonlinear Model Predictive Substrate Feed Control of Biogas Plants*. 20th IEEE Mediterranean Conference on Control and Automation. Barcelona, Spain.

Gaida, D., Wolf, C., Meyer, C., Stuhlsatz, A., Lippel, J., Bäck, T., Bongards, M. and McLoone, S., 2012. State estimation for anaerobic digesters using the ADM1. *Water Science & Technology*, 66 (5), 1088.

Wolf, C., Gaida, D., and Bongards, M., 2012. Geeignete Online-Messtechnik zur Optimierung und Regelung von Biogasanlagen. (Suitable online measurement systems for optimization and control of biogas plants). Plenary talk at 2nd VDI Conference for Process Measurement Systems for Biogas Plants, Fulda.

Wolf, C., Gaida, D., Stuhlsatz, A., Ludwig, T., McLoone, S. and Bongards, M., 2013. Predicting organic acid concentration from UV/vis spectrometry measurements - a comparison of machine learning techniques. Transactions of the Institute of Measurement and Control, 35 (1), 5–15.

References

Bundesministerium für Umwelt, Naturschutz und Reaktorsicherheit (Federal Ministry for the Environment, Nature Conservation and Nuclear Safety), 2011. *Erneuerbare-Energien-Gesetz 2012 (Renewable Energy Law 2012): EEG*.

Da Rosa, A.V., 2013. *Fundamentals of renewable energy processes.* 3rd ed. Oxford: Academic Press.

Eberhart, R.C., Simpson, P.K., and Dobbins, R.W., 1996. Computational intelligence PC tools. Boston: AP Professional.

European Commission (EC), 2009. *Directive 2009/28/EC of the European Parliament and of the Council of 23 April 2009 on the promotion of the use of energy from renewable sources and amending and subsequently repealing Directives 2001/77/EC and 2003/30/EC* [online]. Brussels. Available from: http://eur-lex.europa.eu/LexUriServ/LexUriServ.do?uri=OJ:L:2009:140:0016:0062:EN:PDF [Accessed 25 Feb 2013].

European Commission (EC), 2013. *7th Framework Programme for European Research and Development* [online]. Available from: http://cordis.europa.eu/fp7/home_en.html [Accessed 25 Feb 2013].

Eurostat, 2013a. *Share of renewable energy in gross final energy consumption [%]* [online], Eurostat. Available from: http://epp.eurostat.ec.europa.eu/tgm/table.do?tab=table&plugin=1&language=en&pcode=t2020_31 [Accessed 25 Feb 2013].

Eurostat, 2013b. *Energy statistics: Supply, transformation, consumption - all products - annual data. Energy statistics: Supply, transformation, consumption - renewables and wastes (total, solar heat, biomass, geothermal, wastes) - annual data. Energy statistics: Supply, transformation, consumption - renewables (hydro, wind, photovoltaic) - annual data.* [online]. Available from: http://epp.eurostat.ec.europa.eu/portal/page/portal/energy/data/database.

Fachverband Biogas e.V., 2013. *Biogas Segment Statistics 2013: Development of the number of biogas plants and the total installed electric output in megawatt [MW] (as of 6/2012)* [online]. Available from: http://www.biogas.org/edcom/webfvb.nsf/id/DE_Branchenzahlen/$file/12-06-12_Biogas%20Branchenzahlen%202011_eng.pdf [Accessed 10 Feb 2013].

FNR e.V., 2009. *Biogas-Messprogramm II - 61 Biogasanlagen im Vergleich: (Biogas Measurement Program II - A comparison of 61 German biogas plants).* 1st ed. Gülzow: Fachagentur Nachwachsende Rohstoffe (Agency for Renewable Resources).

Gaida, D., Wolf, C., Bongards, M. and Bäck, T., 2011. MATLAB Toolbox for Biogas Plant Modelling and Optimization. *International Conference Progress in Biogas II - Biogas production from agricultural biomass and organic residues*, 67–70.

Madsen, M., Holm-Nielsen, J.B. and Esbensen, K.H., 2011. Monitoring of anaerobic digestion processes: A review perspective. *Renewable and Sustainable Energy Reviews*, 15 (6), 3141–3155.

Markus Becker, 2012. *Interview mit Dennis Meadows: "Für eine globale Mobilmachung ist es zu spät" (Interview with Dennis Meadows: "It is too late for global mobilization")*. http://www.spiegel.de/wissenschaft/natur/grenzen-des-wachstums-interview-mit-dennis-meadows-a-870238.html.

Matheron, G., 1963. Principles of geostatistics. *Economic Geology*, 58, 1246–1266.

Meadows, D.H., Meadows, D., Randers, J., and Behrens [III], W.W., 1977, c1972. *The limits to growth: A report for the Club of Rome's project on the predicament of mankind.* 2nd ed. New York: Universe Books.

Nuclear and Industrial Safety Agency (NISA), 2011. *The 2011 off the Pacific coast of Tohoku Pacific Earthquake and the seismic damage to the NPPs*.

Observ'ER, 2012. *EurObServ'ER: The State of Renewable Energies in Europe 2011: 11th EurObserv'ER Report*. Paris.

Steyer, J., Bernard, O., Batstone, D. and Angelidaki, I., 2006. Lessons learnt from 15 years of ICA in anaerobic digesters. *Water Science & Technology*, 53 (4-5), 25.

UNPF, 2012. *Annual Report: Delivering Results in a World of 7 Billion*. New York, NY: United Nations Population Fund.

2 Anaerobic Digestion and Agricultural Biogas Plants

Anaerobic Digestion (AD) in general describes the degradation of organic material by several groups of anaerobic bacteria in the absence of oxygen. During this degradation process, the so-called biogas is produced which mainly consists of methane (CH_4), carbon dioxide (CO_2), hydrogen (H_2) and hydrogen sulphide (H_2S). With methane being the primary energy carrier in biogas, the produced biogas is mostly burned in cogeneration units for power and heat production. Other possibilities for biogas processing include its liquefaction to use it as fuel and its enrichment with methane to achieve natural gas quality so that it can be supplied to the gas grid. The applications for AD are multifaceted. It is not only used in the food and pharmaceutical industry but also for the treatment of wastewater and organic waste. For the last 20 years, the use of AD for renewable energy production from waste and energy crops in industrial and agricultural biogas plants (IBPs and ABPs) has become increasingly popular due to the strong legislative support in many countries by Renewable Energy Laws[6].

The aim of this chapter is to provide background information on the AD process (section 2.1) as well as on process and operational parameters that are important for monitoring and control applications (section 2.2). Furthermore, a short introduction to ABPs focusing on modes of operation and digester types is given in section 2.3. Thus, this chapter provides the basis for all subsequent developments and results that are presented in the thesis.

2.1 The Anaerobic Digestion Process

The AD process is a very complex process which is why it took a long time before the four main stages of the AD process, namely hydrolysis, acidogenesis, acetogenesis and methanogenesis, were fully understood. The history of AD is well described by McCarty in 1982 who claimed that an Italian physicist with the name Volta was the first to prove the production of combustible gas from organic material in 1776 (McCarty 1982). Some 92 years after this discovery, Bechamp reported that methane production is caused by a microbiological process and another 22 years went by before Omelianski successfully identified that anaerobic bacteria were responsible for the release of hydrogen, acetic acid and butyric acid during the anaerobic digestion of cellulose (Abbasi *et al.* 2012). Söhngen confirmed these results in 1910 and assumed that there were two different kinds of pathways for methane production, one from hydrogen and carbon dioxide and the other from acetic acid (Ferry 1993). This was the first time that the methanogenesis was fully described. One of the first full descriptions of the AD process was given by McCarty in 1964 who described three stages of the AD process: hydrolysis and acidogenesis as stage I, acetogenesis as stage II and methanogenesis as stage III (McCarty 1964). The most detailed and comprehensive description of the AD process with four process stages and six bacterial populations which was used as basis for the development of the ADM1 simulation model,

[6] http://www.res-legal.eu/home/ - Portal from the European Commision on Renewable Energy Legislation in Europe

was introduced by Gujer and Zehnder (1983). The presently generally accepted process scheme of the AD process is shown in Figure 2-1.

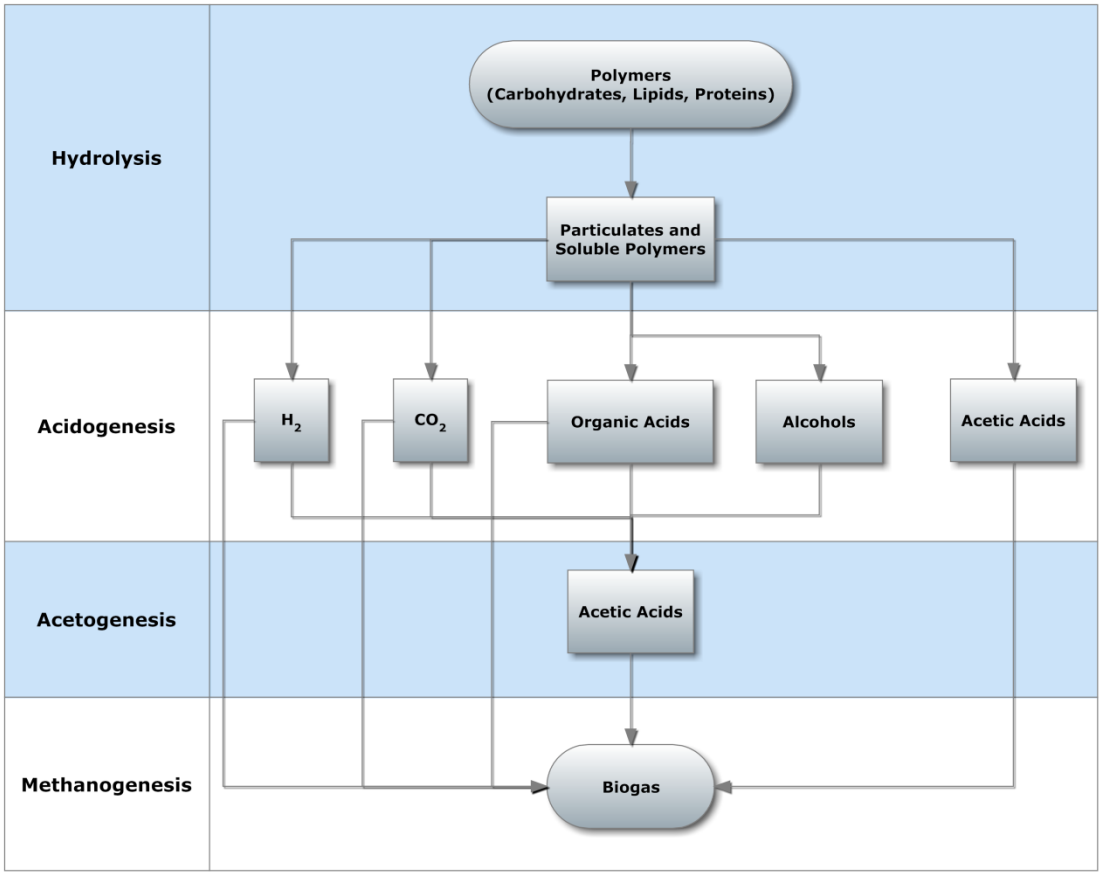

Figure 2-1: The four phases of the AD process adapted from Gruber (2004)

2.1.1 Hydrolysis

Hydrolysis is considered to be the main rate limiting step in the AD process (Pavlosthatis and Gossett 1985) because it is responsible for the enzymatic breakdown of long-chain starch, sugar and protein molecules of the particulate organic fraction of the input substrates. Due to the fact that the subsequent phases of the AD process can only process the hydrolyzed readily degradable soluble substrate, the hydrolysis is the "bottleneck" of the AD process determining the reaction rates of the other process stages. If hydrolysis is slow, substrate limitation is the main reason for an inhibition of subsequent processes. Hydrolysis is mainly performed by exoenzymes which are released by other anaerobic bacteria to perform metabolic reactions, such as the breakdown of nutrients, outside the bacterial cell. Furthermore, exoenzymes act as a catalyst for the other process stages by decreasing their activation energy which leads to an increase in their reaction rates. Therefore, fast hydrolysis is important for a well-balanced AD process and can be achieved due to the short generation time of exoenzymes ranging from several hours up to two days (Thomas 1988).

The reaction pathways (2.1), (2.2) and (2.3) illustrate the hydrolysis for carbohydrates, proteins and lipids (Koppe and Stozek 1993).

Carbohydrates:

$$\begin{aligned} &polysaccharide\ (i.e.\ starch) \longrightarrow oligosaccharide \longrightarrow \\ &disaccharide \longrightarrow monosaccharide\ (i.e.\ glucose\ C_6H_{12}O_6) \end{aligned} \tag{2.1}$$

Proteins:

$$\begin{aligned} &proteins \longrightarrow peptone \longrightarrow polypeptide \longrightarrow oligopeptide \\ &\longrightarrow amino\ acids\ (i.e.\ amino\ acetic\ acid\ \ NH_2 - CH_2 - COOH) \end{aligned} \tag{2.2}$$

Lipids:

$$tri\ palmitic\ acid\ glycerel\ ester \longrightarrow tri\ palmitic\ acid + glycerol \tag{2.3}$$

2.1.2 Acidogenesis

Acidogenesis is the second phase of the AD process which uses the hydrolyzed particulates for the production of organic acids such as butyric, valeric, propionic and in particular acetic acid (CH_3COOH). Acetic acid is then later used by the methanogenic bacteria to produce methane. The acidogenic bacteria feed on monsaccharides, amino acids and long chain fatty acids (LCFA) from hydrolysis and produce the aforementioned volatile fatty acids (VFA). Furthermore, small amounts of hydrogen, carbon dioxides and alcohol are produced.

As acidogenesis is the main acid producing stage, the high production of organic acids strongly affects the *pH* value. The *pH* value itself and the substrate concentration decide which end product is mainly produced by the acidogenic bacteria. Bischofsberger *et al.* (2003) stated that in the case of a neutral *pH* mainly acetic acid as well as hydrogen and carbon dioxide are produced whereas for high substrate concentrations and a $pH < 7$ more propionic and butyric acid are produced. If the *pH* drops below 4.5 the process completely shifts towards the production of lactic acid. Therefore, a detailed monitoring and control of the acidogenic process step is important to prevent high concentrations of propionic and lactic acid which indicate severe process disturbances have an inhibitory effect and acetogenesis and methanogenesis. Furthermore, a stable *pH* is required. For ABPs pH stability is not an issue under normal process conditions due to the high buffer capacity of the substrates.

2.1.3 Acetogenesis

Acetogenesis uses the end and by-products from acidogenesis to produce acetic acid and acetate. The following reactions show the production of acetic acid from propionic and butyric acid as described in the Scientific and Technical Report No. 13 from the IWA (Batstone *et al.* 2002).

Propionic acid:

$$CH_3CH_2COOH + 2H_2O \rightarrow CH_3COOH + CO_2 + 3H_2 \tag{2.4}$$

Butyric acid:

$$CH_3(CH_2)_2COOH + 2H_2O \rightarrow 2CH_3COOH + 2H_2 \quad (2.5)$$

These reactions show that a relatively high amount of hydrogen is produced which affects the hydrogen partial pressure and thus the *pH* value. If the *pH* value drops because of an increase in hydrogen production, the acetogenic bacteria are strongly inhibited as they need a neutral, even slightly alkaline environment to get enough energy from their metabolism. Therefore, a control of the hydrogen concentration is necessary which is realized by the hydrogenotrophic methanogenic bacteria which use hydrogen and carbon dioxide to produce methane. This dependency between acetogenesis and methanogenesis is a symbiotic relationship. If hydrogen production from the acetogenesis is low, the hydrogenotrophic methanogenesis is inhibited due to substrate limitation and if hydrogen consumption from the hydrogenotrophic methanogenesis is low, low *pH* values result in inhibition of the acetogenesis.

2.1.4 Methanogenesis

The last step of the AD process is methanogenesis which uses acetic acid, hydrogen and carbon dioxide produced in the previous processes to produce methane. Two different pathways for methane production exist: (1) hydrogenotrophic and (2) acetoclastic methanogenesis. The hydrogenotrophic methanogenesis uses hydrogen and carbon dioxide to produce methane whereas the acetoclastic methanogenesis only uses acetic acid.

hydrogenotrophic methanogenesis:

$$CO_2 + 4H_2 \rightarrow CH_4 + 2H_2O \quad (2.6)$$

acetoclastic methanogenesis:

$$CH_3COOH \rightarrow CH_4 + CO_2 \quad (2.7)$$

Due to the high dependency on the continuous availability of the end products from acidogenesis and acetogenesis, the main reason for inhibition of methanogenesis is substrate limitation. Furthermore, Thomas (1988) determined the generation time of methanogenic bacteria to be between three and fifteen days which is long compared to the short generation time of exoenzymes as described in section 2.1.1. This means that the methanogenic bacteria need longer to recover from process disturbances, which makes their well-being a priority.

Based on results from Gujer and Zehnder (1983) on the digestion of waste-activated sludge, acetoclastic methanogenesis was considered the main methanogenic pathway with 70% of the total methane production whereas hydrogenotrophic methanogenesis only contributed about 30%. This was proven to be wrong for ABPs by Lübken *et al.* (2010), who stated that hydrogenotrophic methanogenesis is far superior to acetoclastic methanogenesis.

2.2 Process and operational parameters

The description of the AD process shows its complexity due to the four different process steps and the high number of different bacteria involved. Thus, monitoring and control of the AD process is a challenge and requires knowledge about relevant process and operational parameters. The following two sections introduce the main process and operational parameters that are important to monitor and to assess process efficiency.

2.2.1 Process parameters

2.2.1.1 Temperature

Temperature is one of the most important variables for process stability as anaerobic bacteria populations can only survive in certain temperature ranges. Furthermore, sudden changes and permanent fluctuations in the process temperature lead to inhibition of bacteria populations. Therefore, controlling process temperature so that it remains constant at all times is crucial to maintaining stable plant operation. There are three different temperature ranges (Gruber 2004):

- Psychrophilic bacteria - $T < 25°C$
- Mesophilic bacteria - $30°C \leq T \leq 45°C$
- Thermophilic bacteria - $T > 50°C$

This means that an AD process can be operated in one of these three temperature ranges with the corresponding bacteria population. Nevertheless, the mesophilic temperature range is preferred for most AD processes. The main reasons for this are that AD performed by psychrophilic bacteria is slower than by mesophilic and thermophilic bacteria and that it is difficult to maintain such low process temperatures, in particular during the summer time. Furthermore, thermophilic bacteria are known to be very sensitive to disturbances, which requires costly process monitoring and control, although biogas productivity is the highest (Gruber 2004). Therefore, most ABPs are also operated in the mesophilic temperature range.

2.2.1.2 Total Solids (TS) and Volatile Solids (VS)

TS and *VS* concentrations of the substrates as well as the digestate provide useful information about the biogas yield that can be expected and process efficiency. Furthermore, mechanical components of an AD plant such as pumps and stirrers can only safely process material with a certain *TS* concentration.

The *TS* basically describes the dry matter of a substrate as a percentage of the total weight or in grams per kilogram. Therefore, a certain amount of the substrate is weighed and then dried at 105°C for 24 hours until its water content is zero. Finally, the weight after drying is divided by the original weight to get the *TS* value. A detailed description of the measurement procedure is given in DIN EN 12880 (DIN 2001).

The *VS* concentration is defined as the organic fraction of the *TS* and is commonly measured as a percentage of *TS* or in grams per kilogram. To isolate the inorganic from the organic fraction of the *TS*, the already dried substrate is burned in a muffle furnace at 550°C. The residue after incineration is the inorganic fraction. The weight of the dried substrate minus the weight of the inorganic fraction is then divided by the weight of the dried substrate in order to get the VS concentration (DIN 2001).

The *VS* concentration is commonly used to assess AD process efficiency. Not only can the biogas potential of a substrate be estimated based on its *VS* content, but also the degree of degradation achieved by the AD process by comparing *VS* input to the digester and *VS* output. Thus, monitoring of the *VS* concentration is important but very difficult to realize online as shown in chapter 6.

2.2.1.3 pH

The *pH* value of a stable AD process should be between six and nine. A $pH = 6$ is indicative of inhibition due to high VFA concentrations and a $pH \geq 9$ results in a significant increase of ammonia which also has a strong inhibitory effect. Due to the fact that the first two stages of the AD process, in particular the hydrolysis stage, prefer lower *pH* values between four and 7, a two stage digestion with two digesters is often used for the digestion of hard to degradable substrate (FNR e.V. 2010).

Furthermore, the *pH* value of the AD process is often used to assess process stability as high *VFA* concentrations from the acidogenic and acetogenic process steps result in a drop in the pH value. This is basically true but if a sudden change in the *pH* value is detected it is often already too late. The main reason for this can be found in the total alkalinity (*TA*) of the process which acts as a buffer for the *pH* value. This means that as long as the *TA* of an AD process is high, elevated *VFA* concentrations cannot be detected by measuring the *pH* value. In particular for ABPs, *TA* is normally very high so that the pH value cannot be used as an early warning measurement system.

2.2.1.4 VFA and VOA/TIC

The *VFA* concentration in a digester yields important information about process efficiency and stability. In 1982, Braun stated that an AD process for municipal organic waste is stable for *VFA* concentrations below 1,000 mg/l and that concentrations greater than this clearly indicate an inhibition and possible process failure (Braun 1982). On the contrary, Kaiser *et al.* (2007) stated that for ABPs the total *VFA* concentration should be around 4,000 mg/l for stable plant operation. The main problem with such limit values is that biological processes in general and the AD process in particular have the ability to adapt to suboptimal process conditions. The results from Industrial I in chapter 6 support this assumption showing that stable operation at 2,000 mg/l is possible and that inhibition and the eventual breakdown occurred at 3,000 mg/l. Thus, an absolute value of the *VFA* concentration is difficult to interpret but deviations from values during normal operating conditions provide valuable process information. Apart from the total concentration of *VFAs*, the concentration of single *VFAs* is also important for process monitoring. Thus, propionic acid concentration should be lower than 1,000 mg/l

and a ratio to acetic acid of 2:1 is considered to be optimal. Furthermore, the remaining *VFAs* should be below 500 mg/l.

As previously mentioned, the buffer capacity *TA* has a strong influence on *pH* because it alleviates the effect of high VFA concentrations, which is why the ratio of all volatile organic acids (*VOA*) and the total inorganic carbon buffer (*TIC*), which is closely related to *TA*, is the most popular and commonly used measure for AD process stability. The *VOA/TIC* ratio is measured via titration and is defined by the standard VDI 4630 (VDI 2006). A two-point titration is performed using 0.05-mol sulphuric acid (H_2SO_4). The acid consumption until $pH = 5$ determines the *TIC* concentration whereas the titration until $pH = 4.3$ gives the *VOA* concentration. For ABP operation a *VOA/TIC* ratio below 0.3 represents a stable process, whereas higher ratios indicate process disturbances. Nevertheless, ABPs with higher ratios up to 0.6 have been found to be stable after a long adaptation process (VDI 2011).

2.2.1.5 Ammonium (NH_4)

The NH_4 concentration plays a major role in the AD process as NH_4 is transformed into the strong inhibitor ammonia (NH_3) at high temperatures and high *pH* values as described by Emerson *et al.* (1975)

$$NH_3 = NH_4 \frac{10^{pH}}{\exp\left[6344(273+T)^{-1}\right]+10^{pH}} \quad [g\,l^{-1}], \tag{2.8}$$

where NH_4 and NH_3 are the ammonium and ammonia concentrations in gram per liter, *T* is the temperature in °C and *pH* is the *pH* value.

In particular, substrates such as manure and chicken excrement cause high NH_4 concentrations in the digesters of ABPs which results in elevated ammonia levels. According to the FNR[7] NH_4 concentrations below 3,000 mgl^{-1} indicate a stable AD process (FNR 2010), but again the author visited an ABP near Darmstadt, Germany which was stable at NH_4 concentrations of 7,000 mgl^{-1}. Thus, deviations from values acquired during normal operation are more important than absolute measurement values.

[7] Fachagentur für nachwachsende Rohstoffe (Agency for Renewable Resources)

2.2.1.6 Biogas yield and quality

Biogas yield and quality mainly determine the efficiency of an AD process. A change in biogas yield automatically means that the AD process is inhibited, although the reason for the inhibition remains unknown. Thus, close monitoring of the biogas yield, which is measured in m³ per day, is absolutely necessary.

Biogas quality is mainly determined by the composition of the biogas. The biogas consists of CH_4, CO_2, H_2, H_2S and O_2, from which CH_4, H_2 and H_2S are particularly interesting for process monitoring. To guarantee a burnable gas composition, the methane concentration needs to be at least 50%. Furthermore, a decrease in methane concentration indicates problems with the methanogenic process steps due to substrate limitation or substrate abundance. This is automatically reflected in the H_2 concentration in the biogas. If methanogenesis is inhibited, plenty of H_2 is produced by acetogenesis, but cannot be processed to methane by methanogenesis. Thus, H_2 is a perfect parameter to monitor to provide an early warning of process disturbances. In addition, high H_2S concentration also indicates process instability. H_2S is a well-known lethal poisonous gas, which causes a strong inhibition of the anaerobic bacteria populations. Besides its inhibitory effect, H_2S causes aggressive corrosion in motors and pipes as well which makes cleaning of the biogas necessary. Nevertheless, H_2S is normally not a problem at ABPs because of slight aeration of the digesters which is so small that the anaerobic conditions are not endangered. Due to the reaction of H_2S with O_2, H_2S is split into water (H_2O) and elementary sulphur (S_2).

$$2H_2S + O_2 \rightarrow 2H_2O + S_2 \tag{2.9}$$

2.2.2 Operational parameters

2.2.2.1 Hydraulic Retention Time (HRT)

The *HRT* is calculated based on the volume of the anaerobic digester (V_D [m^3]) and daily substrate inflow (x_S [$m^3 d^{-1}$]).

$$HRT = \frac{V_D}{x_S}[d] \tag{2.10}$$

The *HRT* determine the degree of substrate degradation. If the *HRT* is below 20 days, most of the energy crops used in ABPs cannot be fully digested, which results in a loss of energy (Gruber 2004). Thus, it is important to operate at an *HRT* that is appropriate for the amount of substrate fed to a plant.

2.2.2.2 Digester Load

The digester load (L_D) is the main operational parameter to measure the capacity of the AD process. L_D is defined as the ratio of *VS* inflow (VS_{in} [$kgVSd^{-1}$]) and digester volume (V_D [m^3]).

$$L_D = \frac{VS_{in}}{V_D} [kgVSm^{-3}d^{-1}] \quad (2.11)$$

In general, a digester load of 2.5 $kgVSm^{-3}d^{-1}$ is considered to be normal for ABPs. Higher values indicate that the AD process is highly efficient but also potentially unstable. Thus, strong variations of the digester load should be avoided to maintain a stable AD process.

2.2.2.3 Volumetric VS degradation efficiency and degree of VS degradation

The *VS* degradation determines the efficiency of an AD process. If *VS* degradation is high, most of the available organic fraction of the input substrates is fully digested. However, if *VS* degradation is low, most of the input substrate is not fully processed to biogas, which means that the AD process is inefficient.

The volumetric *VS* degradation efficiency [$VS_{deg,eff}$] is defined as the *VS* concentration in the outflow of the digester (VDI 2011).

$$VS_{deg,eff} = VS_{out} [kgVSm^{-3}d^{-1}] \quad (2.12)$$

The degree of *VS* degradation, which is often used, is calculated by the ratio of *VS* inflow [VS_{in}] and *VS* outflow [VS_{out}] of the digester (VDI 2011).

$$VS_{deg} = \frac{VS_{out}}{VS_{in}} 100 [\%] \quad (2.13)$$

2.2.2.4 Biogas and methane rate of yield

The biogas and methane rate of yield describe biogas and methane yield in relation to the *VS* concentration of the substrate inflow, which is another measure of process efficiency (VDI 2011). The higher the biogas and methane rate of yield, the higher the process efficiency. Furthermore, a theoretical biogas yield can be calculated which allows a comparison of the measured biogas rate of yield with the theoretical one. If there is a significant difference, the AD process is inhibited. If the measured value is equal to, or even greater than the theoretical value, process efficiency is high. This is also valid for the methane rate of yield.

$$Y_{gas,rate} = \frac{Y_{gas}}{VS_{in}} [Nm^3_{gas} t^{-1}_{VS_{in}}] \quad (2.14)$$

$$Y_{ch4,rate} = \frac{Y_{ch4}}{VS_{in}} [Nm^3_{ch4} t^{-1}_{VS_{in}}] \quad (2.15)$$

2.2.2.5 Biogas and methane productivity

Instead of using *VS* inflow concentration as a reference for biogas and methane yield, the digester volume ($V_D\,[m^3]$) is used to calculate biogas and methane productivity (VDI 2011). The higher the biogas and methane yield per m³ of digester volume, the higher the efficiency of the AD process.

$$Y_{gas,prod} = \frac{Y_{gas}}{V_D}\,[Nm^3_{gas} m_D^{-3} d^{-1}] \tag{2.16}$$

$$Y_{ch4,prod} = \frac{Y_{ch4}}{V_D}\,[Nm^3_{ch4} m_D^{-3} d^{-1}] \tag{2.17}$$

2.3 Agricultural Biogas Plants (ABP)

ABPs primarily use AD to produce electrical and thermal energy which can be sold. Due to the extremely high increase in the number of ABPs in Germany by 450% during the last 10 years, many different designs of ABPs and modes of operation exist. The aim of this section is to give an overview of the plant designs, process models and modes of operation that are commonly used.

The typical ABP consists of two digesters (primary and secondary digester) of similar size, a final storage tank for the digestate and two cogeneration units for electrical and thermal energy production. Furthermore, drive-in silos and manure tanks are commonly used for substrate storage and a container with shifting bottom plates for the feeding of substrate with high TS content to the digesters. Figure 2-2 shows a 3D scheme of such an ABG, where the red pipes describe the heating grid and the yellow pipes the gas grid.

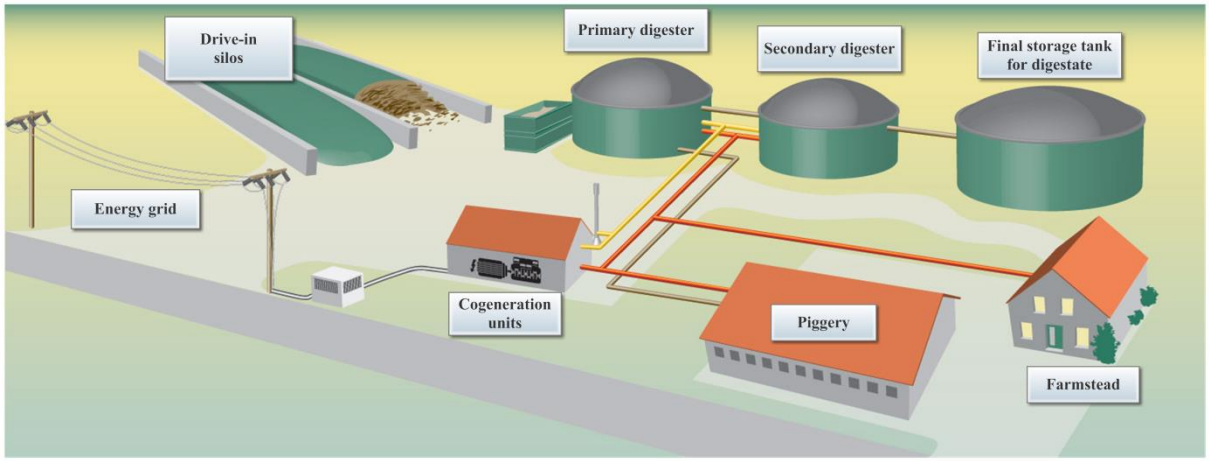

Figure 2-2: Typical design of an ABP[8]

2.3.1 Wet and dry AD

Based on the *TS* content of the substrate inflow, two different kinds of AD can be distinguished, (1) wet digestion for $TS \leq 15\%$ and (2) dry digestion for $TS \geq 25\%$ as defined by (Gruber 2004). AD

[8] used with permission from PlanET Biogas (http://www.planet-biogas.com)

processes with a *TS* concentration between 15% and 25% are considered to be a combination of wet and dry digestion.

In general, wet digestion is preferred for ABPs and mostly used, as plant operation is easier and requires less maintenance because substrates can be pumped and digesters can be stirred properly (FNR 2009). Furthermore, a continuous substrate inflow to the digesters is manageable which also allows for continuous biogas production. This in turn is important for the control of the cogeneration units which require a nearly constant flow of biogas to the gas engines to maximize efficiency of the incineration.

Dry digestion is much more complicated as the substrate inflow is semisolid and not suitable for pumping. Thus, it is difficult to achieve a continuous biogas production. This is why batch digestion is commonly performed in multiple so-called digester garages which are filled at different times. Therefore, biogas production reaches it maximum in each garage digester at a different time so that the average biogas production is stable. Nevertheless, there is one exception, the Valorga[9] system, which is described in more detail in section 6.2.1 of chapter 6. As stirring of the digester content is not possible, a mixing of the substrate is realized by the injection of compressed biogas into the bottom of the digester. Due to these complications dry digestion is rarely used at ABPs.

2.3.2 Number of process stages

Most AD plants have one or two process stages as shown in the biogas measurement program of the FNR (2009), which is why these two fundamental plant designs are discusses in further detail.

ABPs with two separate process stages consider the fact ideal process conditions for hydrolysis and acidogenesis are different from acetogenesis and methanogenesis. Therefore, the idea is to operate one digester under optimal conditions for hydrolysis and acidogenesis, which means a *pH* value between four and seven and temperature normally between 25-35°C, and the second digester operating under normal AD conditions with a *pH* value of seven and at mesophilic temperature. Due to the optimized process conditions, reaction rates can be substantially increased which also results in faster substrate degradation which in turn reduces the *HRT* required to fully digest a substrate.

Nevertheless, most plants only have one process stage (FNR 2009). The main reason is that two separate process stages mean double the costs for digesters as well as the instrumentation and control. Thus, operating conditions for single stage digesters have to be a compromise for all four phases of the AD processes, which is far from optimal due to a higher *HRT* and slower reaction rates. In order to increase substrate degradability and biogas yield under these circumstances, the digestate is often recirculated from the final storage tanks back to the digester. Adjusting the recirculation rate and volume according to the fed substrates, the HRT of the digestate in the digester is increased.

[9] http://www.valorgainternational.fr

2.3.3 Digester types

Many different types of digester have been developed for AD, including many for special applications such as the digester developed by the company Entec[10] who developed a digester with two chambers, one for hydrolysis and the other for the remaining three stages of the AD process. In general, all digesters used for energy production have a liquid phase in which the substrate is digested and a gas phase to collect the produced biogas. The two digester designs that are mainly used for energy production at ABPs are (1) CSTR[11] digesters and (2) plug flow digesters (FNR 2009). The following two sections give a detailed description of these two digester types.

2.3.3.1 CSTR digesters

CSTR digesters are upright tanks that are normally operated using wet digestion. Long and slow turning paddle agitators provide an optimal mixing of the digester content. Generally, two different modes of operation are used for the mixing of the substrate. Continuous mixing, which results in well-homogenized digester content but also involves very high energy consumption due to the high viscosity of the substrate, or discontinuous mixing which is energy efficient but also causes sedimentation that might be difficult to mobilize. As energy efficiency has a high priority for the operator of an AD plant, mostly discontinuous mixing is used, although the disadvantages are obvious (FNR 2010). Figure 2-3 shows two different types of CSTR digesters with different mixing techniques.

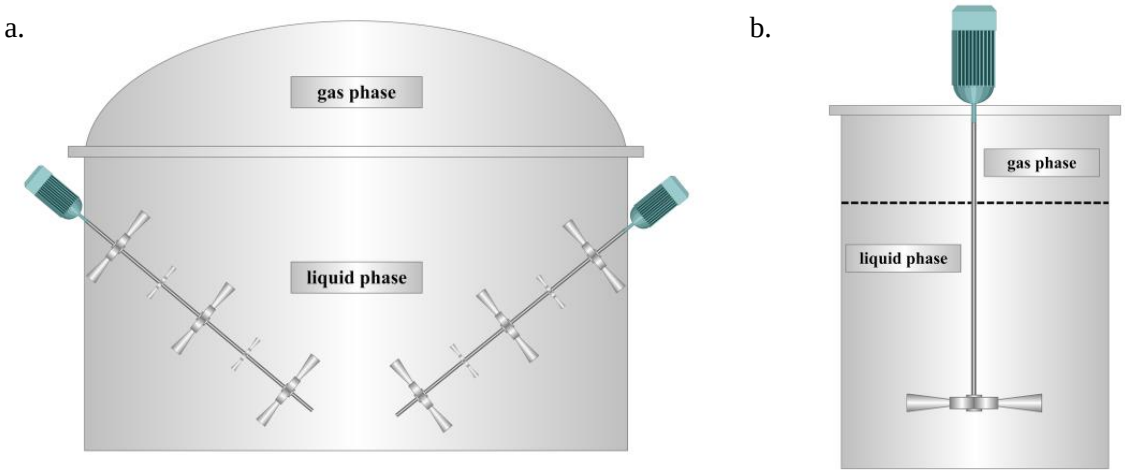

Figure 2-3: Typical CSTR digesters. a. CSTR with paddle agitators and b. tall upright CSTR with central agitator

It is obvious that tall upright CSTRs have one main disadvantage compared to the normal CSTR (a.), which is that the central agitator is very sensitive to lever forces. This means that high substrate viscosity due to high *TS* content can easily cause shearing of the complete agitator, which happened in the case of the ABP Sunderhook which is used for simulation and optimization in this thesis.

[10] http://www.entec-biogas.com
[11] CSTR – **c**ontinuous **s**tirred-**t**ank **r**eactor

Therefore, the *TS* content inside the digester needs to be closely monitored at all times. Nevertheless, tall CSTRs are often used when the available building site is small as it is space-saving.

Both types of CSTR digesters possess one feed pipe for substrate inflow and one outlet pipe for the outflow of the digestate. Because of the homogenized substrate mix inside a CSTR, an outflow of fresh, not fully digested substrate cannot be prohibited. Thus, the *HRT* of substrates may vary substantially between the minimum and maximum *HRT*.

2.3.3.2 Lying plug flow digesters

Lying plug flow digesters were mainly developed for two reasons. Dry digestion can be easily realized using a plug flow process and *HRT* of the substrate is maximized as premature outflow of substrate is prohibited with substrate inflow and outflow located at opposite sides. Nevertheless, mixing of the digester content is necessary to allow the effusion of biogas into the gas phase and to allow the bacteria to evenly access the substrate. Two different types of mixing are commonly used and shown in Figure 2-4.

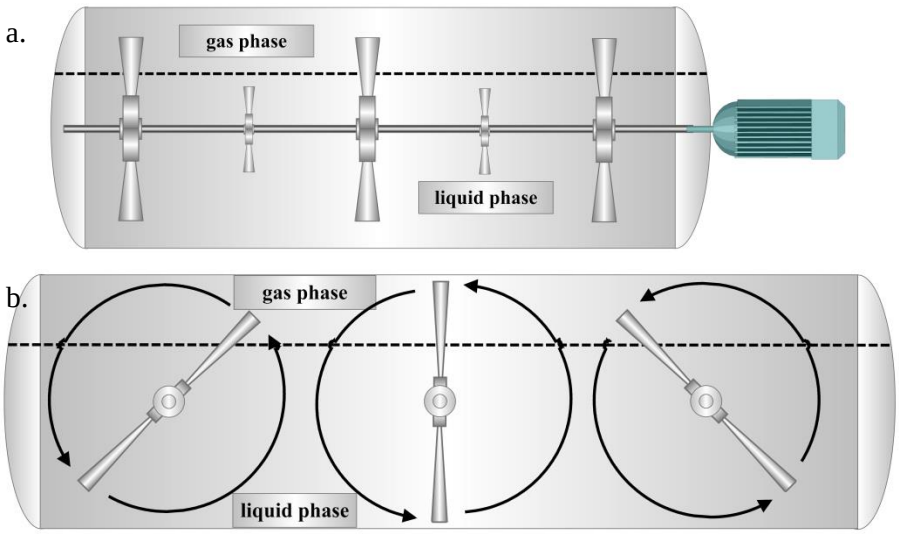

Figure 2-4: Lying plug flow digesters with a. agitators oriented against the longitudinal direction and b. oriented in longitudinal direction.

Mixing with agitators oriented against the longitudinal direction has one major disadvantage as it leads to heavy sedimentation between the paddles, which significantly reduces the digester volume. In order to solve this problem, agitators oriented in the longitudinal direction were developed. These basically shovel the substrate from one paddle to the next, thus preventing sedimentation occurring between the paddles.

2.3.4 Modes of operation

The modes of operation of AD plants are multifaceted, which is why this section focuses on the modes of operation of ABPs. Compared to other processes, the operation of ABPs is difficult because of the long dead times of the AD process and a considerable lack of online instrumentation and control (see

chapter 6). Therefore, operation of ABPs is still in its infancy in many aspects and plant operation is far from optimal (Schmitz 2008).

The investigation of Zimmermann *et al.* (2003) identifies two major modes of operation of ABPs that can be confirmed by the experience of GECO►C: (1) low substrate inflow – high process stability versus (2) high substrate inflow – low process stability.

2.3.4.1 Low substrate inflow – high process stability

To maintain process stability is crucial for efficient ABP operation so that a constant, methane-rich biogas flow to the cogeneration units is guaranteed. In the event of process failure, ABP downtime can vary from several weeks to several months before the AD process is running at its full capacity again. During this time, the financial losses for the plant operator can easily mount up to 50,000€ to 100,000€ if the daily benefit of an ABP is assumed to be between 1,000€ and 2,000€.

Therefore, a common strategy of many ABP operators is to reduce the substrate inflow which in turn reduces the digester load. Thus, plant capacity is not fully used and process stability can be easily maintained. Due to the high remuneration rates for electricity production from ABPs, plant operation is still financially feasible. Nevertheless, governmental support will be substantially reduced in the future, which will require ABPs to tap their full potential.

2.3.4.2 High substrate inflow – low process stability

An increase in substrate inflow always results in an increase in biogas yield, unless the AD process is inhibited. Thus, a high substrate feed is a good way to operate an ABP at its full capacity. Unfortunately, it is also a high risk strategy as a high substrate inflow might also result in an overload, which causes massive production of organic acids leading to process failure, eventually. The main problem in this case is the lack of instrumentation for online process monitoring, which makes a comprehensive assessment of process stability impossible. Therefore, it is very risky to increase the substrate inflow with only limited and delayed feedback from the AD process as process stability remains unknown. Nevertheless, this mode of operation is applied to many ABPs in order to increase biogas yield which in turn increases a plant's net profit.

The solution to this problem is a combination of instrumentation for proper process monitoring and optimization and control methods to maximize biogas yield while maintaining process stability. The following chapters investigate the different aspects of this solution.

References

Abbasi, T., Tauseef, S.M., and Abbasi, S.A., 2012. *Biogas energy*. New York, NY: Springer.

Batstone, D.J., Keller, J., Angelidaki, I., Kalyuzhnyi, S.V., Pavlostathis, S.G., Rozzi, A., Sanders, W.T.M., Siegrist, H., and Vavilin, V.A., 2002. *Anaerobic Digestion Model No. 1 (ADM 1): Scientific and technical Report No. 13*. London: IWA Publ.

Bischofsberger, W., Dichtl, N., Rosenwinkel, K.-H., and Seyfried C. F., 2003. *Anaerobtechnik: Handbuch der anaeroben Behandlung von Abwasser und Schlamm.* 2nd ed. Berlin: Springer.

Braun, R., 1982. *Biogas, Methangärung organischer Abfallstoffe (Biogas, methane digestion of organic waste): Grundlagen und Anwendungsbeispiele (Principles and applications)*. Wien, New York: Springer-Verlag.

Deutsches Institut für Normung e.V. (DIN), 2001. *Charakterisierung von Schlämmen - Bestimmung des Trockenrückstandes und des Wassergehalts (Characterization of sludges - Determination of dry residue and water content)* (DIN EN 12880).

Emerson, K., Russo, R.C., Lund, R.E. and Thurston, R.V., 1975. Aqueous Ammonia Equilibrium Calculations: Effect of pH and Temperature. *Journal of the Fisheries Research Board of Canada*, 32 (12), 2379–2383.

Ferry, J.G., 1993. *Methanogenesis: Ecology, physiology, biochemistry & genetics*. New York: Chapman & Hall.

FNR e.V., 2009. *Biogas-Messprogramm II - 61 Biogasanlagen im Vergleich: (Biogas Measurement Program II - A comparison of 61 German biogas plants).* 1st ed. Gülzow: Fachagentur Nachwachsende Rohstoffe (Agency for Renewable Resources).

FNR e.V., 2010. *Leitfaden Biogas - von der Gewinnung zur Nutzung: (Handbook biogas - from production to exploitation).* 5th ed. Gülzow-Prüzen, Hannover: Technische Informationsbibliothek u. Universitätsbibliothek.

Gujer, W. and Zehnder, A.J.B., 1983. Conversion Processes in Anaerobic Digestion. *Water Science & Technology*, 15 (8-9), 127–167.

Gruber, W., 2004. *Biogasanlagen in der Landwirtschaft.* 2nd ed. Bonn: Aid.

Koppe, P. and Stozek, A., 1993. *Kommunales Abwasser (Municipal wastewater): Seine Inhaltsstoffe nach Herkunft, Zusammensetzung und Reaktionen im Reinigungsprozess einschliesslich Klärschlämme (Its compunds according to origin, composition and reactions during the treatment process including waste-activated sludges).* 3rd ed. Essen: Vulkan-Verl.

References

Lübken, M., Gehring, T. and Wichern, M., 2010. Microbiological fermentation of lignocellulosic biomass: current state and prospects of mathematical modeling. *Applied Microbiology and Biotechnology*, 85 (6), 1643–1652.

McCarty, P.L., 1982. One hundred years of anaerobic treatment. *Proceedings of the International Symposium on Anaerobic Digestion* (2), 3–22.

Pavlostathis, S.G. and Gossett, J.M., 1986. A kinetic model for anaerobic digestion of biological sludge. *Biotechnology and Bioengineering*, 28 (10), 1519–1530.

Schmitz, H., 2008. *Mittlere Auslastung der elektrischen Leistung bei landwirtschaftlichen Biogasanlagen (Average capacity utilization of the electrical power of ABPs)*: Landwirtschaftskammer Nordrhein-Westfalen.

Thomas, S., 1988. *Beitrag zur Protein- und Biogaserzeugung aus hochbelasteten Abwässern . Bd.107. Aachen 1988.* PhD thesis. RWTH Aachen.

Tomei, M.C., Braguglia, C.M., Cento, G. and Mininni, G., 2009. Modeling of Anaerobic Digestion of Sludge. *Critical Reviews in Environmental Science and Technology*, 39 (12), 1003–1051.

Verein Deutscher Ingenieure e.V. (VDI), 2006. *Vergärung organischer Stoffe Substratcharakterisierung, Probenahme, Stoffdatenerhebung, Gärversuche (Fermentation of organic materials Characterisation of the substrate, sampling, collection of material data, fermentation tests)*, 13.030.30; 27.190 (VDI 4630).

Verein Deutscher Ingenieure e.V. (VDI), 2011. *Gütekriterien für Biogasanlagen (Quality criteria for biogas plants)*. Berlin: Beuth Verlag GmbH, 27.190 (4631).

Zimmermann, C., Baalmann, M., and Wulfert, K., 2003. *Prozesskontrolle und Anlagenführung landwirtschaftlicher Biogasanlagen durch dynamische Betriebsweise (Process control and operation of agricultural biogas plants by dynamic mode of operation)*. Bremen.

3 Modeling and Simulation of Biogas Plants

The modeling and simulation of industrial plants and processes is commonly used for their design, optimization and control. In particular, dynamic simulation models are widely applied to chemical and process engineering problems (Ogunnaike and Ray 1994) because they have two main advantages when it comes to process optimization and control: (1) Easy and fast implementation of new optimization and control strategies and; (2) safe testing and evaluation of their negative and positive effects on process and overall plant performance. Both advantages apply especially to the optimization and control of ABPs. Firstly, a variety of optimization and control strategies can be fully implemented in a dynamic simulation model of a plant and then further adapted and optimized based on the simulation results. Secondly, this results not only in faster implementation times but also allows a comprehensive assessment of potential risks and benefits, which can subsequently be minimized or maximized respectively. As the implementation of new optimization and control strategies at ABPs strongly affects the biological process, operational risks are high. Events, such as process overload and plant breakdown in the worst case cause extremely high costs, which can be averted by the application of a dynamic simulation model for process design and control. There is a wide range of applications for dynamic simulation models of anaerobic digestion processes (AD models) which offers great potential for the design, monitoring and control of AD plants whether they are ABPs or AD-WWTPs. Table 3-1 gives a survey of the possible applications of AD models and states the corresponding model requirements. Based on this survey, it is evident that complex and high-dimensional models are needed for the optimization and control of ABPs to capture authentic ABP behavior in the AD model. Therefore, the Anaerobic Digestion Model No. 1 (ADM1) was chosen from a variety of available AD models to optimize the substrate feed of ABPs. Advantages of the ADM1 are that its complexity is high enough to allow a comprehensive development, implementation and evaluation of new optimization strategies and that it is nevertheless computationally manageable.

The main contributions of this chapter are (1) a detailed review of available dynamic AD models to show the variety of AD models and to provide the rationale for selecting ADM1 as the model of choice for ABP simulation in this thesis as well as (2) the design and calibration of an ADM1-based AD model of a full-scale ABP. This model which was developed based on an open source Matlab® toolbox for simulation and modeling which was also developed at the Gummersbach Environmental Computing Center at Cologne University of Applied Sciences during this thesis.

The detailed review of dynamic AD models from the last 40 years is presented in section 3.1 followed by section 3.2 which provides a more complete description of the ADM1 model. Then section 3.3 describes the development and calibration of an ADM1 based AD model for a full-scale ABP. Finally section 3.4 provides a short summary of the achieved results on modeling and simulation of ABPs within this chapter.

Table 3-1: Applications and requirements for AD models adapted from Batstone (2006)

Aim	Application	Technical considerations
Model-based analysis and optimization of existing systems (operational analysis)	An existing AD plant where operational parameters are known and can be optimized. Limitations by plant operation.	Necessary process data is available. Parameters can be specifically adapted for that process. Model needs to consider limiting or controlling mechanisms.
Model-based design	Design of new, full-scale systems.	Model needs to be standardized and accepted. High number of realistic parameter sets needed. Information about inflow characteristics is required. Hydraulics and particle behavior needs to be considered.
Technology development	Development of new technology using AD models. Use of AD models to assess new technology.	Model needs factual, fundamental basis.
Parameter estimation	Estimation of transferable parameters for other applications and design.	Parameter estimation method needs to be robust and adaptive. Highly defined model required.
Integrated system analysis	Process chain evaluation. Process selection and justification.	AD models interact with other models. Models need to be suited for design and selection applications.
Sensor analysis and development	Sensor accuracy, performance. Soft-sensors	Model needs to include relevant underlying processes. Good model accuracy.
Model-based control	Non-linear control of AD systems.	Low-dimensional, fast model that adequately describes I/O system behavior.
Control, optimization and operation system benchmarking	Development and testing of new strategies	Complex, high-dimensional model needed, which is as realistic as possible.

3.1 Literature review

The number of available steady state and dynamic AD models is great and so are the differences between the models in terms of complexity, number of input variables as well as number of kinetic and stoichiometric model parameters. The aim of this literature review is to give a survey of existing AD models by summarizing their features and capabilities and to retrace the historical development over the last 40 years. A comparative overview of all discussed AD models is given at the end of this section in Table 3-2. Furthermore, this literature review justifies the decision to use the ADM1 instead of other available AD models for the simulation and optimization of ABPs.

Table 3-2: Survey of the most relevant AD models developed over the past 40 years

Publication	Model type	Adapted substrate	Growth kinetics	Composition variables	Main processes	Model parameters	Bacteria groups	Hydrolysis kinetics	Inhibition functions	Type of inhibition
(Andrews 1969)	dynamic; steady state	sludge	modified Monod	3	2	7	1	none	2	VFA, pH
(Hill and Barth 1977)	dynamic; steady state	organic waste	modified Monod	5	6	18	2	none	3	VFA, pH and NH_3
(Eastman and Ferguson 1981)	dynamic	sludge	Monod	3 - COD based	3	5	1	first order	none	none
(Pavlostathis and Gossett 1986)	dynamic	sludge	Monod	6 - BOD based	5	12	2	first order	none	none
(Shimizu *et al.* 1993)	dynamic	sludge	first order and Monod	15 - COD based	14	6	4	first order	none	none
(Vavilin *et al.* 1994)	dynamic	complex organic material	first order and Monod	32	13	28	7	first order	5	H_2, pH, NH, H_2S, Propionate
(Angelidaki *et al.* 1999)	dynamic; steady state	organic waste	modified Monod	17	11	11	8	first order	3	LCFA, acetic acid, NH_3
(Massé and Droste 2000)	dynamic	swine manure	modified Monod	11 - COD based	11	48	6	first order	none	none
(Siegrist *et al.* 1993, 2002)	dynamic; steady state	sludge	modified Monod	23 - COD based	18	11	6	first order	4	H_2, pH, NH_3, acetic acid
(Batstone et al. 2002)	dynamic; steady state	wide variety of substrates	modified Monod	24 - COD based	22	55	8	first order	4	H_2, pH, NH_3, butyric acid
(Keshtkar *et al.* 2003)	dynamic	cattle manure	modified Monod	13	25	14	4	first order	3	pH, VFA and NH_3
(Sarti *et al.* 2004)	dynamic	wastewater	first order	8	12	9	1	none	none	none
(Sötemann *et al.* 2005a)	dynamic	sludge	Monod	15 - COD based	10	19	4	Contois	1	H_2
(Sötemann *et al.* 2005b)	steady state	sludge	none	14 - COD based	12	8	none	first order, Monod, saturation	none	none
(Blumensaat and Keller 2005)	dynamic; steady state	sludge	modified Monod	32 - COD based	28	37	8	first order	4	H_2, pH, NH_3, butyric acid
(Gali *et al.* 2009)	dynamic; steady state	agro-waste	modified Monod	41 - COD based	32	80	8	first order	5	H2, pH, iN, NH_3, H_2S

The first dynamic AD model was developed by Andrews (1969) to simulate the anaerobic digestion of waste-activated sludge from WWTPs. Due to advances in computing capacity, the use of dynamic simulation models became possible and feasible. Andrews included three main process steps in his model, namely hydrolysis by exo-enzymes, acid and methane production. Furthermore, the inhibition of the anaerobic digestion process by volatile acids, *pH* and ammonia was considered and modeled using Michaelis-Menten kinetics. To model bacterial growth, Andrews based his model on the achievements of Monod (1949) who was the first to fully describe the growth of bacterial cultures. The only changes compared to standard Monod kinetics were made by integrating inhibition terms into the equations for bacterial growth. Thus, changes in *pH* or volatile acid concentration strongly affect process stability in the model. The three composition variables (*S, X, HS*) of the model come from the wastewater treatment sector and describe the concentration of soluble (*S*), particular (*X*) and unionized substrate in the unit *COD*[12]. Overall, the model possesses seven kinetic and stoichiometric parameters for model calibration and was tested and evaluated in comparison to a lab-scale digester in batch and continuous operation.

In 1974, Graef and Andrews adapted the AD model from 1969 to use it for process stability analysis and control applications (Graef and Andrews 1974). Three control strategies were closely investigated: (1) Scrubbing of carbon dioxide from the gas phase with subsequent gas recycle, (2) addition of a base to increase buffer capacity and (3) recirculation of sludge. Over the following years it became obvious that Andrews' AD model had several limitations such as only one microbial culture and one organic acid, namely acetic acid and a very simple hydrolysis without a disintegration step. Furthermore, the characterization of substrates using just three variables has proven not to be suitable for more complex substrates than sludge. Therefore, Hill and Barth (1977) developed a dynamic AD model for the simulation of animal waste digestion with five composition variables, two microbial cultures and 24 model parameters to capture the characteristics of animal waste. Another approach to improve AD models proposed by Eastman and Ferguson (1981) was to integrate the hydrolysis step into the acid production, modeling it by first order kinetics. Thus, hydrolysis was considered to be the main rate limiting processes. The importance of hydrolysis was confirmed later by Pavlosthatis and Gossett (1985) who closely investigated the kinetics of cell death, lysis as well as acidogenesis and methanogenesis to integrate them into a new BOD[13]-based AD model where cell death, lysis and hydrolysis are the main rate limiting process steps. Cell death and lysis were modeled using first order kinetics and acidogenesis and methanogenesis using the well-known Monod kinetics. Although, this AD model has 12 kinetic and stoichiometric parameters, Pavlosthatis and Gossett argued that less than

[12] "The chemical oxygen demand is a measure of the oxygen equivalent of the organic matter content of a sample that is susceptible to oxidation by a strong chemical oxidant." (American Public Health Association 1981)

[13] "The biochemical oxygen demand measures the molecular oxygen utilized during a specified incubation period for the biochemical degradation of organic material (carbonaceous demand) and the oxygen used to oxidize inorganic material such as sulfides and ferrous iron." (American Public Health Association 1981)

half of theses parameters needed to be adapted for model calibration and that the digestibility of the input substrate is the most important parameter.

In another attempt to further improve substrate characterization, Shimizu *et al.* (1993), divided each substrate into the three substances, carbohydrates, proteins and lipids. Furthermore, hydrogenotrophic methanogenesis was added in addition to acetoclastic methanogenesis to allow a broad range of applications for the model. Nevertheless, Shimizu's model was still far away from being a comprehensive AD model which captures most of the known AD processes.

The first attempt to develop a comprehensive AD model containing hydrolysis, acidogenesis, acetogenesis as well as acetoclastic and hydrogenotrophic methanogenesis was undertaken by Vavilin *et al.* (1994). For the first time sulphur reactions were included in the model to trace hydrogen sulphur (H_2S) production and inhibition during anaerobic digestion of animal waste. However, the complexity of the model with 13 processes, 32 state variables, 28 kinetic and stoichiometric parameters and an additional 72 inhibition constants is difficult to handle as many of the model parameters cannot be measured or have to be determined in long laboratory tests. Nevertheless, using many parameter values from literature good accordance was achieved with measurements from a lab-scale reactor, fed with wastewater from the food industry. Only five years later Vavilin, Angelidaki *et al.* (1999) published an even more complex AD model containing eight different bacterial groups focusing on the hydrolysis of carbohydrates and insoluble proteins and on eight biological reactions within acido-, aceto- and methanogenesis. This model was the first to incorporate inhibition by long chain fatty acids (LCFA) for all process steps. In addition, ammonia inhibition was not modeled with first order kinetics but rather with the Briggs-Haldane equation (Briggs and Haldane 1925). Based on Angelidaki's AD model Vavilin *et al.* (2000) adapted the previously developed AD model from 1994 to include inhibition by *LCFA* and closely evaluated the model with regard to its sensitivity to process disturbances. Results showed that the COD:S ratio is crucial for a well-functioning AD process and that free H_2S and *pH* are the main inhibitions causing system failure. Due to the fact that AD models became more and more complicated over the years and thus difficult to use, Massé and Droste (2000) developed an AD model that only uses measurable parameters and variables. Therefore, several compromises had to be made, so that the effect of *pH* on microbial growth was considered irrelevant and that growth rates of microorganisms are not significantly affected by high *VFA* or ammonium concentrations. Although these assumptions are arguable, results for the simulation of the digestion of swine manure in a lab-scale sequencing batch reactor were consistent with obtained measurements.

The year 2002 was a breakthrough in the development of AD models. Two very similar AD models were published by Siegrist *et al.* (1993, 2002) and Batstone *et al.* (2002) that had only one goal to unify all existing dynamic AD models in one standardized, detailed simulation model. Comparing both models, the AD model from Siegrist is simpler with less processes and parameters. It is focused

on the meso- and thermophilic digestion of waste-activated sludge and aims to capture the process dynamics under varying substrate feed and digester temperature. The ADM1 developed by Batstone aims to be a universally applicable model that can not only be used for different digester temperatures, but also for a broad variety of input substrates. Developed within the IWA[14] Task Group for Mathematical Modeling of Anaerobic Digestion Processes, the ADM1 is a very complex model with 22 processes and over 50 model parameters. Nevertheless, it has gained wide acceptance and has been the standard AD model used and adapted to different applications more often than any other model. Furthermore, over the past decade many issues associated with the application of the ADM1 have been addressed, further enhancing its utility. One of the main advantages of the ADM1 is the disintegration as an additional process step before the hydrolysis. Modeled with first order kinetics, disintegration describes the breakup of the degradable, particulate *COD* fraction into carbohydrates, proteins and lipids, which is especially important for the digestion of complex substrates such as energy crops and organic waste.

Although the ADM1 is one of the most comprehensive AD models available, other models focusing on specific applications were developed and the ADM1 was further improved. For example, Keshtkar *et al.* (2003) included mixing in an AD model using a classic model by Levenspiel (1962) and validated the model on the digestion of cattle manure because until 2003 all available AD models considered the digesters of an AD plant to be CSTRs, which is mostly not true but makes model development much easier. Sarti *et al.* (2004) developed a very simplistic AD model with only 9 model parameters and 8 variables also considering hydrodynamic characteristics. Furthermore, Sötemann *et al.* (2005a) developed a steady state AD model for AD plant design and evaluation of optimal operating conditions as well as a more complex dynamic AD model (Sötemann *et al.* 2005b). Also in 2005, Blumensaat and Keller (2005) adapted the ADM1 model to a two stage digestion process with one thermophilic stage for hydrolysis and acido- and acetogenesis and a subsequent mesophilic stage for methanogenesis. It is remarkable that Blumensaat and Keller used a pilot-scale plant (160 l) equipped with sophisticated online and lab measurement systems to evaluate their AD model instead of a lab-scale digester. To facilitate model calibration parameter values from Siegrist *et al.* (2002) were used. Over all a good agreement between simulation results and measurement data was achieved during normal loading conditions after steady state and dynamic model calibration. Nevertheless, extreme process conditions such as high loadings or process breakdown could not be captured by the model.

Due to the fact that the determination of ADM1 input variables was still very difficult at that time, Jeppson *et al.* (2007) modified the ADM1 and developed two conversion blocks that calculate the ADM1 input variables based on the well-known ASM1 (Henze 2000) parameters. Thus, substrate

[14] http://www.iwahq.org

characterization for the ADM1 became much easier and the fast and easy integration into WWTP models for sludge digestion was possible. Although, determination of the ADM1 input variables was significantly improved by Jeppson *et al.*, the application of the ADM1 for agricultural waste or energy crops was still extremely challenging as standard *COD* measurements are impossible to handle due to the matrix of the substrates. Therefore, Gali *et al.* (2009) modified the ADM1 by adding standard parameters for the characterization of energy crops to the input parameters, such as (*TSS* and *VSS*). The adapted AD model was compared against a four liter laboratory digester and was sufficiently accurate. Nevertheless, the addition of extra input variables made the ADM1 again more complex. A further improvement in handling of the ADM1 was achieved by Zaher *et al.* (2009) who developed a comprehensive simulation toolbox based on the ADM1 and Matlab® Simulink. The purpose of this toolset is the simulation of co-digestion and the evaluation of different waste stream compositions and hydraulic retention times in order to maximize biogas production. As the composition of the input substrates is dynamically changing in terms of their contents of carbohydrates, proteins, lipids, TS and VS, which is difficult to implement in the hydrolysis of the ADM1, hydrolysis was modeled in a separate model. The outputs of the hydrolysis model are then fed to the ADM1. To speed up simulation of the ADM1, a special ADM1 DAE model developed by Rosen *et al.* (2006) for plant-wide WWTP benchmark simulations was used. Due to the economic boom in the biogas market, in particular ABPs, the applications of the ADM1 increased rapidly. Nevertheless, one main problem still remained unsatisfactorily solved; the easy and feasible characterization of the input substrates. One of the best solutions to this problem was presented by Koch *et al.* (2010) who did no longer measure the necessary *COD* fractions of the substrates but rather calculated them based on standard measurements for the characterization of energy crops and waste, the Weender analysis (Basler 1976). Thus, a theoretical *COD* value ($ThCOD$) was introduced. Furthermore, Koch *et al.* suggested a standard procedure for model calibration by setting all model parameters to standard ADM1 values and subsequently varying the sensitive model parameters until the model performance shows good agreement with the measurement values. Model performance was evaluated using the Nash-Sutcliffe coefficient (Nash and Sutcliffe 1970).

In parallel with all the white box dynamic AD models (using a defined set of differential equations), several black box models have been developed in recent years using mainly Computational Intelligence (CI) methods. In 2005, Brus applied recursive system identification techniques to drastically reduce model degree and the number of model parameters of an AD model. The application of the recursive prediction error method (RPEM) for nonlinear identification problems showed that a second order nonlinear model is sufficient to accurately model AD processes. Around the same time, Strik *et al.* (2005) developed a black box ANN model for the prediction of trace compounds such as ammonia and hydrogen sulphide based on experimental data from a 20l lab-scale CSTR. Another application at a full-scale anaerobic digester treating sludge from the primary sedimentation of a

Turkish WWTP with 800,000 PE was developed by Cakmakci (2007) who used a two stage adaptive neuro-fuzzy interference system (ANFIS) to predict VS effluent concentration in the first stage and methane production in the second stage. Also in 2007, ANN were used again by Ozkaya *et al.* when they built a model to predict the methane concentration in the biogas from a landfill site. Based on data from 34 month where the leachate and landfill gas components were monitored, a two layer ANN was trained using back propagation. Another interesting approach was developed by Abu Qdais *et al.* (2010) who trained an ANN with two hidden layers to predict the methane concentration in the biogas. The four process parameters used for ANN training were pH, temperature, VS and TS. Based on the fully trained ANN model Abu Qdais tried to optimize these four parameters with a Genetic Algorithm to maximize methane concentration in the biogas.

To sum up, this survey of existing AD models shows the high number and variety of available AD models as well as the historical development of these models. However, it is not an exhaustive survey. Other reviews by Gavala *et al.* (2003), Batstone (2006) as well as Tomei *et al.* (2009) are therefore recommended to get additional information for a complete and comprehensive overview of AD modeling.

Looking at all the available AD models it seems difficult to decide which one is most suited for the simulation and optimization of ABPs, but due to the high number of publications on ADM1 applications and the variety of model adaptations, the ADM1 was used for the optimization of ABPs. The implementation of the ADM1 used for the developments in this thesis was programmed by the ifak system GmbH[15] and is called ADM1xp (Wett *et al.* 2006). The ADM1xp only differs slightly from the original ADM1 using two different state variables and several modified reaction rates. The following section will give a detailed description of this ADM1xp which will be called ADM1 in the remainder of this thesis.

[15] http://www.ifak-system.com/

3.2 The Anaerobic Digestion Model No. 1 (ADM1)

The ADM1 model is one of the most comprehensive AD models and thus model complexity in terms of number of differential equations and parameters is high. The aim of this section is to explain the ADM1 in detail and to evaluate its strengths and limitations for the simulation of ABPs. Most composition and process variables are expressed in *COD* concentrations (kgCOD/m³) except nitrogen (NH_4^+ and NH_3) and inorganic carbon (CO_2 and HCO_3^-) concentration variables which are expressed in kmolN/m³ and kmolC/m³ respectively. The main two reasons to choose *COD*-based variables are: (1) high compatibility with existing Activated Sludge Models (Henze 2000) developed by the IWA and, (2) use of a standardized unit for most of the model variables. Furthermore, the ADM1 was initially parametrized for the digestion of waste-activated sludge as described in the Scientific and Technical Report No. 13 of the IWA (Batstone *et al.* 2002), which is normally characterized by its soluble and particulate *COD* fractions.

In general, the process of anaerobic digestion can be subdivided in two different kinds of processes:

(1) Biochemical processes, which describe intracellular processes such as the degradation of soluble organic material by different bacterial populations resulting in biomass growth and decay, and extracellular processes such as disintegration of particulate organic material and enzymatic hydrolysis.
(2) Physico-chemical processes, which include ion association and dissociation and liquid-gas transfer. Both processes are needed for comprehensive modeling of AD processes as physico-chemical state variables such as pH, carbon buffer and biogas composition strongly affect the biochemical reactions causing inhibitions and thus a rate-limiting effect.

In the following three sections the state variables of the ADM1 as well as the two main process groups are explained in further detail.

3.2.1 ADM1 state variables

The state of the ADM1 is described by 24 variables that can be divided into two main groups of soluble and particulate components, which are labeled as S and X respectively. These two groups are subsequently split into inert components expressed by S_I and X_I and further degradable components. Those degradable soluble components consist of organic and inorganic compounds whereas the particulate components apart from X_I are considered to be organic as the inorganic compounds are part of X_I.

Table 3-3 shows a list of all soluble as well as particulate state variables of the ADM1 and their corresponding notation.

Table 3-3: ADM1 state variables

Monosaccharides (kgCOD m^{-3})	S_{su}
Amino acids (kgCOD m^{-3})	S_{aa}
Long chain fatty acids (kgCOD m^{-3})	S_{fa}
Total valerate (kgCOD m^{-3})	S_{va}
Total butyrate (kgCOD m^{-3})	S_{bu}
Total propionate (kgCOD m^{-3})	S_{pro}
Total acetate (kgCOD m^{-3})	S_{ac}
Hydrogen gas (kgCOD m^{-3})	S_{h2}
Methane gas (kgCOD m^{-3})	S_{ch4}
Inorganic Carbon (kmoleC m^{-3})	S_{co2}
Inorganic Nitrogen (kmoleN m^{-3})	S_{nh4}
Soluble inerts (kgCOD m^{-3})	S_I
Composites (kgCOD m^{-3})	X_c
Carbohydrates (kgCOD m^{-3})	X_{ch}
Proteins (kgCOD m^{-3})	X_{pr}
Lipids (kgCOD m^{-3})	X_{li}
Sugar degraders (kgCOD m^{-3})	X_{su}
Amino acid degraders (kgCOD m^{-3})	X_{aa}
LCFA degraders (kgCOD m^{-3})	X_{fa}
Valerate and butyrate degraders (kgCOD m^{-3})	X_{c4}
Propionate degraders (kgCOD m^{-3})	X_{pro}
Acetate degraders (kgCOD m^{-3})	X_{ac}
Hydrogen degraders (kgCOD m^{-3})	X_{h2}
Particulate inerts (kgCOD m^{-3})	X_I

Those ADM1 state variables are affected by the biochemical and physico-chemical processes of the AD process. In particular, the degradation of substrates and the biogas production are described by the COD-based state variables. Figure 3-1 shows the COD flux through the different stages of the AD process. In a first step the complex source substrate is split into an inert and a degradable COD fraction, where the degradable fraction disintegrates to carbohydrates, proteins and lipids. The compounds are then degraded to sugars, amino acids and LCFA before they are transformed into organic acids and hydrogen, which are eventually used to produce methane. The different bacteria populations involved in all these conversion steps, so-called degraders, are also represented in particulate COD fractions.

Thus, modeling and simulation of AD processes requires a good characterization of the input substrates used for digestion. In particular, the soluble and particulate inert fractions and the particulate fractions of carbohydrates, proteins and lipids need to be analyzed or properly estimated based on available substrate data.

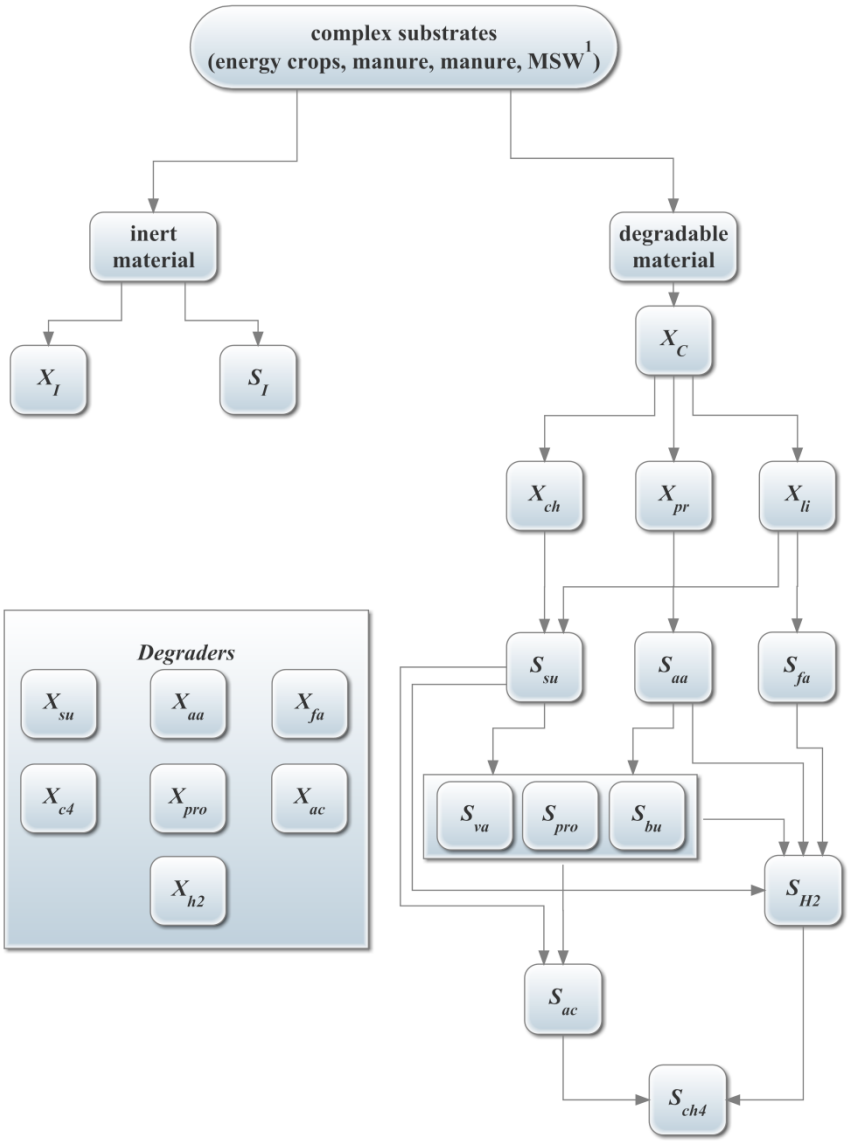

Figure 3-1: Description of the COD flux through the AD process of the ADM1 for complex substrates such as MSW[16] using COD-based state variables (modified from Batstone *et al.* 2002)

3.2.2 Biochemical processes

The ADM1 consists of 19 biochemical processes which describe the five main degradation processes of AD: (1) disintegration, (2) hydrolysis, (3) acidogenesis, (4) acetogenesis and (5) methanogenesis as previously mentioned in chapter 2. Disintegration and hydrolysis are extracellular processes whereas the remaining three main processes are intracellular. As described by Batstone *et al.* (2002) the extracellular processes are modeled by first order kinetics whereas intracellular processes are modeled by Monod-type kinetics to describe substrate uptake as well as bacterial growth and decay. Furthermore, intracellular kinetics of biochemical processes is affected by inhibition. Overall, five

[16] Municipal Solid Waste

different inhibition functions are implemented in the ADM1; two functions modeling pH inhibition and three for the modeling of ammonia as well as butyrate and valerate inhibition.

Table 3-4 gives a survey of all biochemical processes and the corresponding kinetics, which are influenced by the inhibition functions mentioned in Table 3-5. In turn, the complete reaction rates for each state variable consist of several biochemical processes whose effect is determined by stoichiometric model coefficients. (Table 3-6 and Table 3-7) These stoichiometric coefficients need to be defined for each process and state variable based on literature or measurement values. Due to the large amount of stoichiometric coefficients per biochemical reaction and state variable a matrix representation called Peterson matrix (Peterson 1965) is used to give a comprehensive overview of the complete ADM1 implementation. Thus, this form of model presentation is commonly used.

The Peterson matrices for the soluble and particulate state variables are given in Annex I of this thesis.

Table 3-4: Processes and corresponding reaction rates of the ADM1

Process	**Reaction rates**	
p_1: Disintegration	$k_{dis} X_c$	(3.1)
p_2 : Hydrolysis of Carbohydrates	$k_{hyd,ch} X_{ch}$	(3.2)
p_3 : Hydrolysis of Proteins	$k_{hyd,pr} X_{pr}$	(3.3)
p_4 : Hydrolysis of Lipids	$k_{hyd,li} X_{li}$	(3.4)
p_5 : Uptake of Sugars	$k_{m,su} \frac{S_{su}}{K_S + S_{su}} X_{su} I_1$	(3.5)
p_6 : Uptake of Amino Acids	$k_{m,aa} \frac{S_{aa}}{K_S + S_{aa}} X_{aa} I_1$	(3.6)
p_7 : Uptake of LCFA	$k_{m,fa} \frac{S_{fa}}{K_S + S_{fa}} X_{fa} I_2$	(3.7)
p_8 : Uptake of Valerate	$k_{m,c4} \frac{S_{va}}{K_S + S_{va}} X_{c4} \frac{1}{1 + S_{bu}/S_{va}} I_2$	(3.8)
p_9 : Uptake of Butyrate	$k_{m,c4} \frac{S_{bu}}{K_S + S_{bu}} X_{c4} \frac{1}{1 + S_{va}/S_{bu}} I_2$	(3.9)
p_{10} : Uptake of Propionate	$k_{m,pro} \frac{S_{pro}}{K_S + S_{pro}} X_{pro} I_2$	(3.10)
p_{11} : Uptake of Acetate	$k_{m,ac} \frac{S_{ac}}{K_S + S_{ac}} X_{ac} I_3$	(3.11)
p_{12} : Uptake of Hydrogen	$k_{m,h2} \frac{S_{h2}}{K_S + S_{h2}} X_{h2} I_1$	(3.12)
p_{13} : Decay of X_{su}	$k_{dec,X_{su}} X_{su}$	(3.13)

p_{14}: Decay of X_{aa}	$k_{dec,X_{aa}} X_{aa}$	(3.14)
p_{15}: Decay of X_{fa}	$k_{dec,X_{fa}} X_{fa}$	(3.15)
p_{16}: Decay of X_{c4}	$k_{dec,X_{c4}} X_{c4}$	(3.16)
p_{17}: Decay of X_{pro}	$k_{dec,X_{pro}} X_{pro}$	(3.17)
p_{18}: Decay of X_{ac}	$k_{dec,X_{ac}} X_{ac}$	(3.18)
p_{19}: Decay of X_{h2}	$k_{dec,X_{h2}} X_{h2}$	(3.19)
I_1	$I_{pH\_1} I_{nh4}$	(3.20)
I_2	$I_{pH\_1} I_{nh4} I_{h_2,c_4}$	(3.21)
I_3	$I_{pH\_2} I_{nh4} I_{nh_3}$	(3.22)

Table 3-5: Inhibition functions implemented in the ADM1

Inhibiting parameter	Functional description	
pH (form 1)	$I_{pH\_1} = \frac{1+2\cdot 10^{0.5(pH_{LL}-pH_{UL})}}{1+10^{(pH-pH_{UL})}+10^{(pH_{LL}-pH)}}$	(3.23)
pH (form 2)	$I_{pH\_2} = \begin{cases} \exp\left[-3\left(\frac{pH-pH_{UL}}{pH_{UL}-pH_{LL}}\right)^2\right] & pH < pH_{UL} \\ 1 & pH > pH_{UL} \end{cases}$	(3.24)
Ammonia	$I_{nh_3} = \frac{1}{1+\frac{S_{I\,nh_3}}{K_{I\,nh_3}}}$	(3.25)
Hydrogen and butyrate, valerate inhibition	$I_{h_2,c_4} = \frac{1}{1+\frac{S_{h_2}}{K_{I\,h_2c_4}}}$	(3.26)
Nitrogen (mainly NH_4)	$I_{nh4} = \frac{1}{1+\frac{K_{I\,nh4}}{S_{I\,nh4}}}$	(3.27)

Table 3-6: Reaction rates for the soluble ADM1 state variables

Monosaccharides (kgCOD m^{-3})	$\frac{dS_{su}}{dt} = p_1 + (1 - f_{fa,li})\, p_4 - p_5$	(3.28)
Amino acids (kgCOD m^{-3})	$\frac{dS_{aa}}{dt} = p_3 - p_6$	(3.29)
LCFA (kgCOD m^{-3})	$\frac{dS_{fa}}{dt} = f_{fa,li}\, p_4 - p_7$	(3.30)
Total valerate (kgCOD m^{-3})	$\frac{dS_{va}}{dt} = (1 - Y_{aa})\, f_{va,aa}\, p_6 - p_8$	(3.31)
Total butyrate (kgCOD m^{-3})	$\frac{dS_{bu}}{dt} = (1 - Y_{su})\, f_{bu,su}\, p_5 + (1 - Y_{aa})\, f_{bu,aa}\, p_6 - p_9$	(3.32)
Total propionate (kgCOD m^{-3})	$\frac{dS_{pro}}{dt} = (1 - Y_{su})\, f_{pro,su}\, p_5 + (1 - Y_{aa})\, f_{pro,aa}\, p_6 + (1 - Y_{c4})0.54\, p_8 - p_{10}$	(3.33)
Total acetate (kgCOD m^{-3})	$\frac{dS_{ac}}{dt} = (1 - Y_{su})\, f_{ac,su}\, p_5 + (1 - Y_{aa})\, f_{ac,aa}\, p_6 + (1 - Y_{fa})0.7\, p_7 + (1 - Y_{c4})0.31\, p_8 + (1 - Y_{c4})0.8\, p_9 + (1 - Y_{pro})0.57\, p_{10} - p_{11}$	(3.34)
Hydrogen gas (kgCOD m^{-3})	$\frac{dS_{h2}}{dt} = (1 - Y_{su})\, f_{h2,su}\, p_5 + (1 - Y_{aa})\, f_{h2,aa}\, p_6 + (1 - Y_{fa})0.3\, p_7 + (1 - Y_{c4})0.15\, p_8 + (1 - Y_{c4})0.2\, p_9 + (1 - Y_{pro})0.43\, p_{10} - p_{12}$	(3.35)
Methane gas (kgCOD m^{-3})	$\frac{dS_{ch4}}{dt} = (1 - Y_{ac})\, p_{11} + (1 - Y_{h2})\, p_{12}$	(3.36)
Inorganic Carbon (kmoleC m^{-3})	$\frac{dS_{co2}}{dt} = f_{co2,xc}\, p_1 + f_{co2,xli}\, p_4 + f_{co2,su}\, p_5 + f_{co2,aa}\, p_6 + f_{co2,fa}\, p_7 + f_{co2,va}\, p_8 + f_{co2,bu}\, p_9 + f_{co2,pro}\, p_{10} + f_{co2,ac}\, p_{11} + f_{co2,h2}\, p_{12} + f_{co2,xb}\, p_{13} + f_{co2,xb}\, p_{14} + f_{co2,xb}\, p_{15} + f_{co2,xb}\, p_{16} + f_{co2,xb}\, p_{17} + f_{co2,xb}\, p_{18} + f_{co2,xb}\, p_{19}$	(3.37)
Inorganic Nitrogen (kmoleN m^{-3})	$\frac{dS_{nh4}}{dt} = -Y_{su} N_{bac}\, p_5 + (N_{aa} - Y_{aa} N_{bac})\, p_6 - Y_{fa} N_{bac}\, p_7 - Y_{c4} N_{bac}\, p_8 - Y_{c4} N_{bac}\, p_9 - Y_{pro} N_{bac}\, p_{10} - Y_{ac} N_{bac}\, p_{11} - Y_{h2} N_{bac}\, p_{12} + f_{\sin,xb}\, p_{13} + f_{\sin,xb}\, p_{14} + f_{\sin,xb}\, p_{15} + f_{\sin,xb}\, p_{16} + f_{\sin,xb}\, p_{17} + f_{\sin,xb}\, p_{18} + f_{\sin,xb}\, p_{19}$	(3.38)
Soluble inerts (kgCOD m^{-3})	$\frac{dS_I}{dt} = f_{S_I X_C}\, p_1$	(3.39)

Table 3-7: Reaction rates for the particulate ADM1 state variables

Composites (kgCOD m^{-3})	$\frac{dX_C}{dt} = -p_1 + p_{13} + p_{14} + p_{15} + p_{16} + p_{17} + p_{18} + p_{19}$	(3.40)
Carbohydrates (kgCOD m^{-3})	$\frac{dX_{ch}}{dt} = f_{ch,X_C} p_1 - p_2 + f_{ch,xb} p_{13} + f_{ch,xb} p_{14} + f_{ch,xb} p_{15} + f_{ch,xb} p_{16} + f_{ch,xb} p_{17} + f_{ch,xb} p_{18} + f_{ch,xb} p_{19}$	(3.41)
Proteins (kgCOD m^{-3})	$\frac{dX_{pr}}{dt} = f_{pr,X_C} p_1 - p_3 + f_{pr,xb} p_{13} + f_{pr,xb} p_{14} + f_{pr,xb} p_{15} + f_{pr,xb} p_{16} + f_{pr,xb} p_{17} + f_{pr,xb} p_{18} + f_{pr,xb} p_{19}$	(3.42)
Lipids (kgCOD m^{-3})	$\frac{dX_{li}}{dt} = f_{li,X_C} p_1 - p_4 + f_{li,xb} p_{13} + f_{li,xb} p_{14} + f_{li,xb} p_{15} + f_{li,xb} p_{16} + f_{li,xb} p_{17} + f_{li,xb} p_{18} + f_{li,xb} p_{19}$	(3.43)
Sugar degraders (kgCOD m^{-3})	$\frac{dX_{su}}{dt} = Y_{su} p_5 - p_{13}$	(3.44)
Amino acid degraders (kgCOD m^{-3})	$\frac{dX_{aa}}{dt} = Y_{aa} p_6 - p_{14}$	(3.45)
LCFA degraders (kgCOD m^{-3})	$\frac{dX_{fa}}{dt} = Y_{fa} p_7 - p_{15}$	(3.46)
Valerate and butyrate degraders (kgCOD m^{-3})	$\frac{dX_{c4}}{dt} = Y_{c4} p_8 + Y_{c4} p_9 - p_{16}$	(3.47)
Propionate degraders (kgCOD m^{-3})	$\frac{dX_{pro}}{dt} = Y_{pro} p_{10} - p_{17}$	(3.48)
Acetate degraders (kgCOD m^{-3})	$\frac{dX_{ac}}{dt} = Y_{ac} p_{11} - p_{18}$	(3.49)
Hydrogen degraders (kgCOD m^{-3})	$\frac{dX_{h2}}{dt} = Y_{h2} p_{12} - p_{19}$	(3.50)
Particulate inerts (kgCOD m^{-3})	$\frac{dX_I}{dt} = f_{X_I,X_C} p_1$	(3.51)

3.2.3 Physico-chemical processes

The physico-chemical processes make up the second set of equations which are used in the ADM1. For two main reasons, these processes are particularly significant for the modeling of AD systems. Firstly, many of the inhibitors introduced in Table 3-5 rely on the correct implementation of physico-chemical processes. pH, the acid-base equilibrium as well as the concentration of soluble gas compounds in the liquid phase of the bioreactor are calculated based on physico-chemical principles. Secondly, significant state variables such as biogas flow and carbon buffer depend on physico-chemical processes.

Overall, two major types of physico-chemical reactions are implemented within the ADM1.

(1) Liquid-liquid processes (mainly acid-base reactions)
(2) Liquid-gas processes (liquid-gas transfer of the biogas compounds)

In the following two subsections the acid-base reactions and the liquid-gas transfer of the biogas compounds are briefly explained.

3.2.3.1 Acid-base reactions

One of the main liquid-liquid processes is the acid-base equilibrium. Through ion association and dissociation with hydrogen (H^+) and hydroxide (OH^-) ions acid-base pairs react with each other in order to reach an equilibrium. The magnitude of these acid-base reactions is determined by dissociation constants (K_a) for each acid-base pair of the AD process. Large positive dissociation constants are associated with weak acids where the degree of dissociation is very small whereas low positive dissociation constants are characteristic of strong acids whose dissociation is almost complete. As the range of values for K_a is extensive, the negative logarithm of the base 10 is commonly used to scale down the range of K_a. Thus, K_a is mostly denoted as $pK_a = -\log_{10} K_a$. Furthermore, dissociation constant values are strongly temperature dependent which is why temperature compensation is necessary for the dissociation constants of some acid-base equilibria. In the ADM1, temperature compensation is implemented for the acid-base pairs CO_2 / HCO_3^- and NH_4^+ / NH_3. Due to the fact that the pK_a values for organic acids remain mostly constant within the common temperature range of AD processes (273 K – 333 K), temperature compensation is neglected in this case. The importance of these acid-base reactions and the respective dissociation constants becomes obvious in the calculation of the pH value, which is the negative logarithm to the base 10 of the hydrogen protons, $pH = -\log_{10} H^+$. Thus, a correct calculation of the hydrogen proton concentration in the liquid phase mainly depends on the acid-base reactions and the pK_a values.

Table 3-8: Acid dissociation constants for AD acid-base reactions (Batstone *et al.* 2002)

Acid/base pair	pK_a (298 K)
CO_2 / HCO_3^-	6.35
NH_4^+ / NH_3	9.25
H_2S / HS^-	7.05
$H_2O / (OH^- + H^+)$	14.00
HAc / Ac^-	4.76
HPr / Pr^-	4.88
$n-HBu / Bu^-$	4.82
$i-HBu / Bu^-$	4.86
$n-HVa / Va^-$	4.86
$i-HVa / Va^-$	4.78

3.2.3.2 Liquid-gas transfer

The liquid-gas transfer is important for modeling the biogas flux of an AD system as well as the concentration of gas components in both, the liquid and the gas phase. In the ADM1 implementation used, three main gas components are considered in the liquid-gas transfer: H_2, CO_2 and CH_4. The transfers of NH_3 as well as of H_2S were not considered in the ADM1. In particular, H_2S production is not modeled as sulfate reduction is not included in the biochemical processes. Although, dissolved H_2S is a strong inhibitor in the liquid phase of the AD process and it also causes problems for the cogeneration units in the gas phase. Nevertheless, in practice this does not have an impact on the modeling of ABPs because H_2S production is normally controlled by regular dosage of compressed air to the liquid phase.

The transfer of gas between the liquid and the gas phase mainly depends on the gas concentration in the liquid phase ($S_{liq,i}$) and the corresponding partial pressure of the gas phase ($p_{gas,i}$). Based on Henry's law a steady state is achieved between both phases, which can be described for each biogas component i by

$$K_H p_{gas,i} - S_{liq,i} = 0 . \tag{3.52}$$

Unfortunately, the solubility of each gas component is different which affects the liquid-gas transfer and the transfer of relatively insoluble gases such as H_2 and CH_4 which is also inhibited by a liquid film surrounding the gas bubbles. However, CO_2 has a high solubility, which is about 100 times higher than the solubility of CH_4. Therefore, a mass transfer coefficient k_L (ms^{-1}) is introduced which, if multiplied by the specific transfer area a (m^2m^{-3}) of a gas bubble, regulates the specific mass transfer rate $\rho_{T,i}$ for each gas i.

$$\rho_{T,i} = k_L a\left(S_{liq,i} - K_H p_{gas,i}\right) \tag{3.53}$$

Due to the fact that gas concentrations in the ADM1 are modeled by COD-based state variables the Henry constant K_H needs to be corrected by a factor 16 and 64 for H_2 and CO_2 respectively.

3.3 Design and calibration of an AD model for an ABP

The design and calibration of an AD model for the full-scale Sunderhook ABP provides the basis for ABP optimization, which is described in chapter 5. Thus, accurate modeling and calibration is important to achieve realistic substrate feed optimization results which are transferable to full-scale plant operation. Although, high model accuracy is a priority, calibration and substrate characterization was based on commonly available measurement and plant parameters. This results in a slight decrease of model accuracy but also guarantees that model calibration and substrate characterization can be performed relatively easily for full-scale plants without requiring extensive laboratory analysis in addition to available measurement and performance values. Due to the fact, that the goal of the developed substrate feed optimization is to be applicable to full-scale ABPs, the underlying simulation model is a compromise between model accuracy and practicability.

The comprehensive simulation model for the Sunderhook ABP and its calibration will be described in the following two sections.

3.3.1 Design of the simulation model for the Sunderhook ABP

The Sunderhook ABP is a typical agricultural biogas plant with a power production of 750 kW and two digesters (one primary and one secondary digester). Due to the fact, that remuneration rates for electricity are higher if energy crops and manure are used for AD, the substrate feed of the ABP Sunderhook consists mainly of maize, grass silage and bull manure.

Table 3-9: Characteristics of the ABP Sunderhook

	Sunderhook ABP
Substrate feed	maize grass silage oat rye bull manure
Digesters	primary digester - 3,190 m³ secondary digester – 3,435 m³ final storage tank – 3,435 m³
Measurement systems	solid substrate feed (t/d) liquid substrate feed (m³/d) digester temperature (°C) gas analysis (CH_4, H_2S, H_2, O_2) pH, ORP and TS online probes power and heat production (kWh)
Energy production	750 kW_{el} and 790 kW_{th}
Location	Gronau-Epe (GERMANY)

Table 3-9 gives an overview of the characteristics of the Sunderhook ABP whereas the plant's layout and pictures are shown in Figure 3-2 and Figure 3-3 respectively.

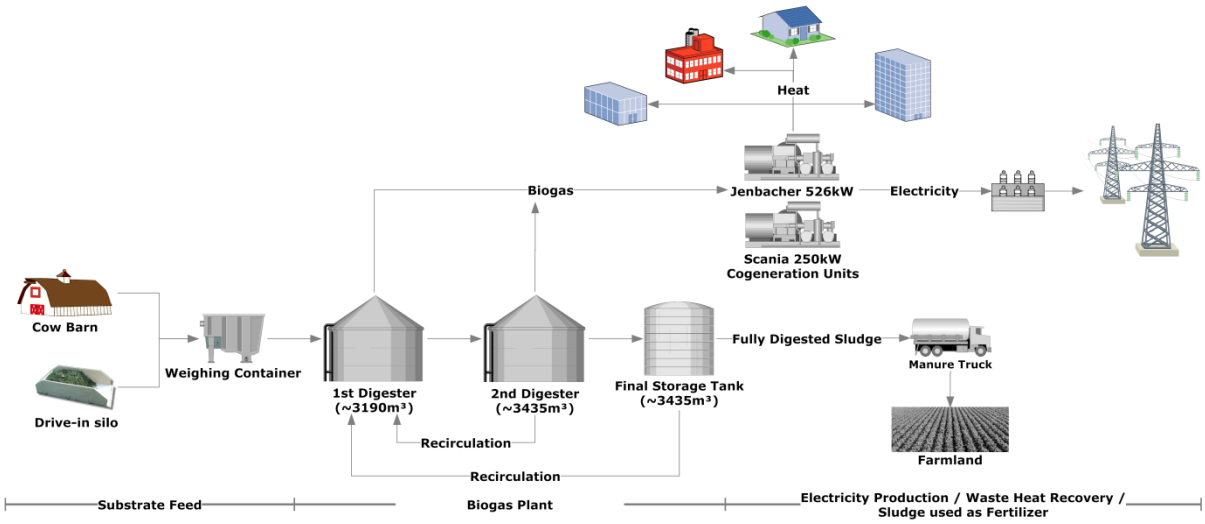

Figure 3-2: Layout of the Sunderhook ABP

Figure 3-3: Sunderhook ABP - a. primary digester with system for solid substrate input, b. primary digester, c. drive-in silo for maize and rye

Based on information about digester sizes and temperatures, electrical and thermal efficiency of the cogeneration units as well as pump characteristics, the simulation model of the Sunderhook ABP was implemented in Matlab®/Simulink using a specially designed Biogas toolbox. This toolbox was developed at the Cologne University of Applied Sciences (Gaida *et al.* 2011) over several years based

on an existing AD toolbox from the ifak system GmbH called SIMBA®[17]. Advantages of this toolbox are: (1) the fast simulation of complex models due to precompiled model blocks programmed in C, (2) compatibility with 64 bit operating systems for faster simulation, and, (3) a substantial toolbox for the optimization and control of biogas plants. To allow for an easy and fast setup of ABP simulation models, the Simulink model is automatically generated based on information which is entered via several GUIs for plant setup, substrate feed and flow paths. Thus, errors in model setup and configuration are minimized. Figure 3-4 shows the GUIs used to define plant structure and to characterize the substrates feed of the ABP, whereas Figure 3-5 shows the complete Matlab®/Simulink simulation model of the Sunderhook ABP.

a.

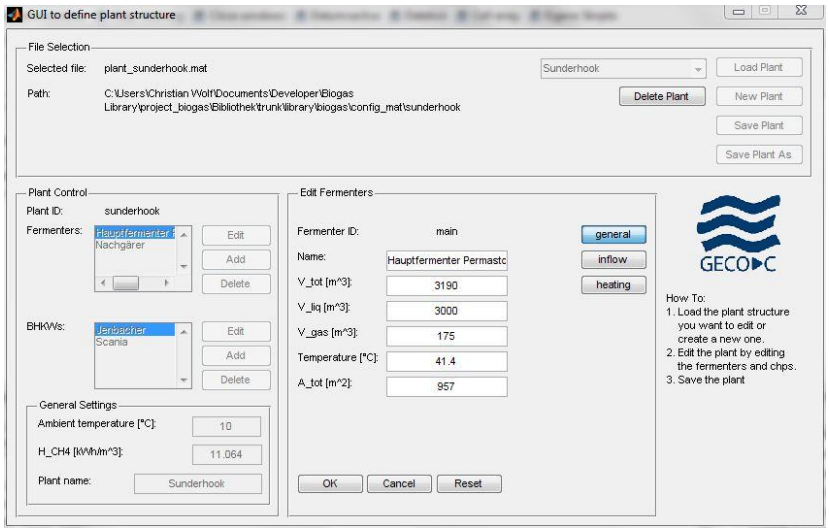

b.

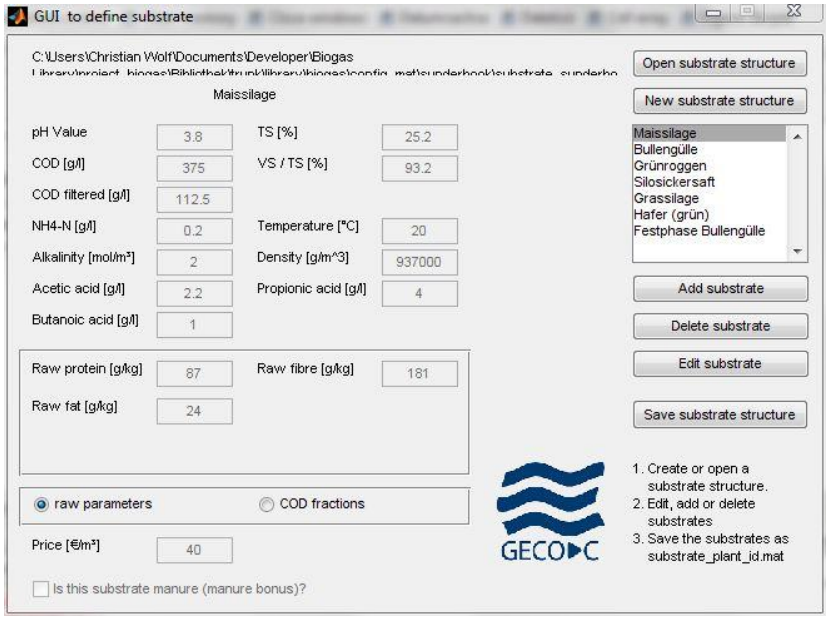

Figure 3-4: GUIs for ABP model design. a. GUI to define plant structure and components, b. substrate characterization

[17] http://simba.ifak.eu/

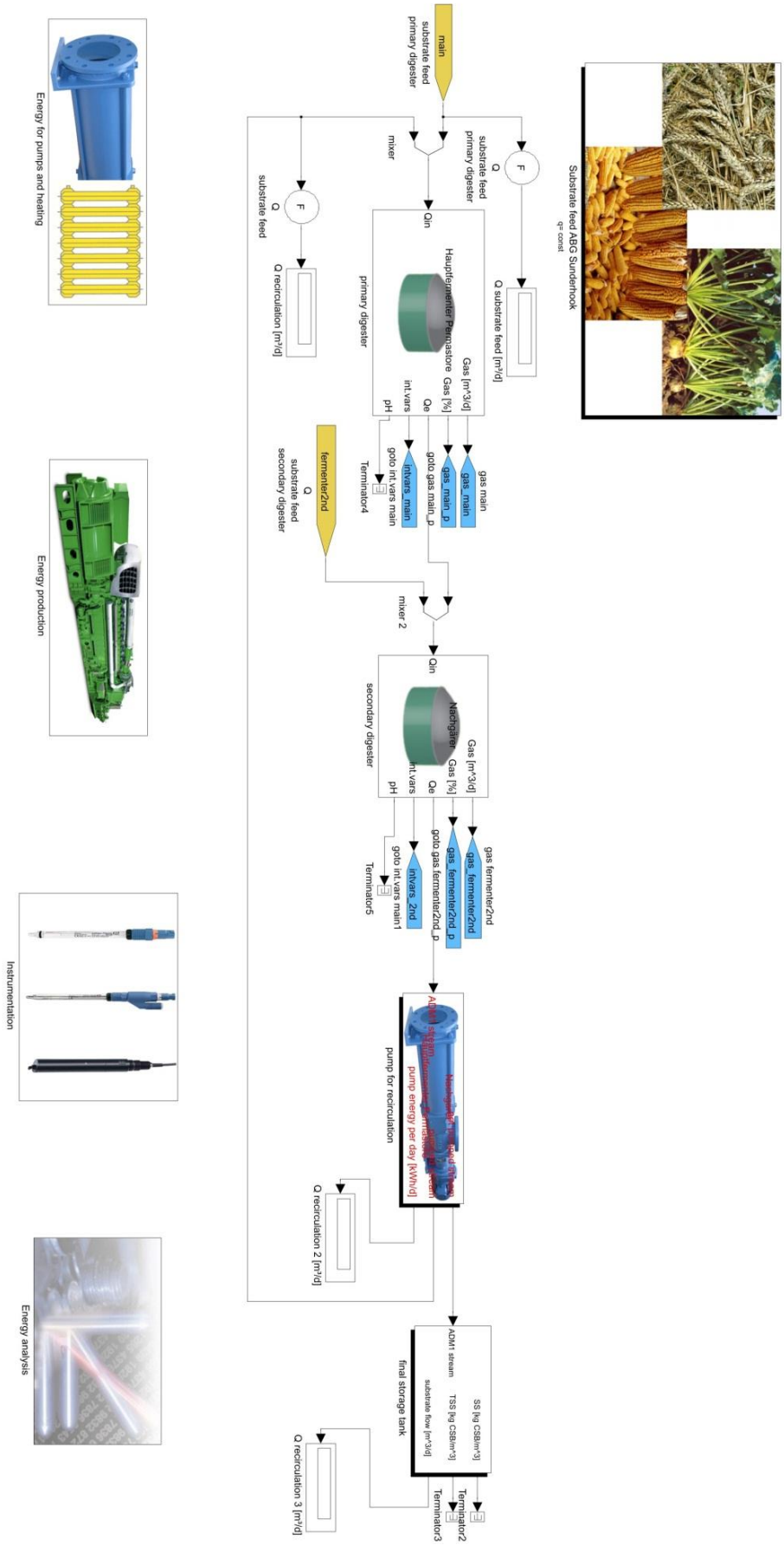

Figure 3-5: Matlab implementation of the simulation model of the Sunderhook ABP based on the ADM1

3.3.2 Calibration of the Sunderhook ABP simulation model

As a proper calibration of the simulation model is needed to allow for good and valid optimization results, two aspects need to be considered for model calibration: (1) substrate characterization, and, (2) adaptation of kinetic model parameters.

3.3.2.1 Substrate characterization

Substrate characterization for the ADM1 requires the determination of degradable and non-degradable COD fractions which were previously described in Figure 3-1 and Table 3-3. Unfortunately, the measurement of the total COD_{tot} is difficult (Buffière *et al.* 2006). One the one hand, online measurement of COD_{tot} is costly and highly inaccurate due to the high *TS* content of the substrates; and on the other side laboratory analysis requires extensive homogenization of the substrate to obtain representative results. Thus, alternatives are required, which allow a calculation of the needed COD_{tot} and its degradable and non-degradable fractions based on standard analytical substrate parameters. Such an alternative was presented by Koch *et al.* (2009) who calculated the $ThCOD$ based on the extended Weender analysis (Basler 1976). The Weender analysis thoroughly analyses the degradable and non-degradable VS fractions by dividing VS into raw protein (RP), raw lipid (RL) as well as carbohydrates consisting of the sum of raw fibre (RF) and nitrogen free extracts (NfE). The carbohydrates are then subdivided into starch which is calculated carbohydrates minus neutral detergent fibres (NDF), cellulose consisting of acid detergent fibre (ADF) minus acid detergent lignin (ADL) as well as hemicellulose ($NDF - ADF$) and lignin (ADL) (Figure 3-6).

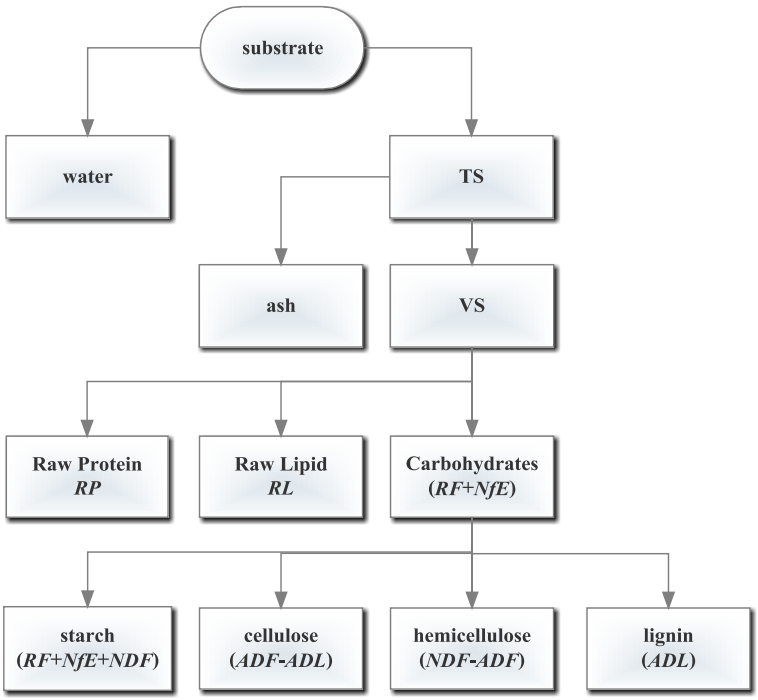

Figure 3-6: Substrate characterization by extended Weender analysis from Koch et al. (2010)

The advantage of the Weender analysis is that the COD-based fractions for proteins, lipids and carbohydrates of the ADM1 can be easily and accurately determined. Thus, the total amount of degradable substrate X_C can be calculated based on Weender fractions, TS, substrate density ρ_s and $ThCOD$ of proteins, lipids, carbohydrates and lignin.

$$X_C = \rho_s TS \begin{pmatrix} RP \cdot ThCOD_{pr} + RL \cdot ThCOD_{li} + \\ (RF + NfE - ADL) ThCOD_{ch} + ADL \cdot ThCOD_I \end{pmatrix} \quad \left[kg_{COD} m^{-3} \right] \text{ (Koch } et\ al. \text{ 2010)} \quad (3.54)$$

The $ThCOD$ of the four fractions of (3.54) is calculated based on the basic chemical formulas of proteins ($C_5H_7O_2N$), lipids ($C_{57}H_{104}O_6$), carbohydrates ($(C_6H_{10}O_5)_n$) and lignin ($C_{11}H_{14}O_6$) as defined by Angelidaki and Sanders (2004) and Koch *et al.* (2010). The formula for the $ThCOD$ developed by Koch *et al.* (2010) is given below.

$$ThCOD = \frac{16(2a + 0.5(b - 3d) - c)}{12a + b + 16c + 14d} \left[\frac{g_{O_2}}{g_{C_aH_bO_cN_d}} \right] \quad (3.55)$$

To calculate the COD fractions X_{pr}, X_{li} and X_{ch} from X_C, constant values determining the percentages of proteins ($f_{pr,xc}$), lipids ($f_{li,xc}$) and carbohydrates ($f_{ch,xc}$) are defined based on the ratios of the respective Weender parameters and the VS concentration in the substrate. The lignin fraction of X_C is considered to be completely inert and thus added to X_I.

$$\begin{aligned} f_{pr,xc} &= \frac{RP}{VS} \\ f_{li,xc} &= \frac{RL}{VS} \\ f_{ch,xc} &= \frac{RF + NfE - ADL}{VS} \end{aligned} \quad (3.56)$$

In the case of the simulation model of the Sunderhook ABP, results from the Weender analysis and actual COD laboratory analysis from each substrate were used to achieve a comprehensive level of substrate characterization and to validate $ThCOD$ and actual COD concentrations of the substrate. Overall, seven substrates which are or were used at the Sunderhook ABP were characterized. These substrates are maize, bull manure, green rye, grass silage, oat, bull manure (solid phase) and silo juice from the drive-in silos. In addition to all biological and physico-chemical substrate parameters, the market price of the substrate was also considered within the simulation model. Although not necessary for the simulation itself, it is important for the optimization of the substrate feed of the Sunderhook ABP as it may be more economical to replace costly substrates with cheaper ones.

Table 3-10: Substrate parameters used for substrate characterization of the Sunderhook ABP simulation model

	maize	bull manure	green rye	grass silage	oat	bull manure (solid phase)	silo sugar juice
pH value	3.8	7.2	4.5	4.08	4	8.8	3.8
COD [g/l]	375	35	144	117.3	100	91.6	312.3
COD filtered [g/l]	112.5	27.3	50.4	29.3	30	37.6	296.7
NH_4-N [g/l]	0.2	1.7	1.71	0.28	1.2	1.3	0.5
TS [%]	25.2	8.9	24.03	22.6	34	14.3	5.1
VS/TS [%]	93.2	82.4	93.2	88.7	80.7	85.8	83.6
Temperature [°C]	20	24	18	18	18	24	20
Density [g/m³]	937,000	900,000	951,610	844,134	864,000	950,000	950,000
Acetic acid [mg/l]	2.2	4.5	1	1	1	1	2.2
Propionic acid [mg/l]	4	2.3	0.5	0.5	0.5	0.5	4
Butanoic acid [mg/l]	1	0.2	0.1	0.1	0.1	0.1	1
Alkalinity [mol/m³]	2	2	5	5	5	2	5
RP [g/kg]	87	122	107	158.9	112	24	87
RF [g/kg]	181	177.9	374	281.6	102	57	181
RL [g/kg]	24	43	20	36.6	45	13	24
Price [€/m³]	40	9.31	30	25.43	10	7	0

3.3.2.2 Adaptation of kinetic model parameters

Following a proper substrate characterization, model parameters need to be adapted for each simulation model of a full-scale ABP to adjust for the specific biological activity of each AD process. Due to the high number of model parameters included in the ADM1, model calibration is time-consuming and complex. Furthermore, values of many sensitive model parameters range over several orders of magnitude which makes model calibration even harder (see Table 3-11). The approach developed by Wichern *et al.* (2009) offers an alternative to extensive model calibration. The results of a sensitivity analysis show that in particular the disintegration rate k_{dis}, hydrolysis parameters $k_{hyd,pr}$, $k_{hyd,li}$ and $k_{hyd,ch}$ as well as the Monod maximum specific uptake rates for propionate acetogenesis ($k_{m,pro}$) and aceticlastic methanogenesis ($k_{m,ac}$) are sensitive model parameters. Thus, these parameters were optimized during model calibration. Furthermore, the yield uptake rates for sugars (Y_{su}), amino acids (Y_{aa}) and acetate (Y_{ac}) were slightly changed to improve model performance. The adaptation of the ADM1 model parameters was performed based on literature values and manual optimization within the ranges given in Table 3-11. The following table (Table 3-11) shows the calibrated ADM1 model parameters and their range as given by Batstone *et al.* (2002).

Table 3-11: Kinetic model parameters after calibration and their range as defined by Batstone *et al.* (2002)

kinetic model parameters	value after calibration	min – literature value	max – literature value
$k_{dis}\ [d^{-1}]$	0.25	0.0041	1
$k_{hyd,pr}\ [d^{-1}]$	10	0.2	10
$k_{hyd,li}\ [d^{-1}]$	10	0.1	10
$k_{hyd,ch}\ [d^{-1}]$	10	0.25	10
$k_{m,pro}$ $[COD \cdot COD^{-1} d^{-1}]$	4	0.16	141
$k_{m,ac}$ $[COD \cdot COD^{-1} d^{-1}]$	3.85	0.14	52
$Y_{su}\ [COD_X COD_S^{-1}]$	0.1	0.1	0.17
$Y_{aa}\ [COD_X COD_S^{-1}]$	0.08	0.058	0.15
$Y_{ac}\ [COD_X COD_S^{-1}]$	0.05	0.025	0.076

3.3.3 Calibration results

The overall goal of the calibration of the Sunderhook ABP model was to perform model calibration based on online measurements that are commonly available at most ABPs to achieve high practicability. Therefore, the online measurement parameters total biogas production (Q_{biogas}), methane concentration of the biogas (CH_4) and total electricity production (P_{el}) were used for model calibration. To properly evaluate model performance, the mean absolute percentage error (MAPE) and the root mean square percentage error (RMSPE) were calculated between the simulated and measured values. Due to the high order of magnitude of Q_{biogas} and P_{el}, these percentage based errors were preferred over the MAE and RMSE methods.

$$MAPE = \frac{100\%}{N} \sum_{n=1}^{N} \left| \frac{m_n - s_n}{s_n} \right| \tag{3.57}$$

$$RMSPE = \sqrt{\frac{1}{N} \sum_{n=1}^{N} \left(\left| \frac{m_n - s_n}{s_n} \right| 100\% \right)^2}\ , \tag{3.58}$$

where m_n and s_n denote the measured and simulated parameter values, respectively.

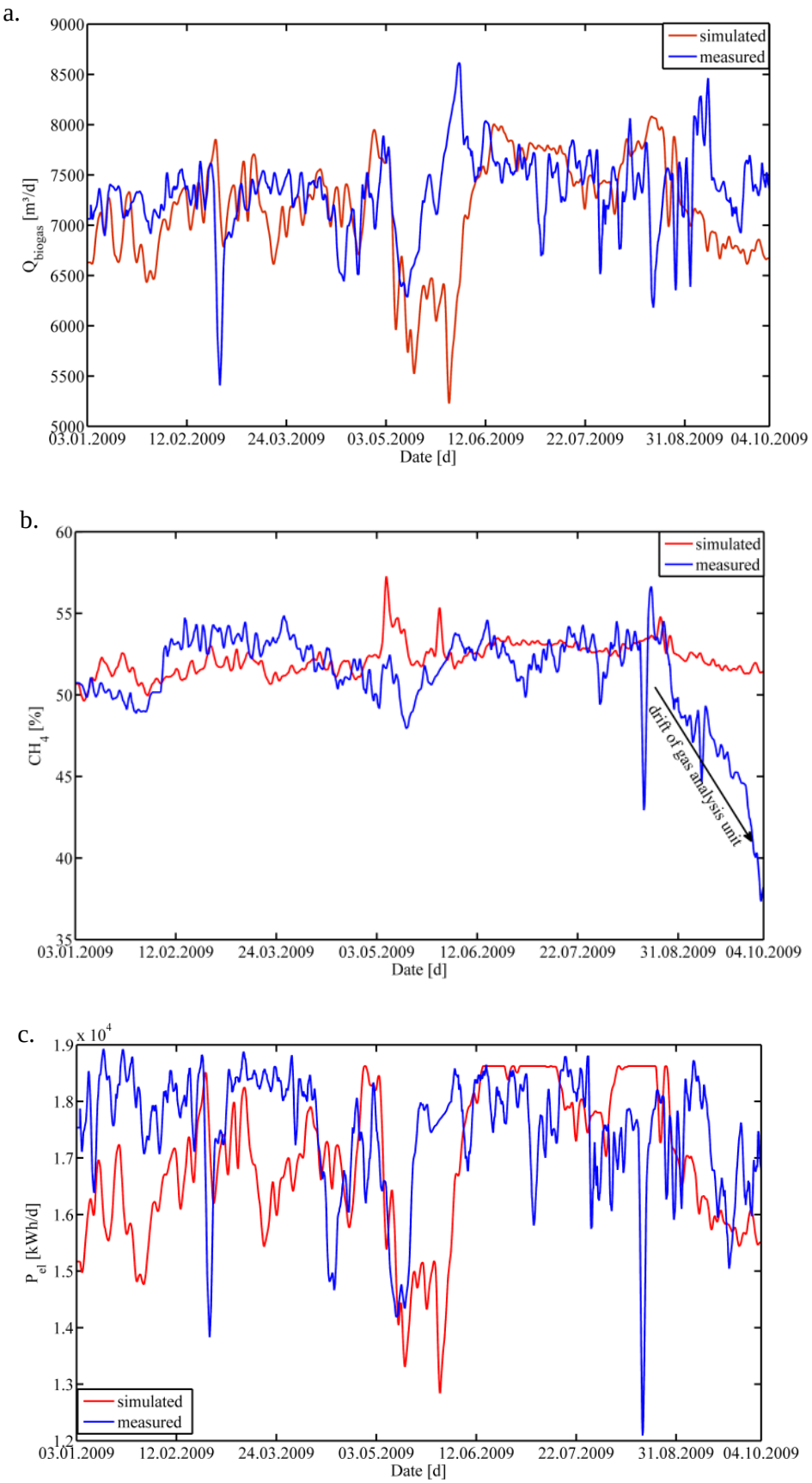

Figure 3-7: Model performance of the Sunderhook ABP simulation model

Figure 3-7 shows the comparison of simulated and measured process parameters during the complete nine month calibration period. It is obvious that measured and simulated values are similar but still differ significantly from each other from time to time. The main issue of simulation model validation against full-scale plant data becomes clear. It is a fact that some disturbances occurring at full-scale plants cannot be captured with a simulation model as a simulation model is always a compromise between model complexity and practicability. The main disturbances are caused by measurement errors of the online-measurement systems and variations in quality of the input substrates. Theses quality changes occur due to rain which strongly affects the *TS* content of maize in the silo and different degrees of ensiling throughout the whole silo. Due to the relatively low number of substrate laboratory analysis once a month or even every two months, these changes in substrate characteristics cannot be detected. Therefore, many periods of the whole calibration period were not considered for the evaluation of the Sunderhook ABP simulation model. A region, where measurement data quality was good due to low drift and regular maintenance was used to evaluate model performance using the aforementioned performance measures. In this region, which spanned from April 2009 to mid-May 2009, a good agreement was achieved between simulated and measured data was achieved.

The percentage error measures prove that the error is well within the acceptance range with values between four and seven percent, which is why calibration of the Sunderhook ABP simulation model is considered to be accurate and practicable enough to be used for the substrate feed optimization of biogas plants. In general, errors below 10% for a simulation model based on measurement data from a full-scale ABP are considered to be acceptable for use with optimization and control methods.

Table 3-12: MAPE and RMSPE errors for the comparison of simulated and measured process data

Process parameter	MAPE [%]	RMSPE [%]
Q_{biogas}	6.4	7.1
P_{el}	7.5	7.1
CH_4	4.0	4.8

3.4 Conclusion on the modeling and simulation of ABPs

This chapter about modeling and simulation of biogas plants presented the basis for the simulation based optimization of biogas plants by (1) describing the history of AD process modeling and its applications, (2) giving a full description of the ADM1, which will be used for substrate feed optimization in chapter 5, and, (3) providing an example for modeling and calibration of a full-scale ABP.

These contributions illustrate that modeling and simulation of AD processes is common for lab-scale applications but very rare for full-scale AD plants. The main reason for this is high model complexity due to many biochemical reactions and even more model coefficients and kinetic parameters. This makes model design, substrate characterization and model calibration extremely difficult. Therefore, manageable methods for model design and calibration are needed, which were presented in section 3.3. The biogas toolbox developed by the Cologne University of Applied Sciences (Gaida *et al.* 2011) facilitates model design and simulation by the centralized configuration of the complete ABP using several GUIs for substrate feed characterization and plant design.

Furthermore, calibration of AD models, requiring proper substrate characterization and adaptation of kinetic model parameters, was explained in detail in sections 3.3.2 and 3.3.3. A fairly new method for substrate characterization by Koch *et al.* (2010) was implemented, which uses substrate parameters that are commonly measured together with the extended Weender analysis. Thus, complex laboratory analysis can be reduced to a minimum, which not only reduces costs but also allows easier and faster substrate characterization for ABP modeling and simulation. The adaptation of kinetic model parameters was performed based on ADM1 standard parameters and literature values based on experiments and experience with ABP modeling.

The overall calibration results show that sufficient agreement between simulation and measured process parameters was achieved, so that the Sunderhook ABP simulation model can be used for optimization purposes in combination with advanced CI and surrogate modeling methods. Nevertheless, the issues involved with modeling and simulation of full-scale ABPs became clear in the calibration results presented in section 3.3.3. Thus, in this case, perfect calibration of simulation models is very hard to achieve as full-scale plant operation is affected by many different kinds of disturbances and the degree of instrumentation and accuracy of online measurement values is normally low. Therefore, simulation model design and calibration always needs to be a compromise between accuracy and practicability.

References

Abu Qdais, H., Bani Hani, K. and Shatnawi, N., 2010. Modeling and optimization of biogas production from a waste digester using artificial neural network and genetic algorithm. *Resources, Conservation and Recycling*, 54 (6), 359–363.

American Public Health Association, 1981. Standard methods for the examination of water and wastewater. 15th ed. Washington: American Public Health Association.

Andrews, J.F., 1969. A Dynamic Model of the Anaerobic Digestion Process. *Journal of the Sanitary Engineering Division*, 1, 95–116.

Angelidaki, I. and Sanders, W., 2004. Assessment of the anaerobic biodegradability of macropollutants. *Reviews in Environmental Science & Bio/Technology*, 3 (2), 117–129.

Bassler, R., 1976. *Die chemische Untersuchung von Futtermitteln*. The chemical examination of animal feed. 3rd ed. Darmstadt: VDLUFA-Verl.

Batstone, D.J., Keller, J., Angelidaki, I., Kalyuzhnyi, S.V., Pavlostathis, S.G., Rozzi, A., Sanders, W.T.M., Siegrist, H., and Vavilin, V.A., 2002. *Anaerobic Digestion Model No. 1 (ADM 1): Scientific and technical Report No. 13*. London: IWA.

Batstone, D.J., 2006. Mathematical Modelling of Anaerobic Reactors Treating Domestic Wastewater: Rational Criteria for Model Use. *Reviews in Environmental Science and Bio/Technology*, 5 (1), 57–71.

Blumensaat, F. and Keller, J., 2005. Modelling of two-stage anaerobic digestion using the IWA Anaerobic Digestion Model No. 1 (ADM1). *Water Research*, 39 (1), 171–183.

Briggs, G.E. and Haldane, J.B., 1925. A Note on the Kinetics of Enzyme Action. *Biochem. J.*, 19 (2), 338–339.

Brus, L., 2005. Nonlinear identification of an anaerobic digestion process. *Proceedings of the 2005 IEEE conference on control applications*, 137–142.

Buffiere, P., Loisel, D., Bernet, N. and Delgenes, J.-P., 2006. Towards new indicators for the prediction of solid waste anaerobic digestion properties. *Water Science & Technology*, 53 (8), 233.

Cakmakci, M., 2007. Adaptive neuro-fuzzy modelling of anaerobic digestion of primary sedimentation sludge. *Bioprocess and Biosystems Engineering*, 30 (5), 349–357.

Eastman, J.A. and Ferguson, J.F., 1981. Solubilization of particulate organic carbon during the acid phase of anaerobic digestion. *Journal of the Water Pollution Control Federation*, 53 (3), 352–366.

References

Gaida, D., Wolf, C., Bongards, M. and Bäck, T., 2011. MATLAB Toolbox for Biogas Plant Modelling and Optimization. *International Conference Progress in Biogas II - Biogas production from agricultural biomass and organic residues*, 67–70.

Galí, A., Benabdallah, T., Astals, S. and Mata-Alvarez, J., 2009. Modified version of ADM1 model for agro-waste application. *Bioresource Technology*, 100 (11), 2783–2790.

Gavala, H.N., Angelidaki, I. and Ahring, B.K., 2003. Kinetics and modeling of anaerobic digestion process. *Advances in biochemical engineering/biotechnology*, 81, 57–93.

Graef, S.P. and Andrews, J.F., 1974. Stability and control of anaerobic digestion. *Journal of the Water Pollution Control Federation*, 46 (4), 666–683.

Henze, M., 2000. *Activated sludge models ASM1, ASM2, ASM2d and ASM3*. London: IWA Pub.

Hill, D.T. and Barth, C.L., 1977. A dynamic model for simulation of animal waste digestion. *Journal of the Water Pollution Control Federation*, 49 (10), 2129–2143.

Jeppsson, U., Pons, M.-N., Nopens, I., Alex, J., Copp, J., Gernaey, K., Rosen, C., Steyer, J.-P. and Vanrolleghem, P., 2007. Benchmark simulation model no 2: general protocol and exploratory case studies. *Water Science & Technology*, 56 (8), 67.

Keshtkar, A.R., Abolhamd, G., Meysssami, B. and Ghanforian, H., 2003. Modeling of Anaerobic Digestion of Complex Substrates. *Iranian Journal of Chemistry & Chemical Engineering*, 22 (2), 61–74.

Koch, K., Lübken, M., Gehring, T., Wichern, M. and Horn, H., 2010. Biogas from grass silage – Measurements and modeling with ADM1. *Bioresource Technology*, 101 (21), 8158–8165.

Levenspiel, O., 1962. Mixed models to represent flow of fluids through vessels. *The Canadian Journal of Chemical Engineering*, 40 (4), 135–138.

Massé, D. and Droste, R.L., 2000. Comprehensive model of anaerobic digestion of swine manure slurry in a sequencing batch reactor. *Water Research*, 34 (12), 3087–3106.

Monod, J., 1949. The Growth of Bacterial Cultures. *Annual Review of Microbiology*, 3 (1), 371–394.

Nash, J. and Sutcliffe, J., 1970. River flow forecasting through conceptual models part I — A discussion of principles. *Journal of Hydrology*, 10 (3), 282–290.

Ogunnaike, B.A. and Ray, W.H., 1994. *Process dynamics, modeling, and control*. New York, NY: Oxford University Press.

Ozkaya, B., Demir, A. and Bilgili, M., 2007. Neural network prediction model for the methane fraction in biogas from field-scale landfill bioreactors. *Environmental Modelling & Software*, 22 (6), 815–822.

Eugene E. Peterson, 1965. Chemical reaction analysis. AIChE Journal, 11 (5), 770–955.

Rosen, C., Vrecko, D., Gernaey, K., Pons, M. and Jeppsson, U., 2006. Implementing ADM1 for plant-wide benchmark simulations in Matlab/Simulink. *Water Science & Technology*, 54 (4), 11.

Sarti, A., Foresti, E. and Zaiat, M., 2004. Evaluation of a mechanistic mathematical model of a packed-bed anaerobic reactor treating wastewater. *Latin American Applied Research*, 34 (2), 127–132.

Shimizu, T., Kudo, K. and Nasu, Y., 1993. Anaerobic waste-activated sludge digestion-a bioconversion mechanism and kinetic model. *Biotechnology and Bioengineering*, 41 (11), 1082–1091.

Siegrist, H., Renggli, D. and Gujer, W., 1993. Mathematical modeling of anaerobic mesophilic sewage sludge treatment. *Water Science & Technology*, 27 (2), 25–36.

Siegrist, H., Vogt, D., Garcia-Heras, J.L. and Gujer, W., 2002. Mathematical Model for Meso- and Thermophilic Anaerobic Sewage Sludge Digestion. *Environmental Science & Technology*, 36 (5), 1113–1123.

Sötemann, S.W., Ristow, N.E., Wentzel, M.C. and Ekama, G.A., 2005. A steady state model for anaerobic digestion of sewage sludges. *Water SA*, 31 (4), 511–528.

Sötemann, S.W., van Rensburg, P., Ristow, N.E., Wentzel, M.C., Loewenthal, R.E. and Ekama, G.A., 2005. Integrated chemical/physical and biological processes modeling Part 2 - Anaerobic digestion of sewage sludges. *Water SA*, 31 (4), 545–550.

Strik, D.P., Domnanovich, A.M., Zani, L., Braun, R. and Holubar, P., 2005. Prediction of trace compounds in biogas from anaerobic digestion using the MATLAB Neural Network Toolbox. *Environmental Modelling & Software*, 20 (6), 803–810.

Vavilin, V., Vasiliev, V., Ponomarev, A. and Rytow, S., 1994. Simulation model 'methane' as a tool for effective biogas production during anaerobic conversion of complex organic matter. *Bioresource Technology*, 48 (1), 1–8.

Vavilin, V.A., Lokshina, L.Y. and Rytov, S.V., 2000. The <methane> simulation model as the first generic user-friend model of anaerobic digestion. *Vestnik Moskovskogo Universiteta. Khimiya*, 41 (6), 22–26.

References

Wett, B., Eladawy, A. and Ogurek, M., 2006. Description of nitrogen incorporation and release in ADM1. *Water Science & Technology*, 54 (4), 67.

Wichern, M., Gehring, T., Fischer, K., Andrade, D., Lübken, M., Koch, K., Gronauer, A. and Horn, H., 2009. Monofermentation of grass silage under mesophilic conditions: Measurements and mathematical modeling with ADM 1. *Bioresource Technology*, 100 (4), 1675–1681.

Zaher, U., Li, R., Jeppsson, U., Steyer, J.-P. and Chen, S., 2009. GISCOD: General Integrated Solid Waste Co-Digestion model. *Water Research*, 43 (10), 2717–2727.

4 Optimization methodology

The optimization of industrial processes, component designs and simulation models is often very complex and time-consuming, in particular, if these optimization problems are of high dimensionality and nonlinear (Simpson *et. al* 2001, Huang *et. al* 2006). Nevertheless, optimization is necessary and widely applied to tap the full potential of industrial processes, to choose optimal design parameters and to calibrate and optimize simulation parameters (Yusup *et. al* 2012, Chandra Mohan and Baskaran 2012). Unfortunately, in most real-world engineering applications the limiting factor for the application of existing optimization methods is the evaluation of so-called cost or fitness functions, which is computationally intensive (Jin *et. al* 2001). These fitness functions typically involve complex engineering simulations from full-scale processes or designs, for example CAD (Computer Aided Design) models of cars, planes and computer chips or detailed dynamic simulation models of process plants such as refineries, wastewater treatment plants and biogas plants. These engineering simulations are often slow and take from several seconds up to several hours to complete for a given set of parameters, which makes an optimization using such simulation models in a fitness function very inefficient.

This means, that given a fitness function $J(\boldsymbol{x})$, which is computationally expensive and where $\boldsymbol{x}$ is the set of parameters to be optimized, the common approach is to seek to estimate $J(\boldsymbol{x})$ with a surrogate model $\hat{J}(\boldsymbol{x})$, estimated on set samples of $[\boldsymbol{x}, J(\boldsymbol{x})]$, where $\hat{J}(\boldsymbol{x})$ is efficient to compute once estimated. These surrogate models $\hat{J}$ are also often called metamodels and there exists a wide variety of different methods to build these models. The main advantage of using metamodels is their short execution time in comparison to the true fitness function J.

When it comes to the optimization of biogas plants, the optimization problem is very similar. The overall goal is to optimize the substrate feed to biogas plants in order to tap their full potential in terms of biogas/energy production, biogas quality and costs. To do this, a dynamic nonlinear simulation model of a biogas plant, which uses the previously explained ADM1, is used to evaluate plant performance for different substrate combinations and compositions. Due to its complexity, an optimization of the substrate feed using the true fitness function, which involves computing the ADM1 simulation model, is very time-consuming and takes from several hours to several days depending on the design parameters of the optimization method and the number of substrates that need to be optimized. To speed up the optimization process two novel and similar global optimization methods using sequential Kriging surrogate models (S-KSM) and Particle Swarm Optimization (PSO) (Clerc 2006) were developed and are introduced in this chapter.

Over all, there are two major contributions in this chapter:

1. The development of two novel Kriging based global optimization methods and
2. an evaluation of the performance of these two methods relative to the original PSO algorithm on four test problems.

The outline of this chapter is as follows. Section 1 gives a short survey of existing and frequently used metamodeling methods and then focuses on the Kriging approximation, which was chosen as the metamodeling method in this work. The PSO optimization method and the selection of its parameters are explained in Section 2. Section 3 then introduces two novel optimization methods using PSO and two different methods to sequentially update the Kriging surrogate model. Method I uses **l**atin **h**ypercube (LH) sampling to update the Kriging model (LH-based S-KSM) and method II uses a separate PSO to update the Kriging model with new positions of the PSO particles (PSO-based S-KSM). The last section investigates the performance of the two novel optimization methods on four test problems and compares the results to conventional PSO optimization.

4.1 Kriging approximation

Kriging as a method for approximation was developed by the engineer Danie G. Krige from South Africa in the early 1950s but it was not published until a few years later by Matheron (1963) who mathematically formulated the method. Further descriptions of Kriging were given by Sacks *et. al* (1989) and Booker *et. al* (1998).

Nevertheless, Kriging is just one of the possible methods for metamodeling. The most common are:

- Polynomial Regression (PR) (Stigler 1974)
- Response Surface Methodology (RSM) (Myers and Montgomery 1995, Box *et. al* 2005)
- Kriging (see above)
- Artificial Neural Networks (ANN) (Smith 1993, Cheng and Titterington 1994)
- Multivariate Adaptive Regression Splines (MARS) (Friedmann 1991)
- Radial Basis Function Approximations (RBFA) (Hardy 1971, Dyn *et. al* 1986)

In this case Kriging was chosen because a good metamodel can be achieved even with a small amount of data samples and because it is known to deliver good results for nonlinear problems (Jin *et. al* 2001, Simpson *et. al* 2001). This does not mean that the other methods are worse than Kriging for the construction of metamodels. In general optimization using a surrogate model, which is introduced in section 4.3, is just as valid with the use of any of the other methods as it is with Kriging. As such, the novel contributions in this chapter relate specifically to the method of generating new data samples to update the metamodels.

4.1.1 Literature review on Kriging

Although developed in the early 1960s, it was relatively late before Kriging was used for the construction of metamodels for real-world engineering applications. One of the first papers on the application of ordinary Kriging is from Currin *et. al* (1988), who used a Bayesian approach. Later on Kriging was used for many engineering applications (Martin and Simpson 2003, 2005). For example, Gao and Wang (2008) used a Kriging model to minimize warpage deformations in injection molding and Kim and Shin (2008) optimized the shape of a staggered dimpled surface to enhance turbulent heat transfer in a rectangular channel. Other applications include aerostructural design optimization (Lam *et. al* 2009), prediction of NO_x concentration in an air quality monitoring network (Kassteele *et. al* 2009), aerodynamic design of a low pressure turbine exhaust hood (Wang *et. al* 2010) and robust design of a bearingless rotation motor (Seo *et. al* 2011).

In addition to the mere direct application of Kriging to engineering applications, Kriging has also been benchmarked against other metamodeling methods and it has been further adapted to enhance surrogate model performance. Lefèbvre *et. al* (1996) investigated the use of Kriging for two test cases from the field of electromagnetics. The results showed that an adequate prediction and estimation of model accuracy is possible with Kriging, although the Kriging model does not have any kind of phenomenological background. Furthermore, it was shown that the parameter θ of the correlation function (introduced later) is one of the most important parameters when it comes to achieving good model accuracy. In case of a small θ the sample points are not linked to each other, whereas a large θ closely links the values of the sample points resulting in a very smooth interpolation. This effect has been intensively investigated by Armstrong and Wackernagel (1988) and Simpson *et. al* (2001) and eventually confirmed by Lin *et. al* (2004). Lefèbvre used a constant regression model and a gaussian covariance function. One of the first comprehensive comparative studies of different metamodeling methods was performed by Jin et. al (2001). In total four metamodeling methods were investigated, namely PR, Kriging, MARS and RBFA. The most important influencing factors were found to be nonlinearity and dimensionality of the underlying simulation as well as the data sampling technique used to choose the sample points for the metamodel and the internal parameter settings of the respective metamodeling method. Kriging was found to be best for large-scale and low order nonlinear problems, although some disadvantages of Kriging are mentioned as well. In general, metamodel construction is time-consuming in the case of high sample numbers and high dimensionality of the underlying simulation, which was also proven by Gano *et. al* (2006). A direct comparison of RSM and Kriging made by Simpson *et. al* (2001) and Jin et. al (2003) shows that both methods deliver similar results. They are both well-suited for deterministic simulations and problems with high dimensionality, though Kriging cannot handle problems with more than 50 variables. A good review of all the applications of Kriging metamodels and the common issues in implementation and use are presented by Kleijnen (2009). In Kleijnen's paper the well-known Kriging Matlab toolbox DACE

developed by Lophaven *et. al* (2002) is used to build Kriging metamodels. The same toolbox is used for Kriging metamodels in the following sections. One important aspect of the DACE toolbox is the fact that it requires lower and upper limits to be defined for θ the covariance function parameters, which have proven to be difficult to specify in practice (Kleijnen 2009).

Due to the rapidly increasing computation time of Kriging models in relation to the number of samples, Sequential Kriging Metamodels (SKM) were introduced by Sasena *et. al* (2002), Huang (2006) and Gano (2006). The advantage of these SKM-methods is that model accuracy can be substantially improved without significantly increasing the computation time of the Kriging model. Sasena *et. al* (2002) introduced a novel algorithm called Efficient Global Optimization (EGO) that uses kriging metamodels. Several sampling criteria to update the Kriging model are reviewed. The results show, that the sampling criterion for each Kriging model update has a strong influence on how efficiently and accurately EGO locates the optimum. EGO was then further developed by Huang (2006), who used a novel function to estimate the expected improvement of the metamodel for new sample points. It is clearly stated that SKM, are in general only suitable for expensive engineering simulations and if small sample numbers are used. The maximum number of dimensions tried by Huang (2006) is ten. Two other sequential update strategies for Kriging metamodels were developed by Gano (2006) who introduced a so-called Trust Region and likelihood ratio Metamodel Update Management Scheme (TR-MUMS and L-MUMS). These update strategies determine whether a new calculation of the Kriging model parameters is necessary or not, based on the ratio of likelihood values or the trust region ratio. Thus, Kriging model parameters are only updated if absolutely necessary, eventually resulting in significant savings in computation time.

All in all, it can be stated that Kriging has been used as a metamodel for the optimization of many engineering and design applications over the last decade. In particular, Kriging was compared to many other metamodel methods and has proven itself due to its good accuracy for small sample numbers and highly nonlinear problems. The development of SKM methods addresses the main issue of relatively high computation times compared to other metamodeling methods and is a valid approach for the optimization of problems with high complexity that are extremely computationally intensive.

4.1.2 Background and formulation of the Kriging approximation

Kriging builds a metamodel for an underlying true model based on a set of input/output data samples from this model. Denoting $\mathbf{X} = [\boldsymbol{x}^1 \cdots \boldsymbol{x}^m]^{\mathrm{T}}$ with $\boldsymbol{x}^i \in \mathbb{R}^n$ as the input sample values and $\mathbf{Y} = [\boldsymbol{y}^1 \cdots \boldsymbol{y}^m]^{\mathrm{T}}$ with $\boldsymbol{y}^i \in \mathbb{R}^q$ as the corresponding output values, the aim is to estimate a model $\hat{y}$ using this data, which represents the deterministic response of the true model $\boldsymbol{y}(\boldsymbol{x}) \in \mathbb{R}^q$ for an n dimensional input vector $\boldsymbol{x} \in D \subseteq \mathbb{R}^n$. In the particular case of using Kriging for optimization purposes the true model is equal to the previously defined true fitness function J.

The idea behind Kriging is that such a model $\hat{y}$ can be realized as combination of a regression function $F(\boldsymbol{\beta}, \boldsymbol{x})$, where $\boldsymbol{\beta}$ is a vector of regression coefficients, and a stochastic Gaussian process $Z(\boldsymbol{x})$

$$\hat{\boldsymbol{y}}(\boldsymbol{x}) = F(\boldsymbol{\beta}, \boldsymbol{x}) + Z(\boldsymbol{x}) \tag{4.1}$$

Furthermore, Z is assumed to have mean zero and covariance

$$Cov[Z(\boldsymbol{x}^i), Z(\boldsymbol{x}^j)] = \sigma^2 \mathbf{R}[R(\boldsymbol{\theta}, \boldsymbol{x}^i, \boldsymbol{x}^j)], \tag{4.2}$$

where $\mathbf{R}$ is the correlation matrix and $R(\boldsymbol{\theta}, \boldsymbol{x}^i, \boldsymbol{x}^j)$ is the correlation model selected by the user with parameters $\boldsymbol{\theta}$. i and j running from 1 to m representing the number of sample data points. $\mathbf{R}$ is always symmetric and possesses unit values along the diagonal. For both, the regression and the Gaussian process functions one can choose between several functions with different characteristics. In the case of the regression function, which is an underlying global trend function, the following functions (4.3, 4.4, 4.5) are most commonly selected.

Constant: $F(\boldsymbol{\beta}, \boldsymbol{x}) = \beta$, where β is a constant value (4.3)

Linear: $F(\boldsymbol{\beta}, \boldsymbol{x}) = \beta_1 + \beta_2 x_1 + \cdots + \beta_{n+1} x_n$ (4.4)

Quadratic: $F(\boldsymbol{\beta}, \boldsymbol{x}) = \beta_1 + \beta_2 x_1^2 + \beta_3 x_1 x_2 + \beta_4 x_2 x_1 + \beta_5 x_2^2 \cdots + \beta_{\frac{1}{2}(n+1)(n+2)+1} x_n^2$ (4.5)

The correlation model can be likewise represented by different correlation functions of the form

$$R(\boldsymbol{\theta}, \boldsymbol{x}^i, \boldsymbol{x}^j) = \prod_{r=1}^{n} R_r(\theta_r, x_r^i - x_r^j) \tag{4.6}$$

Commonly used correlation functions are

Linear: $R(\boldsymbol{\theta}, \boldsymbol{x}^i, \boldsymbol{x}^j) = \prod_{r=1}^{n} \max\left\{0, 1 - \theta_r \left| x_r^i - x_r^j \right|\right\}$ with $i, j = 1, \ldots, m$ (4.7)

Exponential: $R(\boldsymbol{\theta}, \boldsymbol{x}^i, \boldsymbol{x}^j) = \prod_{r=1}^{n} e^{-\theta_r \left| x_r^i - x_r^j \right|}$ with $i, j = 1, \ldots, m$ (4.8)

Gaussian: $R(\boldsymbol{\theta}, \boldsymbol{x}^i, \boldsymbol{x}^j) = \prod_{r=1}^{n} e^{-\theta_r \left(x_r^i - x_r^j \right)^2}$ with $i, j = 1, \ldots, m$ (4.9)

The estimates $\hat{\boldsymbol{y}}(\boldsymbol{x})$ for the true model values $\boldsymbol{y}(\boldsymbol{x})$ at new values of $\boldsymbol{x}$ are predicted by the Kriging model and the mean squared error (MSE) between estimates and true model is calculated as

$$MSE = \mathrm{E}\left[\left(\boldsymbol{y}(\boldsymbol{x}) - \hat{\boldsymbol{y}}(\boldsymbol{x}) \right)^2 \right]. \tag{4.10}$$

A minimization of the MSE over the samples gives the so-called Kriging predictor, which is

$$\hat{\boldsymbol{y}} = \boldsymbol{c}\hat{\beta} + \boldsymbol{r}^{\mathrm{T}}(\boldsymbol{x})\mathbf{R}^{-1}(\boldsymbol{y} - \boldsymbol{c}\hat{\beta}) \tag{4.11}$$

in case of a constant regression function, where $\hat{\beta}$ is a constant. Furthermore, $\boldsymbol{y}$ is the vector of responses to the true model samples $\boldsymbol{x}^i$ for i=1,…, m and $\boldsymbol{c}$ is a constant vector of all ones with length m. $\boldsymbol{r}(\boldsymbol{x})$ is the correlation between the value at untried new location $\boldsymbol{x}$ and the values at the sample locations $\boldsymbol{x}^i$. The two relevant parameters for the Kriging predictor are $\hat{\beta}$ and θ_r, where θ_r is the most significant parameter in determining the correlation factors $\boldsymbol{r}$ and $\mathbf{R}$. The correlation vector is

$$\boldsymbol{r}(\boldsymbol{x})^{\mathrm{T}} = \left[R(\theta_1, \boldsymbol{x}, \boldsymbol{x}^1), \cdots, R(\theta_m, \boldsymbol{x}, \boldsymbol{x}^m) \right]. \tag{4.12}$$

The unknown parameters θ_r and $\hat{\beta}$ are determined using maximum likelihood estimation (MLE) introduced by Giunta and Watson (1998) to best fit the true model observations $\boldsymbol{y}$.

$$L(\theta_r \mid \boldsymbol{y}) = \frac{\exp\left(\dfrac{-(\boldsymbol{y} - \boldsymbol{c}\hat{\beta})^T \mathbf{R}(\theta_r)^{-1}(\boldsymbol{y} - \boldsymbol{c}\hat{\beta})}{2\hat{\sigma}^2} \right)}{\sqrt{(2\pi\hat{\sigma}^2)^m \left|\mathbf{R}(\theta_r)\right|}} \tag{4.13}$$

Due to the fact, that the logarithmic likelihood is much simpler than 4.13, $L(\theta_r \mid \boldsymbol{y})$ is commonly expressed as

$$l(\theta_r \mid \boldsymbol{y}) = \frac{-(\boldsymbol{y} - \boldsymbol{c}\hat{\beta})^{\mathrm{T}} \mathbf{R}(\theta_r)^{-1}(\boldsymbol{y} - \boldsymbol{c}\hat{\beta})}{2\hat{\sigma}^2} \left(-\frac{m\ln(2\pi\hat{\sigma}^2) + \ln(\left|\mathbf{R}(\theta_r)\right|)}{2} \right) \tag{4.14}$$

To find the optimal values for $\hat{\beta}$ and σ^2 the derivatives of 4.14 are set to zero. The optimal values are

$$\hat{\beta} = (\boldsymbol{c}^{\mathrm{T}}\mathbf{R}^{-1}\boldsymbol{c})^{-1}\boldsymbol{c}^{\mathrm{T}}\mathbf{R}^{-1}\boldsymbol{y} \text{ and} \tag{4.15}$$

$$\hat{\sigma}^2 = \frac{1}{m}\left[(\boldsymbol{y} - \boldsymbol{c}\hat{\beta})^{\mathrm{T}} \mathbf{R}^{-1}(\boldsymbol{y} - \boldsymbol{c}\hat{\beta}) \right]. \tag{4.16}$$

The last step then is to find the optimal parameters for the correlation function θ_r, which are determined by maximizing 4.14. This relatively complex problem can be reduced to

$$\begin{aligned} &\underset{\theta_r}{\text{Maximize}} && -\frac{m\ln(2\pi\hat{\sigma}^2) + \ln(\left|\mathbf{R}(\theta_r)\right|)}{2} \\ &\text{subject to:} && 0 < \theta_r \le \infty \end{aligned} \quad . \tag{4.17}$$

4.2 Particle Swarm Optimization (PSO)

Particle Swarm Optimization is one of several methods for global optimization from the field of Computational Intelligence (CI). It was developed by Kennedy and Eberhart (1995) and is a population-based evolutionary computation algorithm for problem solving which simulates social behaviour in swarms. The advantages of PSO are its global search capability and the relatively small population of particles in comparison to other methods, for example Genetic Algorithms (GA) (Ujjin and Bentley 2003), which makes PSO a very fast optimization algorithm. Nevertheless, there are lots of other methods for global optimization, which can be separated into two basic groups of methods: deterministic and probabilistic methods, whereas the probabilistic methods can be subdivided into Monte Carlo algorithms and Evolutionary Computation (EC) algorithms (Figure 4-1).

4.2.1 Short survey of global optimization methods

Deterministic methods such as the simplex algorithm (Nelder 1965) and the quasi-newton method (Shanno 1970) are effective at finding local solutions in the search space, but cannot guarantee that the solution is the global optimum solution if a search space is multi-modal. Users need to be aware of this and decide whether a given local solution is sufficient or not. In practice if the search space is multi-dimensional and highly non-linear, *a priori* knowledge is necessary to select a good starting point near an optimum for deterministic methods to yield good results. Otherwise, they are likely to get stuck in local optima that are far away from the true optimum and consequently deliver poor optimization results. The advantage of deterministic methods is that they require a lot less computation time than probabilistic methods and are able to quickly give sufficient optimization results if appropriately initialized.

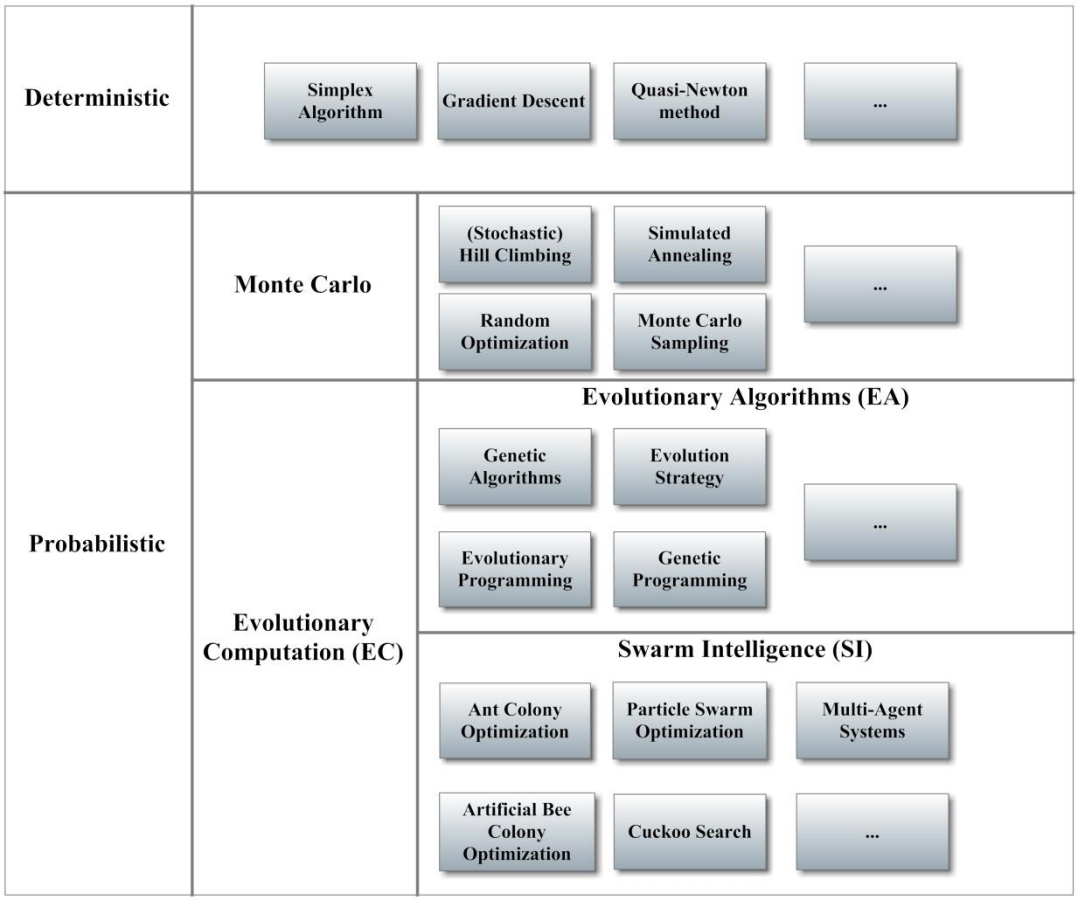

Figure 4-1: Overview of optimization methods derived from (Weise 2009)

In contrast, probabilistic methods possess the ability to globally search for an optimum, but they are not deterministic, which means that no guarantee can be given that the solution obtained is a global optimum. In general, probabilistic methods use a selection process, often random, in order to define the input samples within an allowed input space. Most of these methods follow the following pattern (Fishman 2008):

- Definition of the input space.
- Selection of a group of input samples in the input space at random or based on previous results.
- Evaluation of the input samples using a fitness function.
- Combination of the fitness results into a set of interim results.
- Repetition of the previous steps until a pre-defined end criterion is reached.

Although, these basic steps are similar for all algorithms, they differ significantly in terms of the selection of input or update samples and in the way fitness results are used to converge to an optimum. A detailed description of most of the probabilistic algorithms can be found in Schwefel (1995) and Weise (2009).

For the optimization of the substrate feed at ABPs, PSO was chosen for global optimization due to the following reasons: (1) The ADM1 model is high dimensional and highly nonlinear, which requires the use of a probabilistic optimization method; (2) A study on the feasibility of global optimization methods conducted by Ebel (2009) shows that ES, GA and PSO are well-suited for this kind of optimization problems; (3) Optimization should require as few fitness function evaluations as possible because of the computationally intensive ADM1 model. For this case, PSO has proven to be faster in terms of convergence and more robust than GA (Wolf *et. al* 2008).

4.2.2 Introduction to PSO

PSO belongs to the field of Swarm Intelligence and works on the basis that a group of individuals, called particles, which communicate with each other as they move around, is able to find a global optimum in large, complex and highly nonlinear search spaces. In determining how to move, particles exchange information with their neighbours, thereby influencing their behaviour and eventually the movement of the whole swarm. This process allows a swarm to move towards the most interesting site in a search space, as information about interesting sites is slowly propagated to the whole swarm. Thus, in PSO, the behaviour of each particle in a swarm is governed by two basic principles: *particle communication* and *particle movement*.

Particle communication is controlled by the parameter K_N, defined as the number of neighbouring particles a particle is exchanging information with. To guarantee sufficient particle communication K_N has to be carefully selected. If it is too small the propagation of important information to all particles might take too long and if too large, particles might get stuck in a local optimum. The probability $P_r(t)$ for a particle to be reached at least once after the t^{th} run is described by formula 4.18 (Clerc 2006), where N is the number of particles and K_N is the number of neighbours for information exchange.

$$P_r(t) = 1 - \left(1 - \frac{1}{N}\right)^{(K_N)^t} \tag{4.18}$$

As the probability increases quickly with t, even with a small number of neighbours, K_N, information propagation throughout the whole swarm can be rapid.

The movement of a PSO particle in a search space is defined in terms of its position vector $\mathbf{x}(t)$ and three parameter vectors:

- *Velocity* ($\mathbf{v}$): The speed at which the particle moves through the search space.
- *Personal best position* ($\mathbf{p}$): The best position a particle has currently found.
- *Global best position* ($\mathbf{g}$): The best position found by informants of a particle.

Using these parameters a particle's position and velocity are updated at the t^{th} iteration as follows:

$$\begin{aligned}\mathbf{v}(t+1) &= \varphi(t)\mathbf{v}(t) + c_1\left[\gamma_1(\mathbf{p}(t)-\mathbf{x}(t))\right] + c_2\left[\gamma_2(\mathbf{g}(t)-\mathbf{x}(t))\right] \\ \mathbf{x}(t+1) &= \mathbf{x}(t) + \mathbf{v}(t)\end{aligned} \tag{4.19}$$

The function $\varphi(t)$ and the constants c_1 and c_2 are parameters that determine the importance of the three different vectors $\mathbf{v}(t)$, $\mathbf{p}(t)-\mathbf{x}(t)$ and $\mathbf{g}(t)-\mathbf{x}(t)$, where $\mathbf{v}(t)$ is the actual velocity of a particle, $\mathbf{p}(t)-\mathbf{x}(t)$ is the distance between the actual particle position $\mathbf{x}$ and the personal best position $\mathbf{p}$ and $\mathbf{g}(t)-\mathbf{x}(t)$ is the distance between $\mathbf{x}$ and $\mathbf{g}$. $\varphi(t)$ is a time varying inertia weight as introduced by Yuhui and Eberhart (1998) and represents the confidence of a particle in its direction of movement. Constants c_1 and c_2, so-called acceleration constants, represent the confidence of a particle in its personal best position and its best reported global position, respectively. Furthermore, the influence of $\mathbf{p}$ and $\mathbf{g}$ is manipulated by γ_1 and γ_2, which are random numbers between 0 and 1 and cause a random oscillation of the particles around $\mathbf{p}$ and $\mathbf{g}$. Using these mechanisms a swarm of particles moves through a search space looking for an optimal solution to a defined optimization problem. In a similar fashion to GAs, at each iteration all particles are evaluated using a fitness function and this information is used to update the current position, personal best position and global best position of each particle as can be seen in the following pseudo code.

```
swarm = createSwarm (nParticles);
while (End criteria) // e.g. Max Number of Iterations or expected fitness
        swarm = evaluate (swarm);
        globalBest = getGlobalBest(swarm);
        for i = 1 to numberParticles
                localBest = getLocalBest(swarm(i));
                swarm(i).velocity = updateVelocity(localBest,globalBest);
                swarm(i).position = updatePosition(swarm(i).velocity);
        end;
end;
return globalBest;
```

4.2.3 Literature Review on PSO

As previously mentioned PSO was developed by Kennedy and Eberhart (1995), who developed the algorithm based on the simulations of Stone and Reynolds (1987) and Heppner and Grenander (1990). The main aspect of that original PSO was that particles of a swarm were able to remember their personal best position and global best position in the search space, which is often referred to as autobiographical memory and publicized public knowledge. Kennedy and Eberhart first tested PSO on the well-known Schaffer f6 function, which was used as a benchmark for GA by Davis (1991). Three years later, Yuhui and Eberhart (1998) introduced an extension of the original PSO by implementing inertia weights to counter too fast convergence and improve exploration qualities of the swarm.

Without inertia weights, the original PSO behaves similar to a local search if initial particle positions are badly conditioned. It was found that values of $0.8<\varphi<1.2$ deliver good performance results, which was confirmed later on by Carlisle and Dozer (2000) and Trelea (2003). Eberhart and Shi (2000) further investigated the use of inertia weights and came to the conclusion that a linearly decreasing φ from 0.9 to 0.4 over the whole number of generations delivers good optimization results. A first performance comparison of PSO and GA was made by Angeline (1998). It was shown that PSO finds solutions near the optimum faster than GA, although exploitation is weaker. Due to the problems of too fast conversion of the original PSO, Clerc and Kennedy (2002) performed a detailed analysis of the inner workings of PSO and introduced constriction coefficients to control the dynamical characteristics of the swarm, namely exploration and exploitation. Three different ways of implementing constriction were presented and tested on test problems.

In 2002 and the following years several adapted PSO algorithms were developed. An overview of these methods can be found in Banks *et. al* (2007) and Poli *et. al* (2007). The most relevant are briefly mentioned in this paragraph. The Guaranteed Conversion PSO (GCPSO) was developed by Van Den Bergh and Engelbrecht (2002) and uses an adapted velocity update equation, which causes the best particle to perform a random search within a pre-set radius around $\mathbf{g}$, which is defined by a scaling factor. The disadvantage of GCPSO is that some *a priori* knowledge about the search space is required to properly choose the scaling factor, whereas an advantage lies in the reduced swarm sizes, which significantly reduces the number of true function evaluations. Riget and Vesterstrøm (2002) found out that swarm stagnation is closely related to the diversity of the particles in the swarm. To assure a minimum of diversity, particles attract each other until a minimum diversity level is reached and then go into repulsion mode until they reach maximum diversity again. This PSO is called ARPSO (Attractive and Repulsive PSO). Another method to assure diversity and to prevent quick convergence was introduced by Silva *et. al* (2002) who implemented predator activity for the particle swarm by adding an additional particle, which is attracted to the best particle and drives off the rest of the swarm (PSPPO-Particle Swarm Predator Prey Optimization). The result of that approach is that particles are forced to explore other areas of the search space, which makes this method well-suited for highly nonlinear multimodal optimization problems. To allow particles to move faster through the search space, Kennedy (2003) developed a Gaussian PSO where the velocity vector is replaced by a random number around the mean of $\mathbf{p}$ and $\mathbf{g}$ with a Gaussian distribution. This allows particles to "teleport" to locations in the search space, which should allow for a quick exploration of the search space. On the contrary, Veeramachaneni *et. al* (2003) try to slow down convergence to increase exploration of the search space by introducing another velocity component which represents the influence of the fittest nearest neighbor particle. The method is known as Fitness-Distance-Ratio PSO (FDR-PSO). Another manipulation of the original PSO's velocity vector is presented by Parsopoulos (2004). The constricted PSO is adapted, introducing two velocity vectors one depending on $\mathbf{p}$ and the other depending on $\mathbf{g}$.

These two velocities are then combined to a unified velocity update, which should increase the explorative behavior of the swarm. One last interesting adaptation of the original PSO was developed by Kaewkamnerdpong and Bentley (2005) based on the principle that a particle's perception of its surrounding particles is not optimal but sometimes incorrect or blurred. Thus, particles are no longer allowed to communicate directly but can only observe particles in their pre-set perceptive range. Within this range, information from particles that are closest is considered to be more accurate.

The configuration of PSO is also the topic of several publications, as the global search capability of the algorithm is significantly affected by swarm size, inertia weight and maximum particle speed. Therefore, Carlisle and Dozer (2001) provide guidelines for achieving a working, although not optimal PSO parameter set. Furthermore, Parsopoulos and Vrahatis (2002) developed a method to find optimal initial particle positions using the Nelder Mead Simplex algorithm (NMS) (Nelder 1965). Results show that apart from the additional computational effort for NMS, the improved initial positions may speed up the global search significantly. Last but not least, Zhang et. al (2005) further investigated the guideline from Carlisle and Dozier and tried different parameter combinations on problems of high dimensionality. The results clearly state that greater swarm sizes are necessary to tackle high dimensional optimization problems.

All in all, it can be said that lots of different PSO algorithms exist that mostly address the well-known problems of premature convergence or the tradeoff between true function evaluations and full exploration of the search space. Nevertheless, the basic equations of the original PSO are still used in most of these PSO implementations (O'Reilly *et. al* 2005) and remain mostly unchanged. The high number of publications (18,405[18]) investigating PSO algorithms or using PSO for practical application shows that PSO is one of the most used Swarm Intelligence Optimization methods of our time.

4.3 Global optimization using Sequential Kriging Surrogate Models (S-KSM)

As stated earlier in this chapter, the global optimization of highly complex, nonlinear and multimodal functions or simulations requires a high computational effort. This demands a decision between local optimization, which is fast and deterministic or global optimization, which is slow and probabilistic. In most cases global optimization is the desired choice and the higher computational effort is necessarily accepted. Nevertheless, the all-in-one solution is desired, which does a global search with as few as possible true fitness function evaluations as possible. To provide such an all-in-one solution PSO is used in conjunction with a LH-based S-KSM and a PSO-based S-KSM. Both methods were developed based on the assumption that a perfect Kriging surrogate model (KSM) is not necessary at the beginning of an optimization run to provide useful information for locating an optimum. Thus, a global optimization algorithm is used to find the optimum based on an initial *crude* KSM, which is

[18] general search in the Scopus publications database for "Particle Swarm Optimization" (http://www.scopus.com)

then updated based on the newly found optimum. Then, global optimization is performed again on this improved KSM. This process is repeated until a maximum number of iterations is reached.

The result of this approach is that the KSM is always sequentially updated (S-KSM) at a region of interest and its surroundings and not updated in regions that do not possess an optimum. This serves the main purpose of avoiding costly true fitness function evaluations in areas where they do not provide useful information for finding a new optimum.

The two novel methods are different from existing methods (see 4.1 and 4.1.1) in two ways: (1) The Kriging Surrogate Model (KSM) is sequentially updated ***during*** the optimization run and not before; and (2) the optimization result ($\mathbf{g}$) of the PSO algorithm is used as *a priori* knowledge to determine new sample points for the KSM in each iteration.

It should be noted that while the methods have been developed for the use with PSO and KSM they can be equally used with other sampling or metamodeling paradigm.

In the following two sections 4.3.1 and 4.3.2, LH-based S-KSM and PSO-based S-KSM are explained in detail and in the last section the Kriging and PSO configurations for both methods are introduced.

4.3.1 Optimization using LH-based S-KSM

The LH-based S-KSM uses latin hypercube sampling (LH-sampling) to sequentially update the Kriging surrogate model during optimization. An overview of the method's working principle is given in Figure 4-2. In the following, the different steps of the method will be explained in detail.

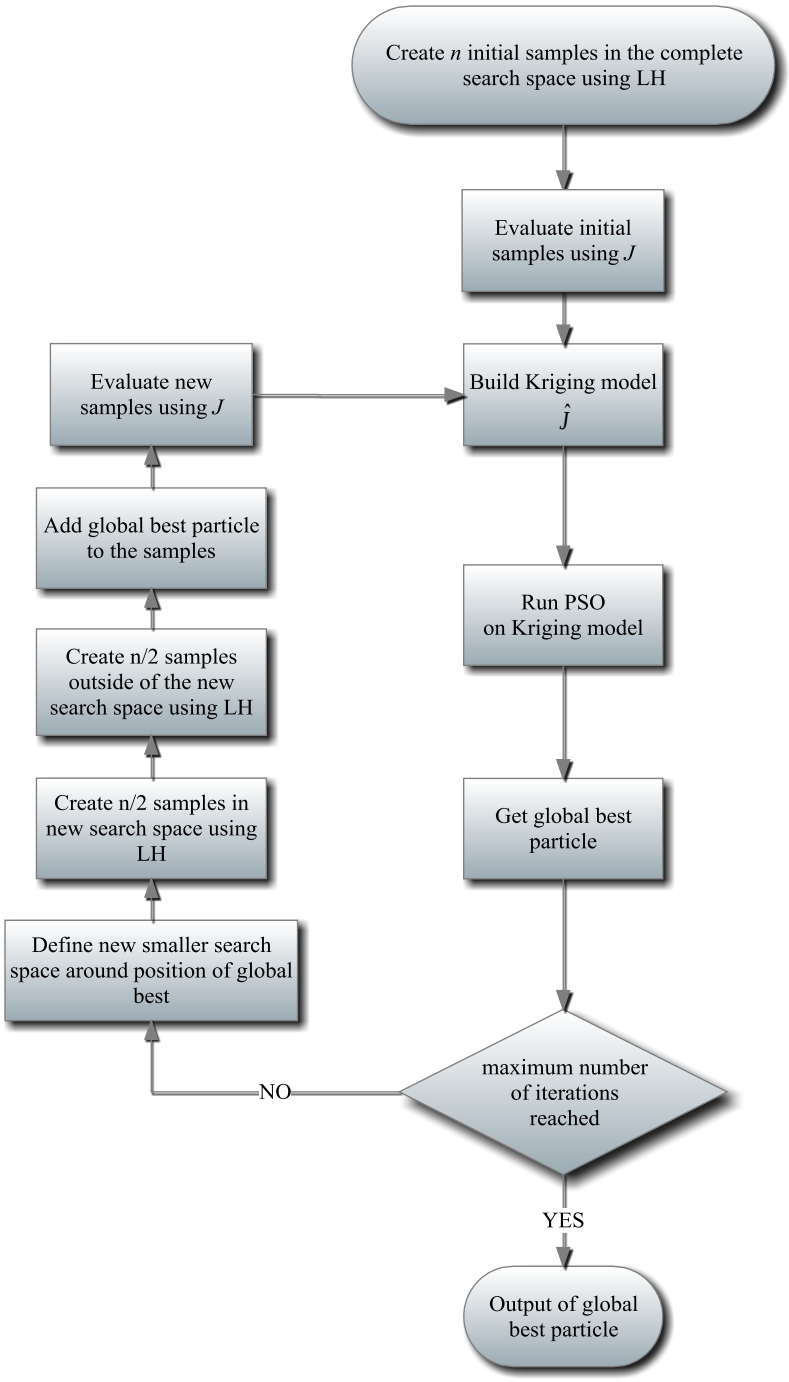

Figure 4-2: Working principle of the LH-based S-KSM optimization

4.3.1.1 Creation of initial and update samples based on LH-sampling

The creation of initial and update samples for LH-based S-KSM is performed using LH-sampling. In general any sampling method can be used instead of LH-sampling as long as they fulfill one major condition. *The samples provide a sparse representation of the search space.* This means that a good coverage of the search space is achieved with as few samples as possible to reduce the computational effort of true fitness function evaluations to a minimum. In this case, LH-sampling was used, because it possesses these characteristics. LH-sampling was developed by McKay *et. al* (1979) and splits each

dimension of the search space into intervals of equal length. Then, for each interval in every dimension one value is randomly generated. In the final step, these values from each dimension are randomly brought together in pairs. The result is a sparse sample distribution in the search space. The following examples in Figure 4-3 show the results of LH-sampling for a 2D and 3D search space, where each dimension is divided into 10 equally spaced intervals.

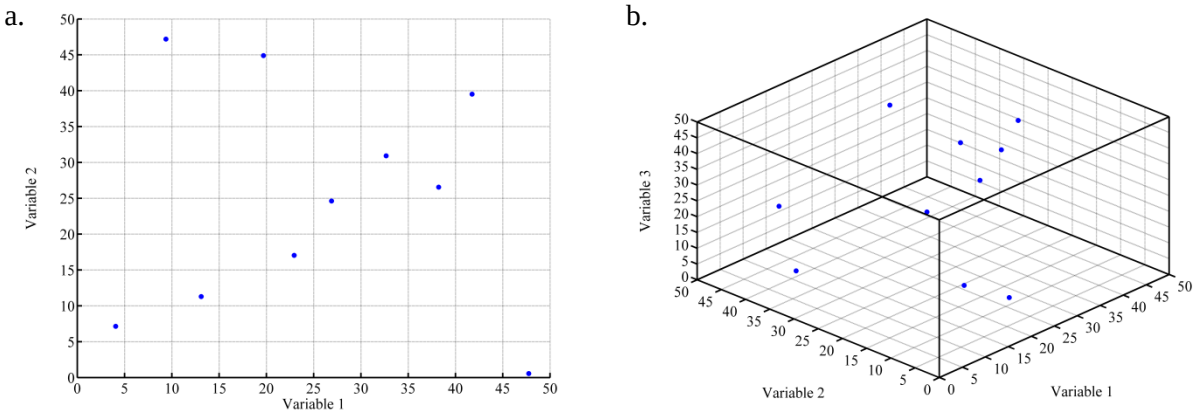

Figure 4-3: Example for LH-sampling: a. 2D example, b. 3D example

Whereas the initial samples cover the complete search space, the update samples are divided into two groups, which are generated separately. Half of the samples are created within the new search space and half outside of the new search space but still within the complete search space. The purpose of this is that on the one hand, the KSM is refined around the found optimum and on the other hand, that the probability of overlooking optima outside the new search space is minimized. The optimum found in the KSM is also added to the generated update samples within the new search space.

4.3.1.2 Construction of KSM and global optimization using PSO

The initial samples, as well as all update samples are evaluated using the true fitness function. The result is a steadily growing set of input/output data pairs, which are used to build a KSM. Due to the increasing number of samples, the KSM becomes more and more accurate and its construction becomes more and more computationally intensive. In every iteration of the optimization with LH-based S-KSM, the global optimum of the KSM is determined using PSO. The found global best particle from the PSO is then used to modify the search space and to update the KSM.

4.3.1.3 Definition of a new search space based on global best particle

The construction of a KSM for the whole search space requires lots of true fitness function evaluations, which has a negative impact on the overall performance of optimization using LH-based S-KSM. Therefore, the search space shrinks around the global best particle with each iteration, allowing the update samples to refine the KSM in that particular area. As the global best particle probably changes throughout the optimization, the shrinking search space *jumps* from one global best particle to the next. This results in a good exploration of the complete search space in the beginning

and guarantees a precise determination of the optimum towards the end of the optimization, when the search space is in the immediate surroundings of the optimum.

The shrinking of the search space is implemented in two different ways depending on the optimization problem: (1) First Search Then Converge (FSTC) and (2) First Converge Then Search (FCTS).

For FSTC a quadratic function of the form $f(x) = ax^2 + bx + c$ is fitted to two points

$$\begin{matrix} P_1(1,1) \\ P_2(i_t, p_{csp}) \end{matrix}, \tag{4.20}$$

where i_t is the total number of iterations, p_{csp} is the final size of the search space given as percentage of the complete search space and $P_1(1,1)$ is the angular point.

For FCTS an exponential function of the form $f(x) = ae^{bx}$ is fitted to the points from 4.20. Figure 4-4 shows examples for the two functions for $i_t = 2000$ and $p_{csp} = 0.0001$.

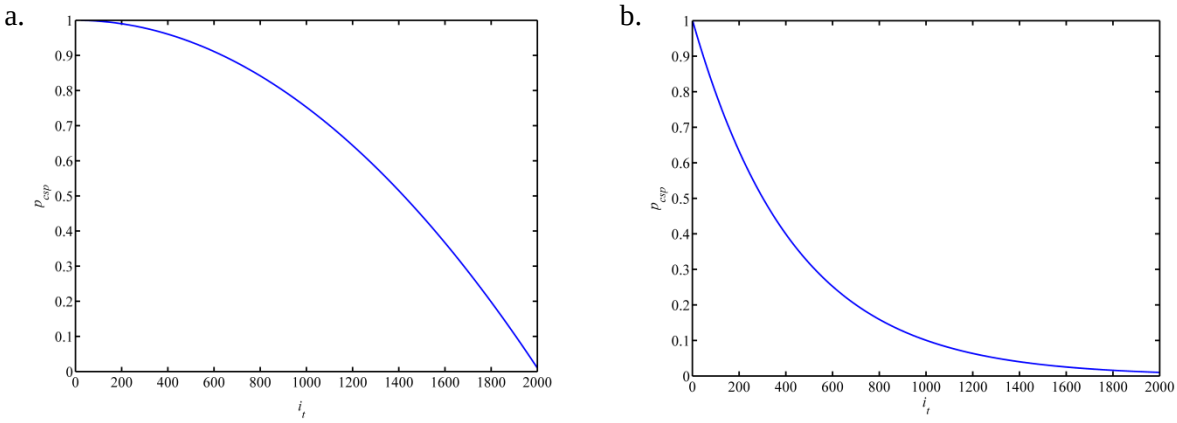

Figure 4-4: a. FSTC example, b. FCTS example

In both cases the new search space boundaries are calculated by the following two equations

$$\boldsymbol{b}_{\min}(i_t + 1) = \boldsymbol{g}(i_t) + \left[\boldsymbol{b}_{\min}(i_t) - \boldsymbol{g}(i_t)\right] p_{csp} \tag{4.21}$$

$$\boldsymbol{b}_{\max}(i_t + 1) = \boldsymbol{g}(i_t) + \left[\boldsymbol{b}_{\max}(i_t) - \boldsymbol{g}(i_t)\right] p_{csp} \tag{4.22}$$

where $\boldsymbol{b}_{\min}$ and $\boldsymbol{b}_{\max}$ are the minimum and maximum boundaries for each dimension of the search space and $\boldsymbol{g}$ is the global best particle found by PSO when applied to the KSM.

4.3.2 Optimization using PSO-based S-KSM

The optimization using PSO-based S-KSM works differently than the LH-based S-KSM when it comes to the update of the KSM. The initial samples are considered particles of a swarm that moves through the search space in the direction of the global optimum based on the standard PSO equations. Thus, the new positions of the particles at every iteration are the new update samples for the KSM

along with the global best particle from the PSO used on the KSM for global optimization. As many parts of the PSO-based S-KSM method are similar to the LH-based S-KSM method, only the generation and initialization of the initial samples as particles will be described in detail. An overview of the method's working principle is given in Figure 4-5.

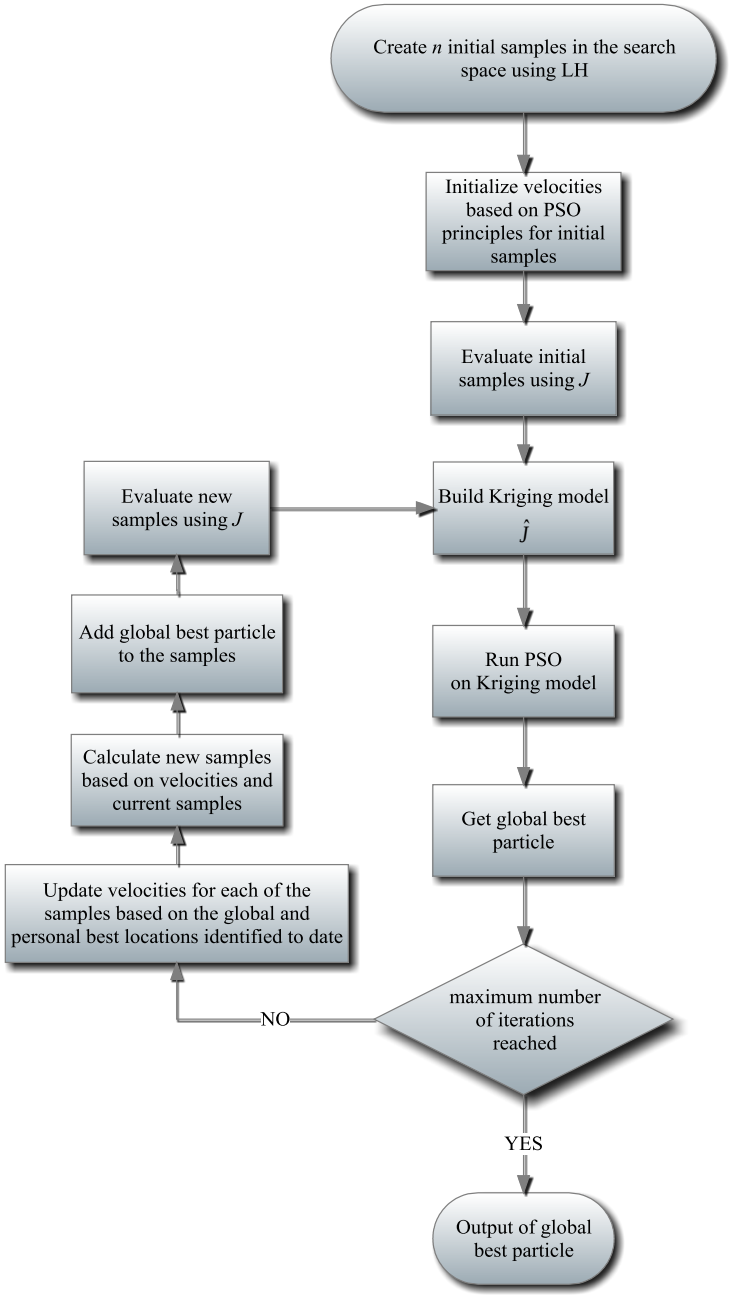

Figure 4-5: Working principle of the PSO-based S-KSM optimization

4.3.2.1 Creation of initial samples and initialization of velocity and personal best positions

Similar to LH-based S-KSM, the initial samples are generated using LH-sampling, which is explained in section 4.3.1.1. As these initial samples are considered particles of a swarm, it becomes necessary to initialize their personal best positions as well as their velocities so that the update samples can be

calculated based on these values and the global best position as previously defined in 4.19. The personal best position is initialized by the actual value of the samples and the initial velocities are defined as

$$\boldsymbol{v}_i = rand\left(0, \frac{\boldsymbol{b}_{\max} - \boldsymbol{b}_{\min}}{2}\right), \tag{4.23}$$

where $\boldsymbol{b}_{\min}$ and $\boldsymbol{b}_{\max}$ are the boundaries of the search space.

4.3.3 Kriging and PSO configurations for the optimization using LH- and PSO-based S-KSM

The Kriging and PSO configurations are the same for both optimization methods and were not only applied to the test problems but also to the substrate feed optimization of an ABP, which is described in detail in chapter 5. The parameter sets for both methods were determined empirically and based on standard parameters. A special optimization of the parameters for each of the test problems or the ABP substrate feed optimization was not performed to make the results comparable.

4.3.3.1 Kriging model configuration

The Kriging model is defined by three parameters: the regression model F, the correlation model R and the parameter θ of the correlation model. Due to the fact that neither the test problems nor the ABP simulation model show a basic underlying trend, the regression model was chosen to be constant (eqt. 4.3). The choice of the correlation model was difficult. At the beginning a gaussian correlation model was chosen as this is reportedly well-suited for the creation of smooth and precise surrogate models (see section 4.1.1). However, the optimization results showed a poor performance with the optimization often sticking in local minima. A direct comparison of Kriging model performance on the alpine function introduced by Clerc (1999) using a Gaussian and piecewise linear correlation model shows that the reason for this poor performance is the Gaussian correlation model because it tends to overshoot at places where only local minima exist and thus creates global minima at wrong positions.

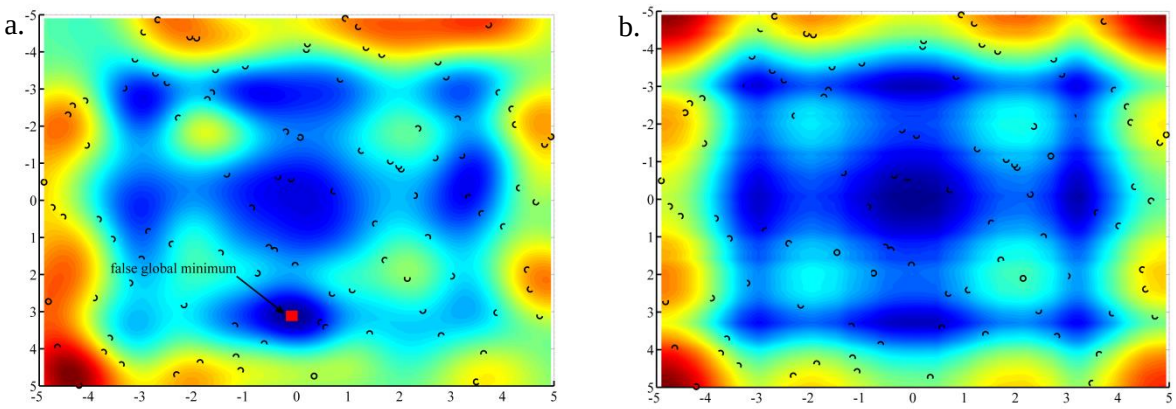

Figure 4-6: Comparison of Kriging model performance on alpine function for a. gaussian correlation and b. piecewise linear correlation model based on 100 sample points (true global minimum at x=y=0)

This behavior of the Gaussian correlation model is not compatible with the two proposed novel optimization methods as the update of the KSM is strongly influenced by the global optimum found by PSO when applied to the KSM. Therefore, a piecewise linear correlation model was chosen, which shows no sign of overshooting.

For the generation of the KSM the freely available DACE Matlab Kriging toolbox from the Department of Informatics and Mathematical Modeling (IMM) of the Technical University of Denmark is used (Lophaven et. al 2002). In this Kriging implementation an optimization of the correlation parameter θ is performed automatically based on pre-set boundaries. For all of the following optimization problems the lower boundary of θ was set to 5 and the upper boundary to 10 because values in this interval are a good compromise between accurate and smooth interpolation.

4.3.3.2 PSO configuration

The PSO was implemented with the PSOt Matlab toolbox by Birge (2003) using a version of the original PSO with inertia weight (Yuhui and Eberhart 1998). The parameters employed with the PSO are shown in Table 4-1.

Table 4-1: PSO parameters based on Eberhart (2000) and Birge (2003)

PSO parameters	Value
Number of runs	300
Number of particles	80
Personal best influence (c_1)	2
Global best influence (c_2)	2
Initial inertia weight (φ_i)	0.9
Final inertia weight (φ_f)	0.6

These parameters (c_1, c_2, φ_i and φ_f) were used with the PSO both for global optimization and for the generation of update samples in the case of the PSO-based S-KSM.

4.4 Performance results on test problems

The use of simulated examples for the testing and validation of new optimization methods is common practice and has several advantages. The computation time of such simulated test problems is short, which allows running of many different configurations of the optimization method. Thus, the performance over several optimization runs can be investigated as well as the use of various parameter configurations of the methods. The four simulated test problems used for validation and their characteristics are discussed in section 4.4.1 and the performance results in comparison to classic PSO

and non-sequential Kriging are given in section 4.4.2. A conclusion on the optimization methods using LH-based KSM and PSO-based KSM is provided in section 4.5.

4.4.1 The test problems

Usually, test problems of different difficulty (number of minima and dimensions) are used to evaluate optimization methods, which is why in this case four test problems were defined. The two novel optimization methods are then applied to 2D, 3D and 5D versions of these functions to investigate their capability to cope with high dimensional problems.

4.4.1.1 Test problem I: The quadratic function

The quadratic function is one of the easiest test problems as it has only one minimum at zero, which can even be found quickly using classic deterministic optimization methods such as gradient descent. The equation of the quadratic function is

$$f(\boldsymbol{x}) = \sum_{i=1}^{n} x_i^2 \,, \tag{4.24}$$

where $\boldsymbol{x} = [x_1, \cdots, x_n]^{\mathrm{T}}$ is a *n*-dimensional vector with $x_i \in \mathbb{R}$. Figure 4-7 shows the quadratic function for $n = 2$ and $n = 3$.

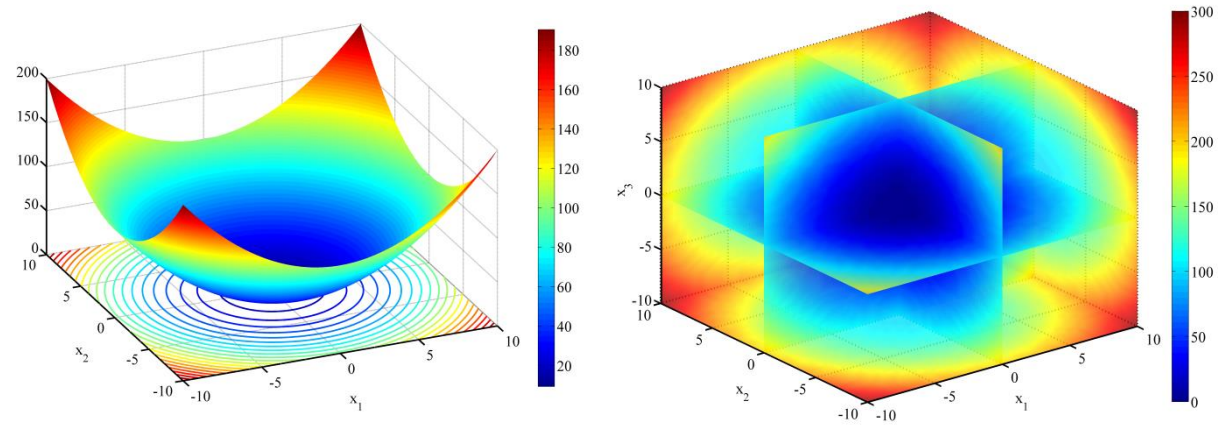

Figure 4-7: Test problem I – the quadratic function

4.4.1.2 Test problem II: RBF with 2 minima

Test problem II has two minima that are very close to each other, with the global minimum being broader and deeper than the local minimum. The three equations 4.25, 4.26 and 4.27 represent the test problem with $\boldsymbol{x} = [x_1, \cdots, x_n]^{\mathrm{T}}$ being a *n*-dimensional vector with $x_i \in \mathbb{R}$ for $n = 2$, $n = 3$ and $n = 5$.

$$f(\boldsymbol{x}) = 5 - \exp\left[-0.02\left(\boldsymbol{x} - (6,2)^{\mathrm{T}}\right)^2\right] - 0.8\exp\left[-0.1\left(\boldsymbol{x} + (5,4)^{\mathrm{T}}\right)^2\right] \tag{4.25}$$

$$f(\boldsymbol{x}) = 5 - \exp\left[-0.02\left(\boldsymbol{x} - (6,2,4)^{\mathrm{T}}\right)^2\right] - 0.8\exp\left[-0.1\left(\boldsymbol{x} + (5,4,-2)^{\mathrm{T}}\right)^2\right] \tag{4.26}$$

$$f(\boldsymbol{x}) = 5 - \exp\left[-0.02\left(\boldsymbol{x} - (6,2,4,-4,5)^{\mathrm{T}}\right)^2\right] - 0.8\exp\left[-0.1\left(\boldsymbol{x} + (5,4,-2,-6,-8)^{\mathrm{T}}\right)^2\right] \tag{4.27}$$

Although there are two minima, it should be fairly easy to find the global minimum. Figure 4-8 shows the RBF functions 4.25 and 4.26.

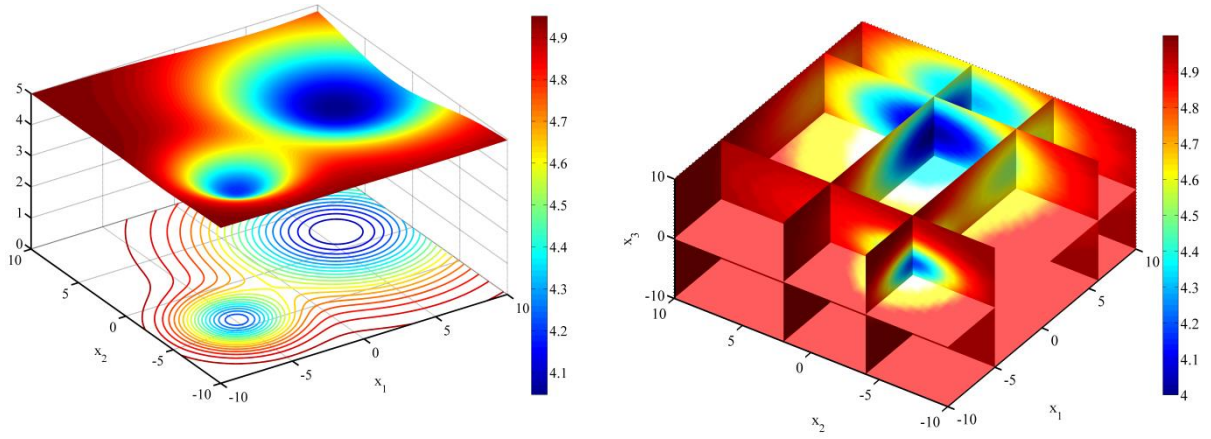

Figure 4-8: Test problem II - RBF with 2 minima

4.4.1.3 Test problem III: RBF with 4 minima

Test problem III is particularly difficult with four minima. The global minimum lies in the corner of the search space and is of small diameter and very steep, which makes it very difficult to detect. The other surrounding minima are broader adding to the complexity of the search, as this increases the probability of the optimization method getting stuck in one of the local and not the global minimum. The three equations 4.28, 4.29 and 4.30 represent the test problem with $\boldsymbol{x} = [x_1, \cdots, x_n]^{\mathrm{T}}$ being a *n*-dimensional vector with $x_i \in \mathbb{R}$ for $n = 2$, $n = 3$ and $n = 5$.

$$\begin{aligned} f(\boldsymbol{x}) = 5 &- \exp\left[-0.02\left(\boldsymbol{x} - (6,2)^{\mathrm{T}}\right)^2\right] - 0.8\exp\left[-0.1\left(\boldsymbol{x} + (5,4)^{\mathrm{T}}\right)^2\right] \\ &-0.5\exp\left[-0.1\left(\boldsymbol{x} + (0,8)^{\mathrm{T}}\right)^2\right] - 2\exp\left[-0{,}1\left(\boldsymbol{x} + (8,-6)^{\mathrm{T}}\right)^2\right] \end{aligned} \tag{4.28}$$

$$\begin{aligned} f(\boldsymbol{x}) = 5 &- \exp\left[-0.02\left(\boldsymbol{x} - (6,2,7)^{\mathrm{T}}\right)^2\right] - 0.8\exp\left[-0.1\left(\boldsymbol{x} + (5,4,-2)^{\mathrm{T}}\right)^2\right] \\ &-0.5\exp\left[-0.1\left(\boldsymbol{x} + (0,8,5)^{\mathrm{T}}\right)^2\right] - 2\exp\left[-0{,}1\left(\boldsymbol{x} + (8,-6,-5)^{\mathrm{T}}\right)^2\right] \end{aligned} \tag{4.29}$$

$$\begin{aligned} f(\boldsymbol{x}) = 5 &- \exp\left[-0.02\left(\boldsymbol{x} - (6,2,7,-4,5)^{\mathrm{T}}\right)^2\right] - 0.8\exp\left[-0.1\left(\boldsymbol{x} + (5,4,-2,-8,-1)^{\mathrm{T}}\right)^2\right] \\ &-0.5\exp\left[-0.1\left(\boldsymbol{x} + (0,8,5,-3,8)^{\mathrm{T}}\right)^2\right] - 2\exp\left[-0{,}1\left(\boldsymbol{x} + (8,-6,-5,1,-9)^{\mathrm{T}}\right)^2\right] \end{aligned} \tag{4.30}$$

Figure 4-9 shows the RBF functions 4.29 and 4.30.

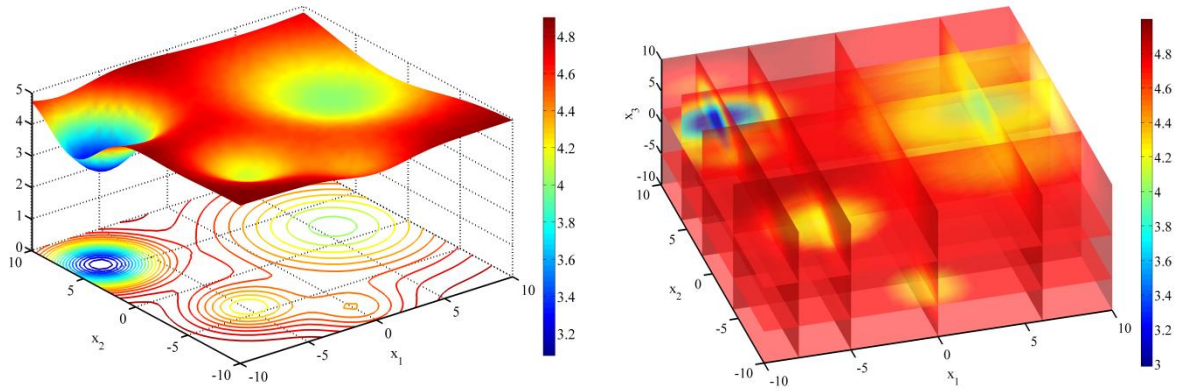

Figure 4-9: Test problem III - RBF with 4 minima

4.4.1.4 Test problem IV: Alpine function

The alpine function developed by Clerc (1999) is a highly nonlinear, multimodal function, which is perfectly suited to testing and validation of optimization methods. Of the four test problems, this poses the greatest challenge due to the high number of local minima and maxima. The equation of the alpine function is

$$f(\boldsymbol{x}) = \sum_{i=1}^{n} \left[\left| x_i \sin(x_i) + 0.1 x_i \right| \right], \tag{4.31}$$

where $\boldsymbol{x} = \left[x_1, \cdots, x_n \right]^{\mathrm{T}}$ is a *n*-dimensional vector with $x_i \in \mathbb{R}$. Figure 4-10 shows the alpine function for $n = 2$ and $n = 3$.

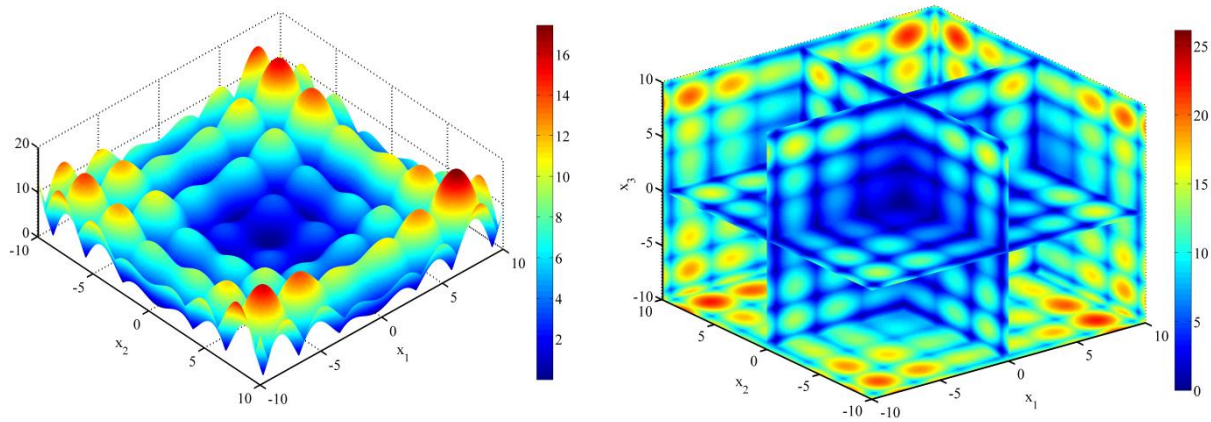

Figure 4-10: Test problem IV - alpine function

4.4.2 Performance results in comparison to classic PSO

The performance of the two novel methods was evaluated on the four test problems introduced in 4.4.1. In the following sections the number of true fitness function evaluations e_J for optimization using LH-based S-KSM and PSO-based S-KSM is compared to the number required when using the original PSO algorithm for optimization. To guarantee comparable and consistent results, optimization

was run ten times on each test problem with the exact same configuration. Optimization was terminated when the global optimum was reached with an accuracy of 0.05. Accuracy is defined as

$$A = \sum_{i=1}^{n} \left(\left| x_i^g - x_i^o \right| \right), \tag{4.32}$$

where $\boldsymbol{x}^g$ represents the coordinates of the global optimum and $\boldsymbol{x}^o$ is the position of the optimum found during optimization. Results shown in this section represent mean and standard deviation values from ten optimization runs. The performance of original PSO on a non-sequential KSM was also investigated but delivered very poor optimization results. The optimization method was not able to reach the desired optimization accuracy of 0.05 for even one of the test problems.

4.4.2.1 Results for test problem I

Problem I being the simplest of all test problems shows that the optimization goal of $A = 0.05$ can be achieved with very low numbers of e_J for the 2D and 3D versions of the quadratic function. The 5D problem requires a significantly higher effort, which was expected due to the higher dimensionality of the problem.

4.4.2.1.1 Results for LH-based S-KSM optimization on test problem I

For the LH-based S-KSM optimization on the 2D quadratic function the lowest $e_J = 152$ was achieved with 70 initial sample points (p_i) and two update samples (p_u) for the KSM. As can be clearly seen in Figure 4-11 the higher the number of update samples, the higher the number of e_J becomes and also the standard deviation of e_J rises significantly. Furthermore, it is interesting to see that the configuration with minimum e_J is not the same as the one with the lowest standard deviation ($p_i = 10$ and $p_u = 12$).

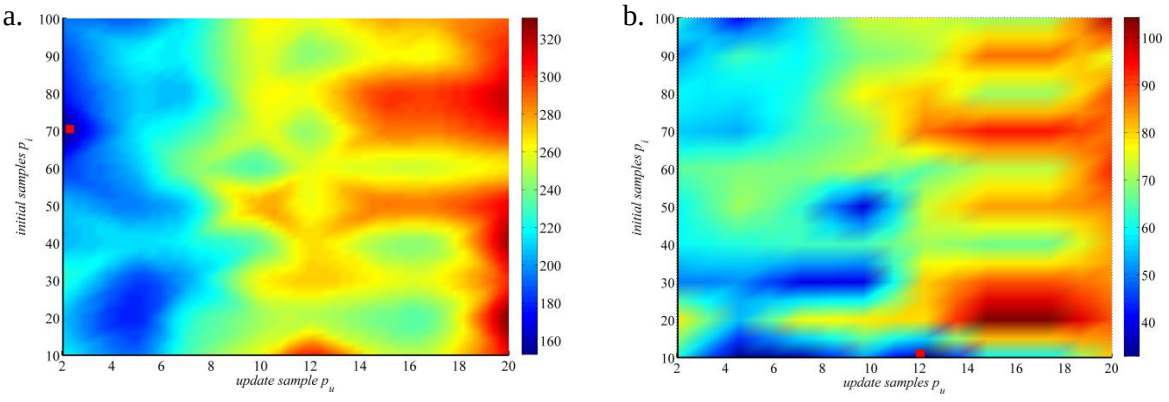

Figure 4-11: Number of true fitness function evaluations e_J for LH-based S-KSM optimization of the 2D quadratic function: a. mean e_J, b. e_J standard deviation

Looking at results for the 3D quadratic function, results are very similar ($p_i = 60$ and $p_u = 10$), although mean e_J and standard deviation of e_J is in average much higher than for the 2D problem.

This effect can be explained by the higher dimensionality of the problem. This hypothesis is supported by the results for the 5D problem shown in Figure 4-13 with $p_i = 40$ and $p_u = 10$.

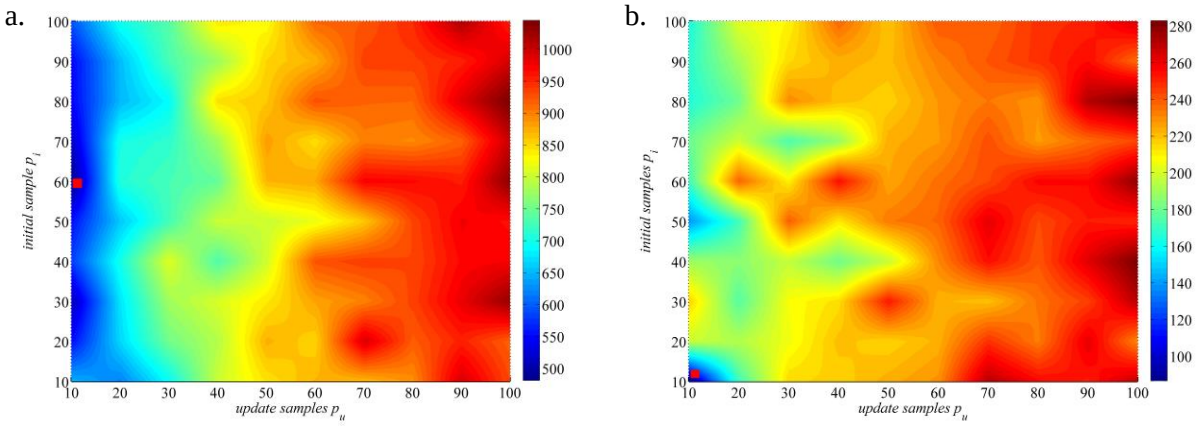

Figure 4-12: Number of true fitness function evaluations e_J for LH-based S-KSM optimization of the 3D quadratic function: a. mean e_J, b. e_J standard deviation

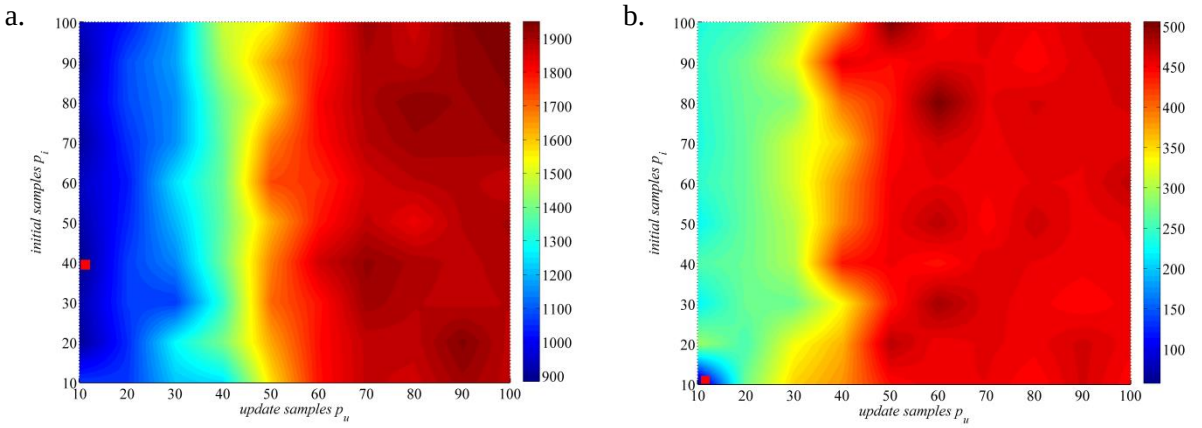

Figure 4-13: Number of true fitness function evaluations e_J for LH-based S-KSM optimization of the 5D quadratic function: a. mean e_J, b. e_J standard deviation

4.4.2.1.2 Results for PSO-based S-KSM optimization on test problem I

The results for the PSO-based S-KSM optimization for the quadratic function are very similar to the ones achieved with LH-based S-KSM optimization. Nevertheless, it is obvious, that e_J largely depends on the number of particles used for the KSM update. With increasing swarm sizes, e_J rises very quickly, so that optimization is often no longer computationally efficient. The best optimization runs show that with a well selected configuration even lower e_J than with LH-based S-KSM can be achieved.

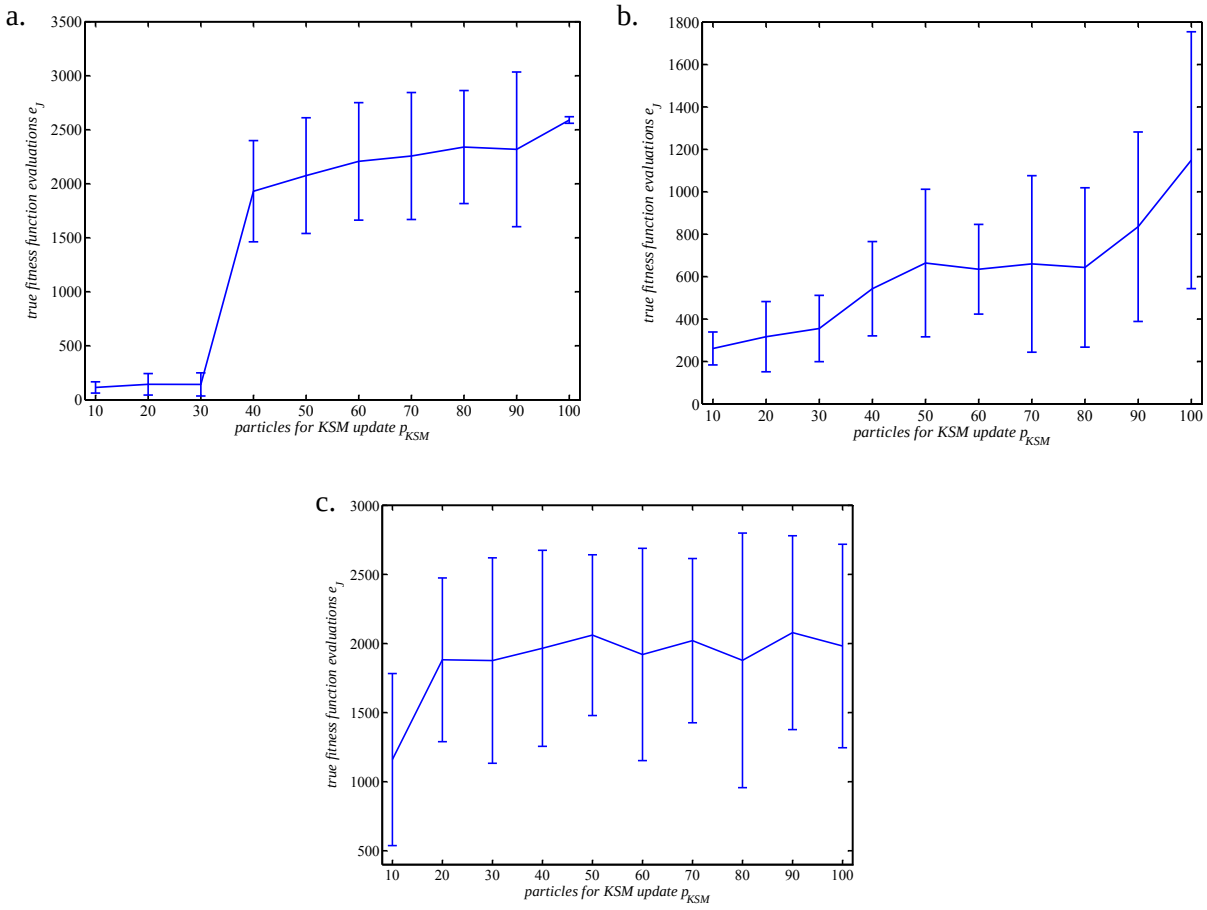

Figure 4-14: Number of true fitness function evaluations e_J for PSO-based S-KSM optimization of the 2D (a.), 3D (b.) and 5D (c.) quadratic function

The best optimization runs are in all cases the ones with the lowest number of particles $p_{PSO} = 10$ and $e_J = 115$ (2D), $e_J = 261$ (3D) and $e_J = 1{,}356$ (5D). With the exception of the 5D version of problem I, a low number of particles also results in a low standard deviation. Thus, the method is robust for these p_{PSO} numbers. However, the 5D results show that a high dimensional problem makes global optimization difficult, resulting in high e_J values and high standard deviations. Although, the PSO-based S-KSM optimization performs better than the LH-based S-KSM optimization on the 2D and 3D version of the problem, the LH-based S-KSM optimization outperforms the PSO-based S-KSM optimization on the 5D quadratic function.

4.4.2.1.3 Performance comparison to original PSO

A direct comparison of the two novel methods and original PSO clearly shows that a significant reduction of e_J of up to 88% for the 2D and 91% for the 3D and 5D quadratic functions can be achieved. The PSO-based S-KSM optimization outperforms the LH-based S-KSM optimization by up to 7% if small swarm sizes are used.

Table 4-2: Performance results of LH-based S-KSM and PSO-based S-KSM optimization in comparison to original PSO based on mean and standard deviation of true fitness function evaluations e_J for the 2D quadratic function

Configuration		LH-based S-KSM		PSO-based S-KSM		original PSO		LH-based S-KSM savings	PSO-based S-KSM savings
LH-based S-KSM	**PSO-based S-KSM / original PSO**	**mean**	**std**	**mean**	**std**	**mean**	**std**		
p_i=70; p_u=2	$p_{KSM} = p_{PSO} = 10$	152	56	115	52	540	384	71.85	78.7
p_i=80; p_u=2	$p_{KSM} = p_{PSO} = 20$	176	59	143	99	937	659	81.22	84.7
p_i=20; p_u=5	$p_{KSM} = p_{PSO} = 30$	179	55	142	107	1,070	1,006	83.27	86.7
p_i=60; p_u=2	$p_{KSM} = p_{PSO} = 40$	182	65	1,931	468	1,025	1,120	82.24	-88.4
p_i=90; p_u=2	$p_{KSM} = p_{PSO} = 50$	185	51	2,075	536	804	1,086	76.99	-158.1
p_i=30; p_u=5	$p_{KSM} = p_{PSO} = 60$	185	51	2,207	544	1,238	1,526	85.06	-78.3
p_i=100; p_u=5	$p_{KSM} = p_{PSO} = 70$	190	41	2,257	588	1,441	1,753	86.81	-56.6
p_i=100; p_u=2	$p_{KSM} = p_{PSO} = 80$	192	62	2,339	523	1,602	1,874	88.01	-46
p_i=10; p_u=2	$p_{KSM} = p_{PSO} = 90$	193	34	2,318	716	1,187	1,683	83.74	-95.3
p_i=50; p_u=5	$p_{KSM} = p_{PSO} = 100$	197	70	2,590	30	1,075	1,553	81.67	-140.9
mean		**183**	**54**	**1,612**	**366**	**1,092**	**1,264**	**82**	**-41**
std		**12.1**	**10.3**	**981.3**	**248.5**	**288**	**468.9**	**4.5**	**87.7**

The results for the 3D quadratic function confirm the 2D results, although it becomes obvious that the PSO-based S-KSM optimization performs particularly well with small swarm sizes and outperforms the LH-based S-KSM optimization with 22% less e_J. Thus, a significant reduction in computation time is achieved. The performance of the PSO-based S-KSM optimization changes completely for the 5D quadratic function, where it performs much worse than the LH-based S-KSM optimization. Only 26% improvement compared to the original PSO is achieved for the smallest swarm size with ten particles, whereas nearly 44% improvement is reached by the LH-based S-KSM optimization. Also for

larger numbers of particles the PSO-based S-KSM optimization performance is in general inferior to the LH-based S-KSM optimization by 10 to 12%.

Table 4-3: Performance results of LH-based S-KSM and PSO-based S-KSM optimization in comparison to original PSO based on mean and standard deviation of true fitness function evaluations e_J for the 3D quadratic function

Configuration		LH-based S-KSM		PSO-based S-KSM		original PSO		LH-based S-KSM savings	PSO-based S-KSM savings
LH-based S-KSM	**PSO-based S-KSM / original PSO**	**mean**	**std**	**mean**	**std**	**mean**	**std**		
p_i=60; p_u=10	$p_{KSM} = p_{PSO} = 10$	481	171	261	776	977	365	50.77	73.3
p_i=30; p_u=10	$p_{KSM} = p_{PSO} = 20$	508	217	317	165	1,760	707	71.14	82
p_i=70; p_u=10	$p_{KSM} = p_{PSO} = 30$	516	180	355	156	2,485	932	79.24	85.7
p_i=80; p_u=10	$p_{KSM} = p_{PSO} = 40$	547	165	543	222	2,796	1,528	80.44	80.6
p_i=90; p_u=10	$p_{KSM} = p_{PSO} = 50$	548	167	664	348	4,007	1,379	86.32	83.4
p_i=20; p_u=10	$p_{KSM} = p_{PSO} = 60$	554	197	634	211	4,913	1,382	88.72	87.1
p_i=50; p_u=10	$p_{KSM} = p_{PSO} = 70$	555	138	660	416	5,460	1,839	89.84	87.9
p_i=40; p_u=10	$p_{KSM} = p_{PSO} = 80$	580	189	643	376	5,377	2,592	89.21	88
p_i=100; p_u=10	$p_{KSM} = p_{PSO} = 90$	594	163	835	447	5,621	3,143	89.43	85.1
p_i=10; p_u=20	$p_{KSM} = p_{PSO} = 100$	620	171	1,148	605	7,549	2,264	91.79	84.8
mean		**550**	**176**	**606**	**372**	**4,095**	**1,613**	**82**	**84**
std		**39.3**	**20.4**	**249.8**	**190.7**	**1946.7**	**820.5**	**12**	**4.2**

A comparison of the overall results shows that for each version of the problem a significant improvement against original PSO is achieved. Considering the fact, that for most optimization problems larger swarm sizes of 30 particles and more are commonly chosen, it becomes evident that e_J savings between 80 and 90% are easily possible.

Table 4-4: Performance results of LH-based S-KSM and PSO-based S-KSM optimization in comparison to original PSO based on mean and standard deviation of true fitness function evaluations e_J for the 5D quadratic function

Configuration		LH-based S-KSM		PSO-based S-KSM		original PSO		LH-based S-KSM savings	PSO-based S-KSM savings
LH-based S-KSM	**PSO-based S-KSM / original PSO**	**mean**	**std**	**mean**	**std**	**mean**	**std**		
p_i=40; p_u=10	$p_{KSM} = p_{PSO} = 10$	883	258	1,160	623	1,570	189	43.76	26.1
p_i=20; p_u=10	$p_{KSM} = p_{PSO} = 20$	899	292	1,882	592	2,866	238	68.63	343
p_i=90; p_u=10	$p_{KSM} = p_{PSO} = 30$	900	241	1,876	743	3,994	477	77.47	53.1
p_i=70; p_u=10	$p_{KSM} = p_{PSO} = 40$	901	234	1,965	709	5,040	359	82.12	65.8
p_i=50; p_u=10	$p_{KSM} = p_{PSO} = 50$	916	224	2,060	582	6,287	527	85.43	65.7
p_i=30; p_u=10	$p_{KSM} = p_{PSO} = 60$	919	221	1,920	768	6,953	1,759	86.78	73.1
p_i=80; p_u=10	$p_{KSM} = p_{PSO} = 70$	926	238	2,020	594	8,427	986	89.01	77.1
p_i=60; p_u=10	$p_{KSM} = p_{PSO} = 80$	942	243	1,878	921	9,334	1,418	89.91	78.4
p_i=100; p_u=10	$p_{KSM} = p_{PSO} = 90$	943	236	2,078	701	10,499	808	91.02	79.5
p_i=60; p_u=20	$p_{KSM} = p_{PSO} = 100$	1,029	268	1,982	736	11,646	715	91.16	81.1
mean		**926**	**246**	**1,882**	**697**	**6,662**	**748**	**81**	**63**
std		**39**	**20.5**	**251**	**100**	**3,164.3**	**487.7**	**14**	**18.8**

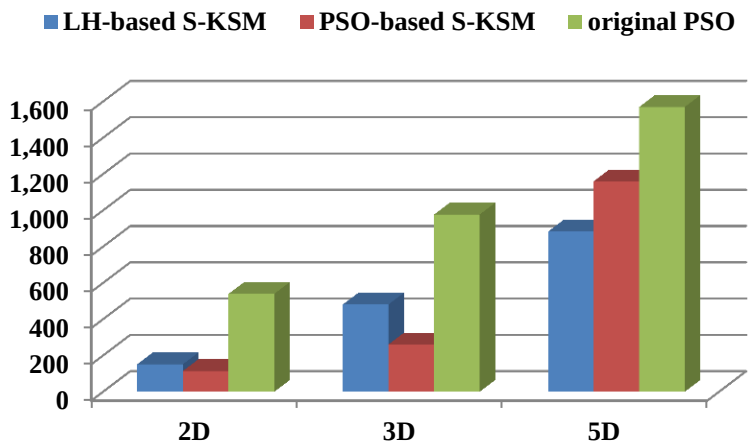

Figure 4-15: Comparison of the lowest e_J for the three evaluated optimization methods applied to test problem I

4.4.2.2 Results for test problem II

Test problem II is more difficult than test problem I as it has two minima instead of one, but is still fairly easy to solve. The global minimum is very broad and deep, whereas the second minimum is narrow and shallow as can be seen in Figure 4-8.

4.4.2.2.1 Results for LH-based S-KSM optimization on test problem II

The best result of the LH-based S-KSM optimization on the 2D version of test problem II is achieved with $p_i = 90$ and $p_u = 2$ with $e_J = 140$. In contrast to the results on test problem I, a higher number of initial samples seems to be beneficial to the overall performance. The detailed initial search grid with 90 samples allows for quicker identification of the global minimum and fast convergence.

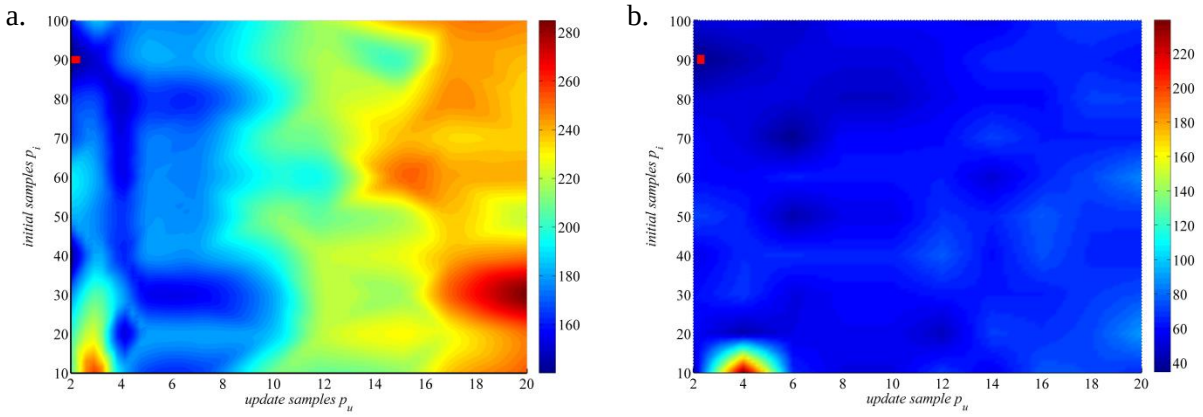

Figure 4-16: Number of true fitness function evaluations e_J for LH-based S-KSM optimization of the 2D version of test problem II: a. mean e_J, b. e_J standard deviation

The results on the 3D version of test problem II are different from the previous 2D results with the best configuration of the LH-based S-KSM configuration being $p_i = 100$ and $p_u = 20$ with $e_J = 532$. Similar to the results for test problem I, e_J rises quickly with the number of dimensions, so that a

higher number of update samples is necessary to cover the search space. Thus, the probability of the optimization method to find the global optimum fast is increased.

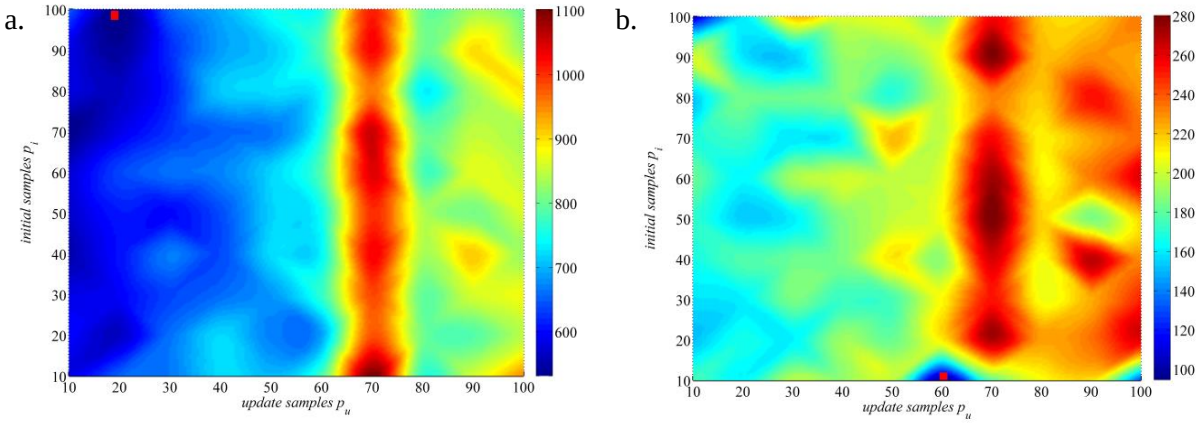

Figure 4-17: Number of true fitness function evaluations e_J for LH-based S-KSM optimization of the 3D version of test problem II: a. mean e_J, b. e_J standard deviation

Looking at the 5D results it is interesting and astonishing to see that e_J is even slightly lower than for the 3D version of test problem II with 483 and $p_i = 10$ and $p_u = 10$. The standard deviation from the ten optimization runs is also the lowest for $p_i = 10$ and $p_u = 10$, which shows the robustness of the method.

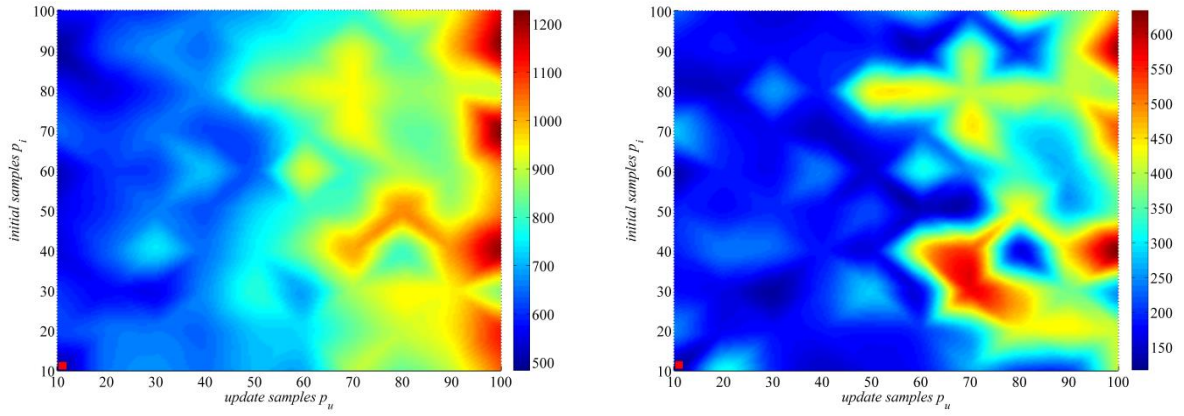

Figure 4-18: Number of true fitness function evaluations e_J for LH-based S-KSM optimization of the 5D version of test problem II: a. mean e_J, b. e_J standard deviation

4.4.2.2.2 Results for PSO-based S-KSM optimization on test problem II

The PSO-based S-KSM optimization is not able to outperform the LH-based S-KSM optimization for the 2D and 5D version of test problem II. Only for the 3D problem the PSO-based S-KSM optimization is slightly better. In general, the lowest e_J is still achieved for the lowest number of particles $p_{KSM} = 10$.

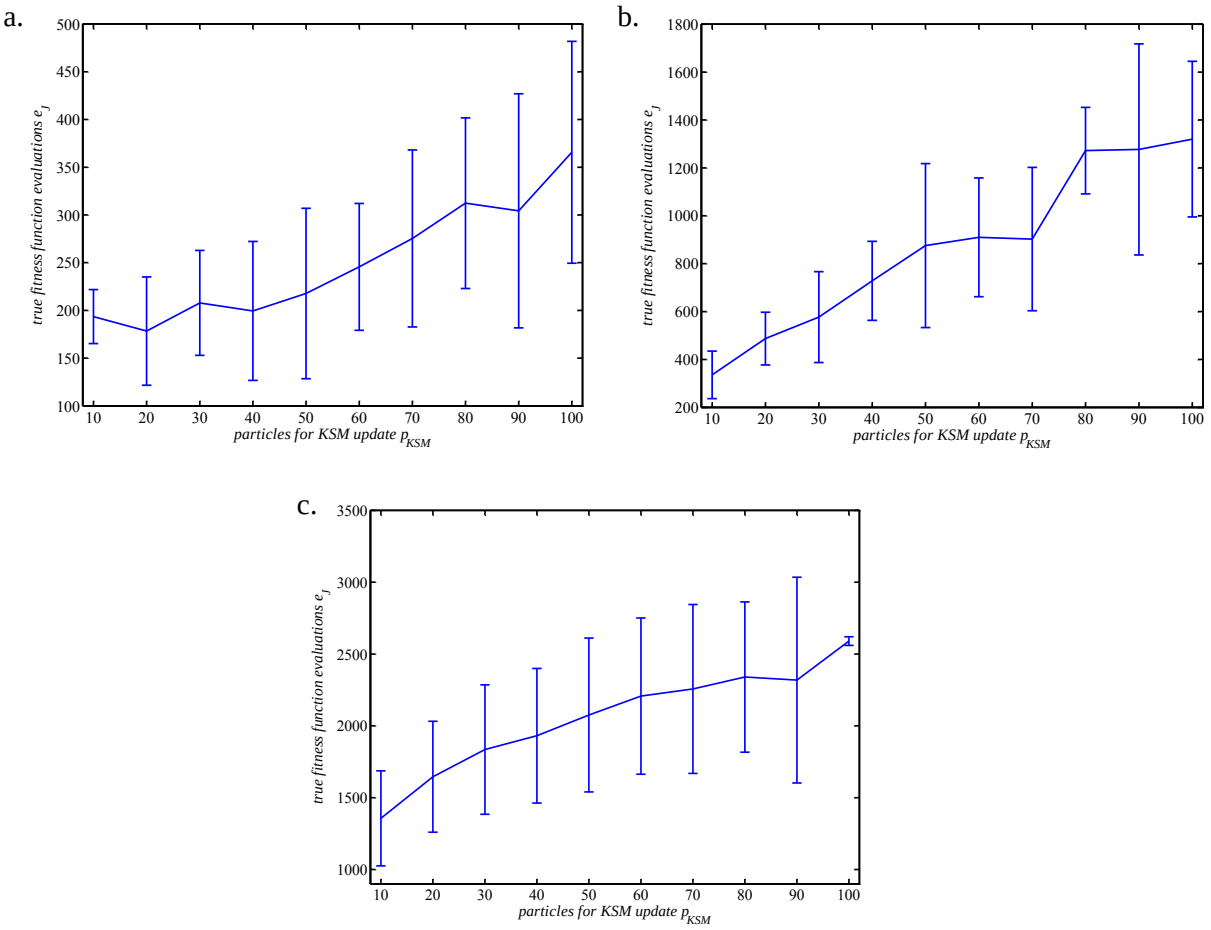

Figure 4-19: Number of true fitness function evaluations e_J for PSO-based S-KSM optimization of the 2D (a.), 3D (b.) and 5D (c.) versions of test problem II

4.4.2.2.3 Performance comparison to original PSO

The comparison of the performance of these two methods to the original PSO for test problem II also shows that a significant reduction in computation time can be achieved. e_J were reduced by more than 95% for the 2D problem, between 85 and 93% for the 3D problem and between 78 and 95% for the 5D test problem II. It is obvious that the advantage of the two novel methods is bigger when applied to problems of lower dimensionality. Nevertheless, savings in computation time are still high and encourage the use of the novel methods instead of the original PSO.

Table 4-5: Performance results of LH-based S-KSM and PSO-based S-KSM optimization in comparison to original PSO based on mean and standard deviation of true fitness function evaluations e_J for the 2D test problem II

Configuration		LH-based S-KSM		PSO-based S-KSM		original PSO		LH-based S-KSM savings	PSO-based S-KSM savings
LH-based S-KSM	**PSO-based S-KSM / original PSO**	**mean**	**std**	**mean**	**std**	**mean**	**std**		
p_i=90; p_u=2	$p_{KSM} = p_{PSO} = 10$	140	35	194	28	1,074	142	86.96	81.9
p_i=40; p_u=2	$p_{KSM} = p_{PSO} = 20$	141	53	178	57	1,958	218	92.8	90.9
p_i=80; p_u=7	$p_{KSM} = p_{PSO} = 30$	149	52	208	55	2,801	337	94.68	92.6
p_i=90; p_u=5	$p_{KSM} = p_{PSO} = 40$	151	43	199	73	3,540	527	95.73	94.4
p_i=70; p_u=7	$p_{KSM} = p_{PSO} = 50$	153	36	218	89	4,410	523	96.53	95.1
p_i=20; p_u=7	$p_{KSM} = p_{PSO} = 60$	154	54	246	66	5,258	658	97.07	95.3
p_i=60; p_u=7	$p_{KSM} = p_{PSO} = 70$	154	64	275	93	5,912	661	97.4	95.3
p_i=30; p_u=10	$p_{KSM} = p_{PSO} = 80$	156	58	312	89	6,690	779	97.67	95.3
p_i=30; p_u=12	$p_{KSM} = p_{PSO} = 90$	155	59	304	123	7,313	1,047	97.88	95.8
p_i=100; p_u=2	$p_{KSM} = p_{PSO} = 100$	159	52	366	116	8,072	963	98.03	95.5
mean		**151**	**51**	**250**	**79**	**4,703**	**586**	**95**	**93**
std		**5.9**	**9.2**	**58.8**	**27.5**	**2,228**	**283.7**	**3.2**	**4**

The performance results for the 2D test problem II show that for all configurations a substantial improvement in comparison to the original PSO is possible.

Table 4-6: Performance results of LH-based S-KSM and PSO-based S-KSM optimization in comparison to original PSO based on mean and standard deviation of true fitness function evaluations e_J for the 3D test problem II

Configuration		LH-based S-KSM		PSO-based S-KSM		original PSO		LH-based S-KSM savings	PSO-based S-KSM savings
LH-based S-KSM	**PSO-based S-KSM / original PSO**	**mean**	**std**	**mean**	**std**	**mean**	**std**		
p_i=70; p_u=10	$p_{KSM} = p_{PSO} = 10$	532	168	336	99	1,143	120	53.46	70.6
p_i=100; p_u=20	$p_{KSM} = p_{PSO} = 20$	533	159	487	110	2,050	232	74	76.2
p_i=90; p_u=20	$p_{KSM} = p_{PSO} = 30$	542	159	577	189	2,937	281	81.55	80.4
p_i=40; p_u=10	$p_{KSM} = p_{PSO} = 40$	553	167	728	165	3,785	389	85.39	80.8
p_i=80; p_u=20	$p_{KSM} = p_{PSO} = 50$	565	183	876	342	4,603	502	87.73	81
p_i=20; p_u=20	$p_{KSM} = p_{PSO} = 60$	566	166	910	248	5,462	481	89.64	83.3
p_i=50; p_u=10	$p_{KSM} = p_{PSO} = 70$	567	172	903	299	6,080	727	90.67	85.1
p_i=60; p_u=10	$p_{KSM} = p_{PSO} = 80$	572	183	1,272	180	6,995	774	91.82	81.8
p_i=80; p_u=10	$p_{KSM} = p_{PSO} = 90$	582	153	1,277	441	7,817	795	92.55	83.7
p_i=30; p_u=10	$p_{KSM} = p_{PSO} = 100$	583	158	1,320	325	8,617	871	93.23	84.7
mean		**560**	**167**	**869**	**240**	**4,949**	**517**	**84**	**81**
std		**17.7**	**9.7**	**327.2**	**105**	**2,362.6**	**250**	**11.6**	**4.2**

For the 3D test problem II, the PSO-based S-KSM optimization achieves a better performance than the LH-based S-KSM optimization for small p_u and p_{KSM}. Nevertheless, both methods provide faster optimization solutions that are also more consistent than the results from the original PSO. Overall standard deviations of both novel methods are smaller than for the original PSO.

The performance results from the 5D test problem II are different as the LH-based S-KSM optimization outperforms the PSO-based S-KSM method with e_J savings over 90%. The fact that even lower e_J than for the 3D version of the problem are achieved is unexpected and difficult to

explain as the standard deviation of e_J is only slightly larger than for the 3D problem. All in all, e_J savings for the PSO-based S-KSM optimization are rather poor with 18.6 and 42.3% for the two smallest swarm sizes. For large swarm sizes with many particles PSO-based S-KSM optimization is able to achieve equally good performance values around 90%.

The best overall results in Figure 4-20 show that both novel methods achieve significant reductions in true fitness function evaluations e_J for all three versions of test problem II.

Table 4-7: Performance results of LH-based S-KSM and PSO-based S-KSM optimization in comparison to original PSO based on mean and standard deviation of true fitness function evaluations e_J for the 5D test problem II

Configuration		**LH-based S-KSM**		**PSO-based S-KSM**		**original PSO**		**LH-based S-KSM savings**	**PSO-based S-KSM savings**
LH-based S-KSM	**PSO-based S-KSM / original PSO**	**mean**	**std**	**mean**	**std**	**mean**	**std**		
p_i=10; p_u=10	$p_{KSM} = p_{PSO} = 10$	483	117	1,424	158	1,665	203	70.99	14.5
p_i=90; p_u=10	$p_{KSM} = p_{PSO} = 20$	495	174	1,746	113	2,849	253	82.63	38.7
p_i=60; p_u=10	$p_{KSM} = p_{PSO} = 30$	520	137	1,835	451	4,089	335	87.28	55.1
p_i=40; p_u=10	$p_{KSM} = p_{PSO} = 40$	544	190	1,931	468	5,264	415	89.67	63.3
p_i=80; p_u=20	$p_{KSM} = p_{PSO} = 50$	547	150	2,075	536	6,397	490	91.45	67.6
p_i=50; p_u=10	$p_{KSM} = p_{PSO} = 60$	549	191	2,207	544	7,574	600	92.75	70.9
p_i=30; p_u=30	$p_{KSM} = p_{PSO} = 70$	562	130	2,257	588	8,644	620	93.5	73.9
p_i=30; p_u=20	$p_{KSM} = p_{PSO} = 80$	570	166	2,340	523	9,762	668	94.16	76
p_i=100; p_u=10	$p_{KSM} = p_{PSO} = 90$	573	228	2,318	716	10,850	744	94.72	78.6
p_i=90; p_u=10	$p_{KSM} = p_{PSO} = 100$	584	174	2,590	30	11,978	789	95.12	78.4
mean		**543**	**166**	**2,072**	**457**	**6,907**	**512**	**89**	**62**
std		**31.9**	**31.6**	**324.9**	**174.9**	**3,282.1**	**194.4**	**7.1**	**19.6**

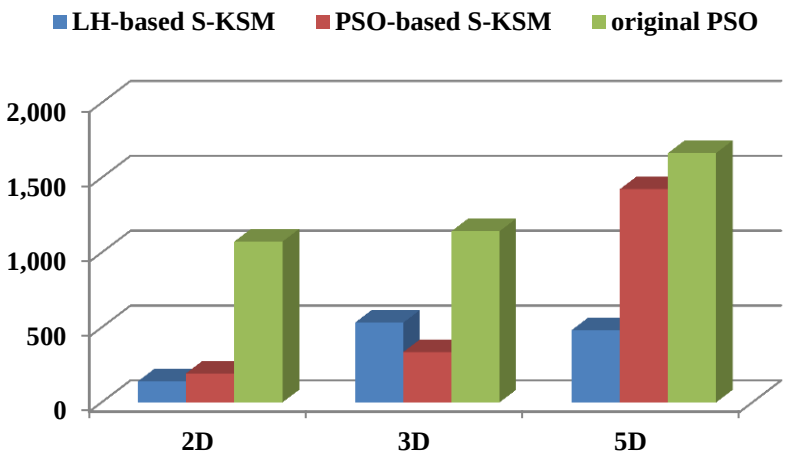

Figure 4-20: Comparison of the lowest e_J for the three evaluated optimization methods applied to test problem II

4.4.2.3 Results for test problem III

Test problem III, which has four minima, can be considered a very difficult optimization problem as the global minimum is very narrow and very deep. Furthermore the global minimum is surrounded by a very broad minimum and two shallow minima. Thus, the probability of getting stuck in one of the local minima or of actually never finding the global minima is very high. Again, test problem III was evaluated in 2D, 3D and 5D, but the 5D results are not shown in this section as neither the two novel methods nor the original PSO was able to find the global optimum in time. Nevertheless, the results for the 2D and 3D test problem III are given in the following sections.

4.4.2.3.1 Results for LH-based S-KSM optimization for test problem III

The LH-based S-KSM optimization for test problem III achieves the best results with very low e_J values. The best result on the 2D test problem III was achieved with $p_i = 90$, $p_u = 2$ and $e_J = 148$. The lowest standard deviation was 34 with $p_i = 30$ and $p_u = 7$.

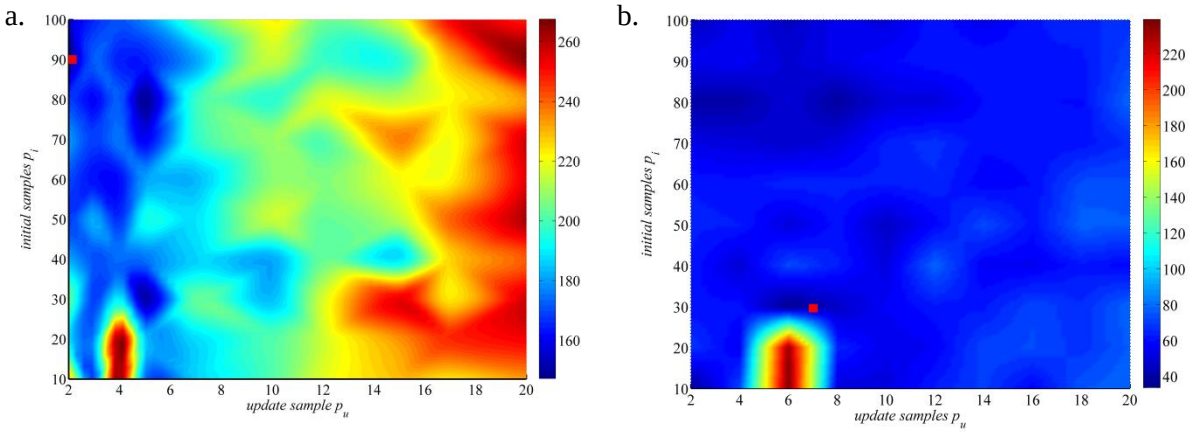

Figure 4-21: Number of true model evaluations e_J for LH-based S-KSM optimization of the 2D version of test problem III: a. mean e_J, b. e_J standard deviation

For the 3D version of test problem III the best $e_J = 913$ is six times higher than for the 2D problem, which clearly shows the high difficulty of this optimization problem. The best configuration was $p_i = 90$ and $p_u = 60$. Thus, a higher number of update samples than for the test problems I and II was necessary to find the global optimum. In general it can be said, that complex problems require a high number of initial samples and update samples to assure a global search with fast convergence. When it comes to the standard deviation, it is interesting to see that the minimum is also at $p_i = 90$ and $p_u = 60$ whereas the surrounding values are much higher. Nevertheless, one reason for such a low standard deviation at this position might also be the relatively low number of optimization runs (10), which does not seem to suffice in this case.

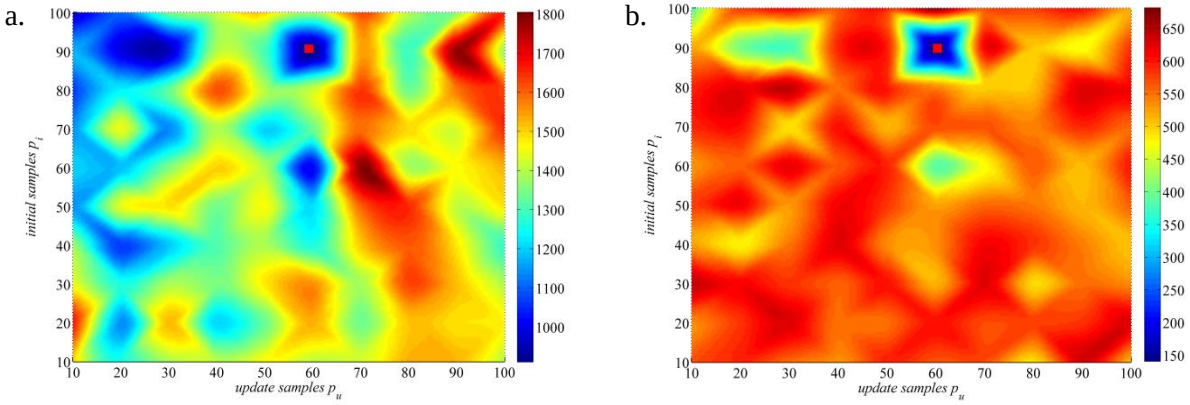

Figure 4-22: Number of true model evaluations e_J for LH-based S-KSM optimization of the 3D version of test problem III: a. mean e_J, b. e_J standard deviation

4.4.2.3.2 Results for PSO-based S-KSM optimization for test problem III

The PSO-based S-KSM optimization performs very poor in comparison to the LH-based S-KSM optimization requiring much more e_J to achieve the same accuracy *A*. For the 2D test problem III, the lowest $e_J = 530$ is achieved with the maximum swarm size $p_{KSM} = 100$. This illustrates the difficulty of this test problem as smaller swarm sizes are not able to cover the complete search space as well as big swarms.

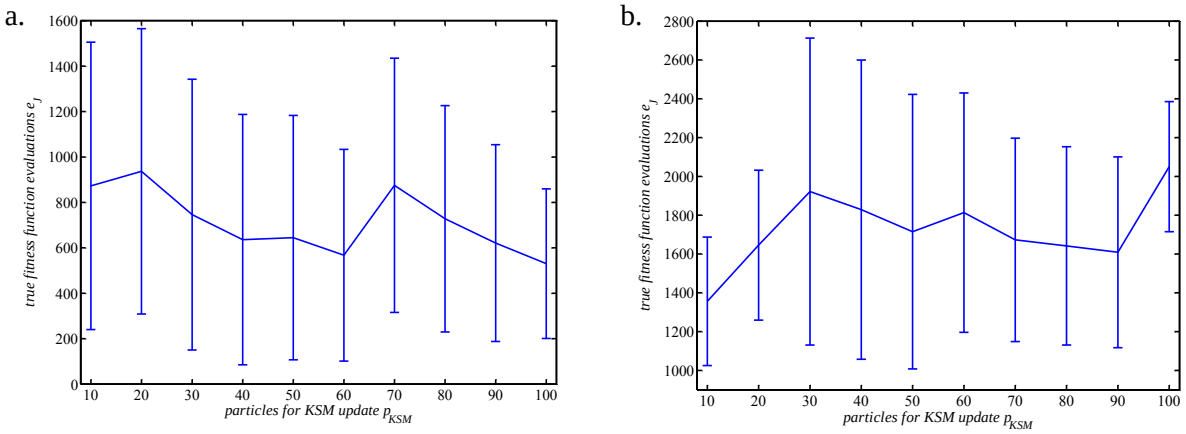

Figure 4-23: Number of true fitness function evaluations e_J for PSO-based S-KSM optimization of the 2D (a.) and 3D (b.) versions of test problem III

The results for the 3D test problem III are similar. Although, the lowest $e_J = 1{,}368$ is achieved with only $p_{KSM} = 10$, it is obvious that bigger swarm sizes cause a slight decrease in e_J. The high standard deviations in both cases clearly indicate that ten optimization runs can only give a first impression and that more runs would give more accurate results. Due to the computation time required for each optimization run, more than ten runs would not have been feasible.

4.4.2.3.3 Performance comparison to original PSO

The performance evaluation of the two novel methods on test problem III in comparison to the original PSO shows that significant improvement of more than 90% is achieved with the LH-based S-KSM optimization, whereas the PSO-based S-KSM optimization fails to considerably improve the overall e_J. In particular for small swarm sizes the improvement of the PSO-based S-KSM optimization is minimal. For larger swarm sizes a reduction of up to 93% can be achieved. The design of test problem III seems to make it particularly difficult for the PSO-based S-KSM optimization as bigger swarm sizes are necessary, which automatically results in higher e_J values.

Table 4-8: Performance results of LH-based S-KSM and PSO-based S-KSM optimization in comparison to original PSO based on mean and standard deviation of true fitness function evaluations e_J for the 2D test problem III

Configuration		LH-based S-KSM		PSO-based S-KSM		original PSO		LH-based S-KSM savings	PSO-based S-KSM savings
LH-based S-KSM	**PSO-based S-KSM / original PSO**	**mean**	**std**	**mean**	**std**	**mean**	**std**		
p_i=90; p_u=2	$p_{KSM} = p_{PSO} = 10$	148	55	873	633	1,147	203	87.1	23.9
p_i=80; p_u=10	$p_{KSM} = p_{PSO} = 20$	148	38	937	628	2,039	253	92.74	54
p_i=30; p_u=10	$p_{KSM} = p_{PSO} = 30$	150	46	746	596	3,299	335	95.45	77.4
p_i=100; p_u=2	$p_{KSM} = p_{PSO} = 40$	155	44	636	551	3,708	415	95.82	82.8
p_i=70; p_u=10	$p_{KSM} = p_{PSO} = 50$	160	51	645	538	4,418	490	96.38	85.4
p_i=80; p_u=5	$p_{KSM} = p_{PSO} = 60$	161	40	567	466	5,287	600	96.95	89.3
p_i=60; p_u=7	$p_{KSM} = p_{PSO} = 70$	162	65	875	560	6,079	620	97.34	85.6
p_i=60; p_u=5	$p_{KSM} = p_{PSO} = 80$	163	60	728	498	6,480	668	97.48	88.8
p_i=90; p_u=7	$p_{KSM} = p_{PSO} = 90$	165	49	621	433	7,466	744	97.79	91.7
p_i=90; p_u=10	$p_{KSM} = p_{PSO} = 100$	165	54	530	329	8,025	789	97.94	93.4
mean		**158**	**50**	**716**	**523**	**4,795**	**512**	**95**	**77**
std		**6.5**	**8.1**	**133.1**	**89.7**	**2,162.5**	**194.4**	**3.2**	**20.7**

Table 4-9: Performance results of LH-based S-KSM and PSO-based S-KSM optimization in comparison to original PSO based on mean and standard deviation of true fitness function evaluations e_J for the 3D test problem III

Configuration		LH-based S-KSM		PSO-based S-KSM		original PSO		LH-based S-KSM savings	PSO-based S-KSM savings
LH-based S-KSM	PSO-based S-KSM / original PSO	mean	std	mean	std	mean	std		
p_i=90; p_u=60	$p_{KSM} = p_{PSO} = 10$	913	141	1,368	1,142	1,368	147	33.26	0
p_i=100; p_u=10	$p_{KSM} = p_{PSO} = 20$	957	382	1,750	998	6,096	2,663	84.3	71.3
p_i=90; p_u=30	$p_{KSM} = p_{PSO} = 30$	962	377	1,922	791	8,259	4,011	88.35	76.7
p_i=90; p_u=20	$p_{KSM} = p_{PSO} = 40$	991	406	1,829	771	10,668	5,130	90.71	82.9
p_i=60; p_u=60	$p_{KSM} = p_{PSO} = 50$	1,010	388	1,715	707	11,135	6,301	90.93	84.6
p_i=40; p_u=20	$p_{KSM} = p_{PSO} = 60$	1,066	480	1,813	617	8,458	4,860	87.4	78.6
p_i=80; p_u=10	$p_{KSM} = p_{PSO} = 70$	1,068	591	1,673	524	7,091	814	84.94	76.4
p_i=100; p_u=20	$p_{KSM} = p_{PSO} = 80$	1,106	580	1,642	511	8,191	820	86.5	80
p_i=70; p_u=30	$p_{KSM} = p_{PSO} = 90$	1,135	489	1,609	492	9,753	2,527	88.36	83.5
p_i=70; p_u=10	$p_{KSM} = p_{PSO} = 100$	1,139	589	2,050	335	11,145	4,505	89.78	81.6
mean		**1,035**	**442**	**1,737**	**689**	**8,216**	**3,178**	**82**	**72**
std		**75.3**	**130.1**	**176.8**	**233.7**	**2,796.3**	**1,996.8**	**16.5**	**24.2**

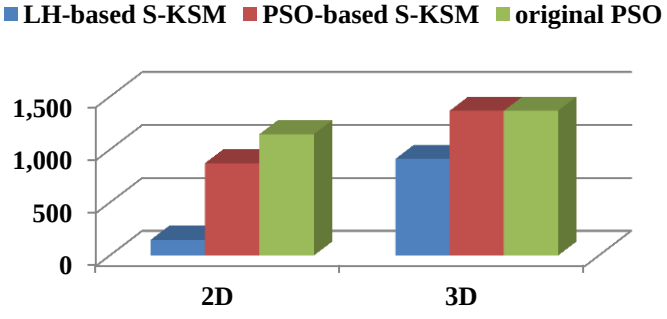

Figure 4-24: Comparison of the lowest e_J for the three evaluated optimization methods applied to test problem III

4.4.2.4 Results for test problem IV

Test problem IV is nearly as challenging as test problem III but it is completely different. The difficulty lies in the many local minima and is highly nonlinear behavior of the alpine function. Because of these characteristics, test problem IV is often used for the test and validation of global optimization methods. For the LH-based and PSO-based S-KSM optimization methods, this test problem is considered to be the most difficult test to determine whether computation time for global optimization can be significantly reduced.

4.4.2.4.1 Results for LH-based S-KSM optimization for test problem IV

The LH-based S-KSM optimization results show that a very low number of e_J is needed to find the global optimum. Furthermore, it is interesting to see that slightly less e_J are needed for the 5D test problem IV than for the 3D problem as was previously observed for test problem II. The reason for this behavior is not clear as a rise of e_J would have been expected.

The best result for the 2D alpine function was achieved with $p_i = 40$, $p_u = 10$ and $e_J = 298$. The lowest standard deviation for the ten optimization runs was 100 for $p_i = 20$ and $p_u = 10$, which is higher than for all the other test problems.

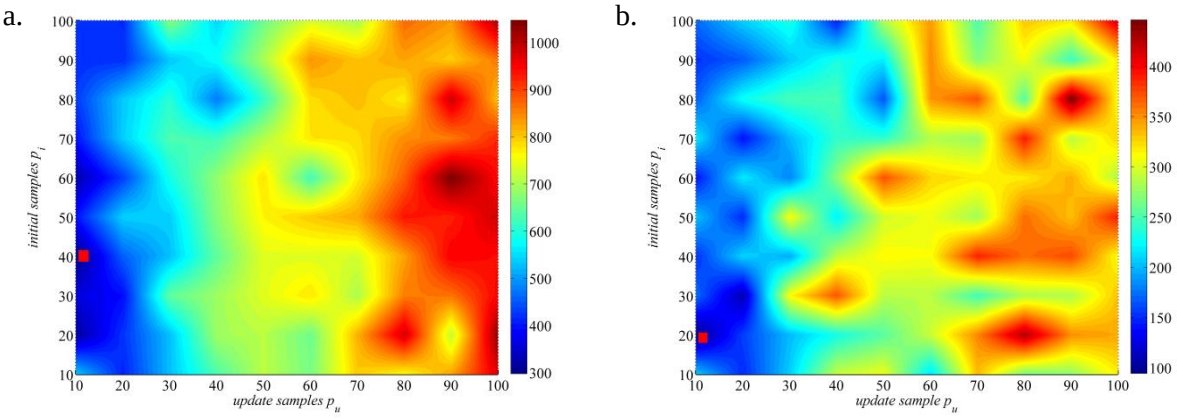

Figure 4-25: Number of true model evaluations e_J for LH-based S-KSM optimization of the 2D version of test problem IV: a. mean e_J, b. e_J standard deviation

The best result for the 3D alpine function with $e_J = 575$ is achieved with the exact same values for $p_i = 40$ and $p_u = 10$ as for the 2D function. The lowest standard deviation of 170 is achieved for $p_i = 90$ and $p_u = 10$. In the case of the 5D alpine function, $e_J = 403$ is considerably lower than for the 3D alpine function, but the number of initial samples is the maximum with $p_i = 100$. Furthermore, the number of update samples is also higher than for the lower dimensional problems with $p_u = 20$. The lowest standard deviation of 36 was achieved with $p_i = 20$ and $p_u = 30$.

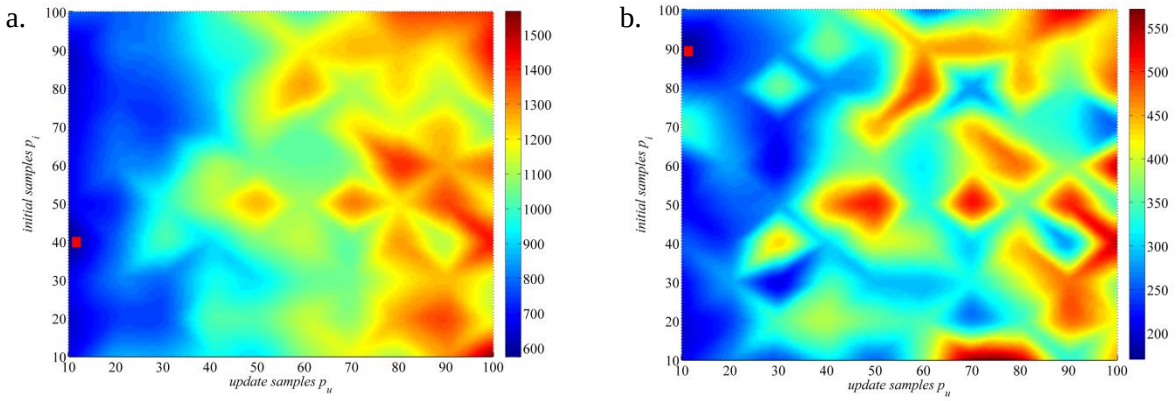

Figure 4-26: Number of true model evaluations e_J for LH-based S-KSM optimization of the 3D version of test problem IV: a. mean e_J, b. e_J standard deviation

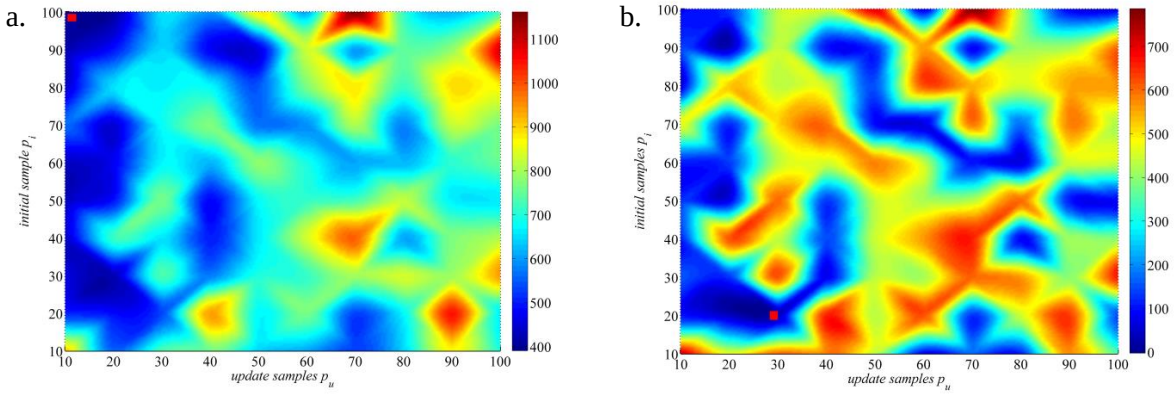

Figure 4-27: Number of true model evaluations e_J for LH-based S-KSM optimization of the 5D version of test problem IV: a. mean e_J, b. e_J standard deviation

4.4.2.4.2 Results for PSO-based S-KSM optimization for test problem IV

The results for the PSO-based S-KSM optimization are much better than the LH-based results on the 2D and 3D alpine function with e_J values that are about 50% lower, which indicates that the method very useful for problems of lower dimensionality. For the 2D alpine function $e_J = 108$ true model evaluations and $p_{KSM} = 10$ particles were needed to find the global optimum. The results for the 3D alpine function with $e_J = 191$ and $p_{KSM} = 10$ as well as for the 5D alpine function with $e_J = 1{,}305$ and $p_{KSM} = 10$ show, that the number of e_J increases steadily with increasing dimensionality as was already discovered for the previous test problems. Nevertheless, standard deviations for all three versions of test problem IV are higher than the standard deviations achieved with the LH-based S-KSM optimization. This indicates, that PSO-based S-KSM optimization might be able to find a global optimum quicker than the LH-based S-KSM optimization, but that it is not that robust.

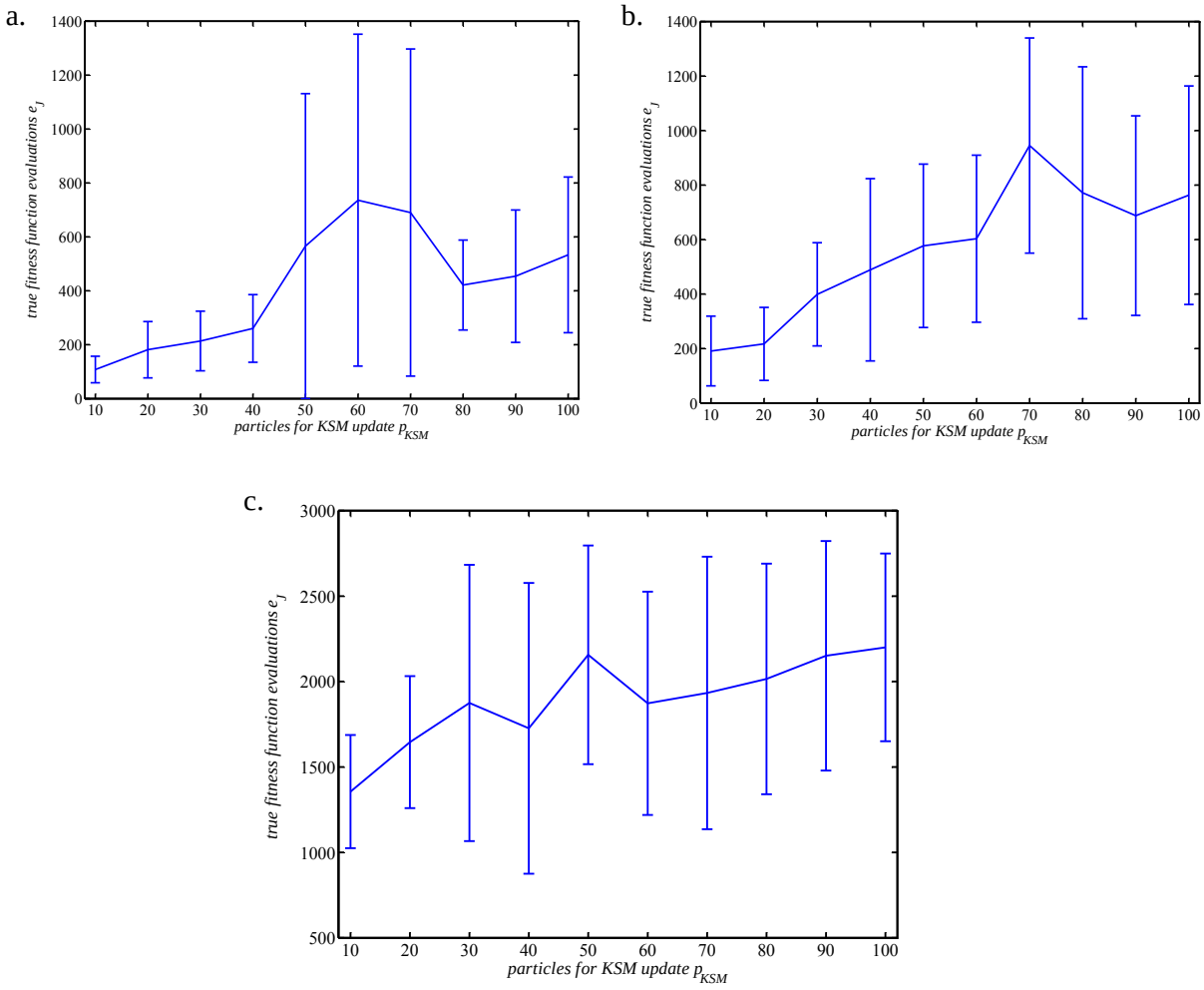

Figure 4-28: Number of true fitness function evaluations e_J for PSO-based S-KSM optimization of the 2D (a.), 3D (b.) and 5D (c.) versions of test problem IV

4.4.2.4.3 Performance comparison to original PSO

The performance comparison of the two novel optimization methods to the original PSO shows that savings in computation time for test problem IV are the biggest compared to the performance results for the previous test problems.

For the 2D alpine function, e_J savings from 82% for LH-based S-KSM optimization and 88% for PSO-based S-KSM optimization are achieved.

Table 4-10: Performance results of LH-based S-KSM and PSO-based S-KSM optimization in comparison to original PSO based on mean and standard deviation of true fitness function evaluations e_J for the 2D test problem IV

Configuration		LH-based S-KSM		PSO-based S-KSM		original PSO		LH-based S-KSM savings	PSO-based S-KSM savings
LH-based S-KSM	**PSO-based S-KSM / original PSO**	**mean**	**std**	**mean**	**std**	**mean**	**std**		
p_i=40; p_u=10	$p_{KSM} = p_{PSO} = 10$	298	152	108	49	556	838	46.4	80.6
p_i=20; p_u=10	$p_{KSM} = p_{PSO} = 20$	316	209	181	104	363	930	12.95	50.1
p_i=60; p_u=10	$p_{KSM} = p_{PSO} = 30$	324	194	214	111	1,829	2,246	82.29	88.3
p_i=30; p_u=10	$p_{KSM} = p_{PSO} = 40$	362	290	260	126	661	1,531	45.23	60.7
p_i=30; p_u=20	$p_{KSM} = p_{PSO} = 50$	392	313	565	647	1912	3,124	79.5	70.4
p_i=50; p_u=10	$p_{KSM} = p_{PSO} = 60$	398	309	736	615	498	1,257	20.08	-47.8
p_i=70; p_u=10	$p_{KSM} = p_{PSO} = 70$	398	389	690	607	1,018	2,341	60.9	32.2
p_i=10; p_u=20	$p_{KSM} = p_{PSO} = 80$	410	362	421	167	1,210	2,889	66.12	65.2
p_i=100; p_u=20	$p_{KSM} = p_{PSO} = 90$	414	374	454	245	725	2,099	42.9	37.4
p_i=90; p_u=10	$p_{KSM} = p_{PSO} = 100$	417	309	533	289	943	2,626	55.78	43.5
mean		**373**	**290**	**416**	**296**	**972**	**1,988**	**51**	**48**
std		**42.4**	**76.2**	**207.4**	**224**	**510.3**	**768**	**21.6**	**36.3**

In the case of the 3D alpine function, e_J savings are considerably higher with a maximum of 95% for both methods.

Table 4-11: Performance results of LH-based S-KSM and PSO-based S-KSM optimization in comparison to original PSO based on mean and standard deviation of true fitness function evaluations e_J for the 3D test problem IV

Configuration		LH-based S-KSM		PSO-based S-KSM		original PSO		LH-based S-KSM savings	PSO-based S-KSM savings
LH-based S-KSM	**PSO-based S-KSM / original PSO**	**mean**	**std**	**mean**	**std**	**mean**	**std**		
p_i=40; p_u=10	$p_{KSM} = p_{PSO} = 10$	575	249	191	128	2,435	1,172	76.39	92.2
p_i=90; p_u=10	$p_{KSM} = p_{PSO} = 20$	636	170	217	134	4,546	1,839	86.01	95.2
p_i=80; p_u=10	$p_{KSM} = p_{PSO} = 30$	641	252	399	189	4,965	3,446	87.09	92
p_i=20; p_u=10	$p_{KSM} = p_{PSO} = 40$	642	200	489	334	8,545	3,159	92.49	94.3
p_i=70; p_u=10	$p_{KSM} = p_{PSO} = 50$	654	342	577	300	7,651	5,398	91.45	92.5
p_i=50; p_u=10	$p_{KSM} = p_{PSO} = 60$	667	211	603	306	11,591	4,729	94.25	94.8
p_i=30; p_u=10	$p_{KSM} = p_{PSO} = 70$	671	214	945	395	6,721	7,631	90.02	85.9
p_i=10; p_u=10	$p_{KSM} = p_{PSO} = 80$	672	208	772	462	11,633	8,315	94.22	93.4
p_i=60; p_u=10	$p_{KSM} = p_{PSO} = 90$	675	216	688	366	14,205	8,748	95.25	95.2
p_i=50; p_u=20	$p_{KSM} = p_{PSO} = 100$	734	251	763	401	13,542	10,508	94.58	94.4
mean		**657**	**231**	**564**	**302**	**8,583**	**5,495**	**90**	**93**
std		**38**	**44**	**232**	**110**	**3,822**	**3,009**	**5.5**	**2.6**

The performance results on the 5D alpine function confirm the very good results for the 2D and 3D problem. With e_J savings of up to 98% (LH-based) and 92% (PSO-based), it is obvious that the two novel global optimization methods are perfectly suited to solve computationally intensive optimization problems.

Table 4-12: Performance results of LH-based S-KSM and PSO-based S-KSM optimization in comparison to original PSO based on mean and standard deviation of true fitness function evaluations e_J for the 5D test problem IV

Configuration		LH-based S-KSM		PSO-based S-KSM		original PSO		LH-based S-KSM savings	PSO-based S-KSM savings
LH-based S-KSM	PSO-based S-KSM / original PSO	mean	std	mean	std	mean	std		
p_i=100; p_u=10	$p_{KSM} = p_{PSO} = 10$	403	90	1,305	834	5,005	982	91.95	73.9
p_i=100; p_u=20	$p_{KSM} = p_{PSO} = 20$	409	135	2,002	634	7,861	2,061	94.8	74.5
p_i=90; p_u=10	$p_{KSM} = p_{PSO} = 30$	418	134	1,875	809	10,940	2,698	96.18	82.9
p_i=30; p_u=20	$p_{KSM} = p_{PSO} = 40$	427	129	1,726	851	14,785	1,703	97.11	88.3
p_i=50; p_u=10	$p_{KSM} = p_{PSO} = 50$	429	128	2,156	640	17,471	3,054	97.54	87.7
p_i=60; p_u=10	$p_{KSM} = p_{PSO} = 60$	434	109	1,873	653	21,130	2,151	97.95	91.1
p_i=80; p_u=10	$p_{KSM} = p_{PSO} = 70$	436	55	1,933	797	23,719	3,088	98.16	91.9
p_i=40; p_u=10	$p_{KSM} = p_{PSO} = 80$	437	104	2,015	675	23,863	8,937	98.17	91.6
p_i=70; p_u=20	$p_{KSM} = p_{PSO} = 90$	452	122	2,151	672	29,007	3,821	98.44	92.6
p_i=30; p_u=10	$p_{KSM} = p_{PSO} = 100$	455	154	2,200	550	31,939	4,714	98.58	93.1
mean		**430**	**116**	**1,924**	**712**	**18,572**	**3,321**	**97**	**87**
std		**16**	**27**	**249.7**	**97.4**	**8,492**	**2,128**	**2**	**6.9**

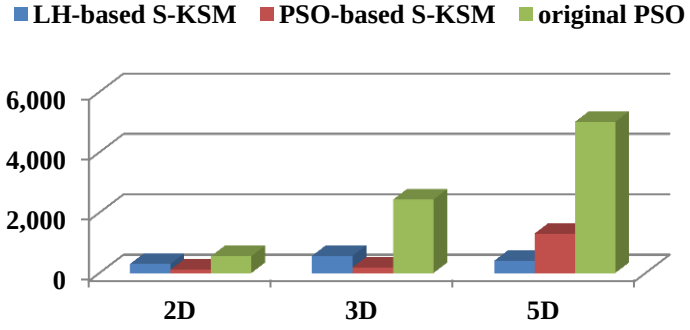

Figure 4-29: Comparison of the lowest e_J for the three evaluated optimization methods applied to test problem IV

All in all, the performance result for test problem IV clearly prove that significant improvement in terms of computation time and e_J in comparison to optimization using the original PSO algorithm can be achieved by the use of LH- and PSO-based S-KSM optimization. Thus, both methods are perfectly suited for high dimensional, highly nonlinear optimization problems.

4.4.3 Computation time of the LH-based S-KSM and PSO-based S-KSM optimization

The investigation of e_J for LH-based and PSO-based S-KSM optimization in comparison to the original PSO is not enough to fully evaluate the performance of the two novel methods. Due to the fact that the regular update of the KSM requires additional computation time t_{KSM}, both the computation time t_J for each e_J and t_{KSM} need to be considered in determining the overall optimization time t_o. Thus, t_o is computed as

$$t_o = k\,t_{KSM} + e_J t_J \text{ with } e_J = e_O + k\,\alpha, \tag{4.33}$$

where k is the number of iterations of the optimization algorithm, e_O the number of initial true fitness function evaluations, α the number of true fitness function evaluations for each KSM update performed during one iteration of the optimization and e_J the number of total true fitness function evaluations. To properly estimate the average computation time of a KSM update, t_{KSM} was measured for a different number of dimensions (2, 3, 4, 5) and a different number of sample points per KSM (100-2,500) for the alpine function. It becomes clear that t_{KSM} increases significantly with higher dimensions and higher number of samples used to build the KSM. The computational complexity of the KSM derived from the results of Figure 4-30 is $O(n^3)$ for n data points, which is confirmed by Cressie and Johannesson (2008).

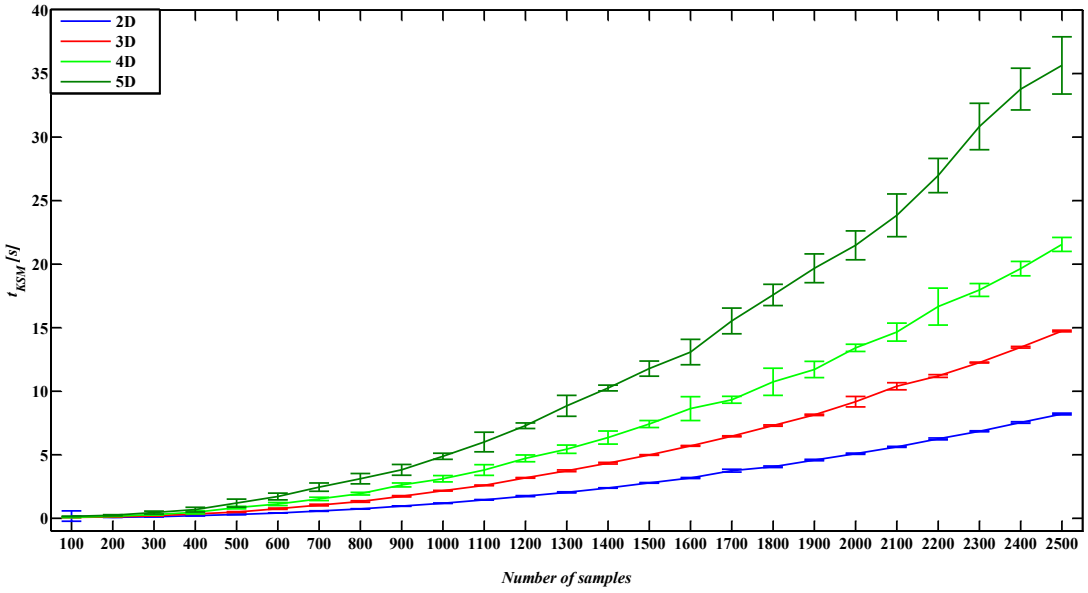

Figure 4-30: Dependency of t_{KSM} on dimensionality and number of samples of the true fitness function (exemplary data for the alpine function)

Based on the data from Figure 4-30 the average computation time t_{KSM} over all KSM updates for the 2D, 3D and 5D versions of the test problems was set as shown in Table 4-13.

Table 4-13: Average t_{KSM} over all KSM updates for the different dimensionalities of the test problems

2D	2.8s
3D	5s
5D	12s

As t_J is the most critical parameter when determining the total optimization time t_o, t_J was estimated to be 30s based on dynamic simulations with a small biogas plant model (one digester). For more complex dynamic models t_J can easily take values from several minutes up to several hours.

Computation time for test problem I

A comparison of the computation times of all three versions of the quadratic function shows that in each case a significant reduction of t_o of several hours can be achieved. Due to the effects described in Figure 4-30, it is obvious that computation time savings are significantly lower with only 41.6% (LH-based S-KSM) and 22.6% (PSO-based S-KSM) for the 5D quadratic function. For the 2D and 3D functions t_o savings are up to 78.5%.

Table 4-14: Computation time savings for test problem I of LH-based and PSO-based S-KSM in comparison to original PSO

Test problem I - 2D	**LH-based S-KSM**	**PSO-based S-KSM**	**original PSO**
$k\,(t_{KSM} = 2.8s)$	41	12	-
$e_J\,(t_J = 30s)$	152	115	540
t_o **[min]**	**77.9**	**58.1**	**270**
t_o **savings [%]**	**71.1**	**78.5**	
Test problem I - 3D			
$k\,(t_{KSM} = 5.03s)$	42	26	-
$e_J\,(t_J = 30s)$	481	261	977
t_o **[min]**	**244**	**132.7**	**488.5**
t_o **savings [%]**	**50**	**72.8**	
Test problem I - 5D			
$k\,(t_{KSM} = 12.05s)$	84	136	-
$e_J\,(t_J = 30s)$	883	1160	1570
t_o **[min]**	**458.4**	**607.3**	**785**
t_o **savings [%]**	**41.6**	**22.6**	

Computation time for test problem II

The computation time results for test problem II are also very good for the 2D and 3D versions of the problem and still acceptable for the 5D version, although the PSO-based S-KSM optimization is only slightly better than the original PSO (11% savings). For the 3D test problem savings of 52.8% (LH-based S-KSM) and 70.1% (PSO-based S-KSM) are very good, resulting in optimization times that are more than six hours faster than the original PSO. Nevertheless, 2D computation times are again much faster with 86.7% (LH-based S-KSM) and 81.8% (PSO-based S-KSM) savings.

Table 4-15: Computation time savings for test problem II of LH-based and PSO-based S-KSM in comparison to original PSO

Test problem II - 2D	**LH-based S-KSM**	**PSO-based S-KSM**	**original PSO**
$k\,(t_{KSM} = 2.8s)$	25	19	-
$e_J\,(t_J = 30s)$	140	194	1074
t_o **[min]**	**71.2**	**97.9**	**537**
t_o **savings [%]**	**86.7**	**81.8**	
Test problem II - 3D			
$k\,(t_{KSM} = 5.03s)$	46	34	-
$e_J\,(t_J = 30s)$	532	336	1143
t_o **[min]**	**269.9**	**170.9**	**571.5**
t_o **savings [%]**	**52.8**	**70.1**	
Test problem II - 5D			
$k\,(t_{KSM} = 12.05s)$	84	142	-
$e_J\,(t_J = 30s)$	483	1424	1665
t_o **[min]**	**258.4**	**740.5**	**832.5**
t_o **savings [%]**	**69**	**11.1**	

Computation time for test problem III

The fact, that test problem III is the most difficult optimization task, is reflected in the computation time that is required to find the global optimum for this problem. In particular PSO-based S-KSM optimization performs rather poorly with 23.2% savings on the 2D problem and no savings on the 3D problem where even more computation time is needed. The performance of LH-based S-KSM optimization is much better with very high 86.9% savings on the 2D and after all 33.1% on the 3D test problem.

Table 4-16: Computation time savings for test problem III of LH-based and PSO-based S-KSM in comparison to original PSO

Test problem III - 2D	LH-based S-KSM	PSO-based S-KSM	original PSO
$k\ (t_{KSM} = 2.8s)$	29	87	-
$e_J\ (t_J = 30s)$	148	873	1147
t_O **[min]**	**75.4**	**440.6**	**573.5**
t_O **savings [%]**	**86.9**	**23.2**	
Test problem III - 3D			
$k\ (t_{KSM} = 5.03s)$	14	136	-
$e_J\ (t_J = 30s)$	913	1368	1368
t_O **[min]**	**457.7**	**695.4**	**684**
t_O **savings [%]**	**33.1**	**-1.7**	

Computation time for test problem IV

As test problem IV is a benchmark for many global optimization methods, computation time results are of particular interest to evaluate the overall performance of LH-based and PSO-based S-KSM optimization. Similar to the previously described results, performance for the 2D and 3D alpine function are good with computation time savings between 80% and 92% in the case of PSO-based S-KSM optimization. Performance of LH-based S-KSM optimization is much poorer than PSO-based S-KSM optimization but still high with 46% (2D) and 76% (3D). In the case of the most complex 5D alpine function, surprisingly both novel methods substantially outperform the original PSO with computation time reduced by 91.7% (LH-based S-KSM) and 72.9% (PSO-based S-KSM). In this case t_O is reduced by more than 38 hours compared to the original PSO.

Table 4-17: Computation time savings for test problem IV of LH-based and PSO-based S-KSM in comparison to original PSO

Test problem IV - 2D	LH-based S-KSM	PSO-based S-KSM	original PSO
$k\ (t_{KSM} = 2.8s)$	25	11	-
$e_J\ (t_J = 30s)$	298	108	556
t_O **[min]**	**150.2**	**54.5**	**278**
t_O **savings [%]**	**46**	**80.4**	
Test problem IV - 3D			
$k\ (t_{KSM} = 5.03s)$	53	19	-
$e_J\ (t_J = 30s)$	575	191	2435
t_O **[min]**	**291.9**	**97.1**	**1217.5**
t_O **savings [%]**	**76**	**92**	
Test problem IV - 5D			
$k\ (t_{KSM} = 12.05s)$	30	130	-
$e_J\ (t_J = 30s)$	403	1305	5005
t_O **[min]**	**207.5**	**678.6**	**2502.5**
t_O **savings [%]**	**91.7**	**72.9**	

4.5 Conclusion for the global optimization with LH- and PSO-based S-KSM

The survey of surrogate models and PSO, given in section 4.1 and 4.2, shows that the use of surrogate models in combination with global optimization methods is not only common but a valid method to reduce optimization time for highly complex problems. Nevertheless, the creation of a surrogate model that adequately matches the true fitness function J based on a small amount of e_J is difficult. To keep these e_J to a minimum, two novel methods were developed and introduced in this chapter, namely LH-based S-KSM and PSO-based S-KSM optimization. These methods update a Kriging surrogate model during the optimization run based on new sample points and the intermediate optimization result, which is new in comparison to existing methods described in section 4.1. Results obtained on four test problems of differing levels of complexity prove that the number of e_J can be reduced by up to 98% in comparison to conventional optimization methods. This translates to a minimum computation time t_O required for the optimization of computationally intensive true fitness functions.

The performance results presented in section 4.4 show that both novel methods are far superior to optimization using standard PSO. Computation time can be reduced by several hours; in the case of test problem IV the reduction was of the order of 1.5 days. Thus, LH-based S-KSM and PSO-based S-

KSM optimization have two major advantages, when used for the optimization of complex true fitness functions.

1. They provide a significant reduction in the number of true function evaluations required for global optimization.
2. The overall computation time to perform the optimization is substantially reduced.

Furthermore, the developed strategies to update a surrogate model are universally applicable, which means that these strategies can be applied to any kind of surrogate model and any kind of global optimization method. In general, the higher the time for one true function evaluation, the higher the reduction of the overall computation time for an optimization run. Thus, if one true function evaluation takes one hour, computation time savings of several days can be easily achieved, which makes such optimization problems perfectly suited for LH-based S-KSM and PSO-based S-KSM optimization. Due to the very good optimization results on the test problems, the optimization of the substrate feed of a biogas plant based on the ADM1 model is performed with these two optimization methods.

References

Angeline, P.J., 1998. Evolutionary optimization versus particle swarm optimization: Philosophy and performance differences. *Lecture Notes in Computer Science (LNCS)*, 1477, 601–610.

Armstrong, M. and Wackernagel, H., 1988. The influence of the covariance function on the Kriged estimator. Geomathematics and Geostatistics Analysts Applied to Space and Time Dependant Data. *Science de la terre, Séries Informatique*, Nancy, 27 (1), 245–262.

Banks, A., Vincent, J. and Anyakoha, C., 2007. A review of particle swarm optimization. Part I: background and development. Natural Computing, 6 (4), 467–484.

Birge, B., 2003. PSOt - a particle swarm optimization toolbox for use with Matlab. *Proceedings of the IEEE swarm intelligence symposium 2003 (SIS 2003), Indianapolis, USA*, 182–186.

Booker, A., J. E. Dennis Jr., Paul, JR., Frank, P.D., Serafini, D.B., Torczon, V. and Trosset, M.W., 1998. A Rigorous Framework for Optimization of Expensive Functions by Surrogates. *Structural Optimization*, 17 (1), 1–13.

Box, G.E.P., Hunter, J.S., and Hunter, W.G., 2005. *Statistics for experimenters: Design, innovation, and discovery*. 2nd ed. Hoboken, N.J: Wiley-Interscience.

Carlisle A. and Dozier G., 2000. Adapting particle swarm optimization to dynamic environments. *Proceedings of the International Conference on Artificial Intelligence* (1), 429–434.

Carlisle, A. and Dozier, G., 2001. An Off-The-Shelf PSO. *Proceedings of the workshop on particle swarm optimization (Indianapolis, IN)*.

Chandra Mohan, B. and Baskaran, R., 2012. A survey: Ant Colony Optimization based recent research and implementation on several engineering domain. *Expert Systems with Applications*, 39 (4), 4618–4627.

Cheng, B. and Titterington, D.M., 1994. Neural networks: a review from a statistical perspective. *Statistical Science*, 9 (1), 2–54.

Clerc, M., 1999. The swarm and the queen: towards a deterministic and adaptive particle swarm optimization. *Proceedings of the 1999 Congress on Evolutionary Computation, Washington DC*, 1951–1957.

Clerc, M. and Kennedy, J., 2002. The particle swarm - explosion, stability, and convergence in a multidimensional complex space. *IEEE Transactions on Evolutionary Computation*, 6 (1), 58–73.

Clerc, M., 2006. Particle swarm optimization. London: ISTE.

Cressie, N. and Johannesson, G., 2008. Fixed rank kriging for very large spatial data sets. *Journal of the Royal Statistical Society: Series B (Statistical Methodology)*, 70 (1), 209–226.

Currin, C., Mitchell, T., Morris M., and Ylvisaker D., 1988. A Bayesian Approach to the Design and Analysis of Computer Experiments: Technical Report ORNL-6498. Oak Ridge, TN: Oak Ridge National Laboratory.

Davis, L., 1991. *Handbook of genetic algorithms*. New York: Van Nostrand Reinhold.

Dyn, N., Levin, D. and Rippa, S., 1986. Numerical Procedures for Surface Fitting of Scattered Data by Radial Functions. *SIAM Journal on Scientific and Statistical Computing*, 7 (2), 639.

Ebel, A., 2009. Application of Computational Intelligence Techniques to Modelling, Control and Optimisation of Wastewater Treatment Plants. National University of Ireland Maynooth.

Eberhart, R. and Shi, Y., 2000. Comparing inertia weights and constriction factors in particle swarm optimization. *Proceedings of IEEE congress evolutionary computation*, 84–88.

Fishman, G.S., 2008. *Monte Carlo: Concepts, Algorithms, and Applications.* 7th ed. New York, NY, USA: Springer.

Friedmann, J.H., 1991. Multivariate adaptive regression splines. *The Annals of Statistics*, 19 (1), 1–141.

Gano, S.E., Renaud, J.E., Martin, J.D. and Simpson, T.W., 2006. Update strategies for kriging models used in variable fidelity optimization. *Structural and Multidisciplinary Optimization*, 32 (4), 287–298.

Gao, Y. and Wang, X., 2008. An effective warpage optimization method in injection molding based on the Kriging model. *The International Journal of Advanced Manufacturing Technology*, 37 (9-10), 953–960.

Giunta A. and Watson, L.T., 1998. A comparison of approximation modeling techniques: polynomial versus interpolating models. *Proceedings of the 7th AIAA/USAF/NASA/ISSMO Symposium on multidisciplinary analysis and optimization*, 392–404.

Hardy, R.L., 1971. Multiquadric Equations of Topography and Other Irregular Surfaces. *Journal of Geophysical Research*, 76 (8), 1905–1915.

Heppner, F. and Grenander, U., 1990. A stochastic nonlinear model for coordinated bird flocks. The Ubiquity of Chaos: AAAS Publications.

References

Huang, D., Allen, T.T., Notz, W.I. and Zeng, N., 2006. Global Optimization of Stochastic Black-Box Systems via Sequential Kriging Meta-Models. *Journal of Global Optimization*, 34 (3), 441–466.

Jin, R., Chen, W. and Simpson, T., 2001. Comparative studies of metamodelling techniques under multiple modelling criteria. *Structural and Multidisciplinary Optimization*, 23 (1), 1–13.

Jin, R., Du, X. and Chen, W., 2003. The use of metamodeling techniques for optimization under uncertainty. Structural and Multidisciplinary Optimization, 25 (2), 99–116.

Kaewkamnerdpong, B. and Bentley, P., 2005. Perceptive particle swarm optimisation: an investigation. *Proceedings of the IEEE Swarm Intelligence Symposium 2005*, 169–176.

Kassteele, J., Stein, A., Dekkers, A.L.M. and Velders, G.J.M., 2009. External drift kriging of NOx concentrations with dispersion model output in a reduced air quality monitoring network. *Environmental and Ecological Statistics*, 16 (3), 321–339.

Kennedy, J. and Eberhart, R., 1995. Particle swarm optimization. In: *Proceedings of the IEEE International Conference on Neural Networks*. Perth, Australia, 1942–1948.

Kennedy, J., 2003. Bare bones particle swarms. *Proceedings of the IEEE swarm intelligence symposium 2003 (SIS 2003), Indianapolis, USA*, 80–87.

Kim, K.-Y. and Shin, D.-Y., 2008. Optimization of a staggered dimpled surface in a cooling channel using Kriging model. *International Journal of Thermal Sciences*, 47 (11), 1464–1472.

Kleijnen, J.P., 2009. Kriging metamodeling in simulation: A review. *European Journal of Operational Research*, 192 (3), 707–716.

Lam, X.B., Kim, Y.S., Hoang, A.D. and Park, C.W., 2009. Coupled Aerostructural Design Optimization Using the Kriging Model and Integrated Multiobjective Optimization Algorithm. *Journal of Optimization Theory and Applications*, 142 (3), 533–556.

Lefèbvre, J., Roussel, H., Walter, E., Lecointe, D. and Tabbara, W., 1996. Prediction from wrong models: the Kriging approach. *IEEE Antennas and Propagation Magazine*, 38 (4), 35–45.

Lin, Y., Mistree, F., Allen, J.K., Tsui, K.-L. and Chen, V.C.P., 2004. Sequential metamodeling in engineering design. *Collection of Technical Papers - 10th AIAA/ISSMO Multidisciplinary Analysis and Optimization Conference.*

Lophaven, S.N., Nielsen, H.B., and Sondergaard, J., 2002. DACE - A Matlab Kriging Toolbox.

Martin, J.D. and Simpson, T.W., 2003. A Study on the Use of Kriging Models to Approximate Deterministic Computer Models. *Proceedings of ASME 2003 design engineering technical conferences and computers and information in engineering conference*, 567–576.

Martin, J. and Simpson, T., 2005. Use of Kriging Models to Approximate Deterministic Computer Models. *AIAA Journal*, 43 (4), 853–863.

Matheron, G., 1963. Principles of geostatistics. *Economic Geology*, 58, 1246–1266.

McKay, M.D., Beckman, R.J. and Conover, W.J., 1979. A Comparison of Three Methods for Selecting Values of Input Variables in the Analysis of Output from a Computer Code. *Technometrics*, 21 (2), 239.

Myers, R.H. and Montgomery, D.C., 1995. Response surface methodology: Process and product optimization using designed experiments. New York: Wiley.

Nelder, J. A. and Mead, R. A., 1965. A Simplex method for Function Minimization. *Computer Journal* (7), 380-313.

O'Reilly, U.-M., Beyer, H.-G., Monson, C.K. and Seppi, K.D., 2005. Bayesian optimization models for particle swarms. *Proceedings of genetic and evolutionary computation conference (GECCO)*, 193–199.

Parsopoulos, K.E. and Vrahatis M. N., 2002. Initializing the particle swarm optimizer using the nonlinear simplex method. *Advances in intelligent systems, fuzzy systems, evolutionary computation*, 216–221.

Parsopoulos, K.E. and Vrahatis, M.N., 2004. UPSO: a unified particle swarm optimization scheme. *Lecture series on computer and computational sciences (Proceedings of international conference on computational methods in sciences and engineering)*, 868–873.

Poli, R., Kennedy, J. and Blackwell, T., 2007. Particle Swarm Optimization: An Overview. *Swarm Intelligence*, 1 (1), 33–57.

Riget, J. and Vesterstrøm, J.S., 2002. *A diversity-guided particle swarm optimizer – the ARPSO.* EVALifeTechnical Report no 2002–2002.

Sacks, W., Welch, J., Mitchell, T.J. and Wynn H.P., 1989. Design and Analysis of Computer Experiments. *Statistical Science*, 4, 409–423.

Sasena, M.J., Papalambros, P. and Goovaerts, P., 2002. Exploration of Metamodeling Sampling Criteria for Constrained Global Optimization. *Engineering Optimization*, 34 (3), 263–278.

References

Schwefel, H.-P., 1995. Evolution and optimum seeking. New York: Wiley.

Seo, S.-I., Lee, M.K., Kim, S.-J. and Kim, N., 2011. Robust optimum design of a bearingless rotation motor using the Kriging model. *International Journal of Precision Engineering and Manufacturing*, 12 (6), 1043–1050.

Shanno, D. F., 1970. Conditioning of Quasi-Newton Methods for Function Minimization. *Mathematics of Computation*, 24, 647–656.

Silva, A., Neves, A. and Costa, E., 2002. An Empirical Comparison of Particle Swarm and Predator Prey Optimisation. *Lecture Notes in Computer Science (LNCS)* (2464), 103–110.

Simpson, T., Poplinski, J., Koch, P.N. and Allen, J., 2001. Metamodels for Computer-based Engineering Design: Survey and recommendations. *Engineering With Computers*, 17 (2), 129–150.

Smith, M., 1993. *Neural networks for statistical modeling*. New York: Van Nostrand Reinhold.

Stone, M.C. and Reynolds, C.W., 1987. Flocks, herds and schools: A distributed behavioral model. *SIGGRAPH '87 Proceedings of the 14th annual conference on Computer graphics and interactive techniques*, 25–34.

Stigler, S.M., 1974. Gergonne's 1815 paper on the design and analysis of polynomial regression experiments. *Historia Mathematica*, 1 (4), 431–439.

Trelea, I.C., 2003. The particle swarm optimization algorithm: convergence analysis and parameter selection. *Information Processing Letters*, 85 (6), 317–325.

Ujjin, S. and Bentley, P. Particle swarm optimization recommender system. *Proceedings of the IEEE swarm intelligence symposium 2003 (SIS 2003)*, Indianapolis, USA, 124–131.

van den Bergh, F. and Engelbrecht, A., 2002. A new locally convergent particle swarm optimiser. *Proceedings of the IEEE International Conference on Systems, Man and Cybernetics*.

Veeramachaneni, K., Peram, T., Mohan, C. and Osadciw, L.A., 2003. Optimization Using Particle Swarms with Near Neighbor Interactions. *Lecture Notes in Computer Science (LNCS)* (2723), 110–121.

Wang, H., Zhu, X. and Du, Z., 2010. Aerodynamic optimization for low pressure turbine exhaust hood using Kriging surrogate model. *International Communications in Heat and Mass Transfer*, 37 (8), 998–1003.

Weise, T., 2009. *Global Optimization Algorithms – Theory and Application*. Available from: http://www.it-weise.de/projects/book.pdf.

Wolf, C., McLoone, S. and Bongards, M., 2008. Biogas plant optimization using genetic algorithms and particle swarm optimization. *IET Irish Signals and Systems Conference (ISSC) 2008*; Galway, Ireland, 244–249.

Yuhui, S. and Eberhart, R., 1998. Modified particle swarm optimizer. *Proceedings of the 1998 IEEE International Conference on Evolutionary Computation*, 69–73.

Yusup, N., Zain, A.M. and Hashim, S.Z.M., 2012. Evolutionary techniques in optimizing machining parameters: Review and recent applications (2007–2011). *Expert Systems with Applications*, 39 (10), 9909–9927.

Zhang, L., Yu, H. and Hu, S., 2005. Optimal choice of parameters for particle swarm optimization. *Zhejiang University Science*, 528–534.

5 Optimization of ABPs

The optimization of ABPs is important to maintain stable operation and to constantly improve process efficiency as previously mentioned in chapter 2. In particular, rising prices for biomass due to high demand and steadily decreasing remuneration rates for electricity and heat from biogas plants driven by revised Renewable Energy Laws (BMU 2011) put additional pressure on biogas plant operators and biogas service providers to maximize biogas production while reducing substrate and energy costs. Thus, the optimization and control of AD plants is a central topic of research and development. Unfortunately, the majority of developments in this area have been largely confined to lab-scale digesters and to the digestion of waste-activated sludge (Steyer *et al.* 2006). The main reasons why research on optimization and control has rarely been applied and validated on full-scale AD plants and particularly on ABPs are the lack of necessary online measurements and the difference in process behavior between lab- and full-scale processes, which make upscaling of such developments very difficult. Therefore, novel and innovative optimization and control methods, that consider the aforementioned challenges and which are (1) suitable for full-scale application and (2) manageable for ABP service providers as well as ABP operators, need to be developed.

This chapter presents such a novel method for the optimization of ABPs by determining the optimal substrate inflow which maximizes plant efficiency by maximizing biogas yield, minimizing costs and guaranteeing process stability. The introduced method is a model based optimization method which combines the fully calibrated simulation model of the Sunderhook ABP from chapter 3 with the newly developed optimization methods using S-KSM and PSO from chapter 4. The combination of these tools allows for a fast and effective optimization of ABP substrate inflows which can be easily implemented in full-scale operation. Thus, the main contributions of the chapter are (1) the definition of the ABP optimal substrate inflow optimization problem, and (2) the evaluation of the performance of the developed optimization method for optimizing the Sunderhook ABP substrate inflow.

The remainder of the chapter is organized as follows. Section 5.1 gives a short survey of advances in the area of optimization and control of AD plants in general and section 5.2 describes the optimization problem of ABPs with regard to an optimal substrate inflow and introduces the fitness function used in the optimization algorithm. The achieved optimization results based on this fitness function are given in section 5.3 where subsections 5.3.1 to 5.3.4 show the main optimization results of this work based on a combination of S-KSM and PSO. To sum up, a conclusion on the results obtained and their relevance in practice is given in section 5.4.

5.1 Short review on optimization and control of AD processes

This short review about developments in the area of optimization and control of AD processes introduces some of the most significant ideas and concepts from the last 20 years. Due to the high

number of publications in this area with more than 140 original research papers on Scopus alone[19], only a small extract is discussed in chronological order.

In 1993 Polihronakis *et al.* developed one of the first model-based control algorithms for AD of waste-activated sludge based on a simplified version of the dynamic simulation model developed by Andrews (1969). Three control strategies were developed; (1) substrate concentration control in the effluent, (2) methane production rate control and (3) a combined control strategy of (1) and (2). The overall goal of the combined controller is to hold both set points for substrate concentration and methane production in the face of process disturbances and highly oscillating inflow concentrations. The practical implementation of the combined control strategy was straight forward. At each sample point the actual value for both controlled variables is compared with the set point. If the deviation from the set point for one controlled variable is greater than a predefined margin the algorithm switches to the controller for this variable. If the actual value is within that margin the controller for the other controlled variable is used. Thus, at each sample point a switching between control strategies (1) and (2) occurs. The control variables for the whole system were the dilution rate of the digester inflow and the feed rate in relation to the digester volume (i.e. the digester load). The developed controllers were tested using the full simulation model by Andrews (1969) and at a full-scale digester with a capacity of 1,600 m³ fed from a municipal WWTP with 110,000 PE[20]. Results show that the controller was able to closely follow changes in substrate concentration and methane production of 10%.

A practical control strategy which is easy to implement was introduced by Steyer *et al.* (1999) who decided to monitor and analyze the reaction of an AD process to sudden changes in substrate inflow and concentration. The disturbances of the substrate inflow were a maximum 20% more than the previous substrate inflow and process reaction was monitored through the controlled variables pH and biogas yield. The idea behind the controller is that an increase in substrate inflow should result in a comparable increase in biogas yield under normal process conditions. If this is not the case, the AD process is inhibited in some way and the substrate inflow needs to be reduced. Therefore, a ratio R between the real and the expected biogas yield is calculated. If R is close to 1 after a step change in substrate inflow, the substrate inflow is increased and if R is between predefined boundaries $R_{\min}$ and $R_{\max}$ the substrate inflow is kept constant. In the case that R is below or equal to $R_{\min}$, the substrate inflow is decreased. This control strategy was validated at a 15 l lab-scale digester and a 120 l pilot-scale digester. Although this method is straight forward its transfer to ABP operation is difficult for two main reasons. Firstly, *pH* is not a reliable process parameter as buffer capacity in ABPs is extremely high. Thus, significant changes in *pH* would already result in complete process failure.

[19] general search in the Scopus publications database for "anaerobic digestion optimization and control" (http://www.scopus.com)
[20] PE – Population Equivalents

Secondly, a step change in substrate inflow of up to 20% is very high and can easily result in severe process inhibition and eventually process breakdown. Therefore, the risks involved in the application to ABPs are too high for ABP operators.

Another highly complex control strategy with a focus on adaptive and robust model-based control of AD processes was developed by Hilgert *et al.* (2000). The aim of the controller was to manipulate the substrate inflow to achieve a set point for the biogas outflow rate. The model employed was an ARMAX (Auto Regressive Moving Average) model of the form

$$A(q)(y_n - y_{eq}) = B(q)(u_n - u_{eq}) + C(q)e_n \tag{5.1}$$

where u_n and y_n are the input and output values of the system at time n and $u_{eq} = 15$ [$\mathrm{lh^{-1}}$] and $y_{eq} = 110$ [$\mathrm{lh^{-1}}$] define the steady state operating conditions of the system. Furthermore, q and e represent a delay operator and white noise and A, B and C are polynomials which need to be determined. As these types of models are trained to represent one specific operating region defined by (u_{eq}, y_{eq}) and do not cope well with disturbances and volatile process parameters, the applied ARMAX model was transformed into a parameter free model using nonparametric estimation for the determination of unknown or uncertain process parameters. Although this procedure is mathematically complex and time-consuming, controller test results at a 120 l pilot plant show that the controller was able to track set point changes quickly and accurately.

Liu *et al.* (2004) a former PhD student of Gustaf Olsson[21] who is well-known for his achievements in the area of industrial automation and control of WWTPs, developed another control strategy using standard PI controllers on the inner level for the control of *pH* and gas flow rate, while using a rule-based supervisory control system on the outer level defining the set points of the gas flow rate. This cascaded controller uses *pH*, gas flow rate and methane concentration in the biogas as controlled variables and the substrate feeding rate as manipulating variable. The whole control setup was tested at a 1.8 l lab-scale reactor under different disturbance conditions which could all be successfully rejected. The main advantage of this control system is the use of different time constants in the inner and outer level of control to adequately react to slow and fast process changes. This allows for plant operation at maximum productivity while guaranteeing process stability. Nevertheless, the use of *pH* as the controlled variable is again not optimal for ABP control applications, which renders this inner control loop useless.

Instead of using *pH* or biogas production as the controlled variable, Boe *et al.* (2008) measured propionate concentration online as high propionate concentration causes strong process inhibition. The overall goal of the controller is to manipulate substrate inflow so that propionate concentration is always below 10 mMol. The controller itself is simple and consists of a feature state controller which

[21] https://www.iea.lth.se/people/gustaf_olsson.html

adjusts the substrate inflow according to fixed ranges of propionate concentration. In total, three different configurations of the feature state controller were tested and manually adapted based on expert knowledge. The performance of the feature state controller was tested at a lab-scale digester (9 l) fed with manure. To allow for a comprehensive evaluation of the control strategy, additional online measurements for *pH*, biogas production, total *VFA* as well as specific *VFAs* were performed on a regular basis. The results show that adaptation of the substrate inflow according to propionate concentration in the digester is far from optimal as high fluctuations in biogas concentration are one of the consequences. Furthermore, there are only three states in each configuration of the feature state controller which results in rapid and drastic changes of the substrate inflow. Therefore, Boe *et al.* (2008) suggests the use of biogas flow rate as controlled variable to maintain a continuously stable biogas production while using propionate concentration as an early warning system for process inhibitions. Even though the feature state controller was successfully evaluated at lab-scale its upscaling is very difficult as the online measurement of *VFA* or even single *VFAs* is very expensive and hard to manage. Nevertheless, in combination with the online measurement system for *VFAs* introduced in chapter 6, this controller could be implemented at full-scale.

An interesting controller design which was developed and validated with the ADM1 was developed by Alferes *et al.* (2008) whose idea was to use equalization tanks to buffer the substrate inflow to digesters of a WWTP treating slaughterhouse waste. Through efficient use of these equalization tanks, the substrate inflow can be flexibly adapted to the current state of the process. Due to the fact that this controller relies on the developments from Liu *et al.* (2004), the same online measurements are used as controlled variables (*pH* and gas flow rate) with the gas flow used as a set point. Although the controller is basically the same as the one from Liu *et al.* (2004) only that the equalization tanks are also controlled, a remarkable amount of testing was performed on ADM1 simulation models of a lab-scale digester (1.2 l), a 1 m³ pilot-scale digester and a full-scale AD plant for slaughterhouse wastewater with two digesters of 68 m³ and 171 m³ capacity respectively. Overall, an average increase of 30% was achieved in the total amount of biogas produced. These results prove the suitability of the ADM1 for AD plant control and optimization.

A good example of the use of Computational Intelligence for ABP control was given by Scherer *et. al* (2009) who designed a fuzzy logic controller (FLC) for an ABP digesting sugar beets as a mono-substrate. The main problem with the digestion of sugar beets is the extremely low pH value (3.3) of the input substrate which makes stabilizing the AD process a major priority as buffer capacity is extremely low. The FLC was implemented in Labview[22] and the rule set was based on the online measurements of pH, biogas flow and methane concentration in the biogas. The control system was evaluated at lab-scale using a 15 l digester and results of a long term study over several years show

[22] http://www.ni.com/labview/d/

that process stability was successfully maintained during that period and that the FLC was able to compensate disturbances caused by changing digester load and temperature.

In 2010, Alferes and Irizar made another attempt to improve AD control based on equalization tanks. A fuzzy-based supervisory module monitoring the state of equalization tanks of AD plants was implemented at the highest level of the previously developed controller (Alferes *et al.* 2008) whose purpose was to optimize methane production in the long run. The maximum methane production set point was defined by the state of the equalization tank determined by fill level and substrate concentration. Control performance was measured through four indexes: (1) Effluent Quality Index (EQI) determined by *COD*, *TSS* and *TKN* concentrations in the effluent, (2) *COD* Removal Efficiency (Ref) determined by the ratio of COD_{in} and COD_{out}, (3) Unitary Methane Production (UMP) described by the ratio of methane production and substrate inflow, (4) Energy Recovery Index ($kwhd^{-1}$). Evaluation of the controller performance showed an increase in effluent quality and methane production by 10-15%.

Another multi-objective cascaded controller was recently developed by García-Diéguez *et al.* (2011) who used *VFA* concentration in the effluent and methane flow rate as controlled variables. The difference in comparison to other existing control strategies is the use of a low-maintenance, easy to manage online measurement system for *VFA* concentration called ANASENSE® (de Neve and Lievens 2004) which makes the transfer of this control strategy to full-scale AD plants possible. The two operational objectives of the controller were to (1) maximize methane production in the inner control loop, and (2) improve effluent quality in the outer control loop. Validation of the controller was performed in two stages. In the first stage the ADM1 simulation model of a 1.15 m³ pilot-scale digester was used before application to the actual pilot-scale reactor. Results show that the controller was able to successfully reject all disturbances during the validation phase.

This small selection of developments in the area of optimization and control of AD processes illustrates that the main manipulated variable is always the substrate inflow. Thus, the challenge in the case of ABP optimization and control is to find the optimal substrate combination for the present state of the AD process. Furthermore, the review shows that model-based approaches as well as the use of CI methods are common in this case due to the high non-linearity of the underlying processes. Therefore, CI methods were used in combination with an ADM1 simulation model for substrate feed optimization of the Sunderhook ABP.

5.2 Description of the optimization problem

The optimization problem for ABPs can best be described by looking at a general description of an ABP system to identify the main input, output variables and the important influencing factors also called disturbances (Figure 5-1). It becomes obvious that the number of manipulated and controlled variables is very small. In addition to the most prominent manipulated variable, the substrate feed $\boldsymbol{x}_S$, mixing of the digester, pH control as well as digestate and biogas recirculation are among the few important manipulated variables. Due to the fact, that the substrate feed $\boldsymbol{x}_S$ has a strong influence on process stability and the produced electrical and thermal energy (y_{Eel}, y_{Eth}), $\boldsymbol{x}_S$ is used as the key manipulated variable in the inflow of an ABP with the view to improving biogas quality and performance of the cogeneration units. Other influencing variables acting as disturbances cannot be controlled because they are very hard to monitor. Most of these disturbances are caused by variations in substrate quality which is determined by *TS*, *VS* and *pH* as well as by inhibition caused by high *VFA*, NO_3, NH_4 and H_2S concentrations.

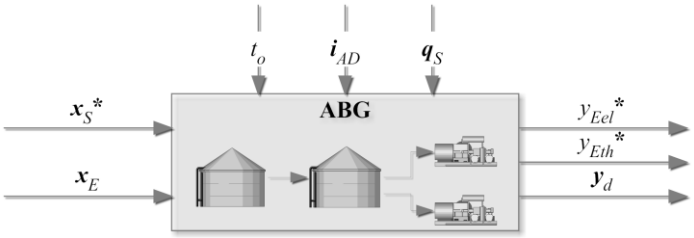

$\boldsymbol{x}_S$ - substrate feed
$\boldsymbol{x}_E$ - energy input/consumption
$\boldsymbol{t}_o$ - outside temperature
$\boldsymbol{i}_{AD}$ - anaerobic digestion inhibitors
$\boldsymbol{q}_S$ - variations in substrate quality
y_{Eel} - electrical energy
y_{Eth} - heat energy
$\boldsymbol{y}_d$ - fully digested sludge
* - controllable variables

Figure 5-1: System description of a standard ABP

For industrial AD plants treating the organic fraction of municipal solid waste (oMSW) the different n substrate components of $\boldsymbol{x}_S = \left[x_{S_1}, ..., x_{S_n} \right]^T$ are normally not known and cannot be properly separated nor characterized which makes optimization of the substrate feed according to the current state of the AD process very difficult. The only possibility is to reduce or increase the total amount of substrate (x_S^T) over time, that is

$$\frac{d\boldsymbol{x}_S^T}{dt}, \text{ where } x_S^T = \sum_{i=1}^{n} x_{S_i} \tag{5.2}$$

Instead ABPs offer diverse possibilities to change and optimize the substrate feed $\boldsymbol{x}_S$. Not only can the number of substrates n be changed if new substrates are available on the market, but also the ratio

of the substrates in $\boldsymbol{x}_S$ can be adapted. Thus, $\boldsymbol{x}_S$ is determined by n and the amount of each single substrate x_{S_i} for $i = 1,...,n$.

$$\frac{d\boldsymbol{x}_S}{dt} = \left[\frac{dx_{S_i}}{dt} \quad \cdots \quad \frac{dx_{S_n}}{dt} \right] \tag{5.3}$$

In the case of the Sunderhook ABP, substrate inflow optimization is performed for $n = 2,3,4,5$ substrates, which are maize, bull manure, green rye, grass silage and oats.

As the literature review from the previous section showed, many of the developed methods used for optimization and control of ABPs are model or state based and involve CI methods, which indicates that the AD process is difficult to optimize and control. What makes optimization difficult is the highly nonlinear behavior of the AD process, which is documented in Figure 5-2. A basic simulation model of an ABP was fed with steadily increasing amounts of maize and green rye which eventually resulted in complete process failure. The sudden drop in biogas production and methane concentration proves the nonlinearity of AD processes. The more substrates are used the more difficult the optimization of the substrate inflow becomes, which is why nonlinear optimization methods such as CI methods are perfectly suited for this problem.

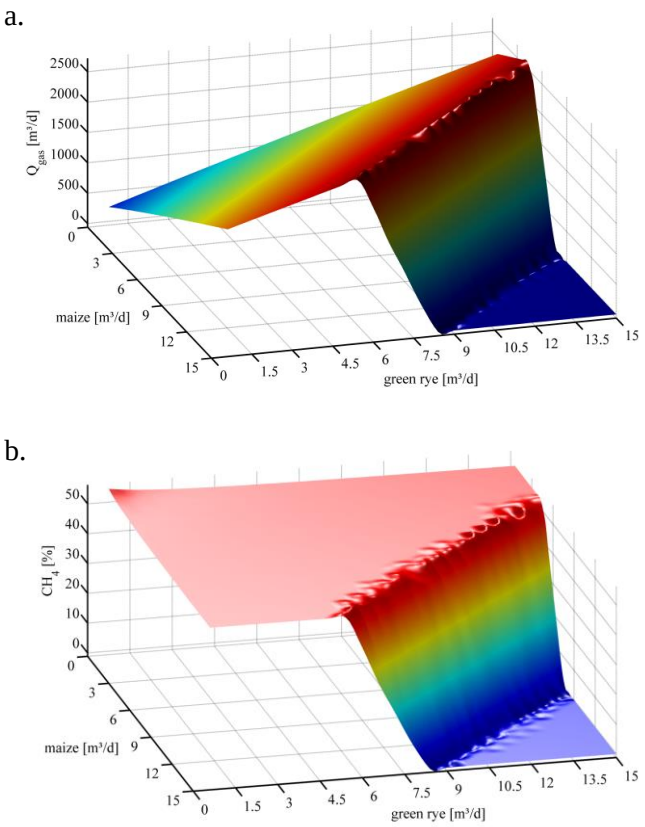

Figure 5-2: Nonlinearity of the AD process shown by simulation results of an ABP fed with steadily increasing substrate inflow, a. biogas production, b. methane concentration

To use CI methods, an assessment of optimization quality is necessary, which is implemented in the form of a fitness function $J(\boldsymbol{x}_S)$. The design of this fitness function is described in the following section.

5.2.1 The fitness function

The fitness function $J(\boldsymbol{x}_S)$ used for the assessment of substrate feed quality in order to achieve a highly efficient AD process is a weighted combination of separate performance measures and penalties. The weights

$$w_i \in \left\{ w_{COD_{\deg}}, w_{pH}, w_{TS}, w_{gas,excess}, w_{fin}, w_{ch4}, w_{COD}, w_{VOA/TIC} \right\} \tag{5.4}$$

for each of the fitness function components were determined based on expert knowledge and in close collaboration with the operator of the Sunderhook ABP. The complete fitness function $J(\boldsymbol{x}_S)$ is defined as

$$\begin{aligned} J(\boldsymbol{x}_S) = {} & w_{COD_{deg}} \left(SS_{fitness}(\boldsymbol{x}_S) + XS_{fitness}(\boldsymbol{x}_S) \right) + w_{pH}\, pH_{fitness}(\boldsymbol{x}_S) + w_{TS} TS_{limit}(\boldsymbol{x}_S) + \\ & w_{gas,excess} Q_{gas,excess}(\boldsymbol{x}_S) + w_{fin} C(\boldsymbol{x}_S) + w_{CH4} CH4_{limit}(\boldsymbol{x}_S) + w_{COD} COD_{limit}(\boldsymbol{x}_S) + \\ & w_{VOA/TIC} VOA/TIC_{limit}(\boldsymbol{x}_S) \end{aligned} \tag{5.5}$$

where the different components are calculated based on the simulation results of the Sunderhook ABP model. The actual fitness value is calculated based on the state of the model after 200 days of simulation when it can be assured that the AD process is again in a steady state. In general, the smaller the fitness value of a substrate inflow, the better its performance. Therefore, the goal of the optimization is to minimize $J(\boldsymbol{x}_S)$.

$$\boldsymbol{x}_S^* := \arg\min_{\boldsymbol{x}_S} J(\boldsymbol{x}_S) \tag{5.6}$$

A detailed description of the fitness function components is given in the following paragraphs and a list of fitness function parameters is shown in Table 5-1.

$SS_{fitness}$ and $XS_{fitness}$

In the case of a stable AD process the total amount of soluble and particulate degradable COD (*SS* and *XS*) is nearly completely degraded and transformed into biogas, which means that the ratios SS_{out} vs SS_{in} and XS_{out} vs XS_{in} describing the degrees of degradation SS_{deg} and XS_{deg} are a measure of the efficiency of the biogas production process. If those ratios are small, substrate degradation is almost complete. If they are close to one, it means that a high percentage of potentially degradable substrate remains unused.

$$SS_{fitness}(\boldsymbol{x}_S) = \frac{SS_{deg}(\boldsymbol{x}_S) - SS_{deg,\min}}{SS_{deg,\max} - SS_{deg,\min}} \tag{5.7}$$

$$XS_{fitness}(\boldsymbol{x}_S) = \frac{XS_{deg}(\boldsymbol{x}_S) - XS_{deg,\min}}{XS_{deg,\max} - XS_{deg,\min}} \tag{5.8}$$

$pH_{fitness}$

The *pH* value is a crucial process parameter which needs to stay within certain boundaries to guarantee stable process conditions. If *pH* is far below its neutral value ($pH = 7$) the *VFA* concentration in the digester is too high, indicating a severe inhibition of the AD process, in particular of the methanogenesis. However, if $pH > 9$, a substantial amount of NH_4 is transformed into NH_3 which also has a strong inhibitory effect. Thus, the overall fitness is punished if the *pH* exceeds predefined lower and upper limits.

$$pH_{fitness}(\boldsymbol{x}_S) = \begin{cases} 1 & pH(\boldsymbol{x}_S) < pH_{\min} \wedge pH(\boldsymbol{x}_S) > pH_{\max} \\ 0 & pH_{\min} \geq pH(\boldsymbol{x}_S) \leq pH_{\max} \end{cases} \tag{5.9}$$

TS_{limit}

A limit for the maximum *TS* concentration of the substrate inflow is introduced because too high concentrations result in heavy operational problems such as deadlock of the stirrers inside a digester or malfunction of pumps. Therefore, substrate inflows with *TS* concentrations greater than a predefined $TS_{\max}$ are punished with a higher fitness value.

$$TS_{limit}(\boldsymbol{x}_S) = \begin{cases} 1 & TS(\boldsymbol{x}_S) > TS_{\max} \\ 0 & TS(\boldsymbol{x}_S) \leq TS_{\max} \end{cases} \tag{5.10}$$

$Q_{gas,excess}$

In some cases, the amount of substrate fed to the ABP might result in such a high biogas yield that it cannot be fully burned in time by the cogeneration units. For safety reasons, this excess gas is burned as a flare so that neither its potential electrical nor thermal energy is supplied to the respective grids. Thus, excess gas is wasted and its production should be avoided. The amount of excess gas is calculated by the difference in the total biogas yield Q_{gas} and the amount of biogas consumed by the cogeneration units $Q_{gas,cog}$.

$$Q_{gas,excess}(\boldsymbol{x}_S) = Q_{gas}(\boldsymbol{x}_S) - Q_{gas,cog}(\boldsymbol{x}_S) \tag{5.11}$$

Costs (C)

The total costs and turnover of ABP operation as a function of different substrate inflows is the most important fitness parameter for the plant operator because an increase in profit directly benefits a

financially secure operation of the ABP in the long run. The main costs, considered in C, are costs for electrical energy of pumps and digester heating (E_{cons}) and the electricity price ($p_{E_{cons}}$) as well as substrate costs (C_S). The turnover is then calculated based on the sales of electrical ($E_{el,gas}$) and thermal energy ($E_{th,gas}$), the respective remuneration rates ($p_{E_{el}}, p_{E_{th}}$) and the manure bonus ($b_{manure}, p_{E_{el},manure}$), if used.

$$C_S(\boldsymbol{x}_S) = \sum_{i=1}^{n} C_{x_{S,i}} x_{S_i} \tag{5.12}$$

$$\begin{aligned} C(\boldsymbol{x}_S) = {} & E_{cons}(\boldsymbol{x}_S) p_{E_{pl}} - E_{el,gas}(\boldsymbol{x}_S) p_{E_{el}} - \\ & b_{manure} E_{el,gas}(\boldsymbol{x}_S) p_{E_{el},manure} - E_{th,gas}(\boldsymbol{x}_S) p_{E_{th}} + C_S(\boldsymbol{x}_S) \quad \left[€\, d^{-1}\right] \end{aligned} \tag{5.13}$$

$CH4_{limit}$

The quality of the produced gas determines whether it can be directly burned in the cogeneration units without needing an additional ignition gas. Therefore, the methane concentration of the gas has to be greater than 50%.

$$CH4_{limit} = \begin{cases} 1 & CH4_{\min} < 50 \\ 0 & CH4_{\min} \geq 50 \end{cases} \tag{5.14}$$

COD_{limit}

As previously explained the degradation rate of the particulate COD (XS) determines the efficiency of the biogas production within the AD process. In order to additionally punish very poor XS_{deg} values, the overall fitness of substrate inflows with $XS_{deg} < 65\%$ is increased by 1.

$$COD_{limit} = \begin{cases} 1 & XS_{deg} < 65 \\ 0 & XS_{deg} \geq 65 \end{cases} \tag{5.15}$$

VOA/TIC_{limit}

The ratio of Volatile Organic Acids (*VOA*) and Total Inorganic Carbon (*TIC*) is the most important stability measure for AD processes. High *VOA* concentrations alone do not necessarily result in process inhibition if the carbon buffer (*TIC*) is high enough to stabilize the *pH*. But if the carbon buffer is low, even small concentrations of *VOA* cause process instabilities which result in a complete process breakdown eventually. Therefore, the VOA/TIC ratio is regularly measured using a titration method. In general, an AD process with a $VOA/TIC \leq 0.3$ is considered to be stable, whereas values above 0.3 indicate an imbalance. Thus, the fitness of substrate inflows with a $VOA/TIC > 0.3$ is increased by 1.

$$VOA/TIC_{limit} = \begin{cases} 1 & VOA/TIC_{\max} > 0.3 \\ 0 & VOA/TIC_{\max} \le 0.3 \end{cases} \tag{5.16}$$

Table 5-1: List of fitness function parameters and their values

fitness function parameters	value	fitness function parameters	value
$pH_{\min}$ (low limit of *pH*)	6	$p_{E_{el}}$* (remuneration for electrical energy)	0.21 €/kWh$_{el}$
$pH_{\max}$ (upper limit of *pH*)	9	$p_{E_{el},manure}$* (remuneration for manure bonus)	0.04 €/kWh$_{el}$
pH_{opt} (optimal *pH*)	7.5	$p_{E_{th}}$* (remuneration for thermal energy)	0.015 €/kWh$_{th}$
$CH4_{\min}$ (lower limit for methane concentration)	50	$w_{COD_{deg}}$ (weighting of COD degradation)	$\frac{1}{9}$
$TS_{\max}$ (upper limit of *TS*)	26	w_{COD} (weighting of punishment of low *XS* degradation)	$\frac{1}{18}$
$SS_{deg,\min}$ (lower limit for *SS* degradation)	0	w_{ch4} (weighting of methane concentration)	$\frac{1}{6}$
$SS_{deg,\max}$ (upper limit for *SS* degradation)	100	w_{fin} (weighting of financial profit)	$\frac{1}{6}$
$XS_{deg,\min}$ (lower limit for *XS* degradation)	0	w_{pH} (weighting of *pH* punishment)	$\frac{1}{6}$
$XS_{deg,\max}$ (upper limit for *XS* degradation)	100	w_{TS} (weighting of TS punishment)	$\frac{1}{6}$
$VOA/TIC_{\max}$ (lower limit for *VOA/TIC*)	0.3	$w_{VOA/TIC}$ (weighting of *VOA/TIC* punishment)	$\frac{1}{6}$
$p_{E_{pl}}$* (energy price paid by the ABP for consumed energy)	0.18 €/kWh	b_{manure} (flag whether manure bonus is considered)	1

* electricity price according to the local power provider and remuneration rates according to the German Renewable Energy Law (BMU 2012)

5.3 Optimization results

The optimization results presented in this section were obtained using the previously developed surrogate optimization method, which was explained in detail in chapter 4. Substrate inflow optimization for the Sunderhook ABP was performed based on the simulation model introduced in chapter 3 and based on the fitness function $J(\boldsymbol{x}_S)$ described in the previous section. In order to account for the nonlinearity of the AD process PSO was used as the nonlinear optimization method for all optimization runs. The necessity of a surrogate model for ABP optimization was proven by Wolf *et al.* (2008) where 12,000 evaluations of $J(\boldsymbol{x}_S)$ were required to find the optimal substrate inflow when using PSO and GA as optimization methods. For a fully calibrated simulation model like the Sunderhook ABP model whose simulation for 200 days takes about 60s, one complete optimization run would take more than 8 days, instead of 16 hours using S-KSM and PSO which requires only 1,000 fitness function evaluations.

The following section shows the optimization results $\boldsymbol{x}_S^*$ for $n = 2,3,4$ and 5 substrates and compares the performance against the original substrate inflow from the Sunderhook ABP. As the Sunderhook ABP currently uses the manure bonus[23], two optimization runs were performed for each n, one including the manure bonus and the other without the manure bonus.

5.3.1 Optimization results for two substrates

In this case, the two most common substrates, maize and bull manure, were used for substrate inflow optimization of the Sunderhook ABP. Figure 5-3 shows a graph of the fitness function $J(\boldsymbol{x}_S)$ for both optimization runs, with and without manure bonus. It becomes clear that J is particularly nonlinear in the border areas of the search space and that local minima can be found in the long extended valley.

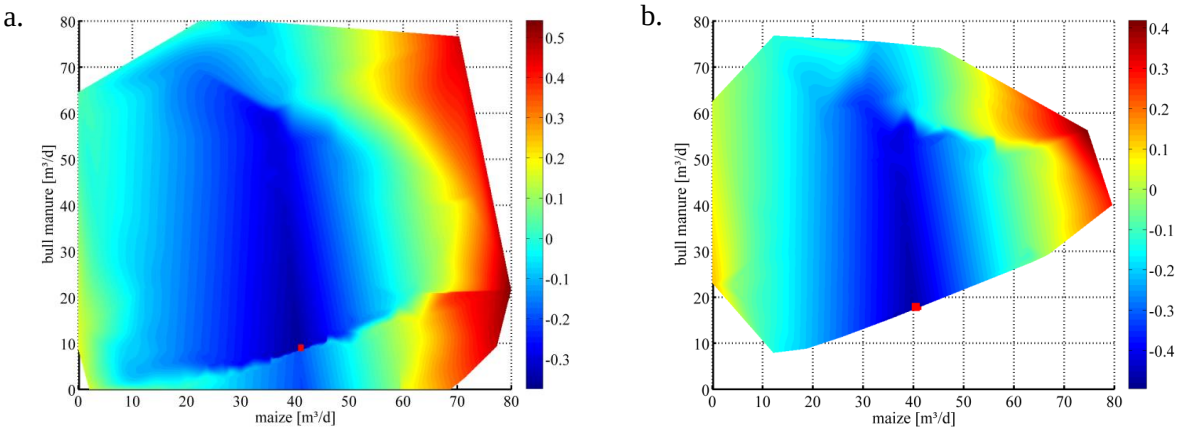

Figure 5-3: Plot of the fitness function *J* for a substrate inflow optimization with 2 substrates. a. b_{manure}=0, b. b_{manure}=1

A comparison of the optimization results with the original substrate inflow of the Sunderhook ABP is given in Table 5-2. It is obvious, that not only is the overall biogas yield per day substantially

[23] To receive the manure bonus, 30% of the total substrate inflow needs to be manure.

improved but also that the AD process seems to be more stable with a significantly lower *VOA/TIC* ratio and a higher degradation rate of *XS*. This indicates that substrate utilization is more efficient.

Table 5-2: Comparison of the original substrate inflow with the optimized substrate inflow for two substrates

	orig. substrate inflow (b_{manure}=1)	opt. Substrate inflow - 2 substrates (b_{manure}=0)	opt. Substrate inflow - 2 substrates (b_{manure}=1)
maize [m³/d]	41.30	40.71	39.92
bullmanure [m³/d]	22.20	8.46	17.62
greenrye [m³/d]	-	0.00	0.00
grass [m³/d]	3.50	0.00	0.00
oat [m³/d]	-	0.00	0.00
stiffmanure [m³/d]	1.78	0.00	0.00
SSdeg [%]	99.46	99.88	99.85
XSdeg [%]	59.14	69.39	69.61
TS [%]	13.63	20.26	18.69
Excess gas [m³/d]	0.00	0.01	0.00
CH4 [%]	54.16	50.00	50.40
gas yield [m³/d]	7521.00	8170.83	8095.62
pH	7.30	7.43	7.40
VOA/TIC	0.31	0.05	0.08
fitness	0.20	-0.36	-0.47

Looking at financial aspects of the optimization results, a higher turnover is already indicated by the higher biogas production. Table 5-3 proves that assumption showing that the daily profit of the Sunderhook ABP can be increased by 599.92 € without the manure bonus and by 545.75 € if the manure bonus is used. This results in a yearly profit increase of 218,969.34 € and 199,198.75 € respectively. Thus, the optimization of the substrate inflow significantly improves ABP efficiency.

Table 5-3: Financial benefits for the substrate inflow optimization with two substrates

	orig. sustrate inflow (b_{manure}=0)	orig. substrate inflow (b_{manure}=1)	opt. Substrate inflow - 2 substrates (b_{manure}=0)	opt. Substrate inflow - 2 substrates (b_{manure}=1)
C_S	1,960.15 €	1,960.15 €	1,707.13 €	1,760.98 €
$C_{E_{cons}}$	331.74 €	331.74 €	188.82 €	208.27 €
$C_{E_{el,gas}+E_{th,gas}}$	4,066.36 €	4,787.92 €	4,270.34 €	5,011.03 €
Daily profit	1,774.47 €	2,496.03 €	2,374.39 €	3,041.78 €
Yearly profit	647,681.55 €	911,050.95 €	866,650.89 €	1,110,249.70 €

5.3.2 Optimization results for three substrates

The optimization with three substrates (maize, bull manure and grass) shows similar results, with the exception that the optimized substrate feed without manure bonus fails to be financially better than the original substrate inflow with manure bonus. This is caused by the higher remuneration rate if the manure bonus is active. Nevertheless, the AD process is again more stable than before (Table 5-4). Figure 5-4 also shows the growing complexity of the four-dimensional fitness function, which makes optimization difficult.

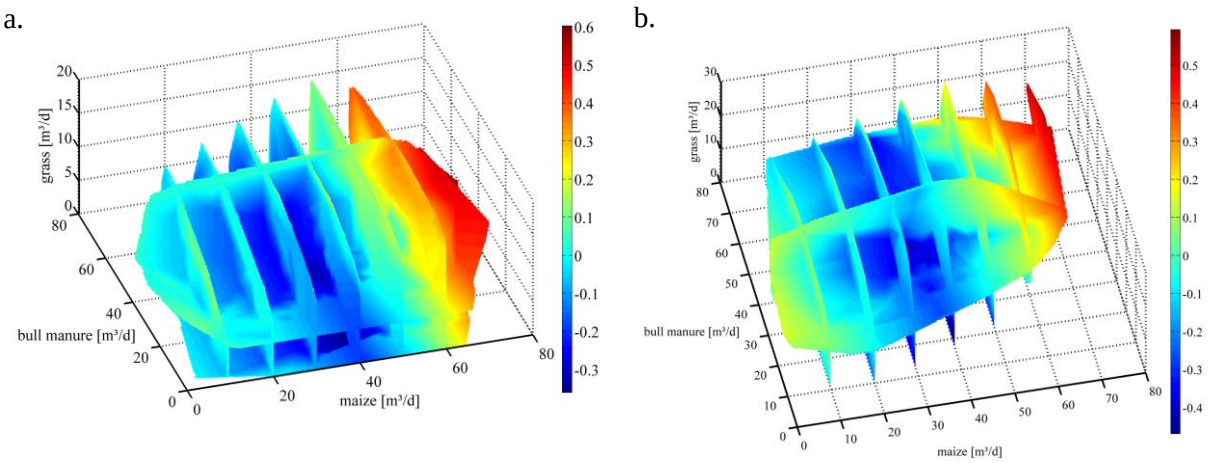

Figure 5-4: Plot of the fitness function *J* for a substrate inflow optimization with 3 substrates. a. b_{manure}=0, b. b_{manure}=1

Table 5-4: Comparison of the original substrate inflow with the optimized substrate inflow for three substrates

	orig. substrate inflow (b_{manure}=1)	opt. Substrate inflow - 3 substrates (b_{manure}=0)	opt. Substrate inflow - 3 substrates (b_{manure}=1)
maize [m³/d]	41.30	37.83	37.95
bullmanure [m³/d]	22.20	26.96	19.02
greenrye [m³/d]	-	0.00	0.00
grass [m³/d]	3.50	3.01	3.65
oat [m³/d]	-	0.00	0.00
stiffmanure [m³/d]	1.78	0.00	0.00
SSdeg [%]	99.46	99.83	99.85
XSdeg [%]	59.14	69.64	69.45
TS [%]	13.63	17.51	18.52
Excess gas [m³/d]	0.00	0.00	0.00
CH4 [%]	54.16	50.54	50.16
gas yield [m³/d]	7521.00	7992.77	7984.75
pH	7.30	7.44	7.43
VOA/TIC	0.31	0.10	0.07
fitness	0.20	-0.32	-0.45

The comparison of the performance measures from Table 5-4 clearly shows that both degradation rates SS_{deg} and XS_{deg} are 10% higher than before the optimization and also that the biogas yield is increased. In addition, the methane concentration in the produced biogas is significantly lower at 50% instead of 54%.

The financial calculations prove that a substantial benefit is generated for the ABP owner through substrate inflow optimization. Without manure bonus, an increase in daily profit of 371.46 € and with manure bonus of 411.32 € is generated. Projected for a whole year, the overall profit of the plant can be increased by 135,581.44 € and 150,133.26 € respectively.

Table 5-5: Financial benefits for the substrate inflow optimization with three substrates

	orig. sustrate inflow (b_{manure}=0)	**orig. substrate inflow (b_{manure}=1)**	**opt. Substrate inflow - 3 substrates (b_{manure}=0)**	**opt. Substrate inflow - 3 substrates (b_{manure}=1)**
C_S	1,960.15 €	1,960.15 €	1,840.77 €	1,787.73 €
$C_{E_{cons}}$	331.74 €	331.74 €	233.94 €	217.45 €
$C_{E_{el,gas}+E_{th,gas}}$	4,066.36 €	4,787.92 €	4,220.63 €	4,912.53 €
Daily profit	1,774.47 €	2,496.03 €	2,145.93 €	2,907.35 €
Yearly profit	647,681.55 €	911,050.95 €	783,262.99 €	1,061,184.21 €

5.3.3 Optimization results for four substrates

The optimization of the substrate inflow with four substrates gives results similar to the aforementioned results but it becomes obvious that the magnitude of improvement is steadily declining with the number of substrates as it becomes more difficult to reduce substrate costs while maintaining or even increasing biogas yield. Nevertheless, the four dimensional solutions for the substrate inflow also manage to reduce the overall substrate costs for more than 100 € while increasing biogas yield. This can only be realized by reducing the fraction of maize, which is a very expensive substrate at 40 €/m³ and to replace it with the much cheaper substrates such as grass and green rye.

The financial calculations reflect this steady decline in improvement in the overall profit. Only 143.98 € without manure bonus and 285.11 € with manure bonus can be gained in addition to the original daily profit. Therefore, the yearly profit is equally reduced to 52,553.06 € and 104,064.79 € respectively.

Table 5-6: Comparison of the original substrate inflow with the optimized substrate inflow for four substrates

	orig. substrate inflow (b_{manure}=1)	opt. Substrate inflow - 4 substrates (b_{manure}=0)	opt. Substrate inflow - 4 substrates (b_{manure}=1)
maize [m³/d]	41.30	32.70	36.00
bullmanure [m³/d]	22.20	19.60	20.96
greenrye [m³/d]	-	11.27	1.73
grass [m³/d]	3.50	1.15	5.01
oat [m³/d]	-	0.00	0.00
stiffmanure [m³/d]	1.78	0.00	0.00
SSdeg [%]	99.46	99.85	99.85
XSdeg [%]	59.14	68.53	69.29
TS [%]	13.63	18.67	18.30
Excess gas [m³/d]	0.00	0.00	0.00
CH4 [%]	54.16	50.17	50.08
gas yield [m³/d]	7521.00	7661.07	7854.78
pH	7.30	7.37	7.42
VOA/TIC	0.31	0.05	0.06
fitness	0.20	-0.28	-0.43

Table 5-7: Financial benefits for the substrate inflow optimization with four substrates

	orig. sustrate inflow (b_{manure}=0)	orig. substrate inflow (b_{manure}=1)	opt. Substrate inflow - 4 substrates (b_{manure}=0)	opt. Substrate inflow - 4 substrates (b_{manure}=1)
C_S	1,960.15 €	1,960.15 €	1,858.16 €	1,814.27 €
$C_{E_{cons}}$	331.74 €	331.74 €	231.54 €	226.24 €
$C_{E_{el,gas}+E_{th,gas}}$	4,066.36 €	4,787.92 €	4,008.14 €	4,821.65 €
Daily profit	1,774.47 €	2,496.03 €	1,918.45 €	2,781.14 €
Yearly profit	647,681.55 €	911,050.95 €	700,234.62 €	1,015,115.74 €

5.3.4 Optimization results for five substrates

Finally, another optimization was performed for five substrates. The results for five substrates show similar improvements in the degradation rates SS_{deg} and XS_{deg} (10%) as well as in the total biogas yield.

The financial profits were slightly increased in comparison to the profits obtained with four substrates but are still lower than the ones obtained for two substrates. All in all, an increase in daily profits of 379.71 € without manure bonus and 364.07 € with manure bonus was achieved. Thus, yearly profits can be enhanced by 138,592.33 € and 132,885.92 €.

Table 5-8: Comparison of the original substrate inflow with the optimized substrate inflow for five substrates

	orig. substrate inflow (b_{manure}=1)	opt. Substrate inflow - 5 substrates (b_{manure}=0)	opt. Substrate inflow - 4 substrates (b_{manure}=1)
maize [m³/d]	41.30	37.11	36.43
bullmanure [m³/d]	22.20	20.89	25.99
greenrye [m³/d]	-	2.00	2.85
grass [m³/d]	3.50	2.00	2.29
oat [m³/d]	-	2.00	3.46
stiffmanure [m³/d]	1.78	0.00	0.00
SSdeg [%]	99.46	99.85	99.84
XSdeg [%]	59.14	69.05	68.75
TS [%]	13.63	18.68	18.36
Excess gas [m³/d]	0.00	0.00	0.00
CH4 [%]	54.16	50.08	50.04
gas yield [m³/d]	7521.00	8011.43	8112.65
pH	7.30	7.41	7.40
VOA/TIC	0.31	0.06	0.07
fitness	0.20	-0.32	-0.44

Table 5-9: Financial benefits for the substrate inflow optimization with five substrates

	orig. sustrate inflow (b_{manure}=0)	orig. substrate inflow (b_{manure}=1)	opt. Substrate inflow - 4 substrates (b_{manure}=0)	opt. Substrate inflow - 4 substrates (b_{manure}=1)
C_S	1,960.15 €	1,960.15 €	1,809.55 €	1,877.22 €
$C_{E_{cons}}$	331.74 €	331.74 €	226.94 €	245.34 €
$C_{E_{el,gas}+E_{th,gas}}$	4,066.36 €	4,787.92 €	4,190.67 €	4,982.66 €
Daily profit	1,774.47 €	2,496.03 €	2,154.18 €	2,860.10 €
Yearly profit	647,681.55 €	911,050.95 €	786,273.88 €	1,043,936.87 €

5.4 Conclusion on ABP substrate inflow optimization

This chapter about ABP substrate inflow optimization gave a brief overview of advances in the area of AD optimization and control showing that the substrate inflow is the main variable used to manipulate the dynamics of the AD process. Thus, ABP optimization has to optimize the substrate inflow in order to maximize plant efficiency by increasing biogas yield, reducing costs and guaranteeing stable ABP operation. Such optimization with multiple optimization criteria was realized using PSO and S-KSM in combination with a fitness function which is particularly adapted to the substrate inflow optimization of ADPs.

The potential of substrate inflow optimization was shown at the Sunderhook ABP by doing five optimization runs for $n = 2,3,4$ and 5 substrates. Results prove that a substantial improvement in terms

of AD process stability and financial profit can be achieved. Figure 5-5 gives a summary of the financial benefits of the optimization results, while Figure 5-6 shows the percentage of profit increase for each optimization result in comparison to the originally applied substrate inflow of the Sunderhook ABP.

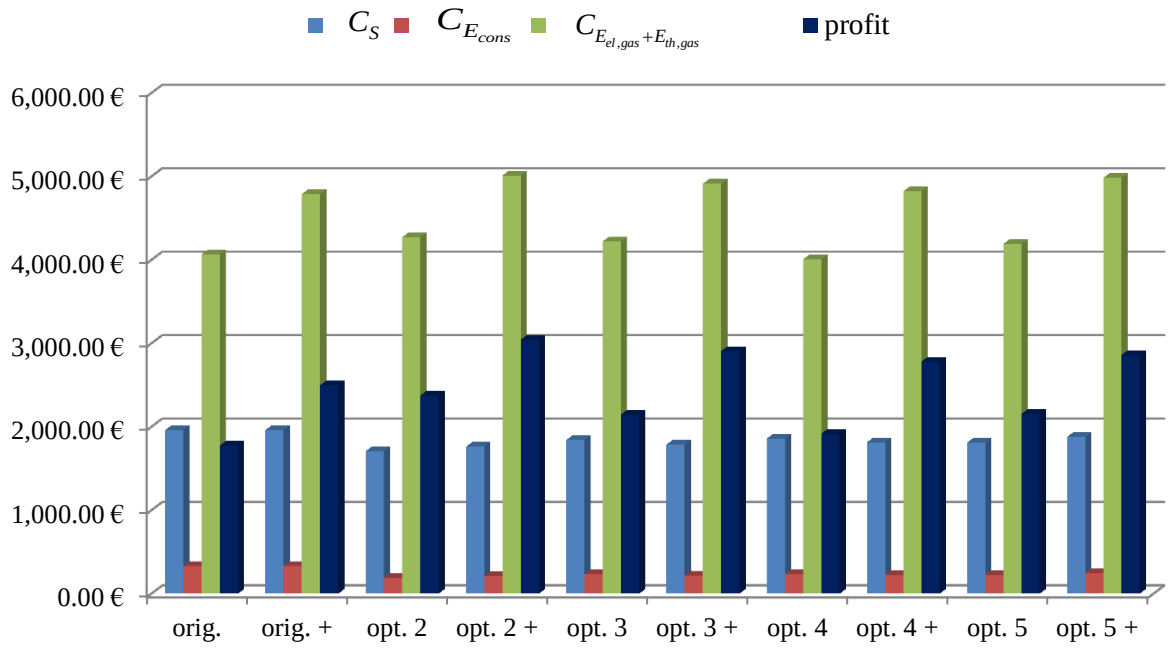

Figure 5-5: Summary of the costs and daily profits of the optimization runs (opt.) for 2, 3, 4 and 5 substrates with (+) and without manure bonus in comparison to the original substrate inflow (orig.)

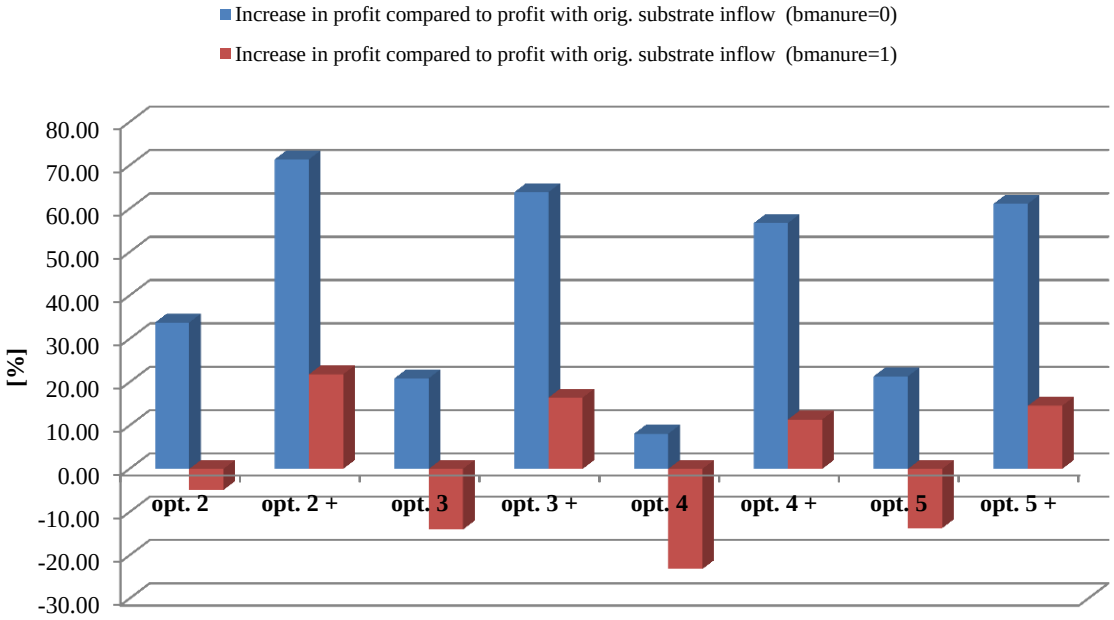

Figure 5-6: Summary of the increase in profit for each of the optimization results (opt.) compared to the profit made with the original substrate inflow (orig.) with (+) and without manure bonus

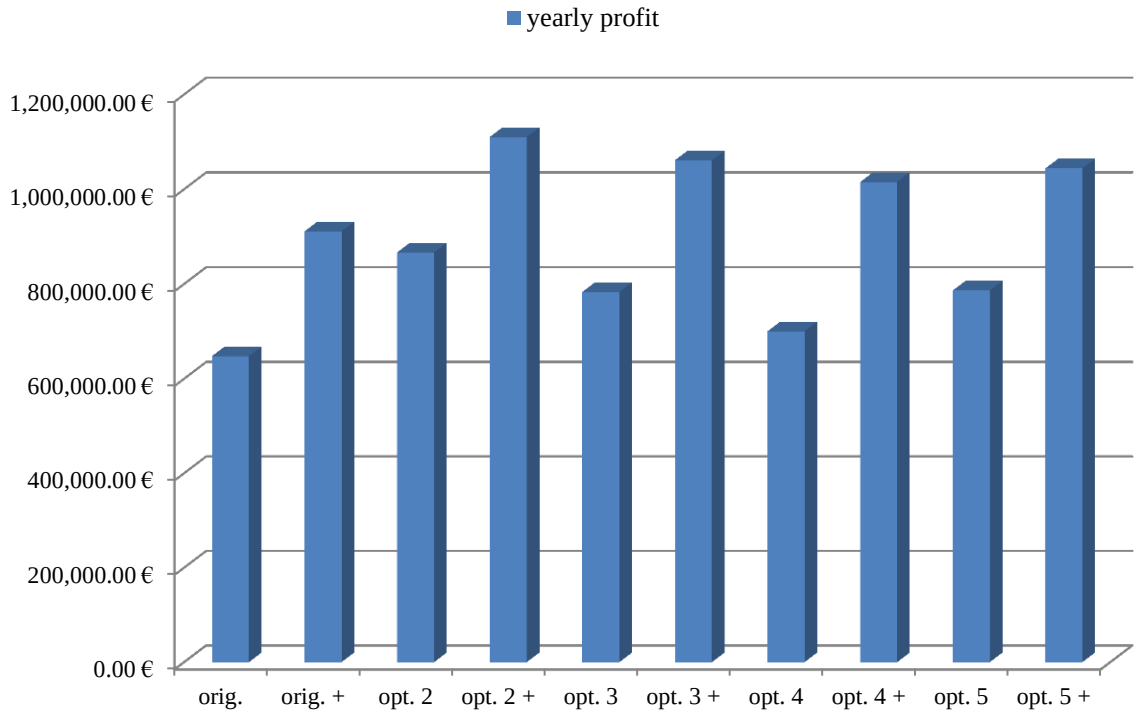

Figure 5-7: Yearly profit of the Sunderhook ABP for each optimization run (opt.) and the original substrate inflow (orig.) with (+) and without manure bonus

All in all, the best optimization result, yielding the highest profit, is achieved for two substrates with manure bonus. The substrate inflow consisting of 39.9 m^3d^{-1} maize and 17.6 m^3d^{-1} bull manure results in an increase in yearly profit of 70% compared to the original substrate inflow without manure bonus and of 21.8% compared to the original substrate inflow with manure bonus. This equals an improvement in net profit of 219,000 € and 199,000 € respectively. Thus, this substrate inflow was suggested to the operator of the Sunderhook ABP and successfully implemented.

The large increase in yearly profits makes this optimization of the ABP substrate inflow an important tool to help ABP operators and service providers to optimize plant efficiency in the long run. The ability to generate a customized fitness function $J(\boldsymbol{x}_S)$ gives the end-user the flexibility to adapt optimization solutions to the actual state of the plants. As hardware costs for the implementation of this optimization are minimal, the return on investment is given within 6 month or earlier depending on the service charge claimed for the optimization service. If steadily decreasing remuneration rates are factored into the financial profit, the optimization of the substrate inflow is absolutely necessary to guarantee sustainable ABP operation in the future.

References

Alferes, J., García-Heras, J.L., Irizar, I., Roca, E. and García, C., 2008. Integration of equalisation tanks within control strategies for anaerobic reactors. Validation based on ADM1 simulations. *Water Science & Technology*, 57 (5), 747.

Alferes, J. and Irizar, I., 2010. Combination of extremum-seeking algorithms with effective hydraulic handling of equalization tanks to control anaerobic digesters. *Water Science & Technology*, 61 (11), 2825-2834.

Andrews, J.F., 1969. A Dynamic Model of the Anaerobic Digestion Process. *Journal of the Sanitary Engineering Division*, 1, 95–116.

BMU (Bundesministerium für Umwelt, Naturschutz und Reaktorsicherheit - Federal Ministry for the Environment, Nature Conservation and Nuclear Safety), 2011. *Erneuerbare-Energien-Gesetz 2012 (Renewable Energy Law 2012): EEG*.

Boe, K., Angelidaki, I. and Steyer, J.-P., 2008. Monitoring and control of the biogas process based on propionate concentration using online VFA measurement. *Water Science & Technology*, 57 (5), 661.

De Neve, K. and Lievens, K., 2004. On-line analyser solves monitoring problem in bio-digester. *Water and Wastewater International*, 19 (6), 28.

García-Diéguez, C., Molina, F. and Roca, E., 2011. Multi-objective cascade controller for an anaerobic digester. *Process Biochemistry*, 46 (4), 900–909.

Hilgert, N., Harmand, J., Steyer, J.-P. and Vila, J.-P., 2000. Nonparametric identification and adaptive control of an anaerobic fluidized bed digester. *Control Engineering Practice*, 8 (4), 367–376.

Liu, J., Olsson, G. and Mattiasson, B., 2004. Monitoring and control of an anaerobic upflow fixed-bed reactor for high-loading-rate operation and rejection of disturbances. *Biotechnology and Bioengineering*, 87 (1), 43–53.

Polihronakis, M., Petrou, L. and Deligiannis, A., 1993. Parameter adaptive control techniques for anaerobic digesters—real-life experiments. *Computers & chemical engineering*, 17 (12), 1167–1179.

Scherer, P., Lehmann, K., Schmidt, O. and Demirel, B., 2009. Application of a fuzzy logic control system for continuous anaerobic digestion of low buffered, acidic energy crops as mono-substrate. *Biotechnology and Bioengineering*, 102 (3), 736–748.

References

Steyer, J.-P., Buffière, P., Rolland, D. and Moletta, R., 1999. Advanced control of anaerobic digestion processes through disturbances monitoring. *Water Research*, 33 (9), 2059–2068.

Steyer, J., Bernard, O., Batstone, D. and Angelidaki, I., 2006. Lessons learnt from 15 years of ICA in anaerobic digesters. *Water Science & Technology*, 53 (4-5), 25.

Wolf, C., McLoone, S. and Bongards, M., 2008. Biogas plant optimization using genetic algorithms and particle swarm optimization. *IET Irish Signals and Systems Conference (ISSC) 2008; Galway, Ireland*, 244–249.

6 Instrumentation of Biogas Plants

The instrumentation of industrial plants in general is a key prerequisite to making efficient and continuous process monitoring and control possible in the first place (Lipták 2003). Looking at biogas plants, both agricultural and industrial, good instrumentation has proven to be essential to maintaining stable and efficient AD processes. In particular, the high volatility of AD processes due to their high sensitivity to varying process conditions such as temperature, *pH*, carbon buffer, acetic acid concentration, ammonia inhibition and substrate composition, requires close monitoring at all times (Kujawski and Steinmetz 2009a). This kind of process monitoring allows the setup of an early detection and warning system for process disturbances to prevent breakdowns and, as such, is of direct monetary benefit to the plant operator. Nevertheless, instrumentation at full-scale biogas plants is still in its infancy as shown by the recent biogas measurement program in Germany (FNR e.V. 2009). Currently 70% of biogas plants in Germany possess measurement systems for biogas production while 60% have systems for measuring biogas composition. Liquid and solid substrate feed are measured at 50% and 80% of the plants, respectively. In contrast, the more sophisticated measurement systems, such as online *pH*, *ORP* or even *VFA* analysis are available at less than 5% of all plants. This leaves lots of potential for the application of innovative online measurements to improve plant performance and presents a huge market for manufacturers of online measurement systems. Furthermore, there is substantial research activity in this area aiming to provide new robust and feasible measurement systems.

However, the research conducted in the field of AD control and optimization shows that in most cases sophisticated lab equipment (online gas chromatography, HPLC, spectrophotometric titration, etc.) is used for detailed process monitoring (Jantsch and Mattiasson 2004, Boe *et al.* 2007b, Méndez-Acosta *et al.* 2008, Ward *et al.* 2011), which delivers very good measurement accuracy but is very expensive and maintenance-intensive at the same time. Thus, transition of such methods and systems to full-scale applications is difficult, and mostly not feasible, due to high installation and maintenance costs. This concerns small and medium-sized agricultural plants in particular, where plant operators also have a lack of the required expert knowledge to operate these complex and sensitive systems. Nevertheless, current research in the area of online measurement systems for anaerobic digestion processes shows that the development of reliable, low-maintenance and feasible systems is far from trivial as the challenges are multifaceted (Spanjers and van Lier 2006). On the one hand, high contents of dry matter with many sharp and hard objects render the use of sensitive electrodes nearly impossible and on the other hand calibration and maintenance procedures need to be simple so that they can be performed by the plant operators themselves (Wolf *et al.* 2011a).

The main contributions of this chapter are:

- a detailed survey of existing online measurement methods and systems
- critical analysis of a biogas plant breakdown
- test and validation of existing online probes for *pH*, *TS* and *ORP* at an agricultural and an industrial biogas plant
- development and validation of a new online UV/vis spectroscopic measurement system for organic acids and buffer capacity
- evaluation of different machine learning methods for spectral analysis to compare their suitability and performance

The remainder of the chapter is organized as follows. In section 6.1 a detailed literature review of the state-of-the-art in online measurement systems is provided together with descriptions of full-scale applications of well-known and innovative monitoring systems. In addition, the current market situation for online measurement systems is analyzed with regard to existing and future technologies. Then section 6.2 introduces and demonstrates the reasons why online measurement systems are urgently needed, giving a practical example from an industrial biogas plant in Germany. Section 6.3 presents and discusses results from a field test of online measurement systems for *pH*, *ORP* and *TS* at an agricultural and an industrial biogas plant highlighting advantages and limitations. The development of a new innovative online measurement system for *VFA* based on UV/vis spectroscopy is introduced in section 6.4 and its full-scale application at an industrial biogas plant described in detail. The analysis of the spectral data set using powerful machine learning techniques is described in section 6.5. A short summary of the results and the derived conclusion are given in section 6.6.

6.1 Literature Review for Online-Monitoring of Anaerobic Digestion Plants

The large number of developments and research papers in the history of monitoring of AD processes illustrates the importance of reliable, low-maintenance and feasible online measurement systems. One of the first papers to consider the topic was McCarty (1982). In this paper McCarty gave a review of the developments in anaerobic digestion in the last century and pointed out that *"recent advances in fundamental understanding of the [anaerobic] process have yet to be translated into practical application for process design, optimization and control."* Therefore, online-monitoring is crucial, but to choose the most viable process parameters for online monitoring is even more important. In 2000 the parameters *pH*, partial alkalinity (*PA*), gas production rate and composition as well as *VFA* concentration were compared under varying organic loading rates (pulse loads) at a lab-scale reactor to evaluate their suitability for monitoring purposes (Björnsson *et al.* 2000). The results showed significant change in *PA* and *VFA* concentration under the pulse loads, whereas a detected decrease in the *pH* could not be separated from normal operating conditions. Thus, *pH* was considered unreliable for early warning purposes as a significant drop in the *pH* only occurred under a heavy organic

overload of the system. Results for gas composition and gas production rate monitoring were also delayed and merely significant in case of overload. These findings are confirmed by Ahring *et al.* (1995) and recently supported by Boe *et al.* (2010), all leading researchers in the AD community. In a substantial study the behavior of *pH*, *VFA* and dissolved hydrogen was investigated under different kinds of disturbances. It became evident that pH is an important parameter in the case of AD systems with low buffering capacity and that the sum of *VFA* concentrations is less meaningful than the separate investigation of acetic, butyric and propionic acid. A fast response to disturbances was also detected in dissolved hydrogen, but an increase was not always related to process instability, which suggests a check against other parameters, such as *VFA* concentration, for the reliable detection of process instability. The use of *pH* and *ORP* online probes for process monitoring in combination with biogas production rate was investigated further in a research project by UTEC GmbH in Bremen, Germany (Zimmermann *et al.* 2003). It was shown at two full-scale biogas plants using co-digestion that a combination of these three process parameters allows a good assessment of process stability. In addition to alkalinity, *VFA*, *pH* and *ORP*, total and volatile solids have proven to be valid process parameters to predict biogas production and to monitor the substrate feed of biogas plants as well as significant indicators like volume load, volatile solids (*VS*) degradation or methane yield (FNR e.V. 2010). These publications as well as a summary of recent developments, online measurement methods and applications for AD were summarized clearly by Madsen *et al.* (2011), who concluded that the most important variables for process monitoring are:

- *VFA*
- alkalinity (*PA* and *TA*)
- *TS* and *VS*
- biogas composition
- biogas yield
- *pH*
- *ORP* and
- temperature

This list of process parameters can be divided into two classes according to the availability of online measurement systems, their reliability and their suitability for practical use at a biogas plant. On the one hand, biogas composition/yield, temperature, *pH* and *ORP* can be considered as state of the art for agricultural biogas plants as the existing technology is sufficiently robust and reliable. On the other hand, the online measurement of alkalinity, *TS/VS* and *VFA* is still subject to substantial research. Even though measurement systems for biogas plants already exist for these parameters, high prices and high maintenance efforts still pose a problem, reducing the acceptance of such technology in practice. Therefore the two classes of process parameters are *state of the art parameters* for process monitoring and *new innovative parameters*. Unfortunately, the state of the art parameters have proven to be less effective at determining the current process state of a biogas pant than the innovative parameters, which emphasizes the need for online measurement systems in the latter field. The following two sections describe the current state of research and practice for these two classes of process parameters.

6.1.1 State of research

Research in the field of online measurement systems for AD processes is mainly focused on a few parameters, such as biogas production and composition, *pH*, *ORP*, *TS*, *VS* as well as alkalinity and *VFA*. Of these parameters *VS*, alkalinity and *VFA*, which belong to the class of innovative parameters, have received lots of attention concerning the development of new measurement methods and systems (Table 6-1). In contrast, several long-term practice tests were conducted for the parameters biogas production/composition, *pH*, *ORP* and *TS* to prove their reliability and capability to detect process disturbances (Wiese and Kujawski 2008, Kujawski and Steinmetz 2009b). Looking at all the publications in this area, as summarized in Table 6-1, it becomes clear that there is a trend to go from direct biochemical measurement of process parameters to indirect measurement using spectroscopic methods in combination with powerful machine learning techniques. In particular, the indirect measurement of *VS*, alkalinity and *VFA* using UV/vis, near-infrared or even mid-infrared spectroscopy has proven to be a good alternative to expensive wet chemistry analyzers (Spanjers *et al.* 2006, Holm-Nielsen *et al.* 2008b, Wolf *et al.* 2010). These spectroscopic measurement systems analyze absorbance or reflection spectra over certain wavelengths using machine learning techniques (ANN, SVM, PLS, etc.) to indirectly measure biochemical parameters. The advantage of such systems is that they offer the possibility of measuring directly inside the measurement medium and to measure several parameters with one system using different basis calibrations. Due to the fact that the description of all published R&D results would be too long, only the most important and relevant developments are briefly described.

Table 6-1: List of developed and tested online measurement methods for AD processes in the past 20 years

	Method	**References**
Biogas yield/ composition	gas chromatography	(Slater *et al.* 1990)
	lab-scale fermentation tests	(Scaglione *et al.* 2008)
	volumetric gas flow meter	(Cadena Pereda *et al.* 2010a)
	near-infrared laser optical spectrometry/ CF-IRMS	(Keppler *et al.* 2010)
	pressure-based near-infrared analyzer	(Bishop *et al.* 2010)
pH/ORP	electro-chemical	(Monzambe *et al.* 1988)
		(Zimmermann *et al.* 2003)
		(Wiese and Haeck 2006)
		(Wolf *et al.* 2011a)
	calculation from bicarbonate and carbon dioxide concentration	(Hawkes *et al.* 1994)
TS/VS	microwave	(Nacke *et al.* 2010)
	backscattered light	(Wiese and Haeck 2006)
		(Wolf *et al.* 2011a)
	near-infrared spectroscopy	(Lomborg *et al.* 2009)

VFA/COD	titration	(Powell and Archer 1989)
PA/TA		(Feitkenhauer *et al.* 2002)
		(Lahav and Morgan 2004)
		(de Neve and Lievens 2004)
	ion-selective electrode arrays	(Witkowska *et al.* 2010)
	membrane-inlet mass spectrometry	(Ward *et al.* 2011)
	spectrophotometric	(Jantsch and Mattiasson 2004)
	multi-wavelength fluorometry	(Morel *et al.* 2004)
	spectrofluoremetric	(Palacio-Barco *et al.* 2010)
	headspace gas chromatography	(Boe *et al.* 2007a)
	saturation with CO_2 and acidification with sulfuric acid	(Guwy *et al.* 1994)
	UV/vis spectroscopy (UV/vis)	(Wolf *et al.* 2011b)
	near-infrared spectroscopy (NIR)	(Tosi *et al.* 2003)
		(Holm-Nielsen *et al.* 2007)
		(Holm-Nielsen *et al.* 2008b)
		(Lomborg *et al.* 2009)
		(Jacobi *et al.* 2009b)
		(Wiese and König 2009b)
	mid-infrared spectroscopy (MIR)	(Steyer *et al.* 2002)
		(Spanjers *et al.* 2006)

Biogas yield/composition

Research to-date on biogas quantity and quality measurements for AD processes primarily focuses on lab-scale applications, where measurement data needs to be as accurate as possible. For this reason the developments are mostly very expensive and their applicability to full-scale biogas plants is limited. Nevertheless the methods developed by Cadena Pereda *et al.* (2010b) and Keppler *et al.* (2010) are worth mentioning. Cadena Pereda used a volumetric cell, where the biogas is isolated from the displacement liquid, with an optical level detection allowing for a measurement range from 10 to 55,000 cm³. Furthermore, the fill level data is automatically analyzed using a FPGA[24] board, which also controls the measurement system. Keppler investigated the measurement of carbon isotope ratios (13C/12C) of methane, which are considered a valuable process parameter to quickly detect changes in AD processes. The use of optical spectrometry in comparison to the conventional method using continuous-flow isotope ratio mass spectrometry was evaluated. Results show that these two methods deliver similar results, with the accuracy of the online spectrometry only varying by 0.7% from the conventional method.

[24] field-programmable gate array

pH/ORP

The use of *pH* and *ORP* probes for online-monitoring of AD processes was strongly suggested by Zimmermann in 2003. It was shown that a combination of biogas production rate, *pH* and *ORP* measurements is well suited to the assessment of process stability. Due to the fact that absolute values for *pH* and *ORP* differ widely from plant to plant, the trends of *pH* and *ORP* measurements were used in this case. Based on this analysis, Wiese and König (2009b) and Wolf *et al.* (2011a) tested the application of *pH* and *ORP* probes of different manufacturers on full-scale agricultural biogas plants. Results indicate that available systems are reliable and sufficiently robust for agricultural plants, if calibration is carried out regularly every two or three weeks. Unfortunately, a correlation between process stability and *pH/ORP* measurement data could only be detected if process instability was imminent, which is in most cases too late. Nevertheless, long-time trends in AD processes can be properly monitored.

TS/VS

The most promising technologies for online *TS/VS* monitoring were introduced by Lomborg *et al.* (2009) and Nacke *et al.* (2010). The use of NIR spectroscopy for *TS/VS* measurement was introduced by Lomborg. Based on the pattern of reflected light in the NIR wavelength range (800nm – 2000nm) by the measurement medium, an indirect measurement of *TS* and *VS* is possible. Lomborg clearly showed that very good results can be achieved for low *TS* and *VS* concentrations (between 4.6 and 6.5), but that further investigation is essential for higher concentrations, as the normal range at agricultural biogas plants goes from 6 to 10% *TS*. The measurement system introduced by Nacke uses a microwave sensor manufactured by hf-sensor GmbH (Leipzig, Germany). The absorption of microwave radiation is measured, because different materials such as polar molecules have very high absorption coefficients and non-polar molecules very low absorption coefficients. Based on these differences *TS* and *VS* content can be measured. Overall, TS concentrations between 6 and 13% were successfully measured. Calibration of the microwave sensor was performed using PLS models.

VFA/COD and PA/TA

The most common methods for *VFA* and *PA/TA* measurement are titration, chromatography and spectroscopy. In 2002, Feitkenhauer (Feitkenhauer *et al.* 2002) developed a robust, online titration system for the two step titration defined by Anderson (Anderson and Yang 1992) for *VFA* measurement. Thereby, the measurement medium is titrated down to pH 5.1 in the first step and down to 3.5 in the second step, which yields the *VFA* and carbon buffer concentrations of the medium. In contrast to other titration methods, the titration cell was specifically designed to cope with the original measurement medium without previous biomass separation. A similar system for online titration of the measurement medium to measure *VFA* and *PA/TA* was developed by de Neve in 2004 (de Neve and

Lievens 2004). It is called AnaSense® and has been distributed by the ***P***rozess***A***nalysen***I***nstrumente GmbH[25] in Germany since 2004. Titration is performed using hydrochloric acid for titration after *pH* stabilization with sodium hydroxide in the case of very low initial *pH* values (< 5). The chemical dosage is added by peristaltic pumps. As the measurement system requires a particle size below 200µm, an additional preprocessing unit is necessary for most applications, in particular for agricultural AD plants. Furthermore, regular maintenance (every week) of the *pH* probe, the peristaltic pumps and the preprocessing unit is necessary to guarantee reliable long-time operation. Looking at these titration based methods, it becomes evident that the *pH* measurement is not only the most important part of these systems but also one, which requires extensive maintenance. Thus, Jantsch and Mattiasson (2004) developed a system to measure *PA* in AD processes based on titration principles but without a *pH* probe. Instead, a *pH* indicator (Methylred) is added to the measurement medium, whose color is detected by a spectrophotometer at the wavelengths 438nm (protonated – red) and 516nm (unprotonated – yellow). During titration, the ratio between absorptions at these two wavelengths indicates the *pH* value. If the *pH* reaches the desired level of 5.75 (titration according to Björnsson *et al.* 2000), acid consumption is measured and *PA* is calculated. To improve measurement quality, pre-filtering of the medium is also necessary. In this case, a nylon cloth with a mesh size of 20µm was used.

Besides titration and chromatographic online measurement systems, spectroscopic methods, be it UV/vis, NIR or MIR spectroscopy, have proven to be very reliable, robust and low-maintenance. Nevertheless, this technology is not widely accepted in practice due to high cost of spectrometers and fiber-optics. At the moment, NIR spectroscopy dominates the market of online measurement systems for AD processes because it has been applied to full-scale bioreactors in several cases as described by Wiese and König (2009a) and Jacobi *et al.* (2009a). It allows not only for online *VFA* measurement but also for *PA/TA* and *VS* measurement. One well-known system is the TENIRS probe (**T**ransflexive **E**mbedded **N**ear **I**nfra-**R**ed **S**ensor) developed by Holm-Nielsen and Andrée in 2007 (Holm-Nielsen *et al.* 2007). The TENIRS probe measures reflection spectra in the wavelength range from 900-1600nm. A first application study under laboratory conditions was published in 2008, showing that good measurement results (up to 96% accuracy) could be achieved for acetic acid, iso-butanoic acid and total VFA concentration (Holm-Nielsen *et al.* 2008a). Further investigation of the TENIRS system at a full-scale 1MW biogas plant in Germany took place in 2009 (Jacobi *et al.* 2009b). During thermophilic plant operation, calibration and online measurement of *VFA*, acetic acid and propionic acid in a bypass was successfully implemented and provided good measurement results for a period of 500 days. It was concluded that calibration for *VFA* and propionic acid yielded very good performance results with coefficients of determination of 0.95 and 0.89 respectively. Unfortunately, results for

[25] http://www.p-a-i.de

acetic acid were relatively poor with 0.69 compared to 0.89 achieved by Lomborg (Lomborg *et al.* 2009).

In comparison to UV/vis and NIR spectroscopy, MIR spectroscopy is the most anticipated alternative because reflection spectra of relevant AD process parameters have a highly distinctive fingerprint in the MIR wavelength range from 3µm to 50µm. Thus, measurability and selectivity is much higher in this wavelength range. Steyer was the first to evaluate applicability of MIR spectroscopic probes for the online monitoring of AD processes in 2002 (Steyer *et al.* 2002). Using FT-IR spectroscopy (**F**ourier **T**ransform **IR**) the absorbance patterns of raw wine distillery effluents which were treated in an AD-WWTP (wastewater treatment plant) were analyzed for wavelengths in the range 2µm to 10µm. Parameters *COD*, *TOC*, *VFA* as well as *PA* and *TA* were successfully measured. Nevertheless, severe problems were caused by the coupling of the fiber-optics with the MIR spectrometer due to high signal losses depending on fiber length and bending. In 2002, production of fiber-optics suitable for online and on site operation was still in its infancy. A few years later, Spanjers *et al.* (2006) used these results and developed and tested an online MIR system for a full-scale AD process to measure *COD*, *VFA*, ammonium and *TKN*. These variables could be measured with sufficient accuracy. To assure reliable long-time operation of the system an automatic preprocessing unit for filtering was necessary. Furthermore, the observation window required regular cleaning once a day.

This overview of research developments in online monitoring of AD processes over the last decade shows that many different systems have been proposed but only a few have been fully developed and deployed in full-scale applications. The reasons for this are multifaceted: high costs, high maintenance, low reliability and very often the failure to develop industrially applicable prototypes. Thus, the development of industry-ready measurement systems is still necessary and highly anticipated due to rising substrate prices and continually reducing remuneration rates, in particular for older biogas plants. The following section will introduce a few available monitoring systems for biogas plants, which allow a more detailed process monitoring compared to common practice and which are already used at several plants in Germany.

6.1.2 State of practice and current market situation

The current state of online monitoring of biogas plants is mostly limited to the state-of-the-art parameters *pH*, *ORP*, temperature, biogas composition and biogas yield. But even their use, excluding temperature, is often limited to innovative biogas plant operators, who are open-minded towards new technology or to large biogas plants with a power production above 500kW that can afford the additional costs. In the course of two research projects PROBIG[26] and MOBIO[27] successfully executed by the Cologne University of Applied Sciences in close cooperation with two biogas plant

[26] Optimal **Pr**ocess **O**peration of **B**iogas Plants using an **I**ntelli**g**ent Adaptive Control System (Grant No.: KA0193201WD5)
[27] **M**odel-based Process **O**ptimization of **Bio**gas Plants (Grant No.: KA0607901WD8)

manufacturers and operators and funded by the BMWi[28], it was clearly stated that only temperature and biogas composition are considered to be standard parameters at agricultural biogas plants.

6.1.2.1 Standard process monitoring at agricultural biogas plants

In general, process monitoring at agricultural biogas plants is done by laboratory analysis at regular intervals. These intervals vary widely from once a week up to once a month depending on the reigning process conditions or operational problems. In the case of a change in input substrates, laboratory analysis of the substrates is necessary to estimate biogas production, quality and possible inhibitory effects. Based on the analytic results, the substrate feed to the plant is properly adjusted. Common monitoring parameters are *TS*, *VS* and *pH* of the input substrates and *VFA*, *PA/TA* and ammonium (NH_4) of the anaerobic sludge in the digesters. In particular, the ratio between *VOA* and *TIC* is considered to be an important process stability measure. In practice, a *VOA/TIC* ratio higher than 0.8 is considered to indicate a severe process disturbance, although some biogas plants operate under higher ratios due to highly adapted bacteria populations (FNR e.V. 2010). As for many other process parameters, the rule of thumb is that deviations from measurement values, which are considered to be normal, are more important than definite limit values. One of the main problems with this kind of offline process monitoring by laboratory analysis is the time delay between sample drawing and analysis, which makes fast reactions to operational problems impossible. Furthermore, costs for regular laboratory analysis are high (between €60 and €120 per sample) (Landwirtschaftskammer Nordrhein-Westfalen 2012) and thus strike most plant operators as unnecessary from a cost-benefit point of view.

Even standard online parameters such as biogas yield and biogas composition are far from maintenance-free. Biogas yield is mostly calculated based on power production of the cogeneration units and not directly measured (Bongards and Wolf 2008), (Wolf *et al.* 2011c). The challenge to accurately measuring the biogas volume flow is how to take account of gas humidity, pressure, temperature and gas flow velocity. Commonly used measurement principles are thermal and Fluidistor measurement as well as pressure difference and bellows-type measurement. Unfortunately, all these measurement principles have considerable disadvantages. The thermal measurement has problems with fouling, is very sensitive to gas humidity and does not cope well with changing biogas composition and the Fluidistor measurement only measures gas volume without considering gas pressure and temperature. Common problems with inaccuracies in pressure difference measurement systems are caused by low gas pressure and unknown gas composition as the gas density needs to be known. Furthermore, pressure difference systems can only be applied to processes with high gas flow velocities. Most problems occur with the bellows-type measurement, which is very susceptible to adhesion caused by an accumulation of humidity and impurities in the gas as well as to abrasion of the

[28] **B**undes**m**inisterium für **Wi**rtschaft und Technologie (German Federal Ministry of Economics and Technology)

mechanical parts. In this case regular maintenance is absolutely necessary. Overall, biogas volume flow measurement is far from trivial if the biogas is not properly dried and cleaned before it is measured. (Keitlinghaus 2011)

For biogas composition commercial measurement systems do exist and are widely applied in agricultural biogas plants. The most common gases measured are methane (CH_4), oxygen (O_2) and hydrogen sulfide (H_2S), whereas gas analyzers are recently often refitted with hydrogen (H_2) units as hydrogen has proven to be very sensitive to process disturbances (Boe *et al.* 2010). The measurement systems commonly use infrared (CH_4, CO_2, H_2, H_2S, O_2), electro-chemical (H_2, H_2S, O_2) and paramagnetic sensors (O_2, H_2) to measure the different gas components. Although all these measurement principles are well developed, impurities in the biogas make an accurate long term gas analysis difficult. Small particles in the biogas as well as high humidity cause the sensors to drift over time (four to twelve weeks), which results in deviations from the actual gas concentrations of up to 10% (PlanET Biogastechnik GmbH and Fachhochschule Köln 2010). Thus, regular calibrations by the manufacturer of the online gas analyzers are absolutely necessary and though costly, highly recommended to maintain measurement accuracy in the long run.

When it comes to *pH*, *ORP* and *TS* online measurement probes, their application at full-scale agricultural biogas plants started more than six years ago and was published by Wiese and Haeck in 2006 (Wiese and Haeck 2006). Nevertheless, the use of these online probes is rare at agricultural biogas plants in Germany with approximately only 240 out of 6,000 plants using one of the above mentioned online measurement systems (FNR e.V. 2009). The main reasons are high costs for probes and installation fittings, which lie between 1.500€ and 5.000€ (all together), depending on probe material and additional equipment and the regular maintenance, which consists of cleaning and recalibration. Throughout several practice tests at agricultural and industrial biogas plants, it was shown that taking measurements at low *TS* concentrations (<10%) does not cause any problems, whereas high *TS* concentrations (>15%) can cause severe damage to the electrodes of *pH* and *ORP* probes (Wolf *et al.* 2011a, Wiese and Kujawski 2008). Therefore, special probes with open aperture for *pH* measurement at high dirt loads and platin ring electrodes for robust *ORP* measurement should be chosen for high *TS* concentrations. For *TS* probes, high *TS* concentrations do not pose a serious threat.

6.1.2.2 Current market situation

The current market situation for online measurement systems for biogas plants will be analyzed in this section, introducing the most important and known manufacturers for such systems and the European biogas market. Thereby, the focus will be on systems that are well established in practice as well as on those that are state of the art and highly innovative products.

Manufacturers of measurement systems for standard process parameters

Online measurement systems for biogas flow meters are produced by all major instrumentation and automation companies in Europe, for example ABB[29], Endress+Hauser (E+H)[30], Siemens[31], Yokogawa[32], etc. Among these only E+H developed a gas flow meter (Proline Prosonic Flow B 200), which is specially designed for biogas and landfill gas and is able to cope with the impurities and the humidity in the gas (Endress+Hauser Messtechnik GmbH & Co. KG 2011).

a.

(ABB AG)

b.

(Endress+Hauser Messtechnik GmbH & Co. KG)

c.

(Siemens AG 2010)

d.

(Yokogawa Electric Corporation)

Figure 6-1: Examples of available gas flow meters: a. ABB Sensyflow FMT 200-D, b. E+H Proline Prosonic Flow B 200, c. Siemens SITRANS FX-300, d. Digital YEWFLOW DY-D

Furthermore, the methane concentration in the biogas is measured as well. Online analyzers for biogas composition are widespread at German biogas plants and mostly manufactured by German small and medium-sized companies. The companies that are well-known are ADOS GmbH[33], ExTox Gasmesssysteme GmbH[34] and Pronova Analysentechnik GmbH & Co. KG[35], whose gas analyzers can be found at most biogas plants in Germany.

a.

(ADOS GmbH)

b.

(ExTox Gasmesssysteme GmbH)

c.

(Pronova Analysentechnik GmbH & Co. KG)

Figure 6-2: Examples of biogas analyzers: a. ADOS Biogas 40, b. ExTox ET-4D2, c. Pronova SSM6000

[29] http://www.abb.com/
[30] http://www.endress.com/
[31] http://www.siemens.com/
[32] http://www.yokogawa.com/
[33] http://www.ados.de/
[34] http://www.extox.de/
[35] http://www.pronova.de/

For process parameters such as *pH*, *ORP* and *TS* in low *TS* environments, Hach-Lange[36] and E+H are the market leaders, offering a broad range of different probes and installation fittings, which even allow for recalibration and maintenance during process operation. Nevertheless, these companies are not able to measure *pH*, *ORP* and *TS* in high *TS* environments, which makes the systems useless for dry digestion or bio-waste processing plants. This is why the company Knick Elektronische Messgeräte GmbH & Co. KG[37] specialized in manufacturing *pH* and *ORP* probes for extreme process conditions such as high temperature/pressure and high *TS* concentration. Furthermore, the company hf-sensor GmbH developed an online measurement system especially for high *TS* concentrations above 15% using microwave sensors.

a.

(Endress+Hauser Messtechnik GmbH & Co. KG)

b.

(Endress+Hauser Messtechnik GmbH & Co. KG)

c.

(Endress+Hauser Messtechnik GmbH & Co. KG)

d.

(Knick Elektronische Messgeräte GmbH & Co. KG)

e.

(Endress+Hauser Messtechnik GmbH & Co. KG)

f.

(hf-sensor GmbH)

Figure 6-3: Example *pH*, *ORP* electrodes and *TS* probes and installation fittings: a. E+H Cleanfit W CPA450 installation fitting for *pH* and *ORP* electrodes, b. E+H Orbisint CPS11D pH electrode, c. E+H Orbisint CPS12D *ORP* electrode, d. Knick SensoGate® WA 130 installation fitting for *pH* and *ORP* electrodes, e. E+H TurbiMax W CUS 41 *TS* probe, f. hf-sensor MWTS PP *TS* probe

[36] http://www.hach-lange.com/
[37] http://www.knick.de/

Manufacturers of measurement systems for non-standard process parameters

The online measurement of *VFA*, *PA/TA*, *COD* and *TOC* is possible but it has been applied to only a few plants in Europe. The main reasons are high costs (between 10,000 and 40,000€) and the fact that most systems require an extensive level of maintenance and expert knowledge, which is mostly not available. The companies S::CAN and Trios manufacture UV/vis spectroscopic probes for online measurement of *COD* and *TOC*, which can also be used to measure *VFA* concentration and *TA*.

a. b.

(s:can Messtechnik GmbH) (TriOS Optical Sensors GmbH)

Figure 6-4: UV-vis spectroscopic probes from a. s::can and b. TriOS

Prices for UV/vis spectroscopic measurement systems range from 10,000 to 20,000€ depending on probe material and number of baseline calibrations, one per measurement parameter. As these online UV/vis spectroscopic systems measure absorption and not reflection, dilution of samples is mostly necessary. In particular, samples with *TS* concentrations above 10% require a high degree of dilution (1:100 or even 1:200) to get clear absorption spectra, which is why such systems are not well suited for processes with high TS contents. Therefore, the companies TENIRS GmbH[38] (recently bought by the m-u-t AG[39]) and art photonics[40] develop spectroscopic probes, which cover the NIR and MIR spectrum and measure the reflection spectra. The advantage of these systems is their ability to measure samples with high *TS* contents (even up to 40%), which makes them perfectly suited to measure substrate feed composition as well as process parameters in the digester. Nevertheless, these systems are still very expensive with approximately 20,000€ for NIR and up to 100,000€ for MIR systems.

a. b.

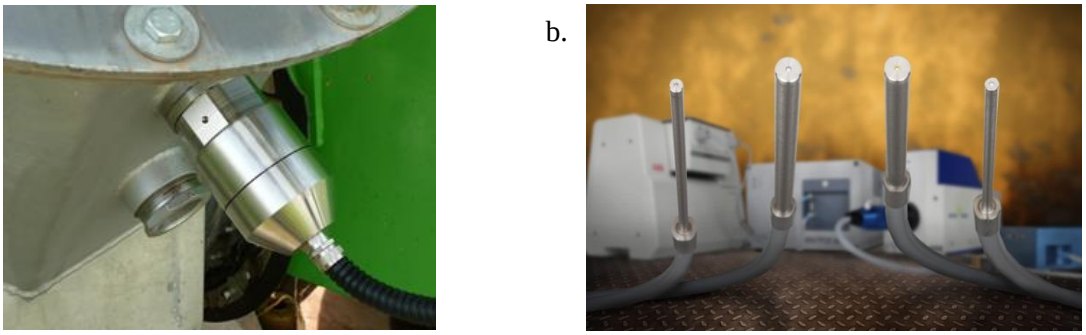

(Andree 2009) (Viacheslav Artyushenko 2010)

Figure 6-5: NIR and MIR measurement systems from a. TENIRS GmbH and b. art photonics GmbH PIR (Polycrystalline InfraRed) fibre probe

[38] http://www.tenirs.de/
[39] http://www.mut-group.com/
[40] http://www.artphotonics.de/

Currently the Cologne University of Applied Sciences works together with art photonics in a research project to develop an online MIR measurement system specially adapted for the use in biogas plants and with a total price between 10,000€ and 15,000€[41].

Other online measurement systems for *VFA* as well as *PA/TA* exist but are rarely applied due to very high prices in the case of online gas chromatography or HPLC analyzers or due to a lack of robustness in the case of systems such as the AnaSense® online titration system, which requires extensive maintenance.

Potential in the European biogas market

The market potential for new online measurement systems for biogas plants in Europe is estimated to be huge, due to the high number of biogas plants in Europe. Based on estimates from the trend:research institute (trend:research 2010) the number of biogas plants will double by 2020 from 8,000 (2010) to 16,000. With more than 7,000 biogas plants in Germany in 2012 alone (Fachverband Biogas e.V. 2011) and a rise in the European biogas production of 31% from 2009 to 2010, it becomes clear that the European biogas market is one of the fastest growing renewable energy markets in Europe (Liébard and Civel 2011). Nevertheless, the market for online measurement systems is smaller than the 16,000 plants envisaged by 2020. In many cases such systems are not feasible for smaller biogas plants with an energy production below 300kW, because of the additional costs for installation and maintenance. In Germany, this leaves us with biogas plants of 300kW and above, which still account for more than 50% of all biogas plants in Germany (FNR e.V. 2009). Overall, these numbers show that the potential market for new online measurement systems for biogas plants is high and will further increase as remuneration rates in most European countries will slowly decrease. This makes efficient plant operation and availability a top priority.

6.2 Necessity for online monitoring for biogas plants – an example from an industrial biogas plant

As long as biogas plants operate under stable process conditions, variations in plant stability and energy production are minimal. Thus, online monitoring does not seem necessary to many plant operators. The following example of an IBG "Industrial I[42]" shows that, in spite of the fact that most process parameters (*pH*, biogas production, biogas quality) were in the range of normal plant operation, plant stability was endangered by high *VFA* concentrations and steadily decreasing buffer capacity (*TA*), which eventually led to complete process failure.

[41] ZIM-KF project „INNO-MIR Biogas - Entwicklung und Automatisierung eines innovativen MIR-Online-Messsystems für Biogasanlagen" funded by the BMWi (Grant No. KF2137807AK1)
[42] Industrial biogas plant using bio-waste near Gummersbach, NRW, Germany

6.2.1 Description of the plant Industrial I

Industrial I is situated on a former landfill site near Gummersbach in Germany and primarily uses bio-waste from private households, which mainly consists of leftovers in the winter months and garden waste and lop in the summer months. The daily amount of bio-waste delivered to the landfill for processing and transportation to other facilities ranges from 100-250t from which 80-150t are digested in the biogas plant Industrial I depending on substrate composition, quality and process stability. Due to the fact that the bio-waste consists of many different kinds of materials and often contains dead animals, straw, tree branches and even sometimes non-degradable waste like stones, bottle caps, glass, car tires and construction waste, a sophisticated preprocessing step to sort and filter the bio-waste is absolutely necessary. After preprocessing, the bio-waste is fed to two digesters with 2,500m³ liquid phase and 500m³ gas phase. Both digesters use dry digestion due to the high *TS* content of the input material, which ranges from 30-50%. The digester uses the Valorga[43] system, which is characterized by a vertical dividing wall that extends up to 75% into the middle of the cylindrical digesters. The substrate input and output are on opposite sides of the dividing wall to maximize the retention time of the digestate by creating a plug flow through the digester. To assure a mixing of the digester content, biogas is pressurized between 10 and 100bar and then injected through gas injection ports at the bottom of the digester. The high pressure of up to 100bar is necessary to prevent sedimentation in the digester and clogging of the gas injection ports, which is mainly caused by the high *TS* content of the substrate feed in such plants and is well-known to become a serious problem after a few years of operation. (Nayono 2010)

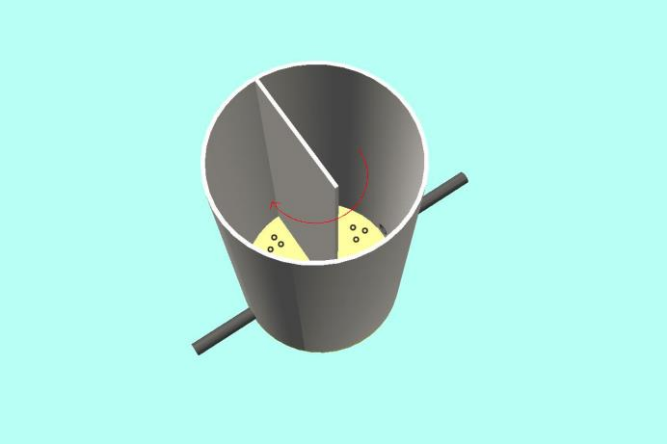

Figure 6-6: Digester Design from Valorga (Etzkorn 2008)

The overall layout of the biogas plant Industrial I is shown in Figure 6-7. The digesters are followed by two dewatering steps for the digestate to separate the liquid from the dry matter, which is then transported by conveyer to a nearby composting plant. The plant has been in operation since 1997 and operational and process data has been available since 1998. Next to flow and temperature

[43] http://www.valorgainternational.fr

measurements, several laboratory measurements are collected on a daily basis: *TS* and *VS* from the input substrates, the digestate and from the press and filter cakes as well as important AD process parameters such as *pH*, *TA* and *VFA* from the press water after the screen drums. Due to operational problems in 2007 an extensive data analysis was conducted to investigate possible reasons and to find out whether these problems could have been detected and prevented in advance. For this data analysis values from the measurement points shown in Figure 6-7 are taken from the years 2003 to 2007.

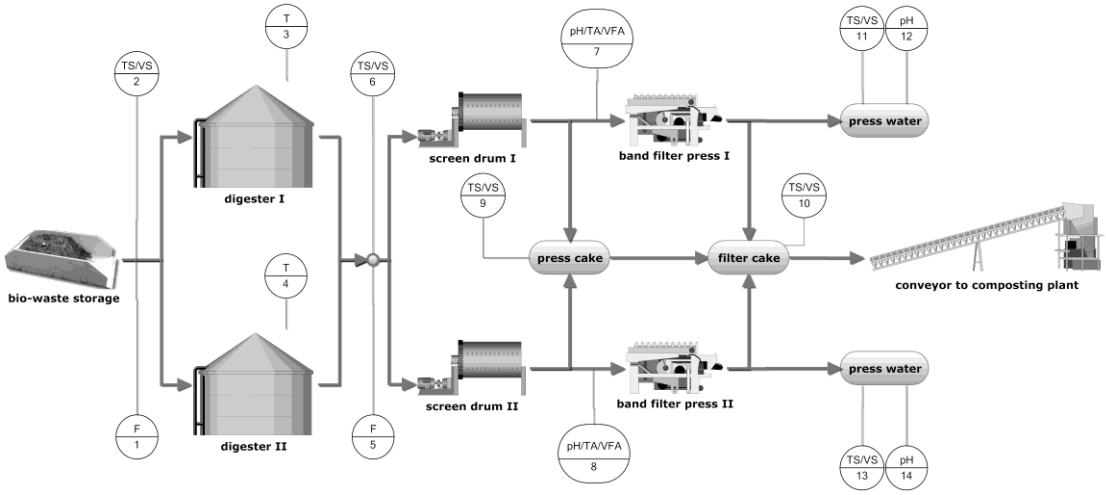

Figure 6-7: Plant layout of the biogas plant Industrial I including flow measurements and laboratory sample points

6.2.2 Data Analysis for Industrial I

The results of the data analysis clearly show that the operational problems could have been detected at least one month in advance by performing a detailed data analysis and could have been prevented if the appropriate counter measures, such as reduction of substrate feed, were taken. Figure 6-8 illustrates that the substrate throughput of Industrial I rose constantly from October 2005 to September 2007, resulting in a rising biogas production and eventually in the complete breakdown of the AD process. Such continuous increase in digester load significantly lowers the overall retention time of the biomass in the digesters, which puts the bacteria under high stress.

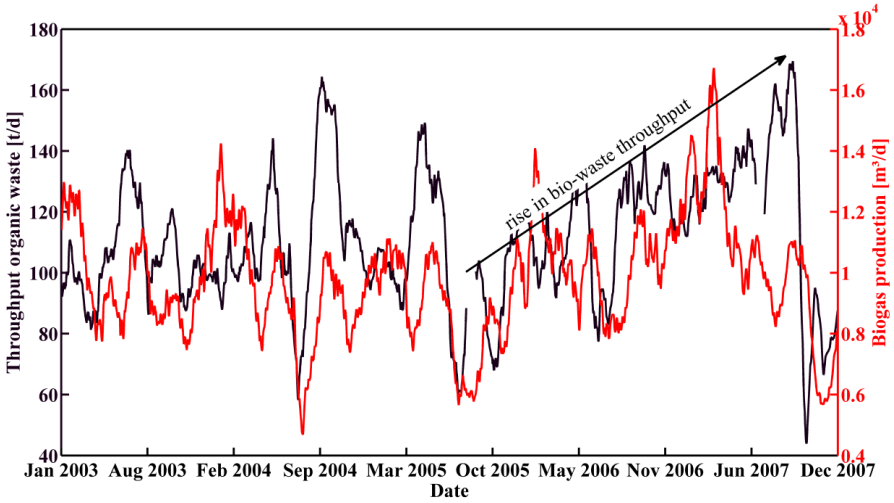

Figure 6-8: Comparison of bio-waste throughput with biogas production between 2003 and 2007

The consequences of such organic overload can be seen very well by looking at the development of *VFA* and *TA*. Caused by the increased bio-waste throughput a high rise in *VFA* concentration was measured, which eventually led to an acidification of the digester biology and the heavy drop in biogas production. Yet, the rise in *VFA* concentration alone would not have led to a complete breakdown of the process if *TA* was high enough to buffer the acids and to stabilize the *pH* value.

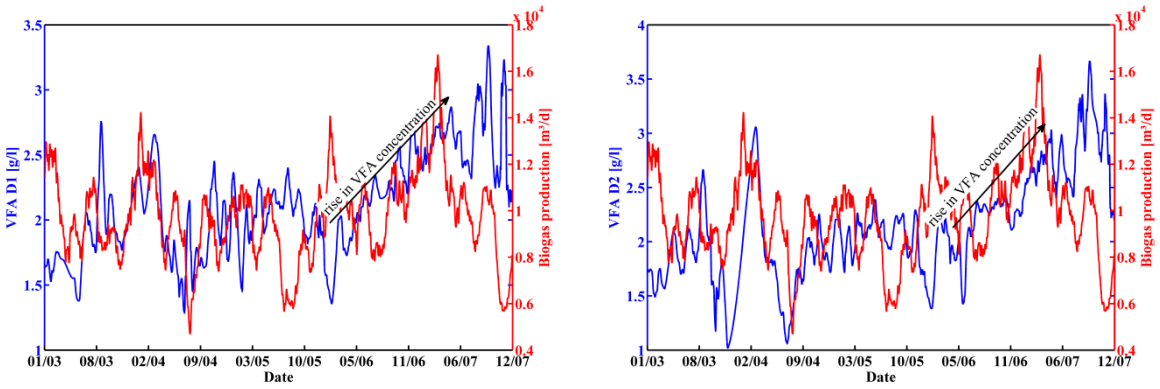

Figure 6-9: Comparison of VFA in digesters D1 and D2 with biogas production between 2003 and 2007

Unfortunately, the buffer capacity also suffered two severe drops as can be seen in Figure 6-10. The first drop occurred at the end of 2006 from which the process recovered before it eventually dropped to an all-time low at the end of 2007, which made a complete recovery impossible.

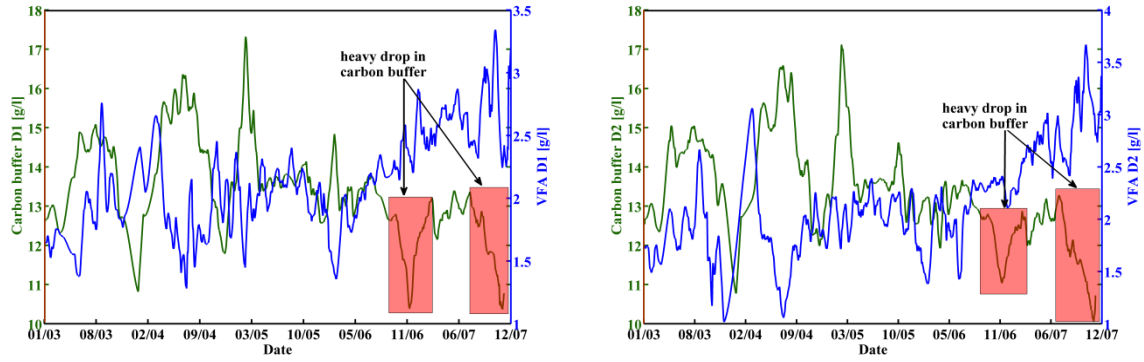

Figure 6-10: Comparison of carbon buffer in digesters D1 and D2 with VFA concentration between 2003 and 2007

One would expect to see comparable drops in the *pH* levels of the digesters because of high *VFA* concentrations and low *TA* values. Nevertheless, no such effects could be clearly detected in the data (Figure 6-11). Variation of the *pH* levels in digester one and two is too small to be of any significance. This corroborates the observations in the literature review that online measurement of *pH* levels does not provide additional valuable information about problematic process conditions in environments with high buffer capacities (Wiese and König 2009b, Wolf *et al.* 2011a). As soon as a considerable drop in *pH* level is detected, it is mostly already too late.

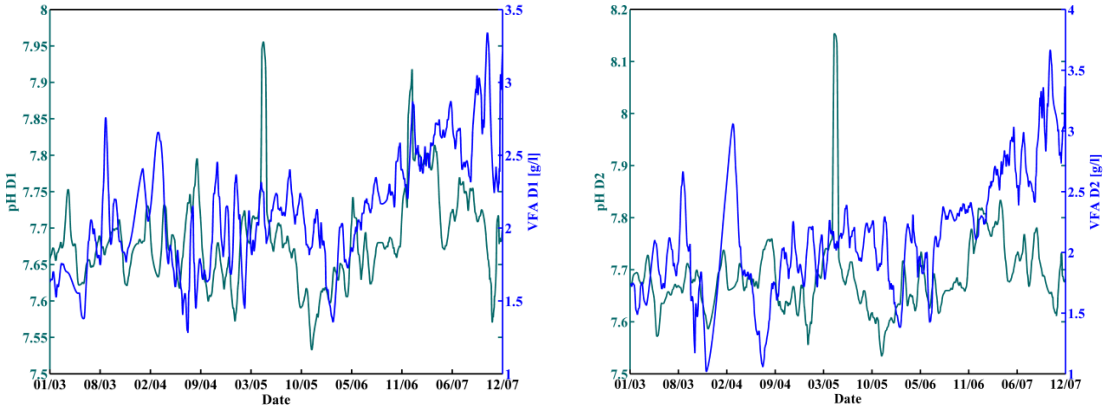

Figure 6-11: Comparison of pH levels in digesters D1 and D2 with *VFA* concentration between 2003 and 2007

Based on these results it becomes obvious that two things are of great importance when it comes to process monitoring of AD processes. Firstly, relevant process parameters (*VFA*, *TA*, *TS*, *VS*) need to be closely monitored on a regular basis. Thereby, online monitoring is recommended due to the availability of consistent process data and documentation as well as faster reaction times in case of operational problems. Secondly, available process data needs to be properly analyzed, if possible automatically to extract valuable process information in time. In particular, the second aspect poses a challenge to many biogas plant operators as process data is mostly not gathered in regular intervals, which makes a comparison among different parameters difficult. Furthermore, most operators do not possess the required expert knowledge for the application of effective data preprocessing methods (filtering, smoothing and interpolation) as well as for the use of more complex data analysis methods (cross-correlation, non-linear regression, Principal Component Analysis, etc.).

The practical example of operational problems from Industrial I shows that online measurement systems do not only create additional costs but help to provide highly valuable information about reigning process conditions, which eventually allows for the early detection of operational problems. In the case of Industrial I, restarting the AD process in the digesters required the complete emptying of one digester and cost several hundred thousand. If such an incident was prevented by the use of online measurement systems, prices of up to 40,000€ for this kind of equipment would still be a good investment.

6.2.3 pH, ORP and TS installation and test at Sunderhook ABP

The probes installed at the Sunderhook ABP are manufactured by E+H and are the same as the ones shown in Figure 6-3. The *pH* and *ORP* probes from E+H, which were used in this case, are called “memosens”-probes because the connection between electrode and controller is an inductive plug connector. This connector allows for easy and fast calibration and replacement of the electrodes and helps to reduce maintenance time. To guarantee a stable long-term operation of the probes, probes and installation fittings are made out of stainless steel. Due to the fact that the immediate surroundings of

the digesters are zone 0 or 1 according to the European ATEX guidelines for explosion prevention and prediction[44,45] installation of the probes directly into the digester wall is not possible. For this reason, the three probes were installed in a pump station, which is used to pump substrates into the first digester and digestate out of the first into the secondary digester. The main advantages are that the installation fittings and measurement controllers do not need to be ATEX certified and that different material flows can be measured and logged with only one installation. Furthermore, the installation fittings are so-called quick-change fittings, which make it possible to pull the probes out of the process under operating conditions. The measurement data of the probes is sent to three small controllers (Liquisys M Endress+Hauser Messtechnik GmbH & Co. KG 2012), one for each probe, and from there sent as current signal (4-20 mA) to a PLC with an OPC server. An OPC client is running on the central computer with the software iPCOIN (**i**ntelligent **P**rocess **C**ontrol **I**ntegration, Bongards *et al.* 2004) developed by the GECO►C research group from Cologne University of Applied Sciences. iPCOIN reads the measurement values from the OPC server and stores them in a PostgreSQL database for further analysis.

Figure 6-12: Installation of pH, ORP and TS probe at the Sunderhook ABP: a. complete installation, b. *TS* probe, c. *pH* and *ORP* probe

6.2.3.1 Comparison of online measurement values with laboratory measurements

A validation of the online measurement values was performed with regular laboratory samples. As the number of laboratory measurements is relatively small in comparison to the number of online measurement values, a t-test is used for an unbiased comparison.

[44] Directive 94/9/EC on equipment and protective systems intended for use in potentially explosive atmospheres (ATEX)

[45] Directive 1999/92/EC on minimum requirements for improving the safety and health protection of workers potentially at risk from explosive atmospheres

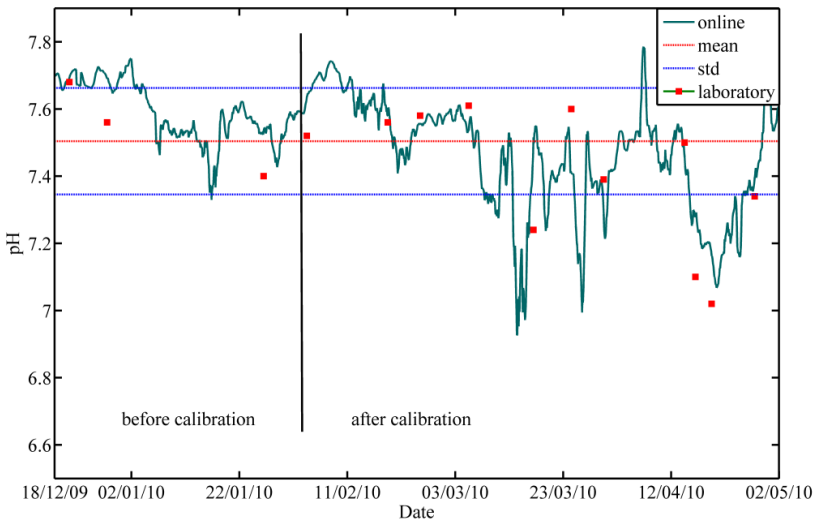

Figure 6-13: Comparison of *pH* online measurement values and laboratory samples

The result of the t-test confirms that both values represent the same normally distributed signal with equal mean and standard deviation as $h=0$ and thus the hypothesis cannot be rejected at the 5% significance level. The results for the f-test are different for the whole validation period and the one after the calibration of the probe. The variance for the whole period is not equal according to the f-test as the hypothesis is rejected ($h=1$) at the 5% significance level, whereas for the period after calibration the hypothesis cannot be rejected ($h=0$) and variances are equal.

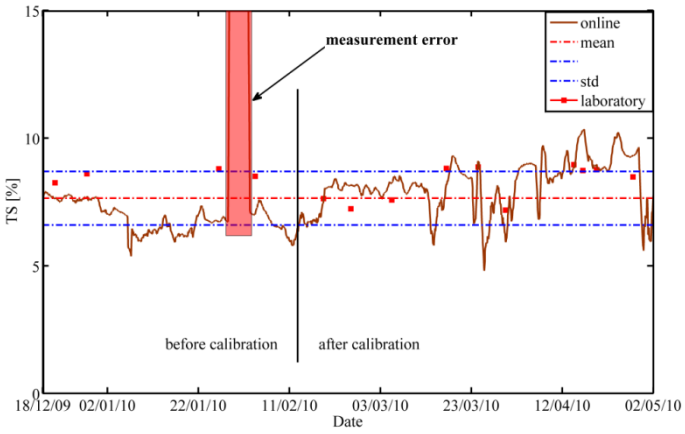

Figure 6-14: Comparison of *TS* online measurement values and laboratory samples

The comparison of *TS* online and laboratory measurements clearly show that before the calibration *TS* values were too low and do not match with the laboratory measurements at all. This is also reflected by the results of the f-test, where the hypothesis that the variances of the two signals are equal is rejected ($h=1$) at the 5% significance level for the period before calibration. For the following period after calibration the hypothesis is confirmed with h being 0. On the contrary, results from the t-test are the same for both periods. The hypothesis, that both signals possess the same mean and the same unknown variances, cannot be rejected ($h=0$).

For the *ORP* probe no laboratory samples were taken, because the exact measurement values do not have any significance in practice. Nevertheless, calibration of the ORP probe was performed on a regular basis every two weeks using calibration fluids. Trends in the overall level of the ORP are much more important and indicative of operational problems (Zimmermann *et al.* 2003). Thus, a steady increase in *ORP* indicates that an organic overload is probable. Figure 6-15 shows the development of the *ORP* values for the investigated period.

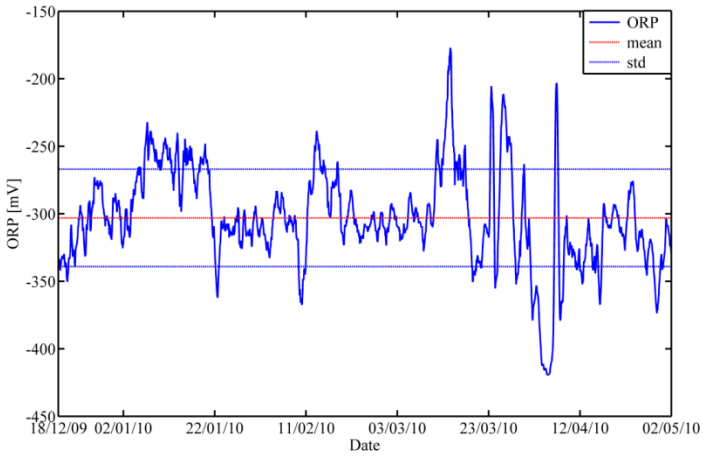

Figure 6-15: *ORP* online measurement values

6.2.3.2 Maintenance and robustness of the probes at Sunderhook ABP

The probes at Sunderhook ABP are low-maintenance products when compared to more complex online measurement systems like online titrators or gas chromatographs. Thus, maintenance is required once every two weeks or once every month depending two main factors: measurement drift and fouling. Due to a slow drift in measurement values over time, regular calibration of the *pH* and *TS* probe is absolutely necessary to gain accurate process data in the long run. The shortest required calibration interval varies from plant to plant and is strongly influenced by substrate composition and *TS* concentration of the digestate. For the Sunderhook ABP calibration of the *pH* probe was performed once every two weeks at the beginning of the test period and later on once every month. For the *pH* probe a two-point calibration at *pH* 4 and *pH* 7 is necessary, which can be easily performed using the Liquisys M controller. Therefore, the probe needs to be pulled out of the installation fitting and to be properly cleaned. Because of the quick-change fittings, the whole procedure of removing the probe from the process, cleaning the electrode and calibration of the electrode, takes between 15 and 20 minutes. For the *TS* probe, the calibration interval was much smaller during the test period. Calibration was performed once every two months, because no significant drift could be detected. In general, there are two calibration procedures available: one-point calibration with an additional damping parameter or two-point calibration. The large maintenance interval is an advantage for the plant operator, as both calibration procedures of the *TS* probe are time-consuming. In both cases, samples from the digestate have to be taken and measured with the *TS* probe. Then, the samples need to be measured in a drying

chamber. After 24 hours the results from these samples are available and can be programmed into the controller along with the *TS* probe results.

When it comes to fouling around the electrodes in case of *pH* and *ORP* probes or at the process window of the *TS* probe, the degree of fouling and its effects on the measurement quality depend mainly on substrate composition. High *TS* concentrations can easily cause clogging of the complete probe heads; in particular fibrous material tends to get stuck between the electrode and the installation fitting. For the *TS* probe, which possesses a flat probe head made from steel with integrated process window for the optics, greasy and oily substances pose a serious problem as they cause schlieren, which are difficult to remove. To counter fouling, the probes were pulled from the process once every two weeks at the beginning of the test period and later on once every month.

Figure 6-16: *pH* (a. & b.), *ORP* (c. & d.) and *TS* (e. & f.) probes after one month of operation before and after cleaning

Figure 6-16 clearly shows that even at low *TS* concentrations, which lie between 6 and 10% at the Sunderhook ABP, regularly cleaning is necessary. Nevertheless, cleaning itself is easy because no special cleaning products are required. Over the whole test period cleaning was performed with normal supply water.

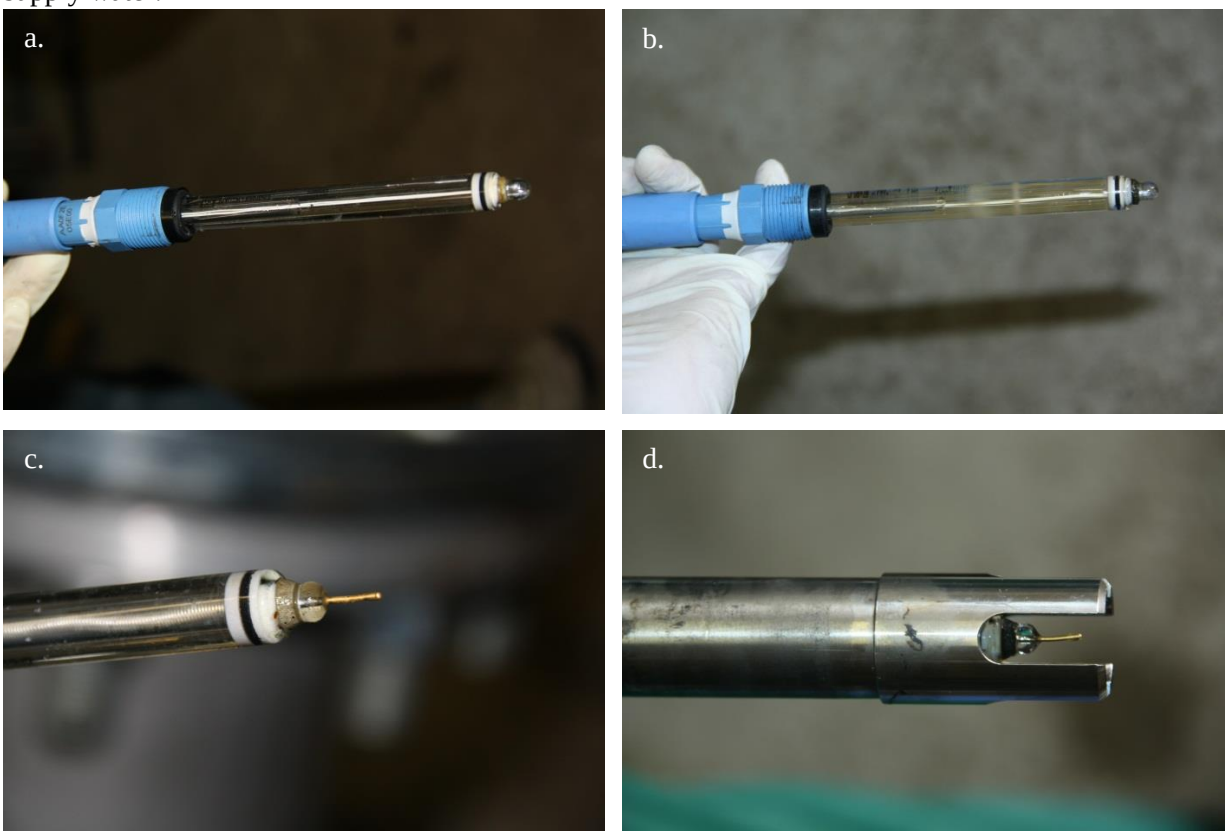

Figure 6-17: Long term effects of the digestate on *pH* and *ORP* probes at Sunderhook ABP

After one year of operation, changes at the *pH* and *ORP* electrodes were detected. The gel inside the *pH* electrode changed its color from clear to a mixture of green and brown, which slowed down the reaction time of the probe significantly. Furthermore, the calibration interval needed to be increased to once a week. Eventually, a replacement of the electrode was necessary. Concerning the *ORP* electrode, a bend, which was caused by the bulking material in the digestate, developed over time. This bend might lead to a break of the electrode in the future, but this has not happened so far. Changes other than these were not detected during the long term operation of the probes, which makes them well-suited for the use in biogas plants.

6.2.3.3 Suitability of pH, ORP and TS probes for online monitoring of the Sunderhook ABP

The purpose of the application of *pH*, *ORP* and *TS* probes at the Sunderhook ABP was also to investigate whether useful process information could be gathered to monitor the AD process and to enable early detection of anomalies. Therefore, the process signals from biogas production and methane concentration in the biogas are compared to the data from the three different probes. Due to different range of values, the process signals were scaled between 0 and 1 according to their min and max values. Unfortunately, a comparison of the curves does not reveal a clear connection between the

signals as can be seen in Figure 6-18. A further investigation of any connection between *pH*, *ORP*, *TS* and biogas production and methane concentration was conducted using cross correlation and k-means clustering. Although cross-correlation does not show a significant similarity in the curve progression between the signals, k-means shows that low biogas production and low methane concentration go hand in hand with low *pH* levels and high *TS* concentrations. *ORP* does not seem to have an influence on either biogas production or methane concentration.

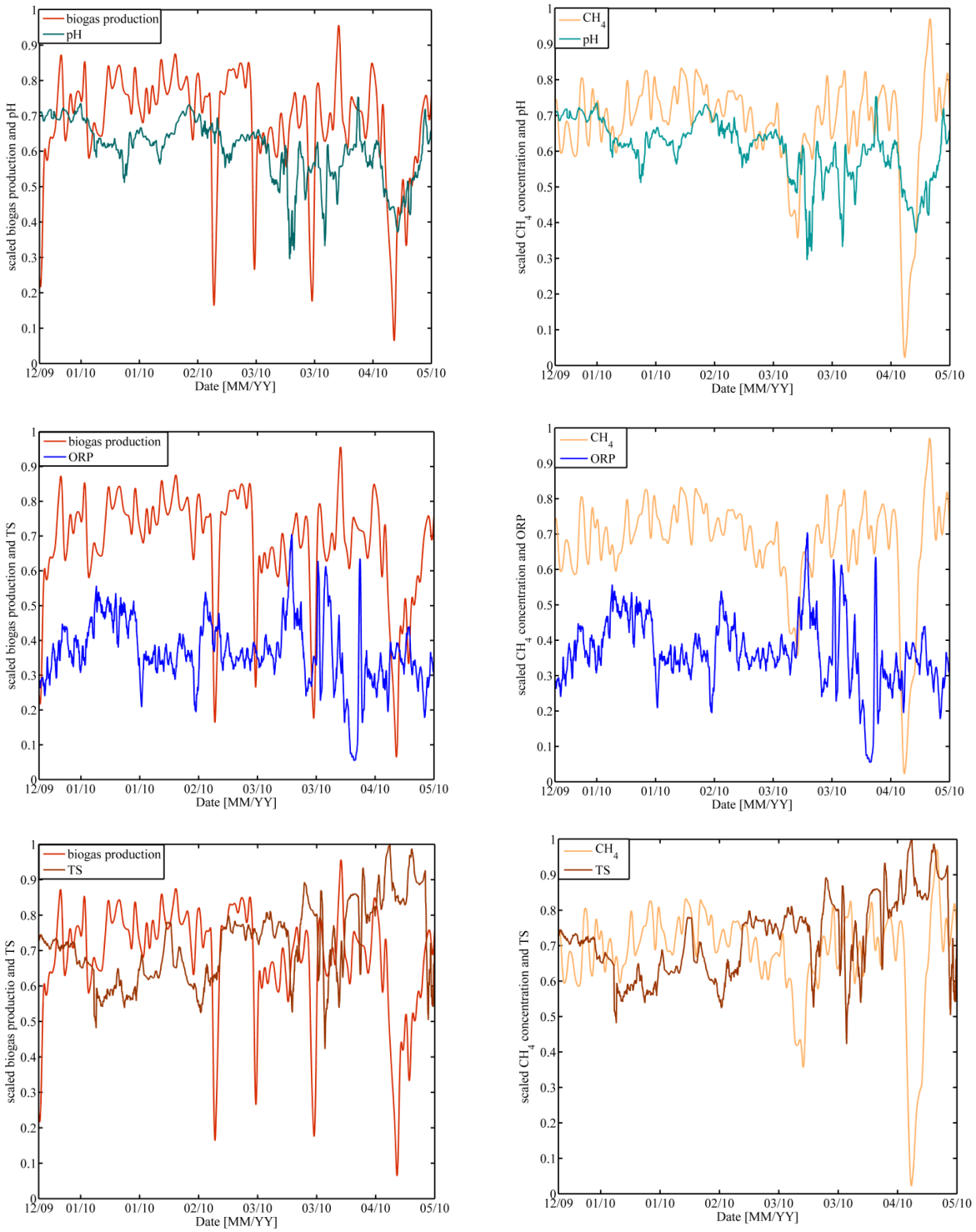

Figure 6-18: Comparison of *pH*, *ORP* and *TS* with biogas production (left) and methane concentration in the biogas (right)

Figure 6-19 shows the results of k-means clustering.

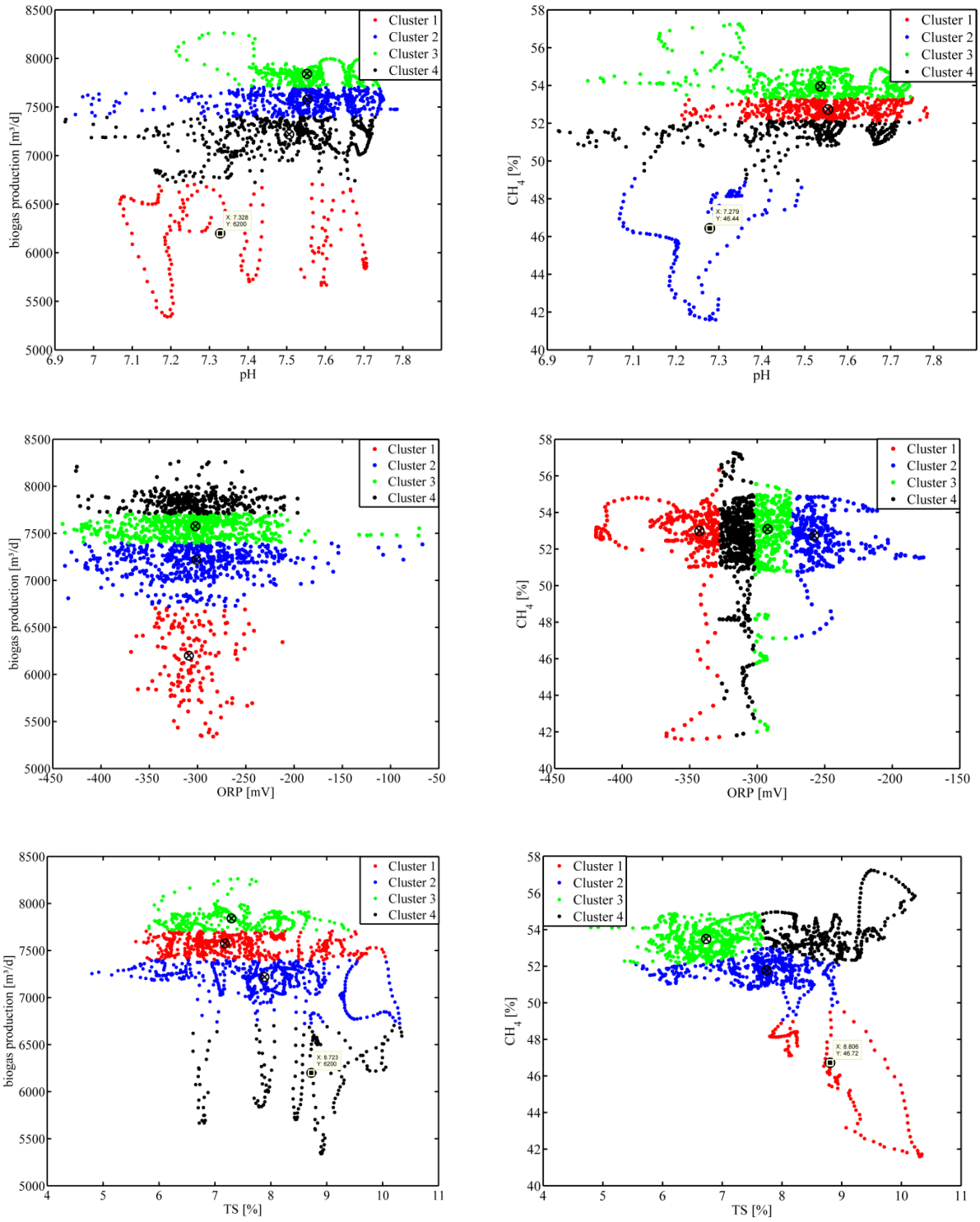

Figure 6-19: k-means clustering of *pH*, *ORP* and *TS* values against biogas production (left) and methane concentration (right)

It becomes obvious that the center of cluster 4 deviates clearly from the other centers of cluster one to three for *pH* and *TS* values, which indicates that low *pH* values and high *TS* values might cause a decrease in biogas production. If the *pH* is low, the AD process is inhibited and the high *TS* makes

mixing much more difficult. The effect of high *TS* concentrations on biogas production was confirmed by the plant operator, who stated that mixing of the digester becomes nearly impossible if *TS* concentration rises to 10% and above. This results in severe operational problems, which cause a drop in biogas production and methane concentration. The following 3D k-means clusters in Figure 6-20 show the influence of *pH* and *TS* on biogas production.

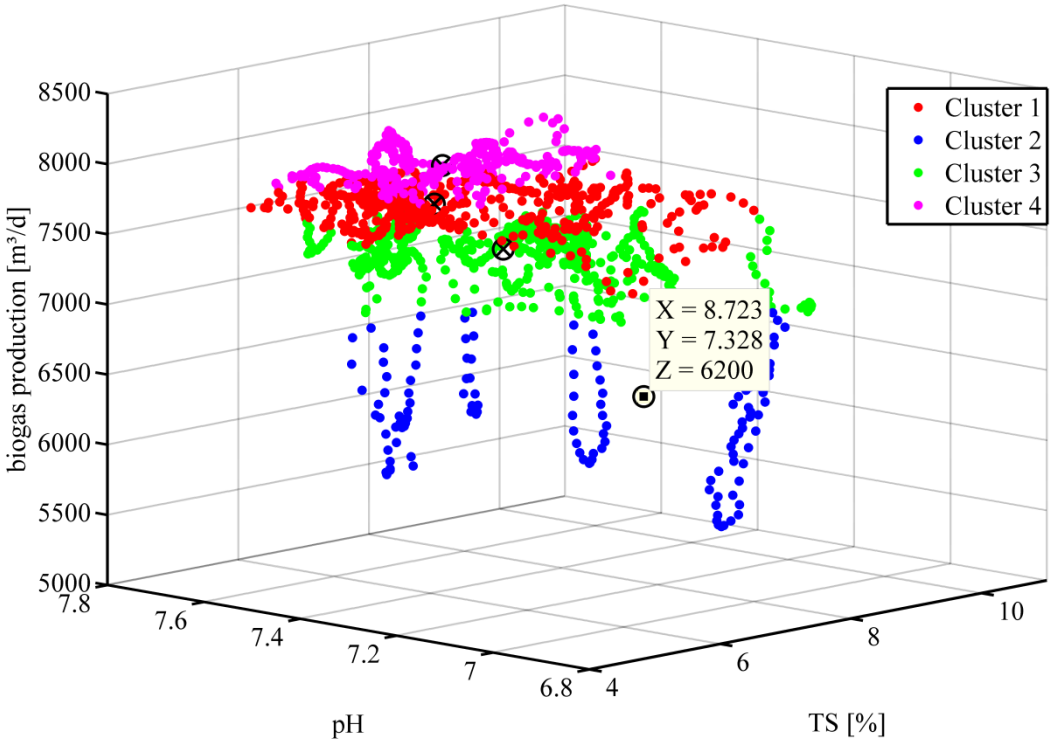

Figure 6-20: k-means clustering of *pH* and *TS* against biogas production

All in all, it can be said that *pH* and *TS* monitoring with online probes seems to be a good additional way to monitor the AD process at the Sunderhook ABP. The *ORP* values do not provide any new knowledge of the process and thus is not deemed necessary. When it comes to long term operation of the probes, all three probes are very well suited for the use at ABPs if *TS* concentration of the digestate is not too high (>12%). The probes are very robust and relatively low maintenance products. Furthermore, maintenance is fairly easy and does not require any expert knowledge, so that the plant operator can take care of the probes himself.

6.3 Field test of online measurement systems for pH, ORP and TS at an agricultural and industrial biogas plant

Online measurement systems for *pH*, *ORP* and *TS* exist for various applications from water, wastewater to AD monitoring. Although, existing probes for *pH*, *ORP* and *TS* are commercially available for biogas plants, they are not widely applied due to a lack of knowledge about their existence and due to the costs for probes and suitable installation fittings. Furthermore, not much

information is available about the suitability of these systems for biogas plants in terms of maintenance intensity and robustness. In 2006 Wiese and Haeck published an article about the instrumentation and automation of a full-scale agricultural biogas plant in Germany, which also mentions the use of *pH*, *ORP* and *TS* probes for online monitoring (Wiese and Haeck 2006). Nevertheless, results in terms of long-term operation and robustness are not presented, which is why *pH*, *ORP* and *TS* probes from two different manufacturers were tested at an agricultural biogas plant and an industrial biogas plant (Industrial I). Probes from E+H were tested at the agricultural biogas plant near Gronau-Epe in Germany (Sunderhook ABP), whereas probes from Hach-Lange[46] were installed at Industrial I. The probes were monitored over a period of several months and the measurement values compared to laboratory samples. The accuracy of the probe measurement values was validated with a t-test and f-test. The t-test examines, whether the null hypothesis, that data in two data vectors $\mathbf{x}$ and $\mathbf{y}$ are independent random samples from a normally distributed process signal with equal means and equal but unknown variances, is true ($h=0$) or false ($h=1$). The f-test is used to check whether data in two data vectors $\mathbf{x}$ and $\mathbf{y}$ are independent random samples from a normal distribution with equal variances ($h=0$) or different variances ($h=1$).

6.3.1 pH, ORP and TS installation and test at Industrial I

The probes installed at Industrial I are from Hach-Lange, which is one of the competitors of E+H on the market for online measurement systems for various environmental applications. Similar to the Sunderhook ABP, the probes were installed in a bypass pipe, which is used to pump digestate out of the two digesters into the following screen drums. The probes were not installed inside the digester walls due to the prevailing ATEX regulations. To allow for as easy maintenance as possible, quick-change fittings were used for all three probes. In general, the test conditions are comparable to the ones at the Sunderhook ABP, except for the extreme TS concentration of around 20%, which is already considered to be dry digestion. Such high TS content is a big threat to the sensitive electrodes of the *pH* and *ORP* probes used in this case.

Figure 6-21: Probes used for the test installation at Industrial I: a. *pH*[47], b. *ORP*[48], c. *TS*[49]

[46] http://www.hach-lange.de
[47] http://www.hach-lange.at/medias/sys_master/8796405006366/67392_L.jpg
[48] http://www.hach-lange.at/medias/sys_master/8796443148318/rd1r-us_L.jpg
[49] http://www.hach-lange.at/medias/sys_master/8796405006366/67392_L.jpg

Control and data acquisition of the probes is managed by a SC1000 (Hach Lange GmbH 2012) controller using three 4-20mA signals. The controller itself is connected to a netbook PC, which is accessible over the internet using the remote monitoring software Teamviewer[50]. An additional computer program accesses the gathered data once a week and sends it by email to the GECO►C research group.

Figure 6-22: Installation of the probes at Industrial I. a. *pH* and *ORP* probes, b. *TS* probe, c. SC1000 controller, d. Overview of probe control and data acquisition

6.3.1.1 Quality of online measurement data

The online measurement results from the test period clearly show that *pH* and *ORP* probes of this kind are not suited for application in high *TS* environments at all. After several weeks, first the *pH* electrode was irreparably destroyed and a month later the *ORP* electrode was shorn off due to sharp particles in the digestate. The moment of destruction of the electrodes becomes obvious in the figures showing the curve progression of the two probes over the test period. The data after the break is meaningless and the electrodes were not replaced as the test proved that they are not robust enough for this environment.

[50] http://www.teamviewer.com/

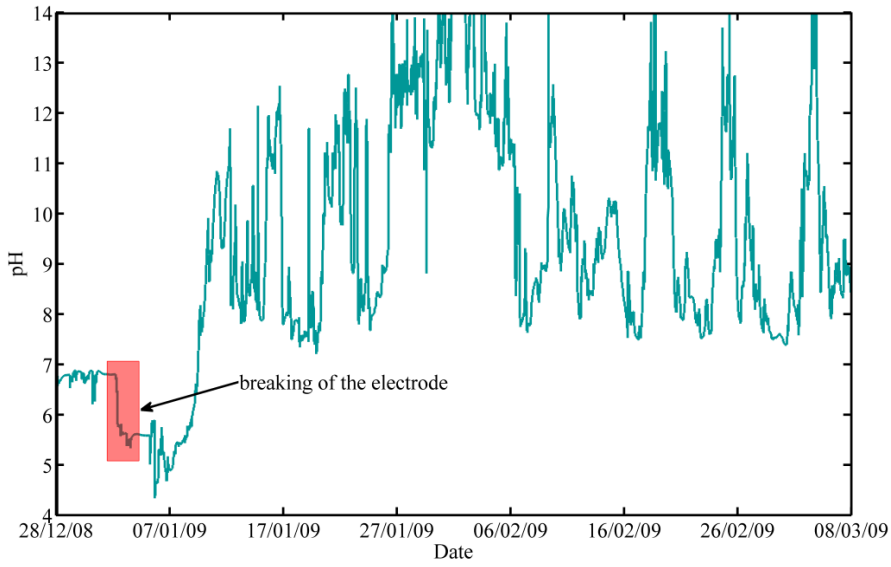

Figure 6-23: Online measurement data from the *pH* probe over the test period. Destruction of the electrode after one week of operation.

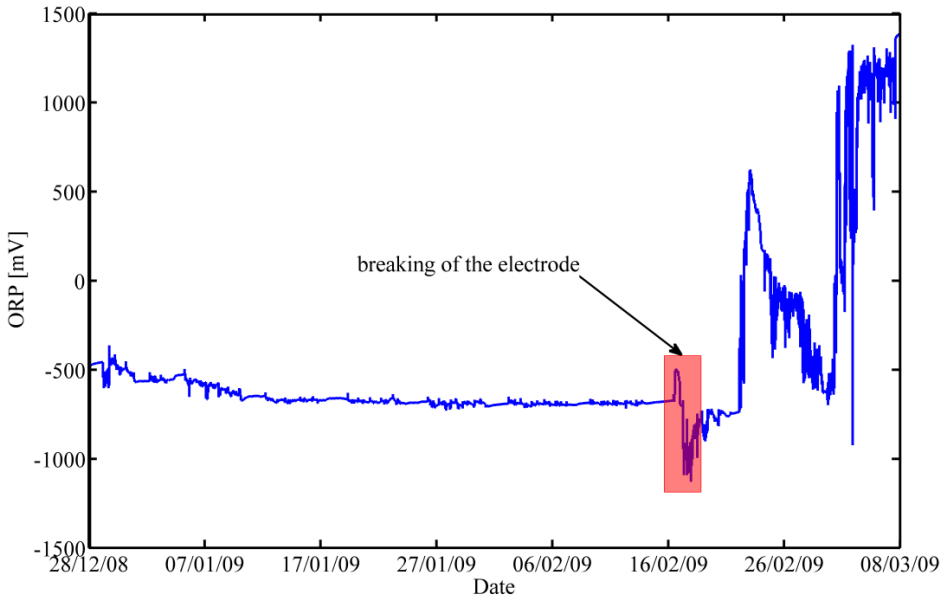

Figure 6-24: Online measurement data from the *ORP* probe over the test period. Destruction of the electrode after seven weeks of operation.

Only the *TS* probe was able to measure correctly over the whole test period, mainly because of the highly robust stainless steel casing and the scratch-resistant sapphire glass. Unfortunately, due to severe operational problems during the test period, the number of comparable laboratory *TS* measurements is very low (4 samples). Thus, the validity and significance of the results is very doubtful, although laboratory samples and online measured *TS* values show a good match. The time period of the *TS* probe test is shorter compared to the ones for the *pH* and *ORP* probes as the installation of the quick-change fitting took longer than expected.

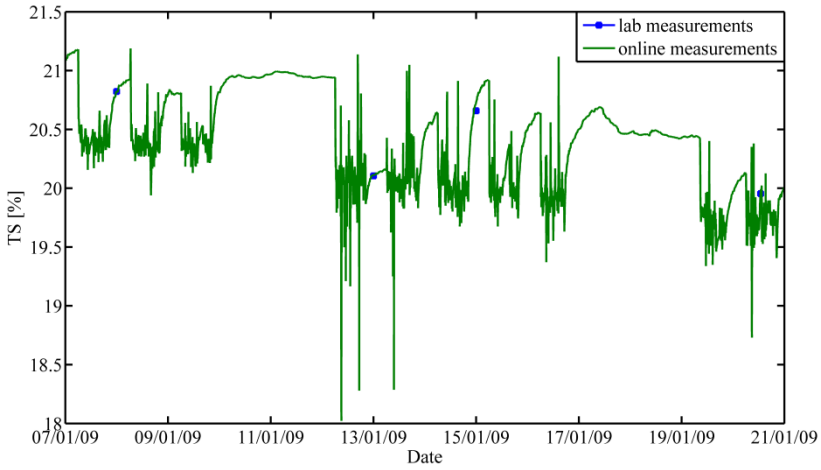

Figure 6-25: Comparison of *TS* online measurement values and laboratory samples

6.3.1.2 Maintenance and robustness of the probes at Industrial I

The *pH* and *ORP* probes used at Industrial I can definitely not be used in environments with high *TS* concentration. It is even doubtful whether more robust probe casings made of stainless steel would allow for a successful long time measurement of *pH* and *ORP*. The sensitive electrodes are the main problem because they come directly in touch with the process and can be easily damaged by sharp objects in the digestate. Without a proper protection no probe with a comparable design is likely to survive long in such a measurement medium. Figure 6-26 makes it obvious that the electrode was shattered at both probes, whereas the *TS* probe was not damaged at all.

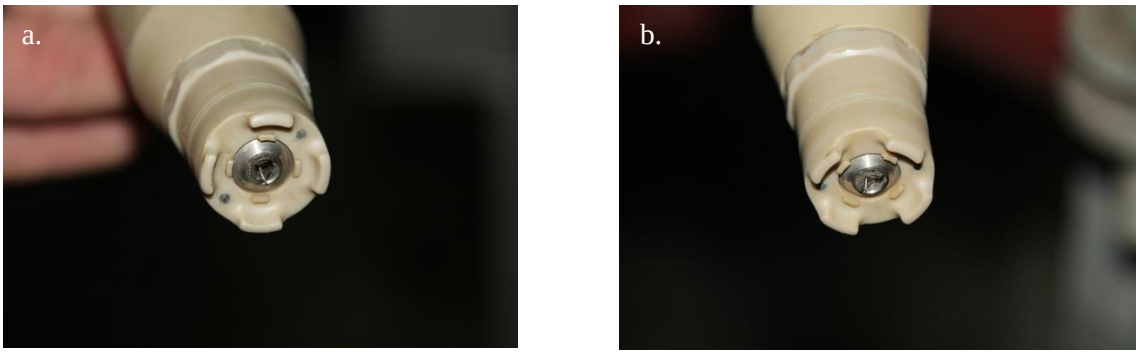

Figure 6-26: Damaged *pH* probe (a.) and damaged *ORP* probe (b.)

Maintenance of the *TS* probe was performed regularly every two weeks. The *TS* probe was properly cleaned and freed from small grains of sand and furring grains, which got stuck around the sapphire glass causing a clogging of the probe in the long run. As the test period was very short with four weeks of operation, no recalibration of the probe was necessary during that time.

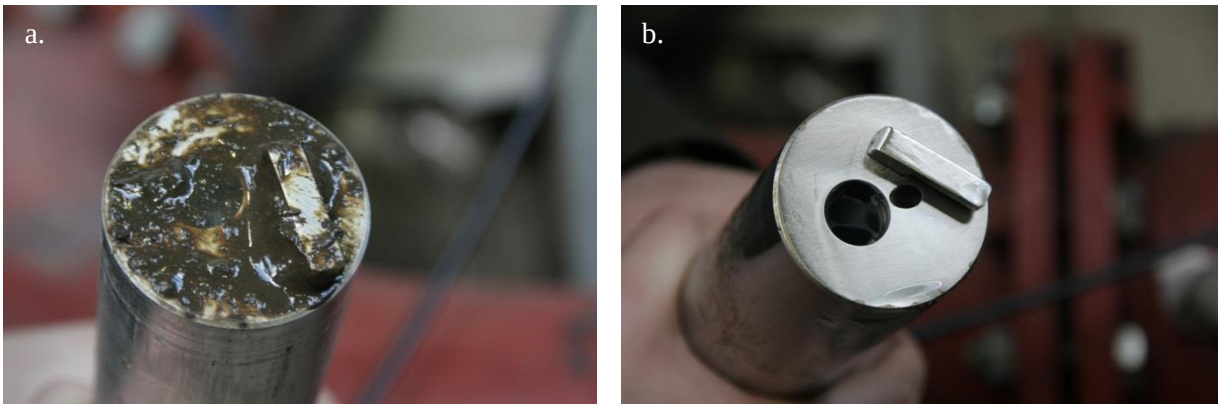

Figure 6-27: *TS* probe after one month of operation before and after cleaning

6.4 A novel method for VFA prediction in biogas plants using UV/vis spectroscopic online measurements

The availability of UV/vis spectroscopic probes offers a new approach to measuring organic acid concentrations indirectly and online. By employing powerful feature extraction and classification methods, organic acid concentrations can be predicted from the absorption spectra measurements taken from diluted fermentation sludge. As the use of UV/vis spectroscopic probes is well established in the wastewater sector for the online-measurement of the *COD* in sewage systems and wastewater treatment plants, these probes have proven to be extremely robust, requiring less maintenance than the alternatives mentioned above (Bongards *et al.* 2007).

Thus, this section presents a novel methodology for the online measurement of *VFA* in biogas plants based on UV/vis spectroscopy. The methodology consists of two key components:

- An online measurement system comprising the UV/vis spectroscopic probe and a dilution system for the fermentation sludge
- Machine learning based analysis software for generating *VFA* concentration predictions from the fermentation sludge absorption spectra measurements

A brief introduction to the practical background, the novel measurement system and its general functional principle is given in section 6.4.1. A key consideration for the proposed methodology is the proper choice of machine learning algorithm. This is addressed in section 6.5 where a detailed evaluation of a number of state-of-the-art machine learning techniques is presented and the optimum approach and configuration identified.

6.4.1 Measurement system methodology and practical application

The newly developed approach is to use UV/vis spectroscopy, which uses ultraviolet light (200nm - 750nm) to determine the concentration of a certain substance in a liquid sample. The general principle of the UV/vis based online measurement system for *VFA* concentration in biogas plants is shown in Figure 6-28. This measurement system is considered to be an indirect measurement as the actual *VFA*

concentration in the fermentation sludge is not measured but predicted based on spectral data from an UV/vis probe. Thus, changes in *VFA* concentration result in varying absorption intensities at certain wavelengths in the UV/vis waveband. The main challenge is to detect these variations in the measured absorption spectra and to translate them into *VFA* predictions. As this translation is a high dimensional, non-linear problem, powerful machine learning methods have proven to be well suited for this task. The final result of the data analysis is a time series of *VFA* concentrations, which can be used to monitor plant stability and to implement control strategies.

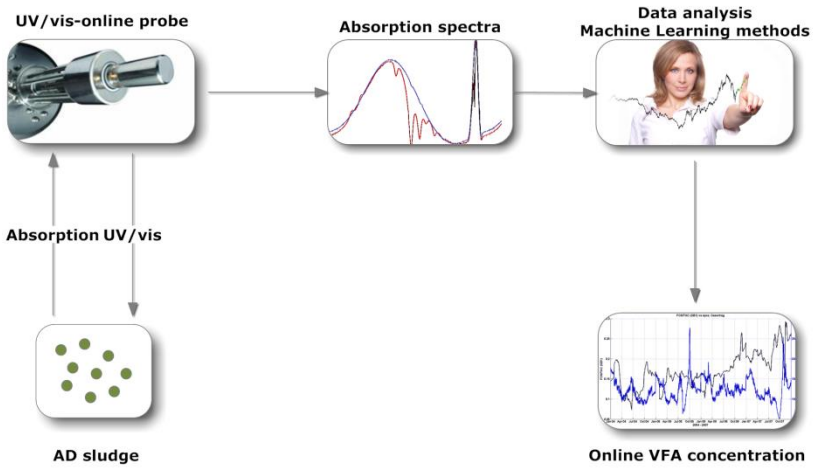

Figure 6-28: Principle of UV/vis based online measurement of *VFA* concentration in biogas plants

The main problem for the application of this measurement system on biogas plants is the high concentration of organic acids in the substrate and also the relatively high concentration of solids. Thus, an automated sample preparation and dilution system has been developed that addresses these issues. This has been installed and validated on Industrial I near Gummersbach, Germany. Industrial I primarily uses biological municipal waste for digestion. In particular high amounts of leftovers, which rapidly increase organic acid production, may compromise plant operation and stability. Due to these operating conditions, the plant operator has a high interest in testing and validating new promising measurement systems.

Laboratory tests conducted with the S::CAN spectro::lyser show that organic acid concentrations can be detected by analyzing the absorption over several wavelengths as shown in Figure 6-29 (Schmidt 2008). Different organic acids (acetic acids, propionic acid, lactic acid) were measured in different concentrations to determine the effect on the measured absorption intensity. It is obvious that with higher concentrations the maximum absorption shifts towards longer wavelengths and that for all three acids the absorption-maximum is at 230nm which makes it very difficult to distinguish between different organic acids. This indicates that organic acid concentrations cannot be measured separately but as a composite parameter, which makes UV/vis spectroscopy well suited for organic acid measurement on biogas plants.

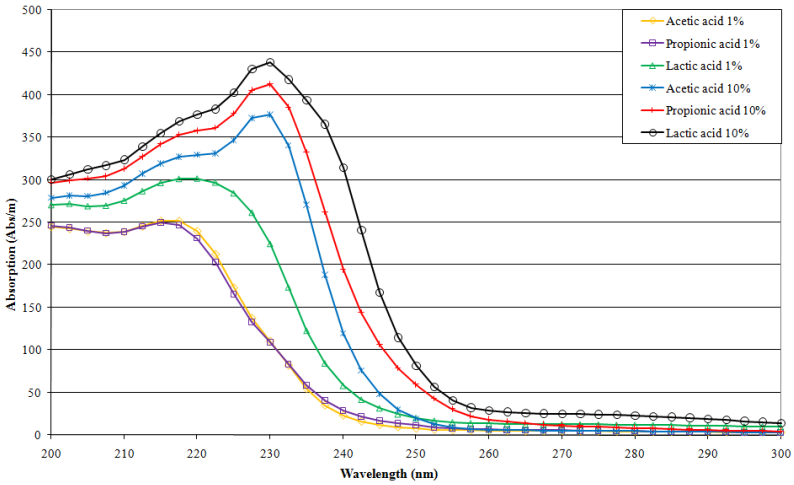

Figure 6-29: Laboratory measurements of different acids and concentrations using an S::CAN UV/vis probe

A very popular machine learning method often used to deduce chemical parameters from UV/vis measurements is Partial Least Squares Regression (PLS) (Langergraber *et al.* 2003). However, an initial investigation of PLS for this problem yielded very poor results with error rates of about 50%. This led us to consider advanced pattern recognition methods in preference to more traditional linear regression tools.

6.4.1.1 Online-measurement apparatus

Due to the fact, that *TS* concentration in the digester is up to 20%, a direct measurement of the absorption of the substrate at different wavelengths is not feasible, as the 1mm gap width of the UV/vis probe (S::CAN spectro::lyser) is easily soiled. For this reason, it is necessary to build up a special dilution system for the fermentation sludge. In this case, water from fermentation sludge dewatering is used for online-measurements, as organic acids are mainly present in the liquid phase of the sludge.

Laboratory tests have shown that the optimal ratio between water and sample is 1:80 to get a clear spectrum. To reach this dilution degree for an accurate measurement with the S::CAN spectro::lyser probe, the dilution unit is filled with four liters of water every 30 minutes (batch process). A peristaltic pump is used to administer a defined amount of the fermentation press water (50ml). Figure 6-30 shows the layout of the measurement and dilution system.

Figure 6-30: a. UV/vis-probe with 1mm gap width; b. Complete layout of the measurement system; c. Online-measurement in progress; d. Control cabinet for the measurement system; e. Flexible-tube pump for exact dosing of the fermentation sludge; f. Collection container for the press water of the fermentation sludge

A baseline calibration of the UV/vis probe is necessary to assure an accurate measurement of the absorption throughout the whole wavelength spectrum. Normally, deionized water is used for baseline calibrations, but in this case the mains water, which is used for dilution of the sample, was used for calibration. The reason is that the mains water itself already contains substances, which cause an additional absorption over the spectrum and thus influence the absorption of the sample. By using mains water for the baseline calibration, this absorption is taken into account so that the measured absorption for the diluted sample represents the sample matrix without the mains water matrix.

6.5 Application and comparison of machine learning techniques

The use of powerful computational intelligence and data analysis methods in conjunction with new and existing online-measurement and advanced control systems allows the development of highly sophisticated and robust systems for efficient process monitoring and optimization. There is a vast range of applications, for example Artificial Neural Networks for modeling and prediction purposes, Fuzzy-Control to include expert knowledge in plant operation, Genetic Algorithms for the optimization of complex processes, and machine learning methods to detect critical operation states or to further process online-measured information in so-called soft sensors (Puñal *et al.* 2003, Strik *et al.* 2005, Ozkaya *et al.* 2007, Steyer *et al.* 2002). The application of feature extraction and classification methods to predict organic acid concentrations in anaerobic digestion processes using UV/vis spectroscopic probes is an example of such a hybrid system.

Two factors support the use of pattern recognition methods for this type of application: (1) Organic acid concentrations can be divided into different concentration ranges/classes, which correspond to different process conditions; (2) a high precision measurement of organic acid concentrations is not necessary as the determination of concentration ranges is sufficient for plant operation. Furthermore, the chosen concentration ranges/classes can be easily applied to the development of Fuzzy-Control systems. In this approach we consider the well-known Linear Discriminant Analysis (LDA) and the Generalized Discriminant Analysis (GerDA), which is a novel and powerful extension of the classical LDA algorithm (Stuhlsatz *et al.* 2010b), to extract features automatically from the raw UV/vis spectrogram measurements. In addition to these feature extractors, we use linear classifiers to classify the extracted features into different concentration ranges. For comparison, we also investigate the use of Random Forest (RF), Neural Networks (Multilayer Perceptron, MLP), Support Vector Machines (SVM) and Relevance Vector Machines (RVM), which have proven to be very efficient methods for multi-class classification (Balabin *et al.* 2011, Guo *et al.* 2011, Wang *et al.* 2010, Yogameena *et al.* 2010). RF is used for feature selection and classification, whereas MLPs are used for the classification of reduced feature spaces created by applying Partial Least Squares regression (PLS), Forward Selection Regression (FSR) and GerDA to the raw measurements. Finally, SVMs and RVMs are investigated for direct classification of the spectrogram as well as for classification of the GerDA and RF features.

A detailed description of the dataset used for training and validation of the machine learning methods is given in section 6.5.1 followed by a short introduction to the feature extraction and classification methods investigated, namely: LDA, GerDA, RF, MLP, SVM and RVM for classification is given in sections 6.5.2 to 6.5.8. The classification results and a comparison of the performance of the different methods are provided in section 6.5.8, which is followed by a final evaluation of the pattern recognition methods considered as well as a discussion of the novel measurement system.

6.5.1 Description of the measurement data set

The measurement data set was created from online measurements using the UV/vis measurement system installed at Industrial I and laboratory measurements, which are regularly taken at Industrial I to monitor organic acid concentration in the two digesters. Thus, no synthetic data set was used for training and validation of the machine learning methods.

The spectrometric measurement device provides a characteristic absorption curve, called a fingerprint, over $p \in \mathbf{N}$ wavelengths. The values are given in $[Au/m]$ and stored as a column vector, where the i^{th} one is denoted by $\mathbf{x}_i \in \mathbf{X}$, with the feature space $\mathbf{X} \subseteq \mathbb{R}^p$. In total we have $N \in \mathbb{N}$ such fingerprints, i.e. $i = 1,\ldots,N$. Associated with each such vector $\mathbf{x}_i$ is the i^{th} *VFA* sample with unit $[g/l]$, denoted by $c_{a,i} \in \mathbb{R}$. To formulate the mapping from $\mathbf{x}_i$ to $c_{a,i}$ as a classification problem the measurements $c_{a,i}$ are clustered into $C = 5$ classes, which account for the whole range of given c_a's. The class $\vartheta \in \Theta$ to which the i^{th} *VFA* measurement belongs to is given by $\vartheta_i \in \Theta$, where $\Theta := \{1,2,3,4,5\}$ are the class labels as defined in table 1. These classes correspond to low, low-normal, normal, normal-high and high *VFA* concentrations, respectively. A total of $N = 4437$ samples were obtained from the biogas plant and these were used to generate training and validation data sets with $N_T = 3326$ and $N_V = 1109$ samples respectively. The distribution of the samples across classes is illustrated in Table 6-2.

Table 6-2: Definition of the class labels and the number of samples in each class ϑ for the complete (N_ϑ), training ($N_{T,\vartheta}$) and validation dataset ($N_{V,\vartheta}$)

Class $\vartheta \in \Theta$	Organic acid concentration $c_a[g/l]$	N_ϑ	$N_{T,\vartheta}$	$N_{V,\vartheta}$
1 (low)	1.1, …, 1.4	228	171	57
2 (low - normal)	1.5, …, 1.8	1528	1146	382
3 (normal)	1.9, …, 2.2	1880	1410	470
4 (normal - high)	2.3, …, 2.6	731	549	182
5 (high)	2.7, …, 3.0	70	52	18

From an initial investigation of the data set for the full spectrum spanning (200nm - 750nm) using LDA it was determined that better results could be obtained by omitting the longer wavelengths, hence as a final pre-processing step wavelengths above 640nm were removed leaving a $p = 176$ dimensional feature vector $\mathbf{x}_i$ for analysis. This cut-off point was determined by optimizing the LDA classification results with respect to *p*. This is simply a reflection of the fact that better generalization can be obtained if irrelevant feature vectors are discarded. The absorption beyond 300nm is very low, which leads to the conclusion that absorption characteristics at higher wavelengths do not have a high impact on the concentration of organic acids. Nevertheless, the inclusion of wavelengths above 300nm is

justified to take account of substrate coloring and the changing matrix of mains water in the measurement. Therefore, the appropriate cut-off point needs to be determined.

6.5.2 Linear Discriminant Analysis (LDA)

Linear Discriminant Analysis searches for a linear transformation $\mathbf{A} \in \mathbb{R}^{m \times p}$, $m \leq p$, such that the transformed data $\mathbf{Y} = \mathbf{A} \cdot \mathbf{X}$, $\mathbf{Y} := (\mathbf{y}_1, \ldots, \mathbf{y}_{N_T}) \in \mathbb{R}^{m \times N_T}$, can be linearly separated better than the original feature vectors $\mathbf{X} := (\mathbf{x}_1, \ldots, \mathbf{x}_{N_T}) \in \mathbb{R}^{p \times N_T}$. The linear transformation $\mathbf{A}$ is determined by solving an optimization problem which corresponds to maximizing the well-known Fisher discriminant criterion:

$$trace(\mathbf{S}_T^{-1} \cdot \mathbf{S}_B), \tag{6.1}$$

where $\mathbf{S}_T$ and $\mathbf{S}_B$ are the total scatter-matrix and between-class scatter-matrix, respectively as defined in Duda et. al. (2001).

The LDA and a subsequent linear classifier are both implemented in MATLAB® (Moore, 2009). An LDA transformation into a feature space of $m = C - 1 = 4$ dimensions yields the best subsequent linear classification results. Nevertheless, it becomes obvious at the 2D and 3D feature space representations of the data set that a clear separation of all five classes using LDA transformation is not possible with a linear classifier.

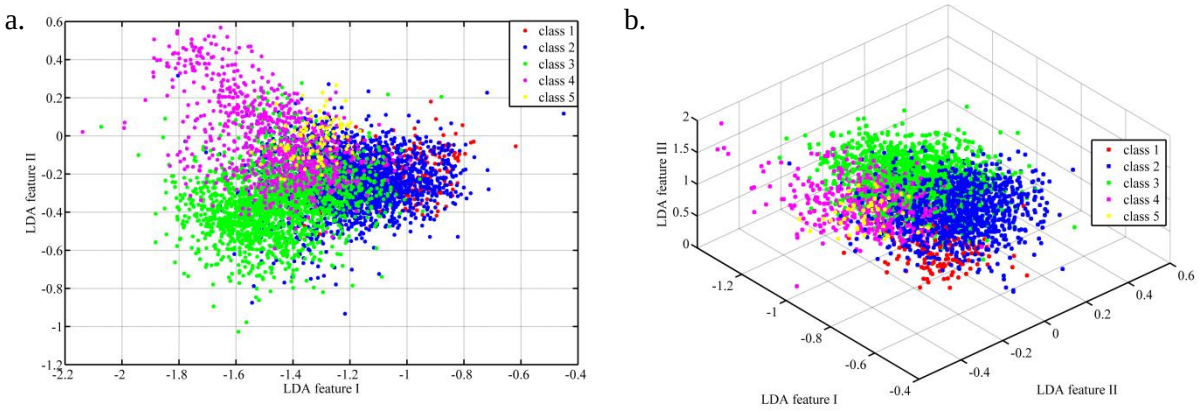

Figure 6-31: Representation of the five VFA concentration classes in (a.) the 2D-LDA-feature space and (b.) the 3D-LDA-feature space

6.5.3 Generalized Discriminant Analysis (GerDA)

LDA is a popular preprocessing and visualization tool used in different pattern recognition applications. Unfortunately, LDA and subsequent linear classification procedures produce high error rates on many real world datasets, because a linear mapping cannot transform arbitrarily distributed features into independently Gaussian distributed ones. A natural generalization of the classical LDA is to still rely on having intrinsic features $\mathbf{h} = f(\mathbf{x})$ with the same statistical properties as assumed for LDA features. Unlike LDA a function space F of nonlinear transformations $f : \mathbb{R}^p \to \mathbb{R}^m$ is used. The idea is that a sufficiently large space F potentially contains a nonlinear feature extractor $f^* \in F$

that can increase the discriminant criterion (6.1) compared to what can be achieved with the optimum linear extractor $\mathbf{A}$.

GerDA defines a large space F using the topology of a Deep Neural Network (DNN), and consequently the nonlinear feature extractor $f^* \in F$ is given by the DNN which is trained with measurements of the data space such that the objective function (6.1) is maximized. Unfortunately, training a DNN with standard methods, like back-propagation, is known to be challenging due to many local optima in the objective function considered. Therefore, randomly initializing the network parameters and restarting until thrown near to a good solution is ineffective for optimizing DNNs.

To efficiently train a large DNN with respect to (6.1), Stuhlsatz *et al.* (2010a, 2010b) have developed a stochastic pre-optimization based on greedily layer-wise trained Restricted Boltzmann Machines (RBM) (Hinton *et al.* 2006). In order to appropriately initialize a full GerDA-DNN, a stack of trained RBMs is used (Figure 6-32). Each RBM is trained with the inputs clamped to the output states of its predecessor RBM via minimizing the difference of two Kullback-Leibler distances d,

$$CD_n(\Theta) := d(P^0 \| P^\infty; \mathbf{\Lambda}) - d(P^n \| P^\infty; \mathbf{\Lambda}) \tag{6.2}$$

with respect to the network parameters $\mathbf{\Lambda}$.
The RBM's states are assumed to be Boltzmann distributed according to the distributions P^0, P^n and P^∞. Minimizing (6.2) can be performed using a very efficient training method for RBMs called Contrastive Divergence (CD) (Hinton 2002). In Stuhlsatz *et al.* (2010b), the CD heuristic is adapted for learning input-output associations by an output RBM (Figure 6-33). Training of all RBMs in a stack is unsupervised, with the exception of the output RBM which requires supervised training through minimization of the Mean Squared Error (MSE) between specific target codes $\vartheta_i \in \Theta := \{\mathbf{t}_1, \ldots, \mathbf{t}_C\}$, $\mathbf{t}_j := [t_{j,1}, \ldots, t_{j,C}]^T \in \mathbb{R}^C$, and the RBM's predictions $\mathbf{v}^{out}(\mathbf{x}_i) \in \mathbb{R}^C$. Minimizing the MSE with respect to the coding

$$t_{j,k} := \begin{cases} \sqrt{N_T / N_k} & \text{if } j = k \\ 0 & \text{otherwise} \end{cases} \qquad j, k = 1, \ldots, C \tag{6.3}$$

where N_k is the number of examples of class k, can be shown to asymptotically maximize the discriminant criterion (6.1) at the hidden units $\mathbf{h} \in \mathbb{R}^m$ (Osman and Fahmy 1994). A layer-wise training, with all weights $\mathbf{W}$ and biases $\mathbf{b}$ up to the last hidden layer $\mathbf{h}$, i.e. the output layer of the output RBM is discarded, is used to initialize a GerDA-DNN. Nevertheless, pre-optimization is suboptimal in maximizing (6.1), thus a subsequent fine-tuning of the GerDA-DNN is performed using a modified back-propagation of the gradients of (6.1) with respect to the network parameters. In Stuhlsatz *et al.* (2010a, 2010b) it is shown that stochastic pre-optimization and subsequent fine-tuning

yields very good discriminative features and training time is substantially reduced compared to random initialization of large GerDA-DNNs.

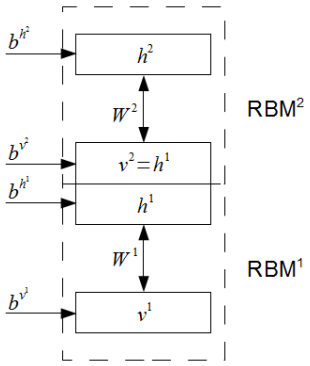

Figure 6-32: A simple stack of two RBMs

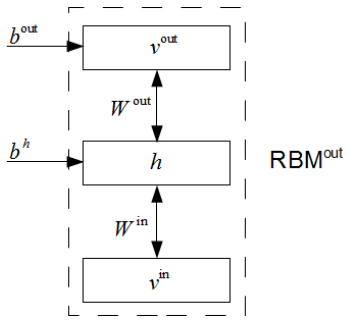

Figure 6-33: An input-output associative RBM

For the extraction of intrinsic features from the raw measurements, we used GerDA with a p-250-50-25-m topology, i.e. a 5 layer DNN consisting of one input layer with p units, 3 hidden layers with 250, 50 and 25 units respectively, and one output layer with m units resulting in more than 265 million free parameters. To avoid the effect of overfitting of the training data, we terminated the fine-tuning after the pre-training stage using an early-stopping criterion dependent on the training error. The topology of GerDA as well as the early-stopping criterion was evaluated on the training data via 5-fold cross-validation. Additionally, the best intrinsic dimensionality $m \geq C-1$ was cross-validated, too. The GerDA-framework is implemented in MATLAB®. The results presented in section 6.5.8 were obtained by using a DNN with the topology p-250-50-25-m, with $p=176$ and $m=4$. A topology with $m=5$ was also examined, but classification performance obtained was slightly inferior. Looking at the GerDA-transformed 2D and 3D feature space for the data set, the good separation capability of GerDA becomes obvious.

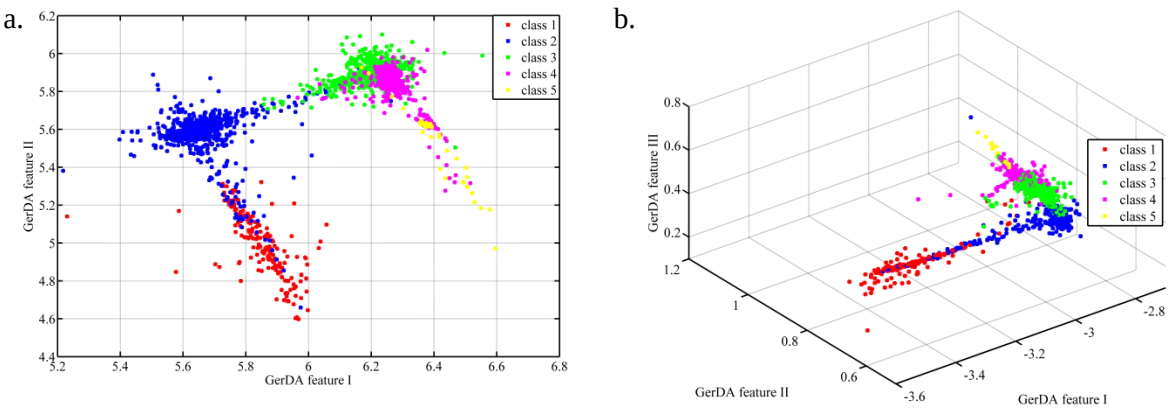

Figure 6-34: Representation of the five VFA concentration classes in (a.) the 2D-GerDA-feature space and (b.) the 3D-GerDA-feature space

6.5.4 Random Forest (RF)

Random Forest is an efficient algorithm for solving complex classification and regression problems, introduced by Breiman (2001). The RF-algorithm used here is the, R based randomForest package for Classification and Regression presented by Liaw and Wiener (2002). R is a free software environment for statistical computing and graphics R (R Development Core Team 2010).

The algorithm is an ensemble of unpruned decision trees. Hence, the classification consists of an ensemble of classification trees, where each tree is trained on a bootstrapped sample of the original training data set (also called in-Bag), and at each new branch the candidate set of variables is a random subset of all variables. For the investigation of the UV/vis spectral data set the number of input variables was set to thirty and the number of trees in the forest set to 800.

One third of the training data set is not present in the in-Bag. This left over data is known as out-of-bag (oob) data and is used to get a running unbiased estimate of the classification error as trees are added to the forest as well as to get estimates of variable importance. The average misclassification over all trees is known as the oob-error estimate. In this case, the algorithm estimates the importance of all variables by looking at how much the oob-error increases for one variable, while all other variables are not considered. This importance information can be used to minimize the number of variables in the dataset in order to minimize computation time and costs. The output of the classifier is determined by a majority vote of the trees.

6.5.5 Neural Networks (MLP)

The Multilayer Perceptron (MLP) is a feedforward artificial neural network, which consists of multiple layers of neurons that are fully connected from one layer to the next. Being an advancement of the standard linear perceptron, MLPs can distinguish data that is not linearly separable, which makes them perfectly suited for learning highly complex and non-linear mappings (Cybenko 1989). Furthermore, MLPs have several desirable properties like universal function approximation capabilities, good generalization properties and the availability of robust efficient training algorithms (Haykin 1999). For the classification problem at hand a single hidden layer MLP is used to map the non-linear relationship between the intrinsic GerDA features $\mathbf{h}_i^* := f^*(\mathbf{x}_i)$ and the corresponding class labels ϑ_i, $i = 1,\ldots,N_T$. Applying PLS and FSR on the original data set two further feature sets are generated which are also mapped to the class labels by a second and third MLP. This feature extraction significantly accelerates MLP design optimization. MLP training is performed using a BFGS training algorithm with stopped minimization used to prevent over-fitting (McLoone *et al.* 1998). The optimum number of neurons in the hidden layer and the optimum number of input features were determined for each model by cross-validation on the test data set. For PLS the optimal MLP design was $p = 30$, $n_h = 40$ and for FSR $p = 25$, $n_h = 60$. Here p is the number of input features and n_h is the number of neurons in the hidden layer.

6.5.6 Support Vector Machines (SVM)

Support Vector Machines (SVMs) offer a computationally efficient method for multi-class classification problems by finding hyperplanes, which separate data sets into classes in a high dimensional feature space. For the classification problem under consideration a C-Support Vector Classification is used with soft margin optimization and a Radial Basis (RBF) Kernel Function (RBF Kernel).

For a simple 2-class classification problem with data set $(\mathbf{x}_i, \vartheta_i)$, $i = 1,\ldots,N$, with $\mathbf{x}_i \in \mathbb{R}^p$ and $\vartheta_i \in \{1,-1\}$ the soft margin hyperplanes of a SVM can be described by the following set of equations, where $\mathbf{w} \in \mathbb{R}^p$ and $b \in \mathbb{R}$ are weight vector and bias, respectively, and $\xi_i \in \mathbb{R}$ is the slack variable for the i[th] set of $(\mathbf{x}_i, \vartheta_i)$ and is the error allowed in the classification (Haussler *et al.* 1992, Cortes and Vapnik 1995).

$$\begin{cases} \mathbf{w}^T \cdot \mathbf{x}_i + b \geq 1 - \xi_i & \text{if } \vartheta_i = 1 \\ \mathbf{w}^T \cdot \mathbf{x}_i + b \leq -1 + \xi_i & \text{if } \vartheta_i = -1 \end{cases} \quad \text{with} \quad \xi_i \geq 0,\ i = 1,\ldots,N \tag{6.4}$$

The optimization goal is to maximize the functional margin

$$\gamma_i := \frac{1}{2}\left(\frac{\mathbf{w}^T}{\|\mathbf{w}\|_2} \cdot \mathbf{x}_i^+ - \frac{\mathbf{w}^T}{\|\mathbf{w}\|_2} \cdot \mathbf{x}_i^- \right) \tag{6.5}$$

between the two classes with class labels 1 and -1 with corresponding data point vectors $\mathbf{x}_i^+$ and $\mathbf{x}_i^-$ while at the same time minimizing the classification error ξ_i. By solving (6.6), where $c \in \mathbb{R}$ is a tradeoff parameter between margin and error, this goal is achieved.

$$\begin{aligned} \min_{\mathbf{w},b,\xi} \quad & \frac{1}{2}\|\mathbf{w}\|_2 + c \cdot \sum_{i=1}^{N} \xi_i \\ \text{subject to} \quad & \vartheta_i \cdot \left(\mathbf{w}^T \cdot \mathbf{x}_i + b \right) \geq 1 - \xi_i \quad i = 1,\ldots,N \end{aligned} \tag{6.6}$$

The dual representation of this optimization problem in the more general kernel-based version can be described as

$$\begin{aligned} \max_{\boldsymbol{\alpha} \in R^N} \quad & \sum_{i=1}^{N} \alpha_i - \frac{1}{2} \sum_{i=1}^{N} \sum_{j=1}^{N} \vartheta_i \vartheta_j \alpha_i \alpha_j \cdot k\left(\mathbf{x}_i, \mathbf{x}_j\right) \\ \text{subject to} \quad & \sum_{i=1}^{N} \vartheta_i \alpha_i = 0 \ \text{ and } \ 0 \leq \alpha_i \leq c \qquad i = 1,\ldots,N \end{aligned} \tag{6.7}$$

where α_i is a Lagrange multiplier and $k\left(\mathbf{x}_i, \mathbf{x}_j\right) := \varphi\left(\mathbf{x}_i\right) \cdot \varphi\left(\mathbf{x}_j\right)$ is the kernel function that maps the training vectors $\mathbf{x}_i$ into a higher dimensional feature space by applying the function $\varphi : \mathbb{R}^p \rightarrow \mathbb{R}$, so that classification can be performed using a linear SVM (Cristianini and Shawe-Taylor 2000).

For classification of the spectral data set a Gaussian RBF kernel of the form

$$k(\mathbf{x}_i,\mathbf{x}_j)=\exp\left(-\lambda\cdot\left\|\mathbf{x}_i-\mathbf{x}_j\right\|^2\right) \quad \text{with} \quad \lambda:=\frac{1}{2\sigma^2} \tag{6.8}$$

is used, because of several advantages. The RBF kernel is perfectly suited for a non-linear relation between class labels and attributes and the linear kernel is a special case of the RBF kernel as proven by Keerthi and Lin (Keerthi and Lin 2003). Furthermore, the number of parameters that have to be optimized is limited to two parameters c (see 6.6) and λ which makes model selection easier and faster, when compared to polynomial kernels. A grid search is performed to determine the best parameters c and λ for the RBF kernel function according to the training data set using the SVM implementation LIBSVM (Chang and Lin 2001). The training is performed with a 5-fold cross-validation procedure (one against one) and different pairs of c and λ values are tested. Finally, the one that yields the best cross-validation accuracy is picked. As suggested by Hsu in 2003, in a first pass exponentially growing sequences of c and λ are evaluated to identify interesting regions for a detailed grid search (Hsu *et al.* 2003). Figure 6-35 shows the result of a global, as well as a detailed grid search for parameter optimization of c and λ on the training data set.

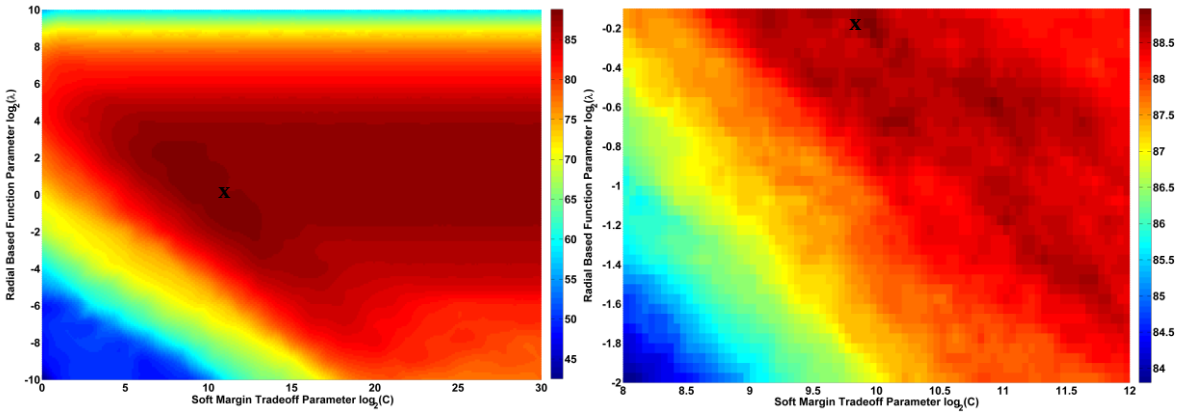

Figure 6-35: RBF and SVM parameter optimization results doing a grid search with LIBSVM.

The best parameters for the data set are shown in Table 6-3.

Table 6-3: Grid search results for the Training data set

	c	λ	MCR [%] (6.9)
N_T	955.425	0.87055	11.0

Due to the biased training and validation data sets, SVM performance on class 5 is rather poor, which made weighting of the classes necessary to achieve better results according to the performance

measure NMCR, which is introduced in section 6.5.8.1. The following results were achieved by a grid search where class 5 was given a weighting factor of 100 compared to 1 for all the other classes.

Table 6-4: Grid search results for the Training data set using a weighted SVM implementation to increase performance on class 5

	c	λ	MCR [%] (6.9)
N_T	4096.0	0.50000	11.1

6.5.7 Relevance Vector Machines

The Relevance Vector Machine (RVM) is a Bayesian formulation of the classification problem with priors selected to encourage sparse representations. They are structurally similar to SVMs and have been shown to provide comparable performance while offering a number of additional benefits. RVM predictions are probabilistic, facilitating the estimation of the uncertainty in predictions, and typically the number of relevance vectors can be reduced significantly compared to SVMs leading to more robust and computationally more efficient predictions. The RVM was introduced by Tipping (2000) as part of a general Sparse Bayesian learning framework in which sparsity is achieved by assigning parameterized priors to the model weights that encourage sparsity (Tipping 2000). As a result predictions for new data are made by estimating the marginal likelihood over the parameters of the priors (referred to as hyperparameters). For the classification at hand the RVM is used with a Gaussian RBF kernel so that it is directly comparable to the SVM implementation employed. The toolbox used for RVM classification is Version 2 of the Sparse Bayesian Modelling toolbox developed by Tipping (2009). Due to the fact that RVM training for data sets of high dimensionality has proven to be very slow, RVMs are applied on the intrinsic 4D-GerDA features and the reduced 30D-RF features only (Silva and Ribeiro 2010). As the toolbox only supports two-class RVMs, a separate RVM is trained and optimized for each class using a one-versus-all methodology and the overall prediction is determined by selecting the RVM with the highest class probability. The width parameter of the RBF kernels, λ, used with each RVM is determined by cross-validation on the test data set. The optimization is performed using Particle Swarm Optimization (Clerc 2006) for λ in the range 1×10^{-5} to 5×10^{-1}.

6.5.8 Classification results and analysis

6.5.8.1 Performance Measures

To validate and compare the classification performances of different methods the mean misclassification rate MCR in percent can be used,

$$\mathrm{MCR} := 100 \cdot \left(1 - \frac{1}{N_V} \cdot \sum_{i=1}^{N_V} 1(\mathbf{x}_i) \right), \ldots\ldots 1(\mathbf{x}_i) := \begin{cases} 1 & \text{if } f_{classifier}(\mathbf{x}_i) = \vartheta_i \\ 0 & \text{otherwise} \end{cases} \tag{6.9}$$

where $f_{classifier} : \mathrm{X} \to \Theta$ is the mapping function. Since in our experiments the number of samples per class is not uniformly distributed, the large classes, such as classes 2 and 3, may dominate the mean MCR too optimistically.

Because our goal is to identify each class with equal certainty performance measure (6.9) is not a good choice. Given the confusion matrix $\mathbf{K} := (k_{j,l}) \in \mathbb{R}^{C \times C}$, with $\sum_{l=1}^{C} k_{j,l} = 100$, $j = 1, \ldots, C$, for each classifier, an alternative measure of performance, called the Normalized MCR (NMCR), that gives equal weighting to each class is given by:

$$\mathrm{NMCR} := 100 - \frac{1}{C} \cdot \sum_{j=1}^{C} k_{j,j} \tag{6.10}$$

We decided to use the latter measure for validation, because it is an unweighted measure of performance independent of the number of samples N_ϑ.

6.5.8.2 Comparison of classification results

In order to compare the machine learning methods used in this case, confusion matrices and MCR and NMCR performance measures were computed for the test data set. These are presented in Table 6-5 and Table 6-7, respectively. The NMCR results show that some machine learning methods substantially outperform others for this classification problem. Significantly, some of the methods that underperform are competitive in terms of their MCR, suggesting that the highly unbalanced data set may be a contributing factor. It is clear that GerDA and RF are both capable of achieving very high accuracy for all classes despite the heavily unbalanced data set. In particular, the combination of the GerDA features and RF classification is very effective and yields one of the best classification results with an NMCR of 12.1%. In contrast, the MLP, SVM and RVM classifiers have serious problems classifying class 5 correctly due to the small number of samples in this class, whereas their recognition of the remaining classes is even better than obtained with GerDA and RF. The MLP results on the PLS features, both weighted and unweighted, were comparable but slightly inferior to the MLP results on the FSR features, so that only the MLP-FSR results are included as representative of both of them in Table 6-5, Table 6-6, Table 6-7.

It can be concluded that distinguishing between classes 4 and 5 seems to be very challenging and even more difficult because of the uneven distribution of training examples. One approach to correct for the unbalanced data set is to apply a weighting to class 5 during the training process. In the case of the SVM implementation, libSVM, this weighting can be introduced directly as a parameter in the optimization process. For the MLP and RVM the weighting can be achieved by replicating the samples in class 5 and adding them to the dataset. Using this approach the SVM, MLP and RVM classifiers were retrained with a 10-fold weighting applied to class 5. The resulting confusion matrices are given in Table 6-6 and the corresponding MCR and NCMR values are recorded in Table 6-7. As can be seen the NMCR performances of SVM, MLP and RVM classifiers have improved significantly. The weighted SVM results yield the best overall performance for the NMCR (12.0%). A comparison of the weighted SVM and weighted RVM results on the 4D GerDA data set shows that both methods provide very good and comparable results with only 0.8% difference in the MCR and 0.2% in the NMCR. However, the number of support vectors used is significantly lower for the RVM, which uses 60 support vectors instead of 398 for the SVM.

Table 6-5: Confusion matrices for different feature extraction and classification methods applied to the UV/vis spectrum data set: (a) LDA used as a feature extractor to get a 4D feature space followed by linear classification; (b) GerDA used as feature extractor to get a 4D feature space followed by linear classification; (c) RF used for feature selection and classification on a 30D feature space; (d) RF used for classification of the 4D GerDA features; (e) MLP used for classification on the 30D FSR features; (f) MLP used for classification on the 4D GerDA features; (g) SVM used for classification on the 30D RF features; (h) SVM used for direct classification on the raw dataset, (i) RVM used for classification on the 4D GerDA features and (j) RVM used for classification on the 30D RF features.

a) LDA — predicted

given [%]	1	2	3	4	5
1	**68.4**	14.0	8.8	8.8	0.0
2	7.1	**64.9**	20.2	6.0	1.8
3	1.9	17.0	**71.1**	8.7	1.3
4	1.6	17.0	30.8	**42.3**	8.2
5	0.0	5.6	5.6	5.6	**83.3**

b) GerDA — predicted

Given [%]	1	2	3	4	5
1	**98.3**	0.0	0.0	0.0	1.8
2	3.1	**91.6**	4.2	0.8	0.3
3	0.0	4.5	**88.7**	4.0	2.8
4	1.1	3.3	12.1	**68.7**	14.8
5	0.0	0.0	11.1	0.0	**88.9**

c) RF — predicted

given [%]	1	2	3	4	5
1	**82.1**	10.7	3.6	3.6	0.0
2	3.4	**87.4**	6.0	2.4	0.8
3	0.0	7.0	**82.1**	8.9	1.9
4	1.1	4.4	12.6	**75.8**	6.0
5	0.0	5.6	0.0	5.6	**88.9**

d) RF — predicted (GerDA features)

given [%]	1	2	3	4	5
1	**91.1**	7.1	0.0	0.0	1.8
2	2.4	**91.9**	4.5	1.0	0.3
3	0.0	4.5	**89.1**	4.0	2.3
4	1.1	3.8	8.8	**73.1**	13.2
5	0.0	0.0	5.6	0.0	**94.4**

e) MLP — predicted (FSR features)

given [%]	1	2	3	4	5
1	**86.0**	12.3	1.7	0.0	0.0
2	5.0	**90.6**	4.4	0.0	0.0
3	0.0	7.4	**89.8**	2.8	0.0
4	0.0	0.0	39.6	**58.8**	1.6
5	0.0	0.0	11.1	66.7	**22.2**

f) MLP — predicted (GerDA features)

given [%]	1	2	3	4	5
1	**86**	12.3	0.0	1.7	0.0
2	2.6	**91.4**	5.7	0.3	0.0
3	0.0	3.8	**92.1**	4.1	0.0
4	0.0	3.3	19.8	**76.9**	0.0
5	0.0	0.0	16.7	83.3	**0.0**

g) SVM — predicted (RF features)

given [%]	1	2	3	4	5
1	**94.6**	3.6	0.0	1.8	0.0
2	3.1	**90.6**	6.0	0.3	0.0
3	0.0	8.7	**88.8**	1.5	1.0
4	3.3	4.9	13.3	**76.9**	1.6
5	0.0	5.6	16.7	38.8	**38.9**

h) SVM — predicted

given [%]	1	2	3	4	5
1	**93**	5.3	1.7	0.0	0.0
2	2.0	**92.4**	5	0.6	1.8
3	0.2	6.0	**89.4**	3.6	0.8
4	2.7	4.4	6.0	**85.2**	1.7
5	0.0	5.5	16.7	33.3	**44.5**

i) RVM — predicted (RVM, GerDA features)

given [%]	1	2	3	4	5
1	**84.2**	12.3	0.0	3.5	0
2	2.1	**92.9**	3.5	1	0.5
3	0.0	3.8	**90.6**	3.7	1.9
4	1.1	2.2	9.9	**83.0**	3.8
5	5.6	0.0	11.1	33.3	**50.0**

j) RVM — predicted (RVM, RF features)

given [%]	1	2	3	4	5
1	**89.3**	5.3	3.6	1.8	0
2	3.4	**88.5**	5.7	2.4	0
3	0.6	5.8	**87.9**	5.1	0.6
4	1.6	3.3	22.0	**71.5**	1.6
5	0.0	5.6	11.1	50.0	**33.3**

Table 6-6: Confusion matrices for different feature extraction and classification methods with weighting introduced to class 5 during training to compensate for the uneven distribution of samples in the training data: (a) MLP classification of the 30D FSR features using a weighted training set; (b) MLP classification of the 4D GerDA features using a weighted training set; (c) SVM classification on the 30D RF features using a weighted SVM optimization; (d) SVM classification from the raw dataset using a weighted SVM optimization; (e) SVM classification on the 4D GerDA features using a weighted training set; and (f) RVM classification on the 4D GerDA features using a weighted training set.

a) W-MLP — predicted (FSR features)

given [%]	1	2	3	4	5
1	**64.9**	31.6	1.8	1.7	0.0
2	4.7	**89.8**	5.2	0.3	0.0
3	0.2	11.0	**84.3**	3.4	1.1
4	0.0	1.7	51.1	**41.2**	6.0
5	0.0	0.0	0.0	33.3	**66.7**

b) W-MLP — predicted (GerDA features)

given [%]	1	2	3	4	5
1	**87.7**	10.5	0	1.8	0.0
2	1.8	**91.6**	6.3	0.3	0.0
3	0.0	3.4	**90.9**	4.7	1.0
4	0.0	2.7	22	**65.9**	9.4
5	0.0	0.0	0.0	22.2	**77.8**

c) W-SVM — predicted (weighted SVM, RF features)

given [%]	1	2	3	4	5
1	**94.6**	3.6	0.0	0.0	1.8
2	3.4	**89.8**	6	0.5	0.3
3	0.0	8.1	**86.0**	4	1.9
4	2.7	4.4	9.9	**72.5**	10.4
5	0.0	0.0	0.0	5.6	**94.4**

d) W-SVM — predicted (weighted SVM)

given [%]	1	2	3	4	5
1	**94.7**	3.5	1.8	0.0	0.0
2	2.4	**91.4**	5.2	1	0.0
3	0.0	6.2	**89.1**	3.2	1.5
4	2.2	3.3	9.9	**75.8**	8.8
5	0.0	5.5	0.0	5.6	**88.9**

e) W-SVM — predicted (weighted SVM, GerDA features)

given [%]	1	2	3	4	5
1	**86.0**	10.5	0.0	1.8	1.7
2	2.3	**92.9**	3.7	0.8	0.3
3	0.0	4.5	**90.6**	3.0	1.9
4	1.6	2.7	11.6	**72.0**	12.1
5	0.0	0.0	0.0	5.6	**94.4**

f) W-RVM — predicted (weighted RVM, GerDA features)

given [%]	1	2	3	4	5
1	**82.5**	12.3	0.0	3.5	1.7
2	2.9	**92.7**	3.1	1	0.3
3	0.6	4.3	**89.6**	3.6	1.9
4	1.6	2.7	9.9	**75.8**	9.9
5	5.6	0.0	0.0	0.0	**94.4**

Table 6-7: Overall results with NMCR and MCR

Feature Extractor	Classifier	NMCR [%]	MCR [%]
LDA	linear	34.0	35.7
GerDA	linear	12.8	13.1
RF	RF	16.7	17.0
GerDA	**RF**	**12.1**	**12.4**
none	SVM	19.1	10.8
RF	SVM	19.1	10.8
RF	RVM	25.9	15.4
GerDA	RVM	19.8	10.8
FSR	MLP	30.5	16.3
GerDA	MLP	30.7	12.4
none	**W-SVM**	**12.0**	**12.0**
RF	W-SVM	12.5	14.3
GerDA	W-SVM	12.8	11.8
GerDA	W-RVM	13.0	11.0
GerDA	W-MLP	17.2	13.3
FSR	W-MLP	30.6	22.1

6.5.9 Summary of classification results for the novel UV/vis measurement system

The developed measurement system demonstrates a new approach for on-line estimation of organic acid concentrations using UV/vis spectrometric measurements, which offers new possibilities for advanced plant operation and control. The close monitoring of anaerobic digestion processes and the development of control strategies for optimal organic acid concentrations will substantially increase process efficiency and stability. However, results show that this online-measurement is far from trivial, such that advanced pattern recognition methods are needed to achieve good results. A comparison of the different feature extraction, selection and classification methods shows that the unbalanced data set available for training is a major problem, when it comes to achieving low NMCR results with some classifiers. However, application of appropriate class weightings during the training process can effectively counter the effect of the very small set of samples available for class 5.

The optimum results were obtained using Support Vector Machines (SVM) and a novel method named Generalized Discriminant Analysis (GerDA) in combination with Random Forest (RF) classification, both of which yielded an NMCR of 12%. This is sufficiently accurate to be of value for the online-measurement of organic acids.

The relatively poor MLP results suggest that the complexity of the classification space cannot be captured adequately with a single hidden layer network. Further tests with multi-hidden layer network designs may lead to better results and are the subject of future work.

Of the methods considered the combination of RF and GerDA yields the best error rate for the unweighted data set (12.1%) and further has many desirable properties. The GerDA-framework is self-contained and easy to use with learning performed in a partly unsupervised and partly supervised manner. It can be used as a pre-processing dimension reduction step for different classification methods. Furthermore, the extracted features are very low-dimensional and particularly suitable for simple linear classification (Stuhlsatz *et al.* 2010b) and data visualization. Consequently classification can be performed very quickly and the method is naturally applicable to multi-class problems. With regards to the weighted data set, SVM achieves the best overall results with an NMCR of 12% without requiring any feature selection or extraction methods. The comparison of the weighted SVM and weighted RVM on the GerDA features reveals that both methods perform equally well on the test data set, but that RVMs are more robust and provide more efficient predictive performance due to the significantly lower number of support vectors. This makes RVM well suited for applications where fast classification is the highest priority. As the dynamics of AD processes are slow (on the order of hours and days), the frequency of measurement of organic acids does not need to be high. Measurement intervals of 30-60 minutes are sufficient. As such the time taken to perform VFA classification is not an issue for this application.

As already noted the non-uniform distribution of class sizes biases the training of the pattern recognition methods in favor of the larger class sizes. To detect this effect it is important to use an unbiased performance measure such as the NMCR for validation and also for the determination and optimization of classifier hyperparameters.

To address the problems posed by having a biased dataset, other possibilities like the sampling with replacement methods exist and can be considered for the generation of balanced datasets for training. Furthermore, the introduction of additional meta-classes, which are constructed by the unification of different classes, offers another solution. Since the organic acid concentration is a continuous quantity, this may facilitate more effective time series analysis.

Summing up, the results obtained show that a variety of methods can successfully deliver sufficient measurement performance to be of practical value, with measurement errors between 12 and 20% (NMCR) for the best methods. In particular GerDA, RVM and SVM and their ability to cope with the highly biased dataset as well as the high dimensionality ($p = 176$), have proven to be perfectly suited to this kind of tasks. Thus, these methods are highly recommended to be used in the future for the analysis of UV/vis spectral data as well as for NIR and MIR spectral data.

6.6 Conclusion on the instrumentation of biogas plants

This chapter has demonstrated that research on instrumentation of biogas plants is multifaceted with many significant advances being made, but that a substantial gap exists between the current state of research and practice as presented in the literature review. Thus, the demand for industry-driven

research is huge and will continue to increase due to the rapid increase in the number of biogas plants across Europe. Sections 6.2 and 6.2.3 have highlighted that the need for online measurement systems in particular, is great, because of the lack of robust and affordable online monitoring systems. These are needed to detect critical process conditions before the AD process collapses and to develop efficient optimization and control strategies for biogas plants. The use of *pH*, *ORP* and *TS* probes can be considered state of the art for ABPs as the practical field trials described in section 6.3 show that they are well suited for ABPs. In general, good agreement between laboratory and online measurement values could be achieved for these properties. Unfortunately, standard *pH* and *ORP* probes from manufacturers such as E+H and Hach-Lange cannot be used with biogas plants which have high *TS* concentration in their digesters, because the sensitive electrodes are quickly damaged.

Due to the fact, that the measurement of *VFA* concentration is of great importance for biogas plant operation, an online measurement system based on UV/vis spectroscopy was successfully developed and tested at the industrial biogas plant Industrial I. The critical step in developing a valid system for analysis of the spectral absorption patterns was the search for suitable machine learning techniques to detect different levels of *VFA* concentration. Several state-of-the-art machine learning methods were tested and validated and SVM and GerDA were recommended as particularly well suited for the analysis of spectral data. This investigation of machine learning methods provides a good overview of existing state-of-the-art techniques and can serve as a useful guideline for their application to the analysis of high dimensional spectral data sets.

All in all, it can be said, that suitable online measurement systems for practical application at ABPs and at IBPs exist and provide good measurement results, which can not only be used for online process monitoring but also for online process control of AD processes in general. The contributions of this chapter show that the existing gap between research and practice can be successfully crossed by industry-driven research and extensive practical field tests.

References

ABB AG. *Datenblatt 10/14-6.73-DE Rev. D, Sensyflow FMT200-D Thermischer Masse-Durchflussmesser* [online], ABB AG. Available from: http://www05.abb.com/global/scot/scot211.nsf/veritydisplay/f598c6fcac4597b8c12577a8003611fb/$file/10_14-673-DE-D-11_2010.pdf [Accessed 14 Mar 2012].

ADOS GmbH. *Biogas 401: Mehrkanal-Gasanalysator* [online]. Available from: http://www.ados.de/Portals/0/ProdSheets/Biogas_401_D.pdf [Accessed 14 Mar 2012].

Ahring, B.K., Sandberg, M. and Angelidaki, I., 1995. Volatile fatty acids as indicators of process imbalance in anaerobic digestors. *Applied Microbiology and Biotechnology*, 43 (3), 559–565.

Anderson, G. and Yang, G., 1992. Determination of bicarbonate and total volatile acid concentration in anaerobic digesters using a simple titration. *Water Environment Research*, 64 (1), 53–59.

Andree, H., 2009. *Effizienzreserven durch optimale Kontrolle und Steuerung im Fermenter: (Efficiency reserves through optimal monitoring and control in the digester)*. Flensburg.

Balabin, R.M., Safieva, R.Z. and Lomakina, E.I., 2011. Near-infrared (NIR) spectroscopy for motor oil classification: From discriminant analysis to support vector machines. *Microchemical Journal*, Article in press.

Bishop, G., Baker, J., Burns, R. and Moody, L., 2010. Developing a pressure-based measuring system for determining biogas and methane production for biochemical methane potentials and anaerobic toxicity assays. *American Society of Agricultural and Biological Engineers Annual International Meeting 2010*, 1, 757–769.

Björnsson, L., Murto, M. and Mattiasson, B., 2000. Evaluation of parameters for monitoring an anaerobic co-digestion process. *Applied Microbiology and Biotechnology*, 54 (6), 844–849.

Boe, K., Batstone, D.J. and Angelidaki, I., 2007a. An innovative online VFA monitoring system for the anerobic process, based on headspace gas chromatography. *Biotechnology and Bioengineering*, 96 (4), 712–721.

Boe, K., Batstone, D.J. and Angelidaki, I., 2007b. An innovative online VFA monitoring system for the anerobic process, based on headspace gas chromatography. *Biotechnology and Bioengineering*, 96 (7), 712–721.

Boe, K., Batstone, D.J., Steyer, J.-P. and Angelidaki, I., 2010. State indicators for monitoring the anaerobic digestion process. *Water Research*, 44 (20), 5973–5980.

References

Bongards, M. and Wolf, C., 2008. *Abschlussbericht Pro-INNO Projekt PROBIG - Optimale Prozessführung von Biogasanlagen mit einem intelligenten, adaptiven Regelungssystem (Final report Pro-INNO project PROBIG - Optimal Process Operation of Biogas Plants using an intelligent, adaptive control system)*. Berlin: BMWi.

Bongards, M., Hilmer, T. and Kern, P., 2007. Online-Konzentrationsmessung in Kanalnetzen - Technik und Betriebsergebnisse. (Online concentration measurement in sewage systems - methods and operational results). *Forschungsbericht der Fachhochschule Köln* (1), 173–176.

Bongards, M., Westenberger, H., and Ebel, A., 2004. *Intelligent Process Control Integration (iPCOIN): Integrationsplattform für intelligente Prozeßsteuerung (integration platform for intelligent process control)*: Cologne University of Applied Sciences.

Breiman, L., 2001. *Machine Learning*, 45 (1), 5–32.

Cadena Pereda, R., Rivera Muñoz, E. and Herrera Ruiz, G., 2010. Automatic volumetric gas flow meter for monitoring biogas production from laboratory-scale anaerobic digester. *Sensors and Actuators B: Chemical*, 147 (1), 10–14.

Chang, C.C. and Lin, C.J., 2001. *LIBSVM: a. library for support vector machines*. Taiwan.

Clerc, M., 2006. *Particle swarm optimization*. London: ISTE.

Cortes, C. and Vapnik, V., 1995. Support-vector networks. *Machine Learning*, 20 (3), 273–297.

Cristianini, N. and Shawe-Taylor, J., 2000. *An introduction to support vector machines: And other kernel-based learning methods*. Cambridge ;, New York: Cambridge University Press.

Cybenko, G., 1989. Approximation by superpositions of a sigmoidal function. *Mathematics of Control, Signals, and Systems*, 2 (4), 303–314.

Endress+Hauser Messtechnik GmbH & Co. KG. *Technical Information Cleanfit W CPA450: Retractable assembly for 12 mm sensors for DO/pH/ORP measurement* [online]. Available from: https://portal.endress.com/wa001/dla/50002269096/000/01/TI183CAE_1109.pdf [Accessed 14 Mar 2012].

Endress+Hauser Messtechnik GmbH & Co. KG. *Technical Information Orbisint CPS11 and CPS11D: pH electrodes, analog or with digital Memosens technology For standard applications in process and environment technology, with dirt-repellent PTFE diaphragm, optional built-in temperature sensor* [online]. Available from: https://portal.endress.com/wa001/dla/50001854171/000/01/TI028CAE.pdf [Accessed 14 Mar 2012].

Endress+Hauser Messtechnik GmbH & Co. KG. *Technical Information Orbisint CPS12/CPS12D/CPS13: ORP electrodes, analog and digital with Memosens technology and reference electrode each with dirt-repellent PTFE diaphragm for standard applications in process and environmental technology* [online]. Available from: https://portal.endress.com/wa001/dla /50001616764/000/00/TI367CAE.pdf [Accessed 14 Mar 2012].

Endress+Hauser Messtechnik GmbH & Co. KG. *Technical Information TI 177C/24/ae: Turbidity sensor TurbiMax W CUS 41: Process and immersion sensor for service water and solids content measurement according to the 90° scattered light method* [online]. Available from: https://portal.endress.com/wa001/dla/50001855766/000/00/TI177CAE.pdf [Accessed 14 Mar 2012].

Endress+Hauser Messtechnik GmbH & Co. KG. *Technische Information Proline Prosonic Flow B 200: Ultraschall-Durchfluss-Messsystem Für genaue, zuverlässige Biogasmessung unter wechselnden Prozessbedingungen* [online]. Available from: https://portal.endress.com/ wa001/dla/50004694917/000/00/TI01018DDE_0111.pdf [Accessed 14 Mar 2012].

Endress+Hauser Messtechnik GmbH & Co. KG, 2011. *Proline Prosonic Flow B 200*. Für die zuverlässige Biogas-Durchflussmessung ohne Kompromisse.

Endress+Hauser Messtechnik GmbH & Co. KG, 2012. *Technical Information - Liquisys M CPM223/253: pH/ORP Measurement Transmitter for analog and digital glass and ISFET sensors*.

Etzkorn, C., 2008. *Modellierung, messtechnische Analyse und praktische Untersuchung des Fermentationsprozesses an industriellen und landwirtschaftlichen Biogasanlagen: Modelling, analysis and practice-oriented investigation of fermentation processes at industrial and agricultural biogas plants*. Gummersbach.

ExTox Gasmesssysteme GmbH. *Betriebsanleitung ExTox Gaswarnzentralen Serien ET-8D und ET-4D2: (Instruction manual ExTox gas warning system series ET-8D and ET-4D2)* [online]. Available from: http://www.extox.de/Gas-Transmitterliste.pdf [Accessed 14 Mar 2012].

Fachverband Biogas e.V., 2011. *Biogas Statistics 2011: Development of the number of biogas plants and the total installed electric output in megawatt [MW] (as of 11/2011)*.

Feitkenhauer, H., Sachs, J. von and Meyer, U., 2002. On-line titration of volatile fatty acids for the process control of anaerobic digestion plants. *Water Research*, 36 (1), 212–218.

FNR e.V., 2009. *Biogas-Messprogramm II - 61 Biogasanlagen im Vergleich: (Biogas Measurement Program II - A comparison of 61 German biogas plants)*. 1st ed. Gülzow: Fachagentur Nachwachsende Rohstoffe (Agency for Renewable Resources).

References

FNR e.V., 2010. *Leitfaden Biogas - von der Gewinnung zur Nutzung: (Handbook biogas - from production to exploitation).* 5th ed. Gülzow-Prüzen, Hannover: Technische Informationsbibliothek u. Universitätsbibliothek.

Guo, L., Chehata, N., Mallet, C. and Boukir, S., 2011. Relevance of airborne lidar and multispectral image data for urban scene classification using Random Forests. *ISPRS Journal of Photogrammetry and Remote Sensing*, 66 (1), 56–66.

Guwy, A.J., Hawkes, D.L., Hawkes, F.R. and Rozzi, A.G., 1994. Characterization of a prototype industrial on-line analyzer for bicarbonate/carbonate monitoring. *Biotechnology and Bioengineering*, 44 (11), 1325–1330.

Hach Lange GmbH, 2012. *sc1000 controller USER MANUAL*.

Haussler, D., Boser, B.E., Guyon, I.M. and Vapnik, V.N., 1992. A training algorithm for optimal margin classifiers. *Proceedings of the fifth annual workshop on Computational learning theory*, 144–152.

Hawkes, F.R., Guwy, A.J., Hawkes, D.L. and Rozzi, A.G., 1994. On-line monitoring of anaerobic digestion: Application of a device for continuous measurement of bicarbonate alkalinity. *Water Science & Technology*, 30 (12), 1–10.

Haykin, S.S., 1999. *Neural networks: A comprehensive foundation.* 2nd ed. Upper Saddle River, N.J: Prentice Hall.

hf-sensor GmbH. *Prozess Mikrowellen-TS-Sensor M W T S PP: (Process microwave TS sensor MWTS PP)* [online]. Available from: http://www.hf-sensor.de/download/mwtspp.pdf.

Hinton, G.E., 2002. Training Products of Experts by Minimizing Contrastive Divergence. *Neural Computation*, 14 (8), 1771–1800.

Hinton, G.E., Osindero, S. and Teh, Y.-W., 2006. A Fast Learning Algorithm for Deep Belief Nets. *Neural Computation*, 18 (7), 1527–1554.

Holm-Nielsen, J., Andree, H., Lindorfer, H. and Esbensen, K., 2007. Transflexive embedded near infrared monitoring for key process intermediates in anaerobic digestion/biogas production. *Journal of Near Infrared Spectroscopy*, 15 (2), 123.

Holm-Nielsen, J.B., Lomborg, C.J., Oleskowicz-Popiel, P. and Esbensen, K.H., 2008. On-line near infrared monitoring of glycerol-boosted anaerobic digestion processes: Evaluation of process analytical technologies. *Biotechnology and Bioengineering*, 99 (2), 302–313.

Hsu, C.W., Chang, C.C., and Lin, C.J., 2003. *A Practical Guide to Support Vector Classification*.

Jacobi, H.F., Moschner, C.R. and Hartung, E., 2009. Use of near infrared spectroscopy in monitoring of volatile fatty acids in anaerobic digestion. *Water Science & Technology*, 60 (2), 339.

Jantsch, T.G. and Mattiasson, B., 2004. An automated spectrophotometric system for monitoring buffer capacity in anaerobic digestion processes. *Water Research*, 38 (17), 3645–3650.

Keerthi, S.S. and Lin, C.-J., 2003. Asymptotic Behaviors of Support Vector Machines with Gaussian Kernel. *Neural Computation*, 15 (7), 1667–1689.

Keitlinghaus, H., 2011. *Gasmengen- und Durchflussmessung (Konzepte und Eignung für Biogasanlagen): gas quantity and flow measurement (Concepts and applicability for biogas plants)*. Braunschweig.

Keppler, F., Laukenmann, S., Rinne, J., Heuwinkel, H., Greule, M., Whiticar, M. and Lelieveld, J., 2010. Measurements of 13C/12C Methane from Anaerobic Digesters: Comparison of Optical Spectrometry with Continuous-Flow Isotope Ratio Mass Spectrometry. *Environmental Science & Technology*, 44 (13), 5067–5073.

Knick Elektronische Messgeräte GmbH & Co. KG. *SensoGate® WA 130 User Manual* [online]. Available from: http://www.knick.de/hps/upload/hxmedia/knick/HBzeCh3o.pdf [Accessed 14 Mar 2012].

Kujawski, O. and Steinmetz, H., 2009. Development of instrumentation systems as a base for control of digestion process stability in full-scale agricultural and industrial biogas plants. *Water Science & Technology*, 60 (8), 2055–2063.

Lahav, O. and Morgan, B.E., 2004. Titration methodologies for monitoring of anaerobic digestion in developing countries?a review. *Journal of Chemical Technology & Biotechnology*, 79 (12), 1331–1341.

Landwirtschaftskammer Nordrhein-Westfalen, 2012. *Angebotsformular - Gärsubstrate aus Biogasanlagen (quotation form - fermentation substate from biogas plants)*. Available from: http://www.landwirtschaftskammer.de/lufa/auftragsformulare/biogas/auftrag-gaerprodukte.pdf.

Langergraber, G., Fleischmann, N. and Hofstädter, F., 2003. A multivariate calibration procedure for UV/VIS spectrometric quantification of organic matter and nitrate in wastewater. *Water Science & Technology*, 47 (2), 63–71.

Liaw, A. and Wiener, M., 2002. Classification and Regression by randomForest. *R News*, 2 (3), 18–22.

References

Liébard, A. and Civel, Y.-B., 2011. *The state of renewable energies in Europe*. EurObserv'ER Report 11. Paris.

Lipták, B.G., 2003. *Instrument engineers' handbook.* 4th ed. Boca Raton, Fla. ; London: CRC Press.

Lomborg, C.J., Holm-Nielsen, J.B., Oleskowicz-Popiel, P. and Esbensen, K.H., 2009. Near infrared and acoustic chemometrics monitoring of volatile fatty acids and dry matter during co-digestion of manure and maize silage. *Bioresource Technology*, 100 (5), 1711–1719.

Madsen, M., Holm-Nielsen, J.B. and Esbensen, K.H., 2011. Monitoring of anaerobic digestion processes: A review perspective. *Renewable and Sustainable Energy Reviews*, 15 (6), 3141–3155.

McCarty, P.L., 1982. One hundred years of anaerobic treatment. *Proceedings of the International Symposium on Anaerobic Digestion* (2), 3–22.

McLoone, S., Brown, M., Irwin, G. and Lightbody, A., 1998. A hybrid linear/nonlinear training algorithm for feedforward neural networks. *IEEE Transactions on Neural Networks*, 9 (4), 669–684.

Méndez-Acosta, H.O., Palacios-Ruiz, B., Alcaraz-Gonza, V., Steyer, J.P., González-Álvarez, V. and Latrille, E., 2008. Robust Control of Volatile Fatty Acids in Anaerobic Digestion Processes. *Industrial and Engineering Chemistry Research*, 47 (20), 7715–7720.

Monzambe, K.M., Naveau Henry P., Nyns, E.-J., Bogaert, N. and Buehler, H., 1988. PROBLEMATICS AND STABILITY OF ON-LINE pH MEASUREMENTS IN ANAEROBIC ENVIRONMENTS: THE JELLIED COMBINED ELECTRODE. *Biotechnology and Bioengineering*, 31 (7), 659–665.

Morel, E., Santamaria, K., Perrier, M., Guiot, S. and Tartakovsky, B., 2004. Application of multi-wavelength fluorometry for on-line monitoring of an anaerobic digestion process. *Water Research*, 38 (14-15), 3287–3296.

Nacke, T., Barthel, A., Pflieger, C., Pliquett, U., Beckmann, D. and Goller, A., 2010. Continuous process monitoring for biogas plants using microwave sensors. *12th Biennial Baltic Electronics Conference, BEC 2010*, 239–242.

Nayono, S.E., ed., 2010. *Anaerobic digestion of organic solid waste for energy production*. Karlsruhe: KIT Scientific Publishing.

Neve, K. de and Lievens, K., 2004. On-line analyser solves monitoring problem in bio-digester. *Water and Wastewater International*, 19 (6), 28.

Osman, H. and Fahmy, M., 1994. On the discriminatory power of adaptive feed-forward layered networks. *IEEE Transactions on Pattern Analysis and Machine Intelligence*, 16 (8), 837–842.

Ozkaya, B., Demir, A. and Bilgili, M., 2007. Neural network prediction model for the methane fraction in biogas from field-scale landfill bioreactors. *Environmental Modelling & Software*, 22 (6), 815–822.

Palacio-Barco, E., Robert-Peillard, F., Boudenne, J.-L. and Coulomb, B., 2010. On-line analysis of volatile fatty acids in anaerobic treatment processes. *Analytica Chimica Acta*, 668 (1), 74–79.

PlanET Biogastechnik GmbH and Fachhochschule Köln, 2010. *Abschlussbericht Projekt MOBIO (Modellbasierte Prozessoptimierung von Biogasanlagen)*. Final project report MOBIO (Model-based process optimization of biogas plants); ProINNO II Grant No.: KA0607901WD8: PlanET Biogastechnik GmbH.

Powell, G.E. and Archer, D.B., 1989. On-Line Titration Method for Monitoring Buffer Capacity and Total Volatile Fatty Acid Levels in Anaerobic Digesters. *Biotechnology and Bioengineering*, 33, 570–577.

Pronova Analysentechnik GmbH & Co. KG. *Gerätefamilie SSM 6000: (Product familiy SSM 6000)* [online].
Available from: http://www.pronova.de/sites/default/files/webfm/uploads/PB_ssm6000_d.pdf [Accessed 14 Mar 2012].

Puñal, A., Palazzotto, L., Bouvier, J.C., Conte, T. and Steyer, J.P., 2003. Automatic control of volatile fatty acids in anaerobic digestion using a fuzzy logic based approach. *Water science and technology : a journal of the International Association on Water Pollution Research*, 48 (6), 103–110.

R Development Core Team, 2010. *R: A language and environment for statistical computing*. Vienna, Austria.

s:can Messtechnik GmbH. *spectro:lyser™ datasheet* [online]. Available from: http://www.s-can.at/medialibrary/datasheets/spectrolyser_ww_eng.pdf [Accessed 14 Mar 2012].

Scaglione, D., Lubello, C., Caffaz, S., Ficara, E. and Malpei, F., 2008. A simple method to evaluate the short-term biogas yield in anaerobic codigestion of WAS and organic wastes. *Water Science & Technology* [online], 58 (8), 1615–1622. Available from: http://search.ebscohost.com.jproxy.nuim.ie/login.aspx?direct=true&db=a9h&AN=35246552&site=ehost-live.

References

Schmidt, H., 2008. *New Online-Measurement Methods for Biogas Plants*. Diploma Thesis. Cologne University of Applied Sciences.

Siemens AG, 2010. *Vortex Durchflussmessgeräte SITRANS FX300* [online]. Available from: http://support.automation.siemens.com/WW/llisapi.dll?func=cslib.csinfo&lang=de&objID=28017661&subtype=133300 [Accessed 14 Mar 2012].

Silva, C. and Ribeiro, B., 2010. *Inductive inference for large scale text classification: Kernel approaches and techniques*. Berlin: Springer.

Slater, W., Merigh, M., Ricker, N., Labib, F., Ferguson, J. and Benjamin, M., 1990. A microcomputer-based instrumentation system for anaerobic wastewater treatment processes. *Water Research*, 24 (1), 121–123.

Spanjers, H., Bouvier, J., Steenweg, P., Bisschops, I., van Gils, W. and Versprille, B., 2006. Implementation of in-line infrared monitor in full-scale anaerobic digestion process. *Water Science and Technology*, 53 (4-5), 55–61.

Spanjers, H. and van Lier J.B, 2006. Instrumentation in anaerobic treatment - Research and practice. *Water Science and Technology* [online], 53 (4-5), 63–76. Available from: http://www.scopus.com/inward/record.url?eid=2-s2.0-33646749693&partnerID=40&md5=edae88c5cb998b0d67695112bf3bd540.

Steyer, P., Bouvier, J.C., Conte, T., Gras, P., Harmand, J. and Delgenes, J.P., 2002. On-line measurements of COD, TOC, VFA, total and partial alkalinity in anaerobic digestion processes using infra-red spectrometry. *Water Science and Technology*, 45 (10), 133–138.

Strik, D.P., Domnanovich, A.M., Zani, L., Braun, R. and Holubar, P., 2005. Prediction of trace compounds in biogas from anaerobic digestion using the MATLAB Neural Network Toolbox. *Environmental Modelling & Software*, 20 (6), 803–810.

Stuhlsatz, A., Lippel, J. and Zielke, T., 2010a. Discriminative Feature Extraction with Deep Neural Networks. *Proceedings of the 2010 International Joint Conference on Neural Networks (IJCNN)*.

Stuhlsatz, A., Lippel, J. and Zielke, T., 2010b. Feature Extraction for Simple Classification. *ICPR '10 Proceedings of the 2010 20th International Conference on Pattern Recognition*, 1525–1528.

Tipping, M.E., 2000. The Relevance Vector Machine. *Advances in Neural Information Processing Systems 12*, MIT Press, 652–658.

Tosi, S., Rossi, M., Tamburini, E., Vaccari, G., Amaretti, A. and Matteuzzi, D., 2003. Assessment of In-Line Near-Infrared Spectroscopy for Continuous Monitoring of Fermentation Processes. *Biotechnology Progress*, 19 (6), 1816–1821.

trend:research, 2010. *Biogas in Europa bis 2020 (Biogas in Europe till 2020): Potenziale, Wettbewerb und Marktentwicklung bis 2020 in 16 europäischen Ländern (Potential, competition and market development till 2020 in 16 European*.

TriOS Optical Sensors GmbH. *ProPS-Kit: NO3, CODeq/TOCeq by spectral UV analysis* [online]. Available from: http://www.trios.de/downloads/Brochures%20-%20English/ProPS-Kit_en_V2.pdf [Accessed 14 Mar 2012].

Viacheslav Artyushenko, 2010. *Fibre Spectroscopy with Clear Process Vision*. Corona.

Wang, D., Leung, H., Kurian, A.P., Kim, H.J. and Yoon, H., 2010. A deconvolutive neural network for speech classification with applications to home service robot. *IEEE Transactions on Instrumentation and Measurement*, 59 (12), 3237–3243.

Ward, A.J., Bruni, E., Lykkegaard, M.K., Feilberg, A., Adamsen, A.P., Jensen, A.P. and Poulsen, A.K., 2011. Real time monitoring of a biogas digester with gas chromatography, near-infrared spectroscopy, and membrane-inlet mass spectrometry. *Bioresource Technology*, 102 (5), 4098–4103.

Wiese, J. and Haeck, M., 2006. Instrumentation, control and automation for full-scale manure-based biogas systems. *Water Science & Technology*, 54 (9), 1–8.

Wiese, J. and Kujawski, O., 2008. Operational results of an agricultural biogas plant equipped with modern instrumentation and automation. *Water Science & Technology* [online], 57 (6), 803–808. Available from: http://search.ebscohost.com.jproxy.nuim.ie/login.aspx?direct=true&db=a9h&AN=31672525&site=ehost-live.

Wiese, J. and König, R., 2009. From a black-box to a glass-box system: the attempt towards a plant-wide automation concept for full-scale biogas plants. *Water Science & Technology*, 60 (2), 321.

Witkowska, E., Buczkowska, A., Zamojska, A., Szewczyk, K.W. and Ciosek, P., 2010. Monitoring of periodic anaerobic digestion with flow-through array of miniaturized ion-selective electrodes. *Bioelectrochemistry*, 80 (1), 87–93.

Wolf, C., Bongards, M. and Sander, A., 2011a. Online-Messtechnik optimiert Biogasanlagen und Faultürme. *wwt - wasserwirtschaft wassertechnik*, 60 (4), 8–16.

References

Wolf, C., Gaida, D., Stuhlsatz, A., Ludwig, T., McLoone, S. and Bongards, M., 2011b. Predicting organic acid concentration from UV/vis spectrometry measurements - A comparison of machine learning techniques. *Transactions of the Institute of Measurement and Control*.

Wolf, C., Gaida, D., Stuhlsatz, A., McLoone, S. and Bongards, M., 2010. Organic acid prediction in biogas plants using UV/vis spectroscopic online-measurements. *Communications in Computer and Information Science* [online], 97 CCIS (PART 1), 200–206. Available from: http://www.scopus.com/inward/record.url?eid=2-s2.0-78149260823&partnerID=40&md5=16c7b274b500a34fc013cc869c6b3a2f.

Wolf, C., Sander, A., Gaida, D., Etzkorn, C., and Bongards, M., 2011c. *Abschlussbericht Pro INNO II Projekt MOBIO - Modellbasierte Prozessoptimierung von Biogasanlagen (Final report Pro INNO II project MOBIO - Model-based process optimization of biogas plants)*. Berlin: BMWi.

Yogameena, B., Veera Lakshmi, S., Archana, M. and Raju Abhaikumar, S., 2010. Human Behavior Classification Using Multi-Class Relevance Vector Machine. *Journal of Computer Science*, 6 (9), 1021–1026.

Yokogawa Electric Corporation. *General Specifications General Specifications DIGI YEFLOW Series GS 01F06A00-01EN* [online]. Available from: http://www.yokogawa.com/fld/pdf/DYF/GS01F06A00-01E.pdf [Accessed 14 Mar 2012].

Zimmermann, C., Baalmann, M., and Wulfert, K., 2003. *Prozesskontrolle und Anlagenführung landwirtschaftlicher Biogasanlagen durch dynamische Betriebsweise (Process control and operation of agricultural biogas plants by dynamic mode of operation)*. Bremen.

7 Discussion and Conclusion

During the last two decades, the production of renewable energy by anaerobic digestion in biogas plants has become increasingly popular due to its applicability to a great variety of organic material from energy crops and animal waste to the organic fraction of MSW, and to the relative simplicity of AD plant designs. Thus, a whole new biogas market emerged in Europe, which is strongly supported by European and national funding and remuneration schemes. In particular, ABPs, which produce biogas from energy crops and animal waste, are strongly supported and form the majority of biogas plants in Europe.

Nevertheless, stable and efficient ABP operation and control can be challenging, due to the high complexity of the biochemical AD process and varying substrate quality. In addition, governmental support for ABPs will decrease in the long run and the substrate market will become highly competitive. Thus, plant efficiency becomes the major priority in order to assure sustainable plant operation going forward (BMU 2011). In order to tap the full potential of biogas plants while maintaining process stability new innovative developments in the area of biogas plant optimization, control and instrumentation are needed.

Thus, the principal aim of the research presented in this thesis was to develop a suite of tools and methodologies comprising developments in the areas of simulation, instrumentation and control in order to cover all aspects, which are relevant for ABP operation. This suite of tools uses dynamic simulation models and computational intelligence (CI) methods for substrate inflow optimization, as well as a novel UV/vis spectroscopic online measurement system for VFA using powerful machine learning techniques. Although, these tools were not combined together to be validated in full-scale operation to quantify the overall improvement, they provide a valuable toolset for process and operational optimization of ABPs.

As a result a simulation based optimization methodology for the optimization of ABP substrate inflows was developed and successfully applied to the full-scale Sunderhook ABP. Results show that significant improvement of plant efficiency can be achieved. The best optimization result for a substrate inflow consisting of maize and bull manure, showed an increase in yearly profit of 219,000 €, which makes the developed substrate inflow optimization strategy very attractive to end users.

In order to achieve these results, a dynamic simulation model of the Sunderhook ABP was successfully developed based on available operational data. As model design and substrate characterization of AD is difficult and normally requires a substantial amount of laboratory analysis, an open source Matlab® toolbox for modeling and simulation of ABPs was developed to facilitate model design and simulation by centralized configuration of the complete ABP using several GUIs for

substrate feed characterization and plant design. Thus, the use of dynamic simulation models for optimization and control purposes becomes manageable as no excessive expert knowledge is required.

Furthermore, two novel optimization methods for the optimization of complex nonlinear and multi-dimensional fitness functions were developed and successfully tested on four test problems and on the Sunderhook ABP model. As global optimization algorithms (such as genetic algorithms or particle swarm optimization) are computationally expensive for the optimization of the substrate inflow of biogas plants, optimization time is the main critical parameter. In this work an alternative method for the optimisation of parameters based on Kriging surrogate models of the fitness function, which are sequentially updated during an optimization run, was proposed. By using these methods the computation time required was substantially reduced. Speed-ups of a factor of 50 or greater were observed in the experiments conducted in chapter 4.

The achievements developed in the area of simulation and optimization show that global optimization of the substrate inflow of ABPs based on dynamic simulation models, or complex optimization problems in general, can be realized by application of the right toolset.

To address the lack of robust and reliable online instrumentation for process monitoring and control of ABPs, state of the art online measurement systems for *pH*, *ORP* and *TS* were tested and evaluated at an ABP and an IBP in order to assess their long term stability. Furthermore, measurement values from the online measurement systems were compared to operational data from the plant to evaluate their ability to recognize process disturbances. Results showed that *pH* and *TS* probes provide valuable information with regard to process stability, whereas *ORP* probes showed no correlation to the operational plant data. Moreover, in the market available *pH* and *ORP* probes were not suitable for the application in dry digestion as the probes were seriously damaged by the high *TS* content in the digester.

As *VFA* concentration is one of the most important process parameters, its online measurement provides real-time information about process stability. What makes the online measurement of *VFA* concentration difficult is the high *TS* content of the substrate. Therefore, a novel UV/vis spectroscopic online measurement system for *VFA* concentration in digesters was successfully developed. The practical testing of the indirect measurement using a UV/vis spectroscopic probe showed that a measurement accuracy of 88% could be achieved.

These results were achieved using powerful machine learning methods for spectral analysis. The analysis of data from spectroscopic probes is needed for calibration but is a challenge due to the large number of wavelengths and the high nonlinearity of absorption. To allow for a fast and thorough analysis of spectral data sets, analysis of the spectral data was performed using six powerful machine learning methods, which are well-suited to this kind of problem. Results show that by applying

dimension reduction and multiple transformations to the data, relevant information can be efficiently extracted, enabling good calibration results to be achieved. The most effective machine learning techniques were a combination of GerDA and RF and SVM with an NMCR of 12.4% and 12% respectively. In particular, GerDA managed to substantially reduce the 176 dimensional data to four dimensions allowing very fast classification using RF. Classification with SVM was slightly slower due to the large number of support vectors required for classification (398). Thus, GerDA in combination with RF and SVM, can be recommended for the analysis of spectral data. Furthermore, the obtained results can be used as a guideline for further developments in the area of spectroscopic online measurements.

All in all, the developed methodologies and optimization strategies as well as the measurement results show that ABP operation can be substantially optimized and improved using dynamic simulation models, CI based optimization strategies, newly developed spectroscopic online measurement systems and powerful machine learning techniques. Thus, sustainable and efficient ABP operation is possible.

7.1 Topics for future research

The methodologies and developments presented in this thesis offer new possibilities for ABP optimization and control.

One of the obvious next steps is the practical implementation of the complete toolset from online measurement system for VFA concentration to substrate feed optimization using dynamic simulation models and CI methods at several full-scale ABP and IBP in order to verify the optimization potential. Therefore, the UV/vis measurement system needs to be further developed into a commercial prototype. In particular, the dilution system needs to be adapted and fully automated to allow for easy and thus fast installation and robust operation. Furthermore, the simulation model needs to be calibrated based on process data from these plants, which requires algorithms to automate the calibration procedure and allow for a continuous recalibration based on newly available process data. The optimization algorithm itself can be implemented on an Industrial PC and connected to the SCADA system of the plants using the OPC protocol. Thus, optimized substrate feed compositions can be transmitted to a local PLC.

The VFA online measurement system could also be further developed into an early warning system for biogas plants similar to a “traffic light” system. Using machine learning techniques, the current VFA measurement could be compared against historical VFA data and integrated with information derived from other available process variables to provide an assessment of the current operational state of a biogas plant. This could then be used to give visual feedback to the operator on the state of his plant: e.g. “green” – everything is in order, “yellow” – light disturbances, “red” – strong inhibition, operational problems are immanent.

In addition, the idea of substrate inflow optimization based on simulation models can be exploited further to develop Nonlinear Model Predictive Controllers (NMPC) for continuous adaptation of the substrate inflow according to the current state of the AD process. Through the development of a state estimator, which predicts the state of the AD process based on available online measurements using a fully calibrated simulation model of an ABP, such a control system could efficiently compensate process disturbances. A first attempt at implementing an NMPC based on the results of this thesis has already made by Gaida *et al.* (2012) showing promising results.

Furthermore, novel online measurement systems for biogas plants should be developed in order to allow the reliable online monitoring of process parameters that are crucial for process stability such as *VFA, VOA/TIC, TA* and concentration of carbohydrates, proteins and lipids. Recent developments in the area of middle infrared spectroscopic diamond-tipped probes show promising results. Due to newly developed polycrystalline fibers (PIR) for signal transmission, signal strength and reflection intensity have been substantially improved. First laboratory trials with anaerobic sludge from an IBG show that *VFA* concentration can be measured (Janz *et al.* 2012).

These are just some examples for future research in the area of optimization, control and instrumentation of biogas plants that show the great potential in this broad field of research.

References

Gaida, D., Wolf, C., Bäck, T., and Bongards, M., 2012. *Nonlinear Model Predictive Substrate Feed Control of Biogas Plants*. 20th IEEE Mediterranean Conference on Control and Automation. Barcelona, Spain.

Janz, S., Trauer, G., Rehorek, A. and Bongards, M., 2012. Entwicklung eines MIR-Online-Messsystems für anaerobe Fermentations-anlagen mit automatischer Kalibrierung. *8. Kolloquium Prozessanalytik.*

Annex I

Biochemical rate coefficients ($v_{i,j}$) and kinetic rate equations (ρ_j) for soluble components (i = 1-12; j = 1-19).

Component →	i	1	2	3	4	5	6	7	8	9	10	11	12	Rate(ρ_j, kg COD.m^{-3}.d^{-1})
j	Process ↓	S_{su}	S_{aa}	S_{fa}	S_{va}	S_{bu}	S_{pro}	S_{ac}	S_{h2}	S_{ch4}	S_{co2}	S_{nh4}	S_I	
1	Disintegration										$f_{co2,xc}$	$f_{sin,xc}$	$f_{SI,XC}$	$k_{dis}X_c$
2	Hydrolysis Carbohydrates	1												$k_{hyd,ch}X_{ch}$
3	Hydrolysis of Proteins		1											$k_{hyd,pr}X_{pr}$
4	Hydrolysis of Lipids	$1-f_{fa,li}$		$f_{fa,li}$							$f_{co2,xli}$			$k_{hyd,li}X_{li}$
5	Uptake of Sugars	−1				$(1-Y_{su})f_{bu,su}$	$(1-Y_{su})f_{pro,su}$	$(1-Y_{su})f_{ac,su}$	$(1-Y_{su})f_{h2,su}$		$f_{co2,su}$	$-(Y_{su})N_{bac}$		$k_{m,su}\frac{S_{su}}{K_S+S_{su}}X_{su}I_1$
6	Uptake of Amino Acids		−1		$(1-Y_{aa})f_{va,aa}$	$(1-Y_{aa})f_{bu,aa}$	$(1-Y_{aa})f_{pro,aa}$	$(1-Y_{aa})f_{ac,aa}$	$(1-Y_{aa})f_{h2,aa}$		$f_{co2,aa}$	$N_{aa}-(Y_{aa})N_{bac}$		$k_{m,aa}\frac{S_{aa}}{K_S+S_{aa}}X_{aa}I_1$
7	Uptake of LCFA			−1				$(1-Y_{fa})f_{ac,fa}$	$(1-Y_{fa})f_{h2,fa}$		$f_{co2,fa}$	$-(Y_{fa})N_{bac}$		$k_{m,fa}\frac{S_{fa}}{K_S+S_{fa}}X_{fa}I_2$
8	Uptake of Valerate				−1		$(1-Y_{c4})0.54$	$(1-Y_{c4})0.31$	$(1-Y_{c4})0.15$		$f_{co2,va}$	$-(Y_{c4})N_{bac}$		$k_{m,c4}\frac{S_{va}}{K_S+S_{va}}X_{c4}\frac{1}{1+S_{bu}/S_{va}}I_2$
9	Uptake of Butyrate					−1		$(1-Y_{c4})0.8$	$(1-Y_{c4})0.2$		$f_{co2,bu}$	$-(Y_{c4})N_{bac}$		$k_{m,c4}\frac{S_{bu}}{K_S+S_{bu}}X_{c4}\frac{1}{1+S_{va}/S_{bu}}I_2$
10	Uptake of Propionate						−1	$(1-Y_{pro})0.57$	$(1-Y_{pro})0.43$		$f_{co2,pro}$	$-(Y_{pro})N_{bac}$		$k_{m,pr}\frac{S_{pro}}{K_S+S_{pro}}X_{pro}I_2$
11	Uptake of Acetate							−1		$(1-Y_{ac})$	$f_{co2,ac}$	$-(Y_{ac})N_{bac}$		$k_{m,ac}\frac{S_{ac}}{K_S+S_{ac}}X_{ac}I_3$
12	Uptake of Hydrogen								−1	$(1-Y_{h2})$	$f_{co2,h2}$	$-(Y_{h2})N_{bac}$		$k_{m,h2}\frac{S_{h2}}{K_S+S_{h2}}X_{h2}I_1$
13	Decay of X_{su}										$f_{co2,xb}$	$f_{sin,xb}$		$k_{dec,Xsu}X_{su}$
14	Decay of X_{aa}										$f_{co2,xb}$	$f_{sin,xb}$		$k_{dec,Xaa}X_{aa}$
15	Decay of X_{fa}										$f_{co2,xb}$	$f_{sin,xb}$		$k_{dec,Xfa}X_{fa}$
16	Decay of X_{C4}										$f_{co2,xb}$	$f_{sin,xb}$		$k_{dec,Xc4}X_{c4}$
17	Decay of X_{pro}										$f_{co2,xb}$	$f_{sin,xb}$		$k_{dec,Xpro}X_{pro}$
18	Decay of X_{ac}										$f_{co2,xb}$	$f_{sin,xb}$		$k_{dec,Xac}X_{ac}$
19	Decay of X_{h2}										$f_{co2,xb}$	$f_{sin,xb}$		$k_{dec,Xh2}X_{h2}$
		Monosaccharies (kgCOD m^{-3})	Amino Acids (kgCOD m^{-3})	Long chain fatty acids (kgCOD m^{-3})	Total valerate (kgCOD m^{-3})	Total buyrate (kgCOD m^{-3})	Total propionate (kgCOD m^{-3})	Total acetane (kgCOD m^{-3})	Hydrogen gas (kgCOD m^{-3})	Methane gas (kgCOD m^{-3})	Inorganic Carbon (kmoleC m^{-3})	Inorganic nitrogen (kmoleN m^{-3})	Solube inerts (kgCOD m^{-3})	Inhibition factors (3.7): $I_1 = I_{pH}I_{IN,lim}$ $I_2 = I_{pH}I_{IN,lim}I_{h2}$ $I_3 = I_{pH}I_{IN,lim}I_{NH3,Xac}$

Biochemical rate coefficients ($\nu_{i,j}$) and kinetic rate equations (ρ_j) for soluble components (i = 13-24; j = 1-19).

Component →	i	13	14	15	16	17	18	19	20	21	22	23	24	Rate(ρ_j, kg COD.m^{-3}.d^{-1})
j	Process ↓	X_c	X_{ch}	X_{pr}	X_{li}	X_{su}	X_{aa}	X_{fa}	X_{c4}	X_{pro}	X_{ac}	X_{h2}	X_I	
1	Disintegration	−1	$f_{ch,xc}$	$f_{pr,xc}$	$f_{li,xc}$								$f_{xI,xc}$	$k_{dis}X_c$
2	Hydrolysis Carbohydrates		−1											$k_{hyd,ch}X_{ch}$
3	Hydrolysis of Proteins			−1										$k_{hyd,pr}X_{pr}$
4	Hydrolysis of Lipids				−1									$k_{hyd,li}X_{li}$
5	Uptake of Sugars					Y_{su}								$k_{m,su}\frac{S_{su}}{K_S+S}X_{su}I_1$
6	Uptake of Amino Acids						Y_{aa}							$k_{m,aa}\frac{S_{aa}}{K_S+S_{aa}}X_{aa}I_1$
7	Uptake of LCFA							Y_{fa}						$k_{m,fa}\frac{S_{fa}}{K_S+S_{fa}}X_{fa}I_2$
8	Uptake of Valerate								Y_{c4}					$k_{m,c4}\frac{S_{va}}{K_S+S_{va}}X_{c4}\frac{1}{1+S_{bu}/S_{va}}I_2$
9	Uptake of Butyrate								Y_{c4}					$k_{m,c4}\frac{S_{bu}}{K_S+S_{bu}}X_{c4}\frac{1}{1+S_{va}/S_{bu}}I_2$
10	Uptake of Propionate									Y_{pro}				$k_{m,pr}\frac{S_{pro}}{K_S+S_{pro}}X_{pro}I_2$
11	Uptake of Acetate										Y_{ac}			$k_{m,ac}\frac{S_{ac}}{K_S+S_{ac}}X_{ac}I_3$
12	Uptake of Hydrogen											Y_{h2}		$k_{m,h2}\frac{S_{h2}}{K_S+S_{h2}}X_{h2}I_1$
13	Decay of X_{su}		$f_{ch,xb}$	$f_{pr,xb}$	$f_{li,xb}$	−1								$k_{dec,Xsu}X_{su}$
14	Decay of X_{aa}		$f_{ch,xb}$	$f_{pr,xb}$	$f_{li,xb}$		−1							$k_{dec,Xaa}X_{aa}$
15	Decay of X_{fa}		$f_{ch,xb}$	$f_{pr,xb}$	$f_{li,xb}$			−1						$k_{dec,Xfa}X_{fa}$
16	Decay of X_{C4}		$f_{ch,xb}$	$f_{pr,xb}$	$f_{li,xb}$				−1					$k_{dec,Xc4}X_{c4}$
17	Decay of X_{pro}		$f_{ch,xb}$	$f_{pr,xb}$	$f_{li,xb}$					−1				$k_{dec,Xpro}X_{pro}$
18	Decay of X_{ac}		$f_{ch,xb}$	$f_{pr,xb}$	$f_{li,xb}$						−1			$k_{dec,Xac}X_{ac}$
19	Decay of X_{h2}		$f_{ch,xb}$	$f_{pr,xb}$	$f_{li,xb}$							−1		$k_{dec,Xh2}X_{h2}$
		Composites (kgCOD m^{-3})	Carbohydrates (kgCOD m^{-3})	Proteins (kgCOD m^{-3})	Lipids (kgCOD m^{-3})	Sugar degraders (kgCOD m^{-3})	Amino acid degraders (kgCOD m^{-3})	LCFA degraders (kgCOD m^{-3})	Valerate and butyrate degrades (kgCOD m^{-3})	Propionate degraders (kgCOD m^{-3})	Acetate degraders (kgCOD m^{-3})	Hydrogen degraders (kgCOD m^{-3})	Particulate inerts (kgCOD m^{-3})	Inhibition factors (3.7): $I_1 = I_{pH}I_{IN,lim}$ $I_2 = I_{pH}I_{IN,lim}I_{h2}$ $I_3 = I_{pH}I_{IN,lim}I_{NH3,Xac}$

Annex I